

THESIS

LIMITING MEMBRANE AND DIFFUSION BEHAVIOR OF A COMPACTED SAND-
BENTONITE MIXTURE FOR HYDRAULIC AND CHEMICAL CONTAINMENT

Submitted by

Cameron John Fritz

Department of Civil and Environmental Engineering

In partial fulfillment of the requirements

For the Degree of Master of Science

Colorado State University

Fort Collins, Colorado

Summer 2017

Master's Committee:

Advisor: Joseph Scalia IV

Co-Advisor: Charles D. Shackelford

Michael J. Ronayne

Copyright by Cameron John Fritz 2017

All Rights Reserved

ABSTRACT

LIMITING MEMBRANE AND DIFFUSION BEHAVIOR OF A COMPACTED SAND-BENTONITE MIXTURE FOR HYDRAULIC AND CHEMICAL CONTAINMENT

Sodium-bentonite (Na-bentonite) commonly is used either as an additive component or as the sole component of engineered barriers used for waste containment applications, because the tendency of Na-bentonite to exhibit high swell can result in the restriction of advective and diffusive contaminant transport. Additionally, compacted mixtures of Na-bentonite and sand can be an effective and economical alternative to barrier materials consisting only of natural clay (e.g., compacted clay liners) if the use of natural clay is not logistically or economically feasible. The existence of membrane behavior, i.e., the ability of a porous material to exhibit selective restriction of migrating chemical species from the clay pores, previously has been shown for typical engineered bentonite-based barriers commonly used in hydraulic and chemical containment applications, including compacted sand-bentonite (SB) mixtures. However, the extent to which clay membrane behavior may persist in the presence of highly concentrated chemical solutions, which have been shown to have an adverse effect on the magnitude of membrane behavior in clays, remains largely unknown, with few studies having quantified the limiting membrane and diffusion behavior of bentonite-based barrier materials. Moreover, the limiting membrane and diffusion behavior of compacted SB mixtures has not yet been evaluated.

Based on these considerations, the purpose of this study was to quantify the limiting membrane and diffusion behavior of two specimens of a compacted SB mixture comprising 15 % Na-bentonite (by dry weight) by determining the threshold salt concentration at which measurable membrane behavior was eliminated. The specimens were exposed to a series of

boundary monovalent salt solutions with increasingly higher source concentrations, C_{ot} , until measured values of the membrane efficiency coefficient, ω ($0 \leq \omega \leq 1$), were effectively nil (i.e., 0.000), representing the limiting condition at which measurable membrane behavior was eliminated. Overall, ω decreased from an average of 0.032 to 0.000 as C_{ot} increased from 160 mM KCl to 3.27 M NaCl, resulting in a threshold concentration between 1.63 M and 3.27 M NaCl for both specimens that was much higher than the range of salt concentrations for which measurable membrane behavior previously was thought to exist. Effective diffusion coefficients, D^* , for nonreactive chloride (Cl^-) also were measured during membrane testing to evaluate possible changes in diffusion behavior corresponding to the progressive destruction of membrane behavior. However, D^* was relatively constant throughout all testing stages ($2.1 \times 10^{-10} \text{ m}^2/\text{s} \leq D^* \leq 3.0 \times 10^{-10} \text{ m}^2/\text{s}$), indicating that the corresponding decrease in ω from 0.032 to 0.000 had little to no effect on the diffusion of Cl^- .

ACKNOWLEDGEMENTS

Being a part of the “Geo Group” at CSU has certainly been one of the most rewarding experiences I’ve had so far. Thank you to all of you, students and professors included, for helping to create such a fun and supportive community.

Of course, many thanks must be given to my committee members. To Professor Joe Scalia, for always being available and willing to provide guidance whenever it was needed, and for spending many hours discussing membrane behavior with me and reviewing my writing. To Professor Charles Shackelford, for his unparalleled expertise and insight which was so invaluable over the course of this project. And to Professor Mike Ronayne, for his time spent reviewing my thesis and serving on my committee, and whose undergraduate geology course helped to confirm for me that I was taking the right path with my choice of careers.

I also would like to extend my thanks to Professor Chris Bareither for cultivating my initial interest in soils and geoen지니어ing as an undergraduate, and for always providing exceptionally challenging and fascinating learning opportunities in the many courses I was able to take with him.

To my parents, John Fritz and Cynthia Hendel, thank you for always supporting me in everything I have pursued in life, and for trusting in me to make the best decisions for myself. Finally, to Megan Comisso, thank you for your endless love and patience as I worked for two years to accomplish this goal and for always providing such a caring and encouraging presence whenever it was needed the most.

TABLE OF CONTENTS

ABSTRACT.....	ii
ACKNOWLEDGEMENTS.....	iv
LIST OF TABLES.....	viii
LIST OF FIGURES.....	ix
CHAPTER 1. INTRODUCTION.....	1
1.1 Background.....	1
1.1.1 <i>Engineered Bentonite-Based Containment Barriers</i>	1
1.1.1.1 <i>Compacted Sand-Bentonite Mixtures</i>	2
1.1.2 <i>Semipermeable Membrane Behavior</i>	3
1.1.2.1 <i>Limiting Membrane Behavior</i>	5
1.2 Research Motivation and Objectives.....	8
REFERENCES.....	9
CHAPTER 2. LIMITING MEMBRANE AND DIFFUSION BEHAVIOR OF COMPACTED SAND-BENTONITE SPECIMENS.....	13
2.1 Introduction.....	13
2.2 Materials and Methods.....	15
2.2.1 <i>Liquids</i>	15
2.2.2 <i>Soils</i>	17
2.2.3 <i>Sand-Bentonite Mixture and Specimen Preparation</i>	17
2.2.4 <i>Hydraulic Conductivity Testing</i>	18

2.2.5	<i>Membrane Behavior and Diffusion Testing Apparatus and Procedure</i>	21
2.2.5.1	<i>Chemico-Osmotic Pressures</i>	24
2.2.5.1.1	<i>Membrane Efficiency Coefficients</i>	30
2.2.5.1.2	<i>Concentration-EC Correlation</i>	32
2.2.5.1.3	<i>Activity Method</i>	38
2.2.5.2	<i>Effective Diffusion Coefficients and Tortuosity Factors</i>	40
2.2.6	<i>Testing Program</i>	45
2.3	<i>Results</i>	46
2.3.1	<i>Hydraulic Conductivity Testing</i>	46
2.3.2	<i>Membrane Testing</i>	47
2.3.2.1	<i>Boundary Electrical Conductivities and Solute Concentrations</i>	48
2.3.2.2	<i>Maximum Chemico-Osmotic Pressure Differences</i>	51
2.3.2.3	<i>Boundary Water Pressures</i>	54
2.3.2.4	<i>Possible Effect of Diffusion Osmosis on Boundary Water Pressures</i>	57
2.3.2.5	<i>Measured Chemico-Osmotic Pressure Differences</i>	58
2.3.2.6	<i>Membrane Efficiency Coefficients</i>	63
2.3.3	<i>Diffusion</i>	67
2.3.3.1	<i>Diffusive Mass Flux</i>	67
2.3.3.2	<i>Effective Diffusion Coefficients</i>	70
2.3.3.3	<i>Tortuosity Factors</i>	73

2.3.4	<i>Effect of NaCl versus KCl</i>	79
2.3.5	<i>Comparison with Previous Research on Limiting Membrane Behavior</i>	81
2.4	Conclusions.....	83
REFERENCES		143
APPENDIX A: WATER ACTIVITY AND SOLUTION DENSITY VALUES FROM THE LITERATURE USED FOR DEVELOPMENT OF THE ACTIVITY METHOD		151
APPENDIX B: MOLALITY TO MOLARITY CONVERSION.....		154
APPENDIX C: COMPARISON OF DIFFERENTIAL PRESSURES OBTAINED USING INLINE VERSUS DIFFERENTIAL PRESSURE TRANSDUCERS.....		156
APPENDIX D: METHOD OF REVERSE FITTING FOR DETERMINATION OF STEADY-STATE NET ACCUMULATED SOLUTE MASS FLUX.....		161

LIST OF TABLES

Table 2.1. Chemical properties of tap water used in this study.	86
Table 2.2. Summary of results obtained using the van't Hoff method ($\Delta\pi_C, \omega_C$) and using the activity method ($\Delta\pi_{aw}, \omega_{aw}$).	87
Table 2.3. Summary of results from membrane efficiency testing.	88
Table 2.4. Summary of diffusion results.	89

LIST OF FIGURES

Figure 2.1. Schematics of the (a) flexible-wall (FW) permeameter (after Meier 2016) and (b) k-testing apparatus with FW permeameter.....	90
Figure 2.2. Schematic of membrane testing apparatus (after Meier 2016).....	91
Figure 2.3. Schematic of the rigid-wall membrane testing cell (after Meier 2016).....	92
Figure 2.4. Activity of water for varying concentrations of aqueous KCl and NaCl solutions, fitted with second-order polynomial regressions. Based on all available data from Robinson and Stokes (1959).	93
Figure 2.5. Values of the theoretical maximum chemico-osmotic pressure difference for a range of Cl ⁻ concentrations using the van't Hoff approximation ($\Delta\pi_C$) and the activity method ($\Delta\pi_{aw}$). Values of $\Delta\pi_{aw}$ calculated using both NaCl water activity relationship ($\Delta\pi_{aw,NaCl}$) and KCl water activity relationship ($\Delta\pi_{aw,KCl}$).	94
Figure 2.6. Percent error of maximum chemico-osmotic pressure differences calculated using the van't Hoff approximation ($\Delta\pi_C$) relative to those calculated using the activity method ($\Delta\pi_{aw}$) for a range of theoretical NaCl and KCl concentrations.	95
Figure 2.7. Concentration vs. EC log-log relationships for KCl and NaCl solutions prepared at varying target concentrations with de-ionized water (DIW) and tap water (TW).	96
Figure 2.8. Sample Cl ⁻ concentrations predicted using calibration curves vs. actual Cl ⁻ concentrations measured using ion chromatography (IC). Samples collected from top boundary circulation effluent by Meier (2016).	97

Figure 2.9. Percent error of sample Cl^- concentrations predicted using calibration curves relative to actual Cl^- concentrations measured using ion chromatography (IC). Samples collected from top boundary circulation effluent by Meier (2016)..... 98

Figure 2.10. Sample Cl^- concentrations predicted using calibration curves vs. actual Cl^- concentrations measured using ion chromatography (IC). Samples collected from bottom boundary circulation effluent by Meier (2016)..... 99

Figure 2.11. Percent error of sample Cl^- concentrations predicted using calibration curves relative to actual Cl^- concentrations measured using ion chromatography (IC). Samples collected from bottom boundary circulation effluent by Meier (2016)..... 100

Figure 2.12. Hydraulic conductivity test results for specimen FW-1: (a) k versus time; (b) k versus pore volumes of flow..... 101

Figure 2.13. Hydraulic conductivity test results for specimen FW-1: (a) $Q_{\text{out}}/Q_{\text{in}}$ versus time; (b) $Q_{\text{out}}/Q_{\text{in}}$ versus pore volumes of flow..... 102

Figure 2.14. Hydraulic conductivity test results for specimen FW-2: (a) k versus time; (b) k versus pore volumes of flow..... 103

Figure 2.15. Hydraulic conductivity test results for specimen FW-2: (a) $Q_{\text{out}}/Q_{\text{in}}$ versus time; (b) $Q_{\text{out}}/Q_{\text{in}}$ versus pore volumes of flow..... 104

Figure 2.16. Measured electrical conductivity values of the top and bottom boundary circulation outflow liquids: (a) specimen RW-1; (b) specimen RW-2. 105

Figure 2.17. Predicted Cl^- concentrations of top and bottom boundary circulation outflow liquids, calculated based on measured EC values: (a) specimen RW-1; (b) specimen RW-2. ... 106

Figure 2.18. Comparison of $\Delta\pi$ calculated based on initial (source) concentrations using the van't Hoff expression ($\Delta\pi_{C,o}$) and the activity method ($\Delta\pi_{aw,o}$) for specimen RW-1: (a) semi-log relationship; (b) log-log relationship. 107

Figure 2.19. Comparison of $\Delta\pi$ calculated based on average concentrations using the van't Hoff expression ($\Delta\pi_{C,o}$) and the activity method ($\Delta\pi_{aw,o}$) for specimen RW-1: (a) semi-log relationship; (b) log-log relationship. 108

Figure 2.20. Comparison of $\Delta\pi$ calculated based on initial (source) concentrations using the van't Hoff expression ($\Delta\pi_{C,o}$) and the activity method ($\Delta\pi_{aw,o}$) for specimen RW-2: (a) semi-log relationship; (b) log-log relationship. 109

Figure 2.21. Comparison of $\Delta\pi$ calculated based on average concentrations using the van't Hoff expression ($\Delta\pi_{C,o}$) and the activity method ($\Delta\pi_{aw,o}$) for specimen RW-2: (a) semi-log relationship; (b) log-log relationship. 110

Figure 2.22. 1:1 plot of $\Delta\pi$ calculated using the van't Hoff expression ($\Delta\pi_C$) vs. $\Delta\pi$ calculated using the activity method ($\Delta\pi_{aw}$) for specimens RW-1 and RW-2: (a) based on initial (source) solute concentrations; (b) based on average solute concentrations. 111

Figure 2.23. Ratio of $\Delta\pi$ calculated using the activity method ($\Delta\pi_{aw}$) to $\Delta\pi$ calculated using the van't Hoff expression ($\Delta\pi_C$) for specimens RW-1 and RW-2: (a) based on initial (source) solute concentrations; (b) based on average solute concentrations. 112

Figure 2.24. Percent error of $\Delta\pi$ calculated using the van't Hoff expression ($\Delta\pi_C$) relative to $\Delta\pi$ calculated using the activity method ($\Delta\pi_{aw}$) for specimens RW-1 and RW-2: (a) based on initial (source) solute concentrations; (b) based on average solute concentrations. 113

Figure 2.25. Boundary water pressures measured via in-line gage transducers: (a) specimen RW-1; (b) specimen RW-2. 114

Figure 2.26. Chemico-osmotic pressure differences across the specimen measured via a differential pressure transducer: (a) specimen RW-1; (b) specimen RW-2..... 115

Figure 2.27. Values of the steady-state chemico-osmotic pressure difference for each two-day circulation cycle, $-\Delta P_c$: (a) specimen RW-1, determined as the geometric mean of the $-\Delta P$ values from the second day of the given cycle; (b) specimen RW-2, determined as the final (maximum) $-\Delta P$ value from the second day of the given cycle..... 116

Figure 2.28. Steady-state chemico-osmotic pressures, $-\Delta P_{ss}$, for each stage of membrane testing for specimens RW-1 and RW-2, measured using a differential pressure transducer. 117

Figure 2.29. 1:1 plot of ω calculated using the van't Hoff expression (ω_C) vs. ω calculated using the activity method (ω_{aw}) for specimens RW-1 and RW-2 based on initial (source) solute concentrations: (a) for all stages of testing (Meier 2016 and this study); (b) for stages of testing conducted during this study..... 118

Figure 2.30. 1:1 plot of ω calculated using the van't Hoff expression (ω_C) vs. ω calculated using the activity method (ω_{aw}) for specimens RW-1 and RW-2 based on average solute concentrations: (a) for all stages of testing (Meier 2016 and this study); (b) for stages of testing conducted during this study..... 119

Figure 2.31. Ratio of ω calculated using the activity method (ω_{aw}) to ω calculated using the van't Hoff expression (ω_C) for specimens RW-1 and RW-2: (a) based on initial (source) solute concentrations; (b) based on average solute concentrations. 120

Figure 2.32. Percent error of ω calculated using the van't Hoff expression (ω_C) relative to ω calculated using the activity method (ω_{aw}) to for specimens RW-1 and RW-2: (a) based on initial (source) solute concentrations; (b) based on average solute concentrations. ... 121

Figure 2.33. Membrane efficiency coefficients calculated for specimens RW-1 and RW-2; (a) based on initial (source) solute concentrations; (b) based on average solute concentrations. 122

Figure 2.34. Comparison of membrane efficiency coefficients calculated for specimens RW-1 and RW-2 based on initial (source) solute concentrations (ω_o) and average solute concentrations (ω_{ave}): (a) difference ($\Delta\omega$) between ω_{RW-1} and ω_{RW-2} ; (b) percent error of ω_{RW-2} relative to ω_{RW-1} ; (c) reduced range of percent error of ω_{RW-2} relative to ω_{RW-1} . . 123

Figure 2.35. Membrane efficiency coefficients calculated based on initial (source) solute concentrations (ω_o) and average solute concentrations (ω_{ave}): (a) specimen RW-1; (b) specimen RW-2..... 124

Figure 2.36. Comparison of membrane efficiency coefficients calculated based on initial (source) solute concentrations (ω_o) and average solute concentrations (ω_{ave}) for specimens RW-1 and RW-2: (a) difference ($\Delta\omega$) between ω_o and ω_{ave} ; (b) percent error of ω_o relative to ω_{ave} 125

Figure 2.37. Membrane efficiency coefficients calculated for specimen RW-1 based on initial (source) solute concentrations (ω_o) and average solute concentrations (ω_{ave}); plotted on a log-log scale..... 126

Figure 2.38. Cumulative mass data for chloride (Cl^-) diffusion through specimen RW-1 for stages of testing conducted in this study: (a) plotted on a linear scale; (b) plotted on a semi-log scale..... 127

Figure 2.39. Net cumulative mass data for chloride (Cl^-) diffusion through specimen RW-1 with steady-state linear regressions: (a) $C_{ot} = 160$ mM KCl; (b) 320 mM KCl; (c) 640 mM KCl; (d) 1.63 M NaCl; (e) 3.27 M NaCl..... 128

Figure 2.40. Net cumulative mass data for chloride (Cl^-) diffusion through specimen RW-2 with steady-state linear regressions: (a) $C_{ot} = 160$ mM KCl; (b) 320 mM KCl; (c) 640 mM KCl; (d) 1.63 M NaCl; (e) 3.27 M NaCl..... 129

Figure 2.41. Slopes of the net cumulative mass plots, $\Delta Q_t'/\Delta t'$, as a function of the difference in the source ($\Delta C_{o,\text{Cl}^-}$) and average ($\Delta C_{\text{ave},\text{Cl}^-}$) solute concentrations: (a) specimen RW-1; (b) specimen RW-2..... 130

Figure 2.42. Comparison of the slopes of the net cumulative mass plots, $\Delta Q_t'/\Delta t'$, as a function of the concentration difference across specimens RW-1 and RW-2: (a) based on the initial (source) solute concentration difference ($\Delta C_{o,\text{Cl}^-}$); (b) based on the average solute concentration difference ($\Delta C_{\text{ave},\text{Cl}^-}$)..... 131

Figure 2.43. Effective diffusion coefficients for Cl^- as a function of initial (source) solute concentrations (D_o^*) and average solute concentrations (D_{ave}^*): (a) specimen RW-1; (b) specimen RW-2..... 132

Figure 2.44. Comparison of effective diffusion coefficients for Cl^- for specimens RW-1 and RW-2: (a) as a function of initial (source) solute concentrations (D_o^*); (b) as a function of average solute concentrations (D_{ave}^*)..... 133

Figure 2.45. Effective diffusion coefficients for Cl^- as a function of the steady-state membrane efficiency coefficients for specimen RW-1, based on initial (source) solute concentrations (D_o^* , ω_o) and average solute concentrations (D_{ave}^* , ω_{ave}): (a) with extrapolated D_p values determined by Meier (2016) and measured D_p values from this study; (b) values plotted on a log-log scale. 134

Figure 2.46. Effective diffusion coefficients for Cl^- as a function of the steady-state membrane efficiency coefficients based on initial (source) solute concentrations (D_{o}^* , ω_o) and average solute concentrations (D_{ave}^* , ω_{ave}): (a) specimen RW-1; (b) specimen RW-2. . 135

Figure 2.47. Comparison of effective diffusion coefficients for Cl^- as a function of steady-state membrane efficiency coefficients for specimens RW-1 and RW-2: (a) based on initial (source) solute concentrations (D_{o}^* , ω_o); (b) based on average solute concentrations (D_{ave}^* , ω_{ave})..... 136

Figure 2.48. Restrictive tortuosity factors for specimen RW-1, based on the measured effective diffusion coefficient, D^* , for Cl^- , as a function of the steady-state membrane efficiency coefficient, ω : (a) including results from Meier (2016) for comparison; (b) reduced range including the results from this study..... 137

Figure 2.49. Restrictive tortuosity factors for specimen RW-2, based on the measured effective diffusion coefficient, D^* , as a function of the steady-state membrane efficiency coefficient, ω : (a) shown on a 1:1 plot (as typically shown); (b) shown over a reduced range..... 138

Figure 2.50. Comparison of restrictive tortuosity factors, based on the measured effective diffusion coefficient, D^* , as a function of the steady-state membrane efficiency coefficient, ω : (a) based on initial (source) solute concentrations; (b) based on average solute concentrations across the specimen boundaries. 139

Figure 2.51. Comparison of restrictive tortuosity factors over a reduced range, based on the measured effective diffusion coefficient, D^* , as a function of the steady-state membrane efficiency coefficient, ω : (a) based on initial (source) solute concentrations; (b) based on average solute concentrations across the specimen boundaries..... 140

Figure 2.52. Comparison of D^* for specimens RW-1 and RW-2 with D^* for a GCL specimen tested by Shackelford et al. (2016), where D^* for the two lowest ω values for specimens RW-1 and RW-2 are estimates of the D^* that would result in the absence of the switch from KCl to NaCl for those two stages; (a) based on initial (source) solute concentrations; (b) based on average solute concentrations across the specimen boundaries. 141

Figure 2.53. Comparison of steady-state membrane efficiency coefficients, ω : (a) based on initial (source) solute concentrations; (b) based on average solute concentrations across the specimen boundaries. 142

CHAPTER 1. INTRODUCTION

1.1 Background

1.1.1 Engineered Bentonite-Based Containment Barriers

Engineered clay barriers are used in a broad assortment of hydraulic and chemical containment applications to prevent the release of potentially harmful contaminants into the environment. Specific applications often include liners, such as compacted clay liners (CCLs), compacted sand-bentonite (SB) liners, and geosynthetic clay liners (GCLs), as well as covers for municipal solid waste and hazardous waste landfills; vertical cutoff walls, such as soil-bentonite backfills (SBBs); and surface impoundments (e.g., aeration ponds, water retention ponds, mine tailings storage facilities, etc.). Generally, the engineered barrier is required to maintain a hydraulic conductivity, k , less than 10^{-9} m/s. Because advective (hydraulic) transport is low, diffusion often is the dominant mechanism of contaminant transport through engineered clay barriers used in chemical containment applications (Shackelford 2013, 2014)

To achieve an engineered barrier with a sufficient capacity for containment, commercially available bentonite commonly is used either as an additive component (e.g., SB liners, GCLs, amended CCLs, and SBBs) or as the sole component of the barrier (e.g., highly compacted bentonite buffers used to contain high-level radioactive waste). The most commonly used type of bentonite in waste containment applications is sodium bentonite (Na-bentonite), in which Na^+ is the dominant exchangeable cation on the bentonite exchange complex (Malusis and Shackelford 2002a; Shackelford et al. 2003). Na-bentonite typically is more desirable as a barrier than bentonites containing a different dominant exchangeable cation (e.g., calcium bentonite) because of the tendency of Na-bentonite to exhibit greater swell, resulting in a lower k , lower

rates of diffusion, and greater potential for semipermeable membrane behavior such that both advective and diffusive transport of contaminants may be further restricted (Kemper and Rollins 1966; Barbour and Fredlund 1989; Shackelford et al. 2000; Malusis and Shackelford 2002a; Bohnhoff and Shackelford 2013).

1.1.1.1 Compacted Sand-Bentonite Mixtures

Compacted mixtures of sand and Na-bentonite can be an effective alternative to CCLs (which consist only of natural clay) as an engineered barrier if the use of natural clay is not logistically or economically feasible. The inclusion of sand results in improved strength, such that the potential for instability and creep is reduced, as well as reduced porosity, n , and increased dry density, ρ_b , due to the presence of the relatively large sand granules that can occupy much of the total volume of the mixture (Dixon et al. 1985). In this regard, consideration of both the amount and distribution of bentonite within the sand pores is critical to a mixture functioning as an effective containment barrier.

According to Kenney et al. (1992), a bentonite content (BC) of between 11 % and 17 % by dry weight of the total mixture is necessary to ensure a suitable distribution of bentonite throughout the sand matrix while simultaneously achieving an adequately low k ($< 10^{-9}$ m/s). Increased BC from 5 % to 15 % has been shown to result in a reduction in k by 1 to 1.5 orders of magnitude, based on permeation with tap water (e.g., Tong 2015). Additionally, Stern and Shackelford (1998) showed that compacted SB mixtures with a BC of 20 % maintained a lower k than did mixtures with BC of 10 % and 15 % when permeated with 500 mM CaCl₂. However, Gillham et al. (1984) concluded that increasing the BC higher than 10 % may not result in additional reduction of the diffusive mass flux through a SB mixture. This conclusion was based

on an observed decrease in ρ_b with increasing BC, as well as an associated increase in the effective diffusion coefficient, D^* .

1.1.2 Semipermeable Membrane Behavior

Membrane behavior in clays is characterized by selective restriction of dissolved solutes from the clay pores resulting from interaction of the electrostatic diffuse double layers (DDLs) surrounding each individual clay particle (Shackelford 2013). The degree to which a clay material exhibits membrane behavior is referred to as the chemico-osmotic or membrane efficiency, and is quantified in terms of the chemico-osmotic or membrane efficiency coefficient, ω . Values of ω range from zero to unity ($0 \leq \omega \leq 1$), with a value of zero indicating no membrane behavior and a value of unity indicating ideal membrane behavior (i.e., complete solute restriction). Because of the heterogeneous nature of clays, considerable variability generally exists in the pore sizes such that some pores may exhibit restrictive properties while others do not, resulting in nonideal membrane behavior and typical values of ω less than unity.

As a result of isomorphous substitution during formation, clay particles develop a net negative charge. When saturated, this net negative charge results in an associated electric field extending into the pore space between adjacent clay particles such that migrating anions can, to some extent, be repelled from the pore space, whereas transport of the neutral solvent (water) remains unaffected (Fritz 1986; Mitchell and Soga 2005). Dissolved cations in the pores are simultaneously influenced by the attractive forces of the negatively charged clay surfaces and the tendency to diffuse towards the (relatively lower concentration) bulk pore fluid, resulting in an immobile "diffuse" layer of cations and adsorbed water molecules known as the DDL, the thickness of which determines the extent of negative potential into the pore space (Mitchell and

Soga 2005). As the thickness of the DDL increases, a greater amount of the pore water becomes immobile such that the cross-sectional area of the pore that is available for flow is decreased, resulting in a reduced rate of advective transport of solutes with the bulk pore water (Shackelford 2013). Additionally, when the DDLs of adjacent clay particles overlap, the negative potential fills the void space such that anions are repelled and cannot enter the pore; assuming this behavior is characteristic of many pores throughout the clay, the overall rate of solute diffusion through the material thus can be reduced (Malusis et al. 2003; Shackelford 2013; Shackelford et al. 2016).

Because the degree of solute restriction within the pore space depends on the proximity of adjacent DDLs, the size of the pores is an important factor in whether a clay material will exhibit membrane behavior. Certain clay minerals, such as kaolinite, contain pores that are sufficiently large to be uncondusive to DDL interaction, such that membrane behavior typically is not observed for these minerals. However, bentonite consists of montmorillonite minerals with relatively small particle sizes and high surface areas, and thus has a greater potential for membrane behavior (Fritz 1986; Shackelford et al. 2003). Membrane behavior has been observed in highly active clays, such as Na-bentonite, by numerous researchers (Kemper and Massland 1964; Kemper and Rollins 1966; Fritz 1986; Barbour and Fredlund 1989; Keijzer et al. 1999; Malusis and Shackelford 2002a,c; Malusis et al. 2001; Shackelford and Lee 2003; Shackelford et al. 2003; Yeo et al. 2005; Henning et al. 2006; Dominijanni and Manassero 2008; Kang and Shackelford 2009, 2010, 2011; Mazzieri et al. 2010; Shackelford 2011; Bohnhoff 2012; Bohnhoff and Shackelford 2013; Dominijanni et al. 2013; Shackelford 2013; Meier et al. 2014; Tang et al 2014a,b, 2015; Sample-Lord 2015; Bohnhoff et al. 2016; Malusis and Daniyarov 2016; Meier 2016; Shackelford et al. 2016).

In addition to reducing rates of advection and diffusion, membrane behavior in clays also results in chemico-osmosis, wherein liquid flows from a region of relatively lower concentration (higher water activity) to a region of relatively higher concentration (lower water activity). In the case of an engineered bentonite-based barrier, chemico-osmotic flow from the dilute (or uncontaminated) side to the contaminated side of the barrier reduces the outward mass flux of chemical species such that the containment function of the barrier can be further enhanced (Shackelford 2013).

1.1.2.1 Limiting Membrane Behavior

The ability of clay specimens to exhibit membrane behavior has been shown to decrease with an increase in the average solute concentration imposed across the specimen, C_{ave} (Kemper and Rollins 1966; Barbour and Fredlund 1989; Malusis and Shackelford 2002a; Kang and Shackelford 2009, 2010, 2011; Shackelford et al. 2016). Higher concentrations in the pore water, as well the presence of ions with higher valence (e.g., Ca^{2+} vs. Na^+), result in a greater charge density near the negatively charged clay particle surfaces and an associated reduction in the thickness of the DDLs. Thus, the introduction of solutions consisting either of relatively high solute concentrations or of dissolved ions with a higher valence (relative to the ions to which the clay previously had been exposed) will result in progressively larger pores such that the degree of solute restriction is reduced (Fritz 1986).

The trend in ω versus $\log(C_{ave})$ typically is approximately semi-log linear, though with nonlinear trends near the limiting values of C_{ave} (i.e., the upper and lower bounds of C_{ave} corresponding to $\omega = 0$ and $\omega = 1$, respectively) (Kemper and Rollins 1966; Shackelford et al. 2003; Dominijanni et al. 2013; Meier et al. 2014). The upper limit for C_{ave} , or the threshold

concentration, marks the limit of measurable membrane behavior for a given clay specimen above which all solute exclusion capabilities are lost. Because few studies have provided a quantifiable evaluation of limiting membrane behavior, threshold concentrations have been estimated based on extrapolation of the semi-log linear portion of the ω versus $\log(C_{ave})$ relationship (e.g., Malusis et al. 2003; Shackelford et al. 2003). However, threshold concentrations determined based on this method typically underestimate the actual threshold concentration because, as previously discussed, the trend in ω versus $\log(C_{ave})$ becomes nonlinear as C_{ave} approaches the threshold concentration (Shackelford et al. 2003).

For example, Malusis et al. (2003) estimated threshold concentrations as high as 0.142 M NaCl based on extrapolation of data from Kemper and Rollins (1966) and Malusis and Shackelford (2002a) for membrane testing of bentonite and GCL specimens, respectively. Although results for the extrapolated threshold concentrations indicated that membrane behavior may not be relevant for many practical waste containment applications involving more aggressive contaminants, including mixtures of multivalent chemical species with high ionic strengths, threshold concentrations still exceeded the maximum contaminant levels (MCLs) for common inorganic contaminants by approximately three to six orders of magnitude (Malusis et al. 2003). Furthermore, traditional in situ treatment methods (e.g., pump and treat) may remove more than 90 % of contaminant mass from the subsurface, with residual concentrations potentially higher than the required MCLs yet lower than the threshold concentrations for membrane behavior. Thus, since the source contaminant concentration could be up to 20 million times higher than the allowable MCLs while still maintaining ω values greater than the minimum threshold value, membrane behavior was shown to be relevant for a broad range of potential containment applications. Assuming the extrapolated threshold concentrations determined by

Malusis et al. (2003) were underestimated compared to the actual threshold concentrations, membrane behavior may thus be relevant for many containment scenarios, since a relatively high threshold concentration would encompass a broader range of potential applications.

Only two previous studies (e.g., Shackelford and Lee 2003; Meier et al. 2014) have quantified limiting membrane behavior for bentonite-based materials used in containment applications. Shackelford and Lee (2003) evaluated the membrane and diffusion behavior of a GCL specimen separating a 5 mM calcium chloride (CaCl_2) solution from de-ionized water (DIW). Measurable membrane behavior was observed immediately following exposure of the GCL specimen to the CaCl_2 solution; however, continual diffusion of Ca^{2+} into the pores contributed to the eventual destruction of the initially observed membrane behavior, which occurred at approximately the same time that steady-state diffusion of Ca^{2+} was attained. Whereas Shackelford and Lee (2003) used a single salt concentration to evaluate limiting membrane behavior, the testing program implemented by Meier et al. (2014) involved multiple stages of membrane testing in which a GCL was exposed to increasingly higher potassium chloride (KCl) concentrations until measurable membrane behavior no longer was observed. The GCL specimen exhibited membrane behavior for KCl concentrations up to 400 mM, which was much higher than the salt concentrations used in previous studies. Furthermore, the reported trend in ω versus $\log(C_{ave})$ was nonlinear, thus confirming the hypotheses of previous studies which had proposed such a trend based only on theory and limited experimental data. In addition to the two aforementioned studies, Shackelford et al. (2016) evaluated the diffusion behavior of the same GCL specimen tested by Meier et al. (2014) based on the data collected during membrane testing. That study found that the limiting value of the effective diffusion coefficient, D^* , for Cl^- measured at $\omega = 0$ was higher than the estimated D^* determined based on

extrapolation of the trend in D^* versus ω , indicating that use of the extrapolation method may result in an unconservatively low D^* .

1.2 Research Motivation and Objectives

The existence and magnitude of semipermeable membrane behavior has been evaluated for typical engineered bentonite-based barriers commonly used in hydraulic and chemical containment applications, including compacted sand-bentonite (SB) mixtures. However, the extent to which membrane behavior may persist for bentonite-based materials in the presence of highly concentrated, monovalent salt solutions remains largely unknown, with only one previous study known to have quantified the limiting membrane and diffusion behavior of a bentonite-based barrier material. Additionally, the limiting membrane and diffusion behavior of compacted SB mixtures has not yet been evaluated. Accordingly, the objectives of this research were to:

- (a) quantify the limiting membrane behavior of a compacted SB mixture suitable for use as a hydraulic and chemical containment barrier by exposing test specimens to increasingly higher concentrations of monovalent salt solutions until membrane behavior ceased to be measurable; and
- (b) simultaneously, evaluate potential changes, if any, in the ability of the same SB mixture to restrict salt diffusion resulting from the progressive destruction of membrane behavior within the test specimens.

REFERENCES

- Barbour, S., and Fredlund, D., 1989. "Mechanisms of Osmotic Flow and Volume Change in Clay Soils." *Canadian Geotechnical Journal*, 26(4), 551-562.
- Bohnhoff, G., 2012. "Membrane Behavior, Diffusion, and Compatibility of a Polymerized Bentonite for Containment Barrier Applications." PhD Dissertation, Colorado State University, Fort Collins, CO.
- Bohnhoff, G.L., and Shackelford, C.D., 2013. "Improving Membrane Performance via Bentonite Polymer Nanocomposite." *Applied Clay Science*, 86, 83-98.
- Dominijanni, A. and Manassero, M., 2008. "Influence of Membrane Behavior on Contaminant Transport Through Geosynthetic Clay Liners." *Characterization, Monitoring, and Modeling of GeoSystems*, Alshawabkeh, A.N. Reddy, K.R., and Khire, M.V. Eds., GeoCongress 2008, ASCE, Reston, Virginia, USA, 814-821.
- Dominijanni, A., Manassero, M, and Puma, S., 2013. "Coupled Chemical-Hydraulic-Mechanical Behavior of Bentonites." *Gèotechnique*, 63(3), 191-205.
- Dixon, D.A., Gray, M.N., and Thomas, A.W., 1985. "A Study of the Compaction Properties of Potential Clay-Sand Buffer Mixtures for Use in Nuclear Fuel Waste Disposal." *Eng. Geol.*, 21, 247-255.
- Fritz, S., 1986. "Ideality of Clay Membranes in Osmotic Processes: A Review." *Clays and Clay Minerals*, 34(2), 214-223.
- Gillham, R.W., Robin, M.J.L., and Dytynyshyn, D.J., 1984. "Diffusion of Nonreactive and Reactive Solutes through Fine-Grained Barrier Materials." *Canadian Geotechnical Journal*, 21, 541-550.

- Henning, J., Evans, J., and Shackelford, C. (2006). "Membrane Behavior of Two Backfills from Field-Constructed Soil-Bentonite Cutoff Walls." *Journal of Geotechnical and Geoenvironmental Engineering*, 132(10), 1243–1249.
- Kang, J., and Shackelford, D., 2009. "Clay Membrane Testing Using a Flexible-Wall Cell under Closed-System Boundary Conditions." *Applied Clay Science*, 44(1-2), 43-58.
- Kang, J. and Shackelford, C., 2010. "Membrane Behavior of Compacted Clay Liners." *Journal of Geotechnical and Geoenvironmental Engineering*, 136(10), 1368-1382.
- Kang, J. and Shackelford, C., 2011. "Consolidation Enhanced Membrane Behavior of a Geosynthetic Clay Liner." *Geotextiles and Geomembranes*, 29, 544-556.
- Keijzer, T., Kleingeld, P., and Loch, J., 1999. "Chemical Osmosis in Compacted Clayey Material and the Prediction of Water Transport." *Engineering Geology*, 53(2), 151-159.
- Kemper, W., and Maasland, D., 1964. "Reduction in Salt Content of Solution Passing through Thin Films Adjacent to Charged Surfaces." *Proceedings of the Soil Science Society of America*, 28(3), 318-323.
- Kemper, W. and Rollins, J., 1966. "Osmotic Efficiency Coefficients across Compacted Clays." *Proceedings of the Soil Science Society of America*, 30(5), 529-534.
- Kenney, T.C., van Veen, W.A., Swallow, M.A., and Sungaila, M.A. 1992. "Hydraulic Conductivity of Compacted Bentonite-Sand Mixtures." *Canadian Geotechnical Journal*, 29(3), 364-374.
- Lo, I., Luk, A., and Yang, X. 2004. "Migration of Heavy Metals in Saturated Sand and Bentonite/Soil Admixture." *Journal of Environmental Engineering*, 130(8), 906–909.
- Malusis, M., and Shackelford, C., 2002a. "Chemico-Osmotic Efficiency of a Geosynthetic Clay Liner." *Journal of Geotechnical and Geoenvironmental Engineering*, 128(2), 97-106.

- Malusis, M., and Shackelford, C., 2002c. "Coupling Effects during Steady-State Solute Diffusion through a Semipermeable Clay Membrane." *Environmental Science and Technology*, 36(6), 3212-1319.
- Malusis, M., Shackelford, C., and Olsen, H., 2003. "Flow and Transport through Clay Membrane Barriers." *Geoenvironmental Engineering, Geoenvironmental Impact Management*, R. Yong and H. Thomas, Eds., *Thomas Telford Publ.*, London, UK, 334-341.
- Mazzieri, F., Di Emidio, G., and Van Impe, P., 2010. "Diffusion of Calcium Chloride in a Modified Bentonite: Impact on Osmotic Efficiency and Hydraulic Conductivity." *Clays and Clay Minerals*; 58(3), 351-363.
- Meier, A., Sample-Lord, K., Castelbaum, D., Kallase, S., Moran, B., Ray, T., and Shackelford, C., 2014. "Persistence of Semipermeable Membrane Behavior for a Geosynthetic Clay Liner." *Proceedings, 7th International Conference on Environmental Geotechnics*, A. Bouazza, S. Yuen, and B. Brown, Eds., Nov. 10-14, 2014, Melbourne, Australia (ISBN 978-1-922107-23-7), 496-503.
- Mitchell, J.K., Soga, K., 2005. *Fundamentals of Soil Behavior*, 3rd Ed., Wiley, New York.
- Shackelford, C., 2011. "Membrane Behavior in Geosynthetic Clay Liners." *Geo-Frontiers 2011: Advances in Geotechnical Engineering*, J. Han and D. Alzamora, Eds., Geotechnical Special Publication 211, ASCE, Reston, VA, 1961-1970.
- Shackelford, C., 2013. "Membrane Behavior in Engineered Bentonite-Based Containment Barriers: State of the Art." *Proceedings of Coupled Phenomena in Environmental Geotechnics (CPEG)*, M. Manassero, A. Dominijanni, S. Foti, and G. Musso, eds., July 1-3, Torino, Italy, CRC Press/Balkema, Taylor & Francis Group, London, 45-60.

- Shackelford, C., and Lee, J., 2003. "The Destructive Role of Diffusion on Clay Membrane Behavior." *Clays and Clay Minerals*, 51(2), 187-197.
- Shackelford, C., Malusis, M., and Olsen, H., 2003. "Clay Membrane Behavior for Geoenvironmental Containment." *Soil and Rock America Conference 2003*, P. J. Culligan, H. H. Einstein, and A. J. Whittle, Eds., Verlag Glückauf GMBH, Essen, Germany, Vol. 1, 767-774.
- Shackelford, C., Meier, A., Sample-Lord, K., 2016. "Limiting Membrane and Diffusion Behavior of a Geosynthetic Clay Liner," *Geotextiles and Geomembranes*, 44(5), 707-718.
- Stern, R.T. and Shackelford, C.D. 1998. "Permeation of Sand-Processed Clay Mixtures with Calcium Chloride Solutions." *Journal of Geotechnical and Geoenvironmental Engineering*, 124(3), 231-241.
- Tang, Q., Katsumi, T., Inui, T., Li, Z., 2014a. "Membrane Behavior of Bentonite-Amended Compacted Clay." *Soils and Foundations*, Japanese Geotechnical Society, 54(3), 329-344.
- Tang, Q., Katsumi, T., Inui, T., Takai, A., Li, Z., 2014b. "Influence of Compaction Degree on Membrane Behavior of Compacted Clay Amended with Bentonite." *Geo-Congress 2014*, February 23-26, 2014, Atlanta, Georgia, GSP 234, ASCE.
- Tong, S., 2015. "Standardized Hydraulic Conductivity Testing of Compacted Sand-Bentonite Mixtures." MS Thesis, Colorado State University, Fort Collins, CO.
- Yeo, S., Shackelford, C., and Evans, J., 2005. "Membrane Behavior of Model Soil-Bentonite Backfills." *Journal of Geotechnical and Geoenvironmental Engineering*, 131(4), 418-429.

CHAPTER 2. LIMITING MEMBRANE AND DIFFUSION BEHAVIOR OF COMPACTED SAND-BENTONITE SPECIMENS

2.1 Introduction

The existence of semipermeable membrane behavior in highly active clays, such as sodium bentonite (Na-bentonite), is well documented (Kemper and Massland 1964; Kemper and Rollins 1966; Fritz 1986; Barbour and Fredlund 1989; Keijzer et al. 1999; Malusis and Shackelford 2002a,b; Malusis et al. 2001; Shackelford and Lee 2003; Shackelford et al. 2003; Yeo et al. 2005; Henning et al. 2006; Dominijanni and Manassero 2008; Kang and Shackelford 2009, 2010, 2011; Mazziari et al. 2010; Shackelford 2011; Bohnhoff 2012; Bohnhoff and Shackelford 2013; Dominijanni et al. 2013; Shackelford 2013; Meier et al. 2014; Tang et al 2014a,b, 2015; Sample-Lord 2015; Bohnhoff et al. 2016; Malusis and Daniyarov 2016; Meier 2016; Shackelford et al. 2016). Since semipermeable membrane behavior results from the restriction in the migration of chemical species or solutes (e.g., contaminants), the existence of membrane behavior may be an important consideration in the design of engineered bentonite-based barriers due to the potential for improved containment function. However, the extent to which bentonite-based materials exhibit membrane behavior in the presence of more realistic chemical solutions, such as those comprising relatively high concentrations of chemical species, must be quantified before the relevance of membrane behavior for many practical containment applications can be fully understood.

The first systematic evaluation of membrane behavior for a compacted sand-bentonite (SB) mixture suitable for use as an engineered barrier in hydraulic and chemical containment applications was conducted by Meier (2016). In that study, duplicate test specimens of a

compacted SB mixture comprising 15 % Na-bentonite by dry weight were exposed to potassium chloride (KCl) solutions with source concentrations, C_{ot} , ranging from 5 mM to 80 mM. Reported values of the membrane efficiency coefficient, ω , for the two specimens were in good agreement, with values ranging from 0.395 ± 0.053 to 0.063 ± 0.012 for C_{ot} of 5 mM KCl and 80 mM KCl, respectively. The observed decrease in ω with increasing C_{ot} was consistent with previously reported trends, and was attributed to the progressive reduction in the thickness of the electrostatic diffuse double layers (DDLs) surrounding individual clay particles. Diffusion of Cl^- and K^+ through the specimens also was evaluated simultaneously during membrane testing, and the results indicated that diffusion of both solutes was restricted as a result of the observed membrane behavior (Meier 2016).

Although the ability of a compacted SB mixture to exhibit measurable membrane behavior was demonstrated by Meier (2016), the full extent to which the SB specimens would act as a membrane remained unknown, in that the upper threshold concentration corresponding to the limits of observable membrane behavior (i.e., corresponding to $\omega = 0$) was not determined. Therefore, the purpose of this study was to extend the results previously reported by Meier (2016) by exposing the same test specimens to increasingly higher salt concentrations beyond 80 mM KCl, until any observed membrane behavior was eliminated. Membrane and diffusion testing continued uninterrupted, with the first testing stage in this study (i.e., $C_{ot} = 160$ mM KCl) commencing immediately following the end of the final testing stage conducted by Meier (2016) (i.e. $C_{ot} = 80$ mM KCl). The result was a comprehensive evaluation of membrane and diffusion behavior for a compacted SB mixture encompassing the full range of monovalent salt concentrations (with the exception of $C_{ot} < 5$ mM KCl) over which membrane behavior may be relevant for containment applications.

2.2 Materials and Methods

2.2.1 Liquids

The liquids used in this study were de-ionized water (DIW), tap water (TW), potassium chloride (KCl) solutions with target concentrations of 160 mM, 320 mM, and 640 mM, and sodium chloride (NaCl) solutions with target concentrations of 1.63 M and 3.27 M. The TW, KCl solutions, and NaCl solutions were used as circulating liquids for membrane testing, whereas the DIW was used as the solvent for preparation of the KCl and NaCl solutions. De-ionized water and TW also were used as solvents for preparation of additional KCl and NaCl solutions for creation of concentration versus electrical conductivity (*EC*) calibration curves.

Simple, monovalent salt solutions generally have been used as circulating liquids when testing for membrane behavior, because of the simpler calculations associated with determining membrane efficiency coefficients, and because of the tendency for solutions containing salts with a monovalent cation, such as potassium (K^+), to result in more measurable membrane behavior than those containing salts with a divalent cation, such as calcium (Ca^{2+}) (Shackelford et al. 2003; Yeo et al. 2005). Specifically, KCl was used to maintain consistency between the initial stages of membrane testing conducted by Meier (2016) and the later stages of testing conducted on the same sand-bentonite specimens during this study, as well as to allow for comparison of results with previous research on membrane behavior of other types of bentonite-based barriers, including GCLs and CCLs (Malusis and Shackelford 2002a,b; Kang and Shackelford 2009; Kang and Shackelford 2010; Shackelford et al. 2016). The use of NaCl solutions for the final two stages of testing resulted from human error in the laboratory, but is not believed to have compromised the overall results of the study. A more detailed discussion of the implications of this error can be found in Section 2.3.4.

The primary focus of the study was on the use of compacted SB mixtures as containment barriers for low-level radioactive waste (LLRW) containment. The use of nonradioactive salt solutions in this study was considered acceptable as an alternative to radioactive solutions based on the study by Tian and Benson (2015), who reported that the hydraulic conductivity of sodium-bentonite based GCLs in LLRW disposal facilities remained relatively unchanged when the GCLs were permeated with nonradioactive synthetic leachates versus synthetic leachates containing radionuclides.

The *EC* of all liquids was measured using an Orion Conductivity Cell (Orion 013005MD), Waltham, MA), and the pH was measured using an Orion Ross Ultra pH/ATC Triode (Orion 8157BNUMD, Waltham, MA). The *EC* at 25 °C for DIW and TW were 6×10^{-5} S/m and 0.0119 S/m, respectively, and pH were 6.8 and 6.9, respectively. The results of chemical analysis of the TW conducted by Meier (2016) are provided in Table 2.1. Biocide (OK-20 Antimicrobial, Dow Chemical Company, Midland, MA) was added at a concentration of 500 ppm to the TW, KCl solutions, and NaCl solutions based on the results of Tong and Shackelford (2016) to inhibit potential biological activity and any associated clogging over the long duration of the membrane testing (e.g. 1-2 years).

Anion concentrations were determined based on measured *EC* and concentration versus *EC* calibration curves constructed using both solutions prepared in the laboratory as well as manufactured stock solutions with known *EC* and concentrations. A detailed description of the creation and use of the calibration curves is presented in Section 2.2.5.1.2.

2.2.2 Soils

The soils used in this study were the same as those used by Meier (2016) and Tong and Shackelford (2016), and included Ottawa silica fine sand (F-60, U.S. Silica, Frederick, MD) and powdered bentonite (Natural Gel, Wyo-Ben Inc., Billings, MT). The fine sand was classified as poorly-graded sand (SP) and the bentonite as high-plasticity clay (CH) per the Unified Soil Classification System (ASTM D2487). The bentonite comprised 98 % fine-grained ($< 75 \mu\text{m}$) particles, 87 % clay-sized particles based on the standard definition of particles $< 5 \mu\text{m}$ (ASTM D422), and 82.8 % clay-sized particles based on a definition of $< 2 \mu\text{m}$. The bentonite was considered a sodium bentonite (Na-bentonite), although a significant amount (40 %) of the exchange sites were occupied by bound calcium (Ca^{2+}) ions. Further details on the mineralogy, physical properties, and chemical properties of the bentonite are presented in Meier (2016) and Tong and Shackelford (2016).

2.2.3 Sand-Bentonite Mixture and Specimen Preparation

The sand-bentonite (SB) specimens used in this study were the same specimens prepared and tested by Meier (2016). These specimens comprised a bentonite content, BC (defined as the dry mass of bentonite per total mass of dry soil) of 15 % primarily on the basis that the sand was a clean sand (no fines), and a BC ranging from 10 to 20 % is common for LLRW containment applications, albeit somewhat high for nonradioactive waste containment (e.g., municipal solid waste). Also, Kang and Shackelford (2010) recommended BC greater than 5 % to achieve sustained membrane behavior across a wide range of salt concentrations. The results of other studies have indicated rapid increases in the hydraulic conductivity (k) of SB liners as BC fell below a value of roughly 8 % (Lundgren 1981; Kenney et al. 1992). Although liners used for the

containment of hazardous or radioactive waste may require BC values as high as 30 % due to the greater risks and long design lives (e.g. 1,000 – 10,000 years) associated with high-consequence containment applications (Akgün et al. 2015; Tong and Shackelford 2016), $BCs \geq 20$ % generally are not considered for most engineering applications since there may not be a significant decrease in k beyond this threshold (Lundgren 1981; Garlanger et al. 1987; O’Sadnick et al. 1995), resulting in a potentially impractical and economically unfeasible design. Finally, Kenney et al. (1992) determined that ideal mixture conditions (i.e. adequate distribution of bentonite throughout the pore space of the sand and $k \leq 10^{-9}$ m/s) were best achieved with a BC in the range $11 \% \leq BC \leq 17$ %.

Specimens were compacted following the standard (Proctor) compaction procedure (ASTM D 698), but using molds with a thickness of 29.1 mm instead of the standard 116.4 mm thickness to more quickly achieve steady-state diffusion compared to a thicker specimen (Meier 2016). Optimum water content, w_{opt} , and maximum dry unit weight, $\gamma_{d,max}$, of the compacted specimens were 12.2 % and 17.4 kN/m³, respectively (Meier 2016; Tong and Shackelford 2016). A more detailed description of the specimen preparation and compaction procedure can be found in Meier (2016).

2.2.4 Hydraulic Conductivity Testing

Following the same methods described in Section 2.2.3, replicated compacted SB specimens also containing 15 % bentonite (by dry weight) were prepared by Meier (2016) to determine k with the same electrolyte solutions used for membrane testing. Specimens with a diameter of 102 mm (4 in) were compacted to a thickness of 29.1 mm (1.15 in), placed in a flexible-wall (FW) permeameter, back-pressured with tap water to achieve a B -value ≥ 0.95 , and

permeated in accordance with ASTM D5084. Further details on the specimen and FW cell preparation are provided by Meier (2016).

Hydraulic conductivity testing was performed using an applied hydraulic gradient ≤ 29.2 (Meier 2016), with head-water, tail-water, and cell-water pressures of 318 kPa (46.2 psi), 310 kPa (45.0 psi), and 345 kPa (50.0 psi), respectively, applied using a panel board (M100000 Standard Panel and M116000 Standard Add-Panel, Trautwein, Houston, TX), such that an average effective stress of 30.4 kPa (4.4 psi) was sustained across the specimen. Initial prehydration of the specimens using biocide-spiked TW was initiated by Meier (2016) in accordance with the constant-head permeation method (Method A) described by ASTM D5084. Upon completion of prehydration, the specimens were permeated with biocide-spiked 80 mM KCl (corresponding to the highest-concentration solution used for membrane testing in that study) to test for chemical compatibility in accordance with ASTM D7100 (Meier 2016).

For this study, the same SB specimens first were permeated with biocide-spiked 640 mM KCl, which initially was believed to be the source concentration at which the specimens would cease to exhibit membrane behavior, using the falling-head, rising-tail method (Method C) described by ASTM D5084. However, because membrane behavior ultimately persisted well beyond a source concentration of 640 mM KCl, an additional stage of *k*-testing was implemented to evaluate the chemical compatibility of the specimens when permeated with the actual salt solution at which membrane behavior was eliminated, i.e., 3.27 M NaCl, which also was spiked with biocide.

Because of the potentially harmful effect of storing high-concentration solutions in the panel board accumulators, 37.8-mm-diameter external accumulators were used for both the head-water and tail-water liquids (see Fig. 2.1). The two external accumulators were connected via

flexible tubing to the panel board and independently pressurized to establish an air-pressure head difference (Δh_p) across the specimen. An elevation head difference, Δh_z , also was established across the specimen resulting from the difference in water levels between the head-water and tail-water accumulators.

For the 640 mM KCl permeation stage, the applied head-water, tail-water, and cell-water pressures (and thus the pressure head difference) were the same as those used for the tap water and 80 mM KCl permeation stage (i.e. $-\Delta h_p = 0.85$ m). Because the difference in head-water and tail-water elevations was as high as approximately 0.22 m (i.e. $-\Delta h_z \leq 0.22$ m), a hydraulic gradient as high as 36.5 was observed, though this value decreased as the water levels changed during permeation. As a result, this stage of k -testing did not adhere to the requirement by ASTM D 5084 for a maximum gradient of 30 for materials with $k < 1 \times 10^{-9}$ m/s. Because the 3.27 M NaCl permeation stage was expected to result in a k greater than 1×10^{-9} m/s, a maximum gradient of 20 was established in accordance with ASTM D 5084 by reducing the head-water and tail-water pressures to 316 kPa (45.9 psi) and 312 kPa (45.3 psi), respectively, while maintaining a cell-pressure of 345 kPa (50.0 psi). Thus, the Δh_p across the specimen was reduced by one-half (i.e. $-\Delta h_p = 0.42$ m) while maintaining an average effective stress of 30.4 kPa (4.4 psi). The difference in head-water and tail-water elevations during this stage of permeation was limited to a maximum of 0.16 m (i.e. $-\Delta h_z \leq 0.16$ m), resulting in a maximum gradient of 19.9. Values for k for both the 640 mM KCl and 3.27 M NaCl permeation stages were calculated based on the following equation (Method C, ASTM D 5084):

$$k = \frac{a \cdot L}{2 \cdot A \cdot \Delta t} \ln \left(\frac{\Delta h_1}{\Delta h_2} \right) \quad (2.1)$$

where a is the cross-sectional area of the external head-water and tail-water accumulators, L is the specimen length (thickness) in the direction of flow, A is the specimen cross-sectional area, Δt is the time interval over which permeation occurs, and Δh_1 and Δh_2 are the average head loss across the specimen at the start and end of the permeation period, respectively.

All stages of k -testing adhered to the termination criteria established by ASTM D 5084 requiring four consecutive data points in which values for k and the ratio of the volumetric outflow rate to the volumetric inflow rate, or Q_{out}/Q_{in} , are steady and exhibit no upward or downward trend, and Q_{out}/Q_{in} remains within a value of 1.00 ± 0.25 . The permeant liquid was changed from a 640 mM KCl solution to a 3.27 M NaCl solution prior to attainment of chemical equilibrium because, as previously stated, the k of primary interest was that resulting from exposure to the maximum salt concentration used during membrane testing. Therefore, the measured k for the 640 mM KCl permeation stage should only be considered an estimate of the true k , since terminating k -tests prior to establishing chemical equilibrium may result in unconservatively low k values (Shackelford et al. 2000).

2.2.5 Membrane Behavior and Diffusion Testing Apparatus and Procedure

The apparatus used in this study was the same as that used by Meier (2016) to evaluate membrane behavior, and comprised a rigid-wall cell and a flow pump with two stainless-steel, dual-acting syringes (actuators) connected to the cell by stainless-steel tubing as shown in Fig. 2.2. Stainless-steel components were used to prevent corrosion and volume change inside the testing apparatus. A schematic of the rigid-wall cell used for membrane testing is presented in Fig. 2.3. Within the cell, the compacted sand-bentonite specimen was confined axially by an acrylic cylinder (inner diameter of 71.0 mm) and secured between a base pedestal and top piston

in such a way as to eliminate any potential change in volume (Meier 2016). To ensure evenly distributed circulation of liquids across the entirety of the specimen boundaries, porous disks (GenPore porous sheet TO-6, General Polymer Corp., Reading, PA) were placed between the specimen and base pedestal and between the specimen and top piston, with filter paper (Whatman™ 42 Grade Ashless Filter Paper, GE Healthcare UK Limited, Buckinghamshire, UK) placed between the disks and the specimen to inhibit clogging of the disks by soil particles (Meier 2016). Circulation liquids displaced by the syringes entered the porous disks via ports through both the base pedestal and top piston, then circulated through the disks before exiting via separate outflow ports leading back to the syringes. One syringe supplied liquid for (and collected liquid from) circulation across the top boundary of the specimen, whereas the other syringe did the same for circulation across the bottom boundary of the specimen.

The flow-pump system was the same as that described by Malusis et al. (2001) and Meier (2016). The two previously-mentioned syringes, powered by the dual-carriage syringe pump (Model 55-1382 or 944, Harvard Apparatus, Holliston, MA), moved liquid through the system at a constant rate of $2.3 \times 10^{-10} \text{ m}^3/\text{s}$, such that the inflow and outflow rates through both the base pedestal and top piston remained constant and equal. Both the top and bottom circulation loops were closed and completely filled with the circulation liquids, and the specimen was saturated and restrained against volume change. Thus, there was no possibility for volume change in the closed system, such that flow through the specimen was prevented during circulation of the liquids across the bottom and top boundaries of the specimen.

The syringes had a limited available capacity (approximately 40 mL) for circulation and collection of liquids, such that testing was performed in recurring 48-h cycles for the purpose of collecting effluent samples and refilling the syringes with fresh circulating liquids for each

subsequent circulation cycle. This circulation cycle was the same as that used by Meier (2016) and by Bohnhoff and Shackelford (2013, 2015). At the end of each 48-h cycle the flow-pump system was turned off and the rigid-wall cell was isolated by closing the valves located at all entry and exit points. The displacement direction of the syringes then was reversed such that the effluent liquid stored in the back chamber of each syringe was expelled from the flow-pump system at a constant rate of $6.4 \times 10^{-7} \text{ m}^3/\text{s}$. The front chambers of the syringes simultaneously were refilled with either fresh tap water or salt solution from two separate reservoirs. Sampling tubes (50 mL) were used for the collection and subsequent measurement of *EC* and pH of the circulation outflows from both the top and bottom boundaries of the specimen. The sampling/refilling process was completed in much less time (i.e. < 5 min) than the 48-h cycle used for circulation across the specimen.

During each circulation cycle, a salt solution (e.g. KCl, NaCl) was circulated across the top boundary of the specimen while tap water was circulated across the bottom boundary, establishing a concentration gradient and resulting in downward diffusion of solutes through the specimen. If the rate of diffusion is less than the rate of replenishment of the source liquids, then circulation outflow concentrations for the top (C_t) and bottom (C_b) boundaries are equal to the source concentrations introduced to the top piston (C_{ot}) and to the base pedestal (C_{ob}) such that $C_t \sim C_{ot}$ and $C_b \sim C_{ob}$ (Malusis and Shackelford 2002a). However, the high source concentrations and associated large concentration gradients used in this study resulted in measurable diffusion of solutes into the top boundary of the specimen and out of the bottom boundary, causing a net decrease in the concentration of the top boundary circulation outflow and a net increase in the concentration of the bottom boundary circulation outflow (i.e. $C_t < C_{ot}$ and $C_b > C_{ob}$).

Multiple-stage membrane testing, consisting of sequential increases in the concentration of the circulating solutions introduced to the top boundary of the specimen, was conducted in this study based on a similar testing program established by Meier (2016) for the purpose of defining the trend in ω with increasing C_{ot} . That study began by circulating 5 mM KCl across the top of the specimen (i.e. $C_{ot} = 5$ mM KCl), with C_{ot} for each subsequent stage doubling that of the previous stage up to a concentration of 80 mM KCl. Because this study was a continuation of the work performed by Meier (2016), the first stage of testing for this study comprised a C_{ot} of 160 mM KCl, which subsequently was doubled to 320 mM KCl and then 640 mM KCl. A C_{ot} of 1.28 M KCl was intended for the ensuing stage. However, NaCl inadvertently was used to prepare the source solution, resulting in a C_{ot} of 1.63 M NaCl. The higher value was the result of using the molar mass of KCl, which is larger than that of NaCl (e.g. 74.55 g mol⁻¹ vs. 58.44 g mol⁻¹), in the calculation of the required mass of solute when in fact NaCl was the salt mixed with the solvent. The final stage of membrane testing in this study included a C_{ot} of 3.27 M NaCl, or double that of the previous stage, based on the same convention as had been implemented prior to the 1.63 M NaCl stage.

2.2.5.1 Chemico-Osmotic Pressures

In addition to the ports used to supply and remove circulating liquids to and from the specimen boundaries, a central port in both the base pedestal and top piston allowed for measurement of boundary liquid pressures via in-line (gage) pressure transducers (PX26 and PX 209 Series, Omega, Stamford, CT). A differential pressure transducer (PX26 Series, Omega, Stamford, CT) also was used to measure the chemico-osmotic pressure difference, ΔP , across the specimen resulting from semipermeable membrane behavior.

Differential pressure across the specimen is generated as a result of the no-flow conditions imposed by the closed system used during testing. Upon addition of solutes to a solution, the total water potential (or activity) of that solution decreases as more water molecules are locked up in hydration shells around the ions (Essington 2004). In the case of a membrane separating two reservoirs, one containing water and the other a concentrated salt solution, the result is a propensity for flow of water from the side of lower concentration (higher potential) to the side of higher concentration (lower potential) until equilibrium (i.e. equal potential across the membrane) is established. In an open system consisting of a reservoir with sufficient capacity to accommodate a rise in the water level, equilibrium is achieved via an increase in pressure head on the concentrated side as water flows through the membrane (Tinoco et al. 1995; Shackelford 2013). However, the closed system and constant circulation rates implemented in this study prevent any flow through the specimen such that equilibrium must be attained in a different manner, viz., the development of a chemico-osmotic pressure on the concentrated side of the membrane to compensate for the lower potential and counteract the tendency for chemico-osmotic flow from the bottom (dilute side) to the top (concentrated side) of the specimen (Malusis et al. 2001; Shackelford 2013). The resulting ΔP across the specimen can be defined as the equilibrium pressure difference required to prevent flow of solvent (water) through the membrane (Katchalsky and Curran 1965).

The pressure difference should remain constant as long as the concentration gradient and, thus, the difference in osmotic potential, across the specimen remains unchanged, as is the case where "perfectly flushing" boundary conditions are maintained by the constant and equal circulation rates across both specimen boundaries. Without constant replenishment of the salt solution by the flow-pump system, diffusion of solutes eventually would result in dissipation of

the pressure difference across the specimen as the concentration gradient and associated tendency for chemico-osmotic flow are eliminated (Malusis et al. 2001).

The theoretical maximum possible chemico-osmotic pressure difference, $\Delta\pi$, resulting from the complete restriction of solute migration associated with ideal membrane behavior (i.e., $\omega = 1$), is defined as follows (Kemper and Rollins 1966; Fritz 1986):

$$\Delta\pi = \pi_1 - \pi_2 = \left(\frac{RT}{V_w}\right) \ln\left(\frac{a_{w,1}}{a_{w,2}}\right) \quad (2.2)$$

where π_1 and π_2 are the theoretical maximum chemico-osmotic pressures of the two solutions separated by the membrane, R is the universal gas constant ($8.314 \text{ L}\cdot\text{kPa}\cdot\text{K}^{-1}\cdot\text{mol}^{-1}$), T is the absolute temperature (298 K for this study), V_w is the mean partial molar volume of water ($0.01802 \text{ L mol}^{-1}$), and $a_{w,1}$ and $a_{w,2}$ are the water activities of the two solutions. For the testing apparatus and conditions used in this study, $a_{w,1}$ represents the water activity of the TW circulated along the bottom boundary of the specimen, whereas $a_{w,2}$ represents the water activity of the salt solution circulated along the top boundary of the specimen. Based on this assumed sign convention, where the pressure difference is taken in the direction of the imposed concentration gradient (i.e., from the top to the bottom of the specimen), the natural log term in Eq. 2.2 will be positive (because $a_1 > a_2$) such that values of $\Delta\pi$ also will be positive.

An approximation of $\Delta\pi$, valid for ideal and dilute solutions, may be determined using the van't Hoff expression (Fritz 1986; Malusis et al. 2001):

$$\Delta\pi = vRT\Delta C \quad (2.3)$$

where ν represents the number of constituent ions of the dissolved salt (e.g., $\nu = 2$ for KCl and NaCl; $\nu = 3$ for CaCl_2) and ΔC is the concentration difference across the membrane.

Although dilute behavior of a solution generally is defined qualitatively, numerical values for the upper threshold concentration at which such behavior no longer is exhibited have been presented in the existing literature, though with widely variable magnitudes. For example, Fritz (1986) calculated values for $\Delta\pi$ using Eq. 2.3 within 5 % of those calculated using Eq. 2.2 for solutions containing 1:1 electrolytes (e.g., KCl, NaCl) with ΔC values as high as 1 M. Alternatively, Tinoco et al. (1995) defined a dilute solution as having a molality less than 0.1 m (equivalent to a concentration of 0.1 M for both the KCl and NaCl solutions used in this study).

Values of the activity of water, a_w , for KCl and NaCl solutions at 25 °C with concentrations (in molality) ranging from 0.1 m to 4.4 m and 0.1 m to 6.0 m, respectively, were obtained from Robinson and Stokes (1959) and plotted versus solute concentration (in molarity) in Figure 2.4. A deviation from ideal behavior ($a_w = 1$) is evident as concentration increases beyond 0.1 M. This also is indicative of a deviation from infinitely dilute conditions, as infinite dilution is characterized by an a_w of unity for the electrolyte solution (Robinson and Stokes 1959).

To determine the applicability of the van't Hoff approximation (Eq. 2.3) for the stages of membrane testing conducted in this study, values of $\Delta\pi$ were calculated using both Eq. 2.2 and Eq. 2.3 designated as $\Delta\pi_{a_w}$ and $\Delta\pi_C$, respectively, for a hypothetical membrane separating tap water ($C \sim 0$ M) from KCl or NaCl solutions with concentrations ranging from 100 mM to 3.5 M (Fig. 2.5). This particular range of concentrations was chosen to encapsulate the range of salt concentrations used during membrane testing. Note that $\Delta\pi_C$ increases linearly whereas $\Delta\pi_{a_w}$ increases nonlinearly for both KCl and NaCl solutions, as $\Delta\pi_C$ is calculated based on the linear

relationship between $\Delta\pi$ and ΔC in Eq. 2.3, whereas the a_w values used in Eq. 2.2 to calculate $\Delta\pi_{a_w}$ are determined based on the second-order polynomial relationship between a_w and solute concentration shown in Fig. 2.4. As a result, the relationships intersect, such that $\Delta\pi_C$ is equal to $\Delta\pi_{a_w}$ at a concentration of 2.34 M for KCl solutions and 1.67 M for NaCl solutions, although distinct differences in $\Delta\pi_C$ and $\Delta\pi_{a_w}$ are evident at both lower and higher concentrations.

The percent error associated with calculating $\Delta\pi$ using Eq. 2.3 as opposed to Eq. 2.2 for the 100 mM to 3.5 M source Cl⁻ concentration range is shown in Fig. 2.6. For concentrations greater than 0.1 M but less than 1 M, differences between $\Delta\pi_{a_w}$ and $\Delta\pi_C$ as high as 10 % for KCl solutions and 8 % for NaCl solutions were identified, indicating a potentially greater error associated with using Eq. 2.3 than was previously suggested by Fritz (1986) for concentrations in this range. The relationships shown in Fig. 2.6, as well as the deviation of a_w from ideal and infinitely dilute conditions (Fig. 2.4), illustrate that the use of the van't Hoff expression for calculating $\Delta\pi$ may not be appropriate for cases where concentrations are greater than 0.1 M. Therefore, calculations of $\Delta\pi$ were performed for this study using the same definition of a dilute solution as that provided by Tinoco et al. (1995) (i.e., $C < 0.1$ M) to obtain values for $\Delta\pi$ with the smallest possible error (i.e., relative to the exact thermodynamic relationship expressed in Eq. 2.2). The specific methods used to obtain $\Delta\pi_{a_w}$ are discussed in greater detail subsequently (see Section 2.2.5.1.3).

As previously discussed, diffusion of solutes through the specimen during membrane testing results in a slight decrease in the concentration (increase in a_w) of the solution circulated across the top of the specimen, as well as a concomitant increase in the concentration (decrease in a_w) of the solution circulated across the bottom of the specimen. Therefore, $\Delta\pi_{a_w}$ may be determined based either on the water activities of the source solutions circulated across the

specimen boundaries, or on the average water activity of the liquid circulated across both boundaries of the specimen (Malusis et al. 2001; Malusis and Shackelford 2002a). Although the former approach may not result in an assessment of true conditions for cases such as this study where diffusion through the specimen does occur, both methods are presented here for comparison. Using initial (source) a_w to calculate $\Delta\pi_{aw}$, Eq. 2.2 can be re-written specifically for the conditions associated with this study as follows:

$$\Delta\pi_{aw,o} = \left(\frac{RT}{V_w} \right) \ln \left(\frac{a_{wb,o}}{a_{wt,o}} \right) \quad (2.4)$$

where $a_{wb,o}$ represents the initial water activity of the TW circulated across the bottom boundary of the specimen, and $a_{wt,o}$ represents the initial water activity of the salt solution circulated across the top boundary. If average boundary water activities are used to calculate $\Delta\pi$, Eq. 2.2 again may be re-written:

$$\Delta\pi_{aw,ave} = \left(\frac{RT}{V_w} \right) \ln \left(\frac{a_{wb,ave}}{a_{wt,ave}} \right) \quad (2.5)$$

where $a_{wb,ave}$ and $a_{wt,ave}$ are defined as:

$$a_{wb,ave} = \frac{a_{wb,o} + a_{wb,f}}{2} \quad (2.6)$$

$$a_{wt,ave} = \frac{a_{wt,o} + a_{wt,f}}{2} \quad (2.7)$$

where $a_{wb,f}$ and $a_{wt,f}$ are the final water activities of the circulation outflow liquids collected from the bottom and top boundaries, respectively. The calculations presented in Eqs. 2.4 – 2.7 are similar to those discussed by Shackelford (2013) and used by Meier (2016) and Meier and Shackelford (2017), where calculations for $\Delta\pi$ instead were based on initial and average solute concentrations (as opposed to activities) using variations of Eq. 2.3.

2.2.5.1.1 Membrane Efficiency Coefficients

Because of the natural variation in pore sizes within clays, engineered barriers constructed with clay materials generally exhibit imperfect membrane behavior (i.e. $\omega < 1$) because some of the pores may be too large to restrict the passage of solutes (Shackelford 2013). In this case, the actual chemico-osmotic pressure difference developed across the specimen, ΔP , represents only a portion of $\Delta\pi$. This actual ΔP can then be measured and used together with the $\Delta\pi$ to calculate the membrane efficiency coefficient, ω , as follows (Katchalsky and Curran 1965; Groenevelt and Elrick 1976; Fritz 1986; Malusis et al. 2001; Shackelford 2013; Meier 2016):

$$\omega = \pm \frac{\Delta P}{\Delta\pi} = \pm \frac{\Delta P_{ss} - \Delta P_{TW}}{\Delta\pi} = \pm \frac{\Delta P_e}{\Delta\pi} \quad (2.8)$$

where ΔP_{ss} is the chemico-osmotic pressure difference measured upon achievement of steady-state conditions at the end of each stage of testing, ΔP_{TW} is the chemico-osmotic pressure difference measured at the end of the initial stage of testing when tap water was circulated across

both specimen boundaries to establish a baseline pressure condition, and ΔP_e is the effective (net) chemico-osmotic pressure difference after accounting for baseline pressure conditions. The assumed sign convention for all measured chemico-osmotic pressure differences in this study is based on the direction of the imposed concentration gradient (i.e., from the top to the bottom of the specimen), such that a negative pressure difference would indicate a higher pressure along the top, or concentrated boundary of the specimen. The condition where ΔP_{ss} is positive would indicate higher pressures along the bottom of the specimen, implying that the specimen no longer acts as a membrane. When Eq. 2.2 is used to calculate $\Delta\pi$, the negative sign in Eq. 2.8 is used so that resulting values of ω are positive as long as the specimen exhibits membrane behavior (i.e., because $\Delta\pi > 0$ and $\Delta P < 0$). However, if Eq. 2.3 instead is used to calculate $\Delta\pi$, then the resulting values for $\Delta\pi$ will be negative (assuming the concentration difference is taken in the direction of the concentration gradient) such that the positive sign in Eq. 2.8 is used.

Because of the brief pause (< 5 min) in liquid circulation at the end of each 48-h circulation cycle required to refill the syringes with fresh circulating liquid and sample the collected circulation outflow, the chemico-osmotic pressure along the top of the specimen rapidly dissipates due to the short loss of "perfectly flushing" boundary conditions (Malusis et al. 2001). However, once circulation is resumed, the pressure difference gradually increases again until reaching a relatively steady value for the specific cycle (i.e., specific ΔC).

In this study, the overall value of ΔP_{ss} for each testing stage was calculated as the average of the ΔP values for the final four circulation cycles for a given ΔC once the pressures maintained a steady state, defined as having a value within $\pm 3\%$ of the average of those same four values and showing no visible upward or downward trend (Meier 2016).

The baseline pressure difference (i.e. ΔP_{TW}) was established by Meier (2016) to account for potential differences in the circulation rates across the top and bottom boundaries resulting from slight variations in the hydraulic properties of the porous disks and/or differences in the machined dimensions of the flow pump components controlling the circulation across each specimen boundary (Malusis et al. 2001; Shackelford 2013). This baseline ΔP ideally should be zero in the case of equal hydraulic resistance in each porous disk, although either a positive or negative value (e.g. $\Delta P_{TW} < 0$ or $\Delta P_{TW} > 0$) can result due to differences in the hydraulic resistances of the disks.

Values of ω can be calculated based on either of the two variations for the maximum chemico-osmotic pressure difference (e.g. $\Delta\pi_o$ or $\Delta\pi_{ave}$) given by Eqs. 2.4 and 2.5 as follows:

$$\omega_o = \pm \frac{\Delta P_e}{\Delta\pi_o} \quad (2.9)$$

$$\omega_{ave} = \pm \frac{\Delta P_e}{\Delta\pi_{ave}} \quad (2.10)$$

Because $a_{w,ot} < a_{w,t,ave}$ and $a_{w,ob} > a_{w,b,ave}$, the magnitude of $\Delta\pi_o$ will be greater than that of $\Delta\pi_{ave}$ such that ω_o will be lower than ω_{ave} as long as ΔP_e remains unchanged. Membrane efficiency coefficients calculated using Eq. 2.9 thus will be more conservative than those calculated using Eq. 2.10 (Malusis et al. 2001; Malusis and Shackelford 2002a).

2.2.5.1.2 Concentration-EC Correlation

The membrane efficiency coefficients determined by Meier (2016) for 5, 10, 20, 40, and 80 mM KCl stages were calculated based on measured KCl concentrations for both the

circulation inflows and outflows across the boundaries of the specimen. Potassium concentrations were measured using inductively coupled plasma-atomic emission spectrometry (ICP-AES), whereas chloride concentrations were measured using ion chromatography (IC). Because the ICP and IC instruments were calibrated for a limited range of concentrations, i.e., 1-60 mg/L and 0.01-3 mg/L, respectively, samples were subjected to dilution factors ranging from 1:1 to 1:1600, with the highest dilution factors used for the IC samples collected during the 80 mM KCl stage. However, several disadvantages associated with using the same procedure for this study were identified as follows.

Samples from the first stage of this study (i.e. $C_{ot} = 160$ mM KCl) required dilution factors up to 1:2500 to fall within the calibrated range of the IC, resulting in measured Cl⁻ concentrations as much as 40 % lower than the target concentration (i.e. approximately 99 mM vs. 160 mM, hypothesized to be the result of dilution errors). As a result, dilution and subsequent IC/ICP analyses were determined to be ineffective methods for accurately determining salt concentrations of samples collected during this study since the error associated with measured Cl⁻ concentrations was anticipated to continue to increase as higher dilution factors became necessary for successive stages with $C_{ot} > 160$ mM.

The additional costs and delays associated with sending samples to an external laboratory for analysis were deemed detrimental to the progress of the testing program. Because concentrations were necessary to determine when each stage of testing had reached steady state, the inability to obtain results in a timely manner could potentially have led to stages lasting well past the point of attainment of a steady-state ΔP and an unnecessary increase in the overall length of the test.

Testing conducted by Meier (2016) consisted of stages in which soluble salts had not yet been washed out of the specimen, since the specimens were not fully flushed prior to the start of membrane testing (Meier 2016). In that study, sufficiently low source KCl concentrations were used such that the presence of Na^+ in the initial pore fluid, as well as other ions (e.g. Ca^{2+} , SO_4^{2-} , Mg^{2+} , Br^-) in the circulation outflow, resulted in additional non-negligible contributions to the overall concentration used to calculate $\Delta\pi$, thus requiring that concentrations be known for all dominant ions present. However, as shown in Meier (2016), the vast majority of the measurable soluble salts had been flushed from the specimens by the end of testing. Furthermore, the salt solutions used in this study were of such high concentration that the presence of residual salts was masked, thus negating the need to distinguish the contribution of each ion using IC/ICP.

Malusis and Shackelford (2002a) and Malusis et al. (2015) proposed an alternative method for determining effective salt concentrations while mitigating problems associated with high dilution factors, and to more rapidly obtain KCl and NaCl concentrations. In this method, concentrations are predicted based on the measured *EC*, which is obtained using full-strength (i.e., not diluted) solution samples. Since the specimens used in testing conducted by Meier (2016) were not fully flushed of soluble salts prior to membrane testing and contained multiple ions contributing to the overall *EC* of the effluent solutions, and the prediction method is based only on the *EC* of either KCl or NaCl, this method likely would not have accurately predicted KCl concentrations during the initial stages of testing (i.e., 5 to 80 mM KCl) reported by Meier (2016). However, as testing progressed during this study, these soluble salts were removed and replaced by the K^+ ions introduced to the system via the top boundary of the specimen during the 160 – 640 mM KCl stages, such that the steady state *EC* of the circulation outflows for the first three stages of this study was due primarily to the contributions of the source K^+ and Cl^- .

Following the change in the source solution from 640 mM KCl to 1.63 M NaCl for the fourth stage of membrane testing, the exchange of K^+ for Na^+ on the bentonite exchange complex, as well as the requirement for electroneutrality within the pore fluid, led to the diffusion of K^+ from the bottom boundary of the specimen and into the circulation outflow. Consequently, both K^+ and the source Na^+ contributed to the overall *EC* of the circulation outflow, though the contribution of Cl^- likely remained unchanged due to the nonadsorbing behavior of the anion. Because of the observed close correlation between the concentration-*EC* relationships for KCl and NaCl (shown subsequently), a negligible difference between the *EC* based on a combination of K^+ and Na^+ and the *EC* based only on Na^+ was expected. Also, the steady-state *EC* for the 1.63 M NaCl stage was expected to be due only to the contributions of Na^+ and Cl^- , since the source NaCl solution was of such high concentration that all K^+ ions had been replaced by Na^+ ions on the exchange complex and removed from the system.

To demonstrate the removal of soluble salts from the specimen with increasing source concentration, results for measured Cl^- concentrations for the 5-80 mM KCl stages from Meier (2016) were compared with KCl concentrations obtained using concentration-*EC* calibration curves (Fig. 2.7) as well as *EC* values corresponding to the measured Cl^- concentrations. Due to the requirement for electroneutrality in solution, and the nonadsorbing behavior of Cl^- , the steady-state KCl concentration was assumed to be the same as the steady-state Cl^- concentration (Shackelford et al. 1999; Malusis and Shackelford 2002a). Thus, only measured Cl^- concentrations from Meier (2016) were used for comparison.

During preparation of solutions used to produce the calibration curves, DIW was used as the solvent for those calibration curves used to predict top boundary circulation outflow concentrations, since the source solutions circulated across the top boundary also were prepared

with DIW. However, TW was used as the solvent for those calibration curves implemented to predict bottom boundary circulation outflow concentrations, since effluent samples comprised only the source TW plus any solutes that had diffused out of the bottom boundary of the specimen during membrane testing. Biocide also was added at 500 ppm to all solutions, matching stock solutions used for membrane efficiency tests.

Predicted Cl^- concentrations for the top boundary circulation outflow were determined using the curve for KCl solutions prepared with DIW (KCl+DIW) shown in fig. 2.7, which was established using standard KCl solutions with known concentrations and *EC* (Fisher Scientific, Waltham, MA). Both the standard solutions and the top boundary source solutions consisted of KCl dissolved in DIW, with biocide added at a concentration of 500 ppm. In general, the predicted and measured Cl^- concentrations for a given effluent sample became increasingly correlated at higher concentrations, with the closest correlation observed during the 80 mM KCl stage (i.e., percent error $\leq 5\%$), as shown in Fig. 2.8. Meier (2016) reported a higher *EC* for the top boundary circulation outflow relative to that of the source solution (i.e. $EC_t > EC_{ot}$) during the 5 mM and 10 mM KCl circulation stages, even though concentrations of the chemical species in the source solution (K^+ , Cl^- , and Br^-) decreased following circulation across the top of the specimen (i.e. $C_t < C_{ot}$), indicating that soluble salts (e.g. Na^+ , Ca^{2+} , and Mg^{2+}) were diffusing from the specimen into the top boundary circulation outflow and increasing the overall *EC* of the effluent. However, as membrane testing progressed and more highly concentrated solutions were introduced to the top boundary of the specimen, this outward diffusion ceased as the soluble salts were removed from the system and inward diffusion by the source chemical species dominated, such that $EC_t < EC_{ot}$ for $C_{ot} > C_t$. Evidence of this observation is shown in Fig. 2.9, in which the error associated with predicted Cl^- concentrations relative to measured Cl^- concentrations

decreased by approximately 10-15 % as the top boundary source concentration increased from 5 to 80 mM KCl. Thus, the approach for determining Cl^- concentrations became more accurate at higher source concentrations as a result of the dominant contribution of Cl^- anions to the overall *EC* of the effluent solution relative to the contributions of other residual ions.

Predicted Cl^- concentrations for the bottom boundary circulation outflow were determined using the curve for KCl solutions prepared with TW (KCl+TW) shown in Fig. 2.77, which was established by preparing KCl solutions with TW at target concentrations ranging from 4 to 160 mM and measuring the associated *EC* values. Because of the very low measured Cl^- concentrations in the bottom boundary TW at the start of the 5 mM KCl circulation stage (~ 0.015 mM), soluble salts diffusing out of the specimen into the TW were the dominant chemical species in the effluent solution (e.g., Na^+ concentration ~ 1 mM) (Meier 2016). Therefore, since the determination of Cl^- concentrations was based only on *EC*, and the initial *EC* of the effluent was based almost entirely on other salts in solution, relatively large differences were observed between predicted and measured values at the lowest Cl^- concentrations (Fig. 2.10). However, the results shown in Fig. 2.10 exhibited a rapid increase in correlation between predicted and measured Cl^- concentrations at higher concentrations, with the percent error based on the predicted concentrations relative to the measured concentrations (Fig. 2.11) decreasing by approximately 850 %, to values as low as 2 %, as the measured Cl^- concentration of the bottom boundary circulation outflow increased from 0.1 to 5 mM and the soluble salts were flushed from the system.

Based on the trends observed in this analysis, the assumption that soluble salts were washed from the system at lower source concentrations (i.e. $C_{ot} = 80$ mM KCl), such that only the constituent ions of the source solutions (K^+ , Na^+ , and Cl^-) contributed to the overall *EC* at

higher concentrations, was validated. Therefore, the alternative method for determining effluent concentrations based on *EC* was considered applicable (given the observed <5 % error) for the concentration stages of testing (i.e. $C_{ot} \geq 160$ mM) conducted in this study.

In addition to the two calibration curves used in the aforementioned analysis, two calibration curves were created for the 1.63 M and 3.27 M NaCl stages to determine NaCl concentrations in the circulation outflow (Fig. 2.7). The two additional curves were established by preparing NaCl solutions using DIW for target salt concentrations ranging from 320 mM to 3.27 M corresponding to the higher concentrations along the top boundary of the specimen, and using TW for target salt concentrations ranging from 6.4 mM to 1.63 M corresponding to the lower concentrations along the bottom boundary of the specimen.

2.2.5.1.3 Activity Method

Previously, values of $\Delta\pi$ used to calculate ω have been obtained using the van't Hoff expression (Eq. 2.3) (Kemper and Rollins 1966; Barbour and Fredlund 1989; Malusis 2001; Malusis et al. 2001; Malusis and Shackelford 2002a,b,c; Malusis et al. 2003; Shackelford and Lee 2003; Yeo et al. 2005; Kang and Shackelford 2009; Kang and Shackelford 2010b; Kang and Shackelford 2011; Bohnhoff 2012; Bohnhoff and Shackelford 2013; Meier et al. 2014; Tang et al 2014; Sample-Lord 2015; Meier 2016; Bohnhoff et al. 2016; Shackelford et al. 2016). However, as previously discussed, the use of this expression to calculate $\Delta\pi$ is dependent on the assumption that the solutions separated by the membrane are both ideal and dilute. Because all salt solutions used in this study were considered neither ideal nor dilute, values of $\Delta\pi$ were calculated based on a more exact thermodynamic relationship (Eq. 2.2) of which the van't Hoff

expression is an approximation. The use of Eq. 2.2, as well as the intermediate steps required for application, hereafter is referred to as the "activity method."

To calculate $\Delta\pi$ using the activity method, all source and effluent liquid concentrations (determined based on measured *EC* as described in the previous section) were converted into equivalent water activities using the relationships shown in Fig. 2.4. These relationships were derived from tabulated values of the activity of water, a_w , of KCl and NaCl solutions at 25 °C for molalities ranging from 0.1 m to 4.4 m and 0.1 m to 6.0 m, respectively, obtained from Robinson and Stokes (1959) and shown in Table A1 in Appendix A. However, concentrations determined using the previously described concentration-*EC* correlations were expressed in units of molarity (mol/L), whereas the a_w values in Table A1 are listed for given solution molalities (mol/kg). Therefore, to obtain a direct relationship between a_w and solution molarity, the range of molal concentrations shown in Table A1 was converted to an equivalent range of molar concentrations using the following relationship (see Appendix B for derivation):

$$C = \frac{\rho}{\frac{1}{m} + \frac{M}{1000}} \quad (2.11)$$

where C is the concentration in molarity (mol/L), m is the molality (mol/kg), ρ is the solution density associated with the given m (Mg/m³), and M is the molar mass of the chemical species in solution (g/mol; e.g., 74.55 g/mol for KCl and 58.44 g/mol for NaCl). Tabulated values of KCl and NaCl solution densities at 25 °C for molalities ranging from 0 m to 4.50 m and 0 m to 6.10 m, respectively, obtained from Romankiw and Chou (1983) are presented in Table A2. These densities were plotted for the given range of molalities (Fig. A1) and fitted with lines of best fit,

such that a value of ρ could be calculated for any given value of m within the range of molalities in Table A2, and subsequently used in conjunction with m in Eq. 2.11. Each curve in Fig. A1 was well represented by a quadratic regression, as reflected by values for the coefficient of determination (R^2) of 1.0000 in each case.

Following conversion of the concentrations in Table A1 from units of molality to units of molarity using Eq. 2.11, the direct relationship between water activity and molar concentration (Fig. 2.4) for the KCl and NaCl solutions used in this study could be formulated. Quadratic regressions also were fit to the data in Fig. 2.4, such that a_w could be calculated for any solution concentration within the range of molarities shown. Therefore, because all concentrations determined in this study using the concentration-*EC* correlations were within the range of concentrations shown in Fig. 2.4, membrane efficiency coefficients could be calculated for each stage of testing based on the calculated a_w values of the circulating solutions. For solutions with predicted concentrations less than 0.1 M, as with the majority of bottom boundary circulation outflow samples collected during this study, values of a_w were considered to be equal to unity ($a_w = 1$), since concentrations below this threshold were, as previously discussed, shown to be representative of an ideal solution with a water activity essentially equivalent to that of pure water.

2.2.5.2 Effective Diffusion Coefficients and Tortuosity Factors

In the absence of ideal membrane behavior, salt diffusion will occur through the specimen from the side of higher concentration to the side of lower concentration in response to an imposed concentration gradient (Shackelford 1991). In the membrane and diffusion testing conducted in this study, diffusion through the test specimen will result in increased solute

concentrations in the bottom boundary circulation outflow relative to those in the bottom circulation inflow, and decreased solute concentrations in the top boundary circulation outflow relative to those in the top circulation inflow (i.e. $C_b > C_{ob}$ and $C_t < C_{ot}$). The stepwise increase in the concentration of the source solution circulated across the top boundary from one stage of testing to the next resulted in an initial period of transient diffusion. However, because of the maintenance of a constant concentration gradient via continual replenishment of the source solutions circulated across both boundaries, a steady-state solute flux through the bottom boundary of the specimen eventually is established during each testing stage. The aforementioned boundary conditions are consistent with the through-diffusion method (also referred to as the steady-state or time-lag method) to calculate the effective diffusion coefficient, D^* , for chemical species diffusing through porous media (e.g., Shackelford 1991; Shackelford and Lee 2003; Shackelford and Moore 2013).

The through-diffusion method was used to calculate D^* based on the area-normalized cumulative mass of the solute species diffusing through the specimen per unit time, Q_t (Bohnhoff and Shackelford 2015; Meier 2016). Because samples were collected continuously from the bottom boundary outflow for each circulation cycle during membrane and diffusion testing, incremental values for the total diffused solute mass per time increment ($\Delta Q_{t,i}$) were calculated by converting the effluent concentrations to solute mass using the volumes from each circulation cycle, as follows (Bohnhoff and Shackelford 2015; Meier 2016):

$$\Delta Q_{t,i} = \frac{\Delta m_i}{A \cdot \Delta t_i} = \frac{\Delta(C_b \cdot V_b)_i}{A \cdot \Delta t_i} \quad (2.12)$$

where Δm_i is the incremental solute mass collected per circulation cycle, Δt_i is the incremental time for each circulation cycle, A is the cross-sectional area of the specimen, C_b is the concentration (determined using Fig. 2.7) of the effluent sample collected from the bottom boundary of the specimen, V_b is the volume of effluent corresponding to C_b , and i is the index number corresponding to the particular circulation cycle (expressed as an integer ranging from 1 to the total number of incremental samples). Values of Q_t were calculated as the sum of the incremental masses per unit time for all consecutive circulation cycles within the testing stage, or:

$$Q_t = \sum_{i=1}^N \Delta Q_{t,i} \quad (2.13)$$

with the requirement that sampling remain continuous such that all solute mass was collected and accounted for in the calculations. Values of Q_t were plotted as a function of the cumulative elapsed time, t , representing the elapsed time from the start of testing to the end of a specific time increment, or:

$$t = \sum_{i=1}^N \Delta t_i \quad (2.14)$$

where Δt_i represents the increment in time corresponding to $\Delta Q_{t,i}$. Following the initial period of transient diffusion characterized by a generally nonlinear Q_t -versus- t relationship, steady-state diffusion was established such that the trend in Q_t versus t became linear, indicating a constant diffusive mass flux (Shackelford 1991).

Values of D^* can be calculated based on the data within the steady-state portion of the Q_t -versus- t relationship as follows (e.g. Shackelford 1991):

$$D^* = -\left(\frac{\Delta Q_t}{\Delta t}\right)\left(\frac{L}{nw_A\Delta C}\right) \quad (2.15)$$

where $\Delta Q_t/\Delta t$ is the slope of the linear regression fitted to the steady-state portion of the Q_t -versus- t relationship, L is the specimen thickness, n is the specimen porosity, w_A is the atomic weight of the diffusing solute (Cl⁻ in this study, therefore $w_A = 35.45$ g/mol), and ΔC (<0) is the difference in the solute concentration (in molarity) across the specimen. The linear regression used to calculate $\Delta Q_t/\Delta t$ was obtained by "reverse fitting" a line to an increasing number of data points, i.e., fitting a regression beginning with the final two data points then individually adding each previous data point until the coefficient of determination, R^2 , deviated significantly from unity (Shackelford and Lee 2003), or in the case of this study became lower than 0.9998. This value was determined based on visual assessment of the Q_t -versus- t plots for all stages of testing conducted in this study, with the conclusion that a R^2 of 0.9998 appeared to represent a threshold value below which deviation from linear behavior was observed. This threshold was assumed to be the point of transition from transient to steady-state diffusion, with the time required to reach this transition point designated as the time to steady state, or t_{ss} .

Values of D^* calculated from Eq. 2.15 also may be defined using the following relationship (Shackelford and Daniel 1991; Malusis and Shackelford 2002b; Shackelford and Moore 2013):

$$D^* = D_o\tau_a \quad (2.16)$$

where D_o is the aqueous-phase (or free solution) diffusion coefficient and τ_a is the apparent tortuosity factor, which represents the product of the matrix tortuosity factor, τ_m (representing the tortuosity due only to the geometry of the interconnected pores), and the restrictive tortuosity factor, τ_r , or:

$$\tau_a = \tau_m \tau_r = \tau_m \prod_{i=1}^N \tau_i = \tau_m (\tau_1 \cdot \tau_2 \cdots \tau_N) \quad (2.17)$$

where τ_r represents the product of N factors (τ_i), aside from pore geometry, that act to reduce the diffusive flux of solutes through the porous medium and thus contribute to the overall (apparent) tortuosity (Malusis and Shackelford 2002c; Shackelford and Moore 2013; Shackelford 2014). Such additional factors may include anion exclusion due to membrane behavior, as well as increased water viscosity of the adsorbed water near the clay particle surfaces relative to the bulk water in the open pore space (Malusis and Shackelford 2002c; Bohnhoff and Shackelford 2015).

Because τ_m ($0 \leq \tau_m \leq 1$) and τ_r ($0 \leq \tau_r \leq 1$) presently cannot be directly measured, an additional diffusion coefficient, referred to as the pore diffusion coefficient (D_p), can be used to back-calculate τ_m and τ_r as follows (Shackelford and Moore 2013):

$$D_p = D_o \tau_m = \frac{D^*}{\tau_r} \quad (2.18)$$

such that:

$$\tau_r = \frac{D^*}{D_p}; \quad \tau_m = \frac{D_p}{D_o} \quad (2.19)$$

where D_p represents the diffusion coefficient for a solute in the case where the tortuous nature of flow through a porous medium is only attributed to the geometric restriction (i.e. is only a function of τ_m), and therefore is equivalent to the limiting value of D^* at $\omega = 0$ (Shackelford et al. 2016). Values of D_p can be obtained either by extrapolation of D^* versus ω to estimate the value of D^* at $\omega = 0$, or by simultaneously measuring D^* and ω for a case where membrane behavior is eliminated (as in this study) such that the actual value of D_p is measured.

2.2.6 Testing Program

Testing was conducted on duplicate specimens prepared by Meier (2016) and designated as rigid-wall specimens one (RW-1) and two (RW-2). The specimens were prepared with similar methods and compaction characteristics (see Meier 2016) and, in this study, were tested for membrane behavior with the intent of obtaining comparable results using the same procedure and stage termination criteria. However, the testing duration for specimen RW-1 of 722 d (i.e., including stages of testing conducted by Meier 2016) was considerably longer than that of 396 d for specimen RW-2. This difference was a result of the different stage termination criteria implemented for each specimen during testing conducted by Meier (2016), in which specimen RW-1 was required to exhibit steady-state diffusion of solutes prior to switching to any subsequent testing stage, whereas specimen RW-2 was required only to achieve a steady-state ΔP across the specimen (attained in approximately half the time as steady-state diffusion during that study) before being subjected to the next concentration difference.

However, because both specimens were analyzed for diffusion in this study, termination criteria for all stages of testing in this study for both specimens RW-1 and RW-2 were the same as those used for specimen RW-1 by Meier (2016). As previously discussed, the measured ΔP in response to a particular concentration gradient across the specimen was considered to be at steady state once the values for four consecutive circulation cycles were within $\pm 3\%$ of the average of the same four values with no visible upward or downward trend.

2.3 Results

2.3.1 Hydraulic Conductivity Testing

The results of the hydraulic conductivity tests using 80 mM KCl (Meier 2016), 640 mM KCl, and 3.27 M NaCl as the permeant liquid are presented in Figs. 2.12 through 2.15. The k resulting from permeation of the sand-bentonite mixture with tap water can be found in Meier (2016) and Tong and Shackelford (2016). Increasing the concentration of the permeant KCl solution from 80 mM to 640 mM resulted in an increase in k from 6.6×10^{-12} m/s to 1.6×10^{-10} m/s and from 5.4×10^{-12} m/s to 5.3×10^{-11} for specimens FW-1 and FW-2, respectively. Increasing the permeant solution concentration to 3.27 M NaCl was expected to result in a corresponding increase in k ; however, the resulting k values of 1.1×10^{-10} m/s and 4.7×10^{-11} m/s for specimens FW-1 and FW-2, respectively, actually were slightly lower than those measured for 640 mM KCl. Based on these results, in the presence of monovalent salt solutions with concentrations as high as 3.27 M, the measured k for both specimens remained below the maximum value of 10^{-9} m/s that typically is required of liners used in waste containment applications (Daniel 1987, 1993; Benson et al. 1994, 1999).

The concentration of the permeant liquid was increased from 640 mM KCl to 3.27 M NaCl before chemical equilibrium was attained during the 640 mM KCl permeation stage for reasons previously discussed in Section 2.2.4. Furthermore, due to the relatively low k of the sand-bentonite mixture, chemical equilibrium was not achieved for the 3.27 M NaCl permeation stage within the time constraints of this study. Following collection of approximately 2 pore volumes of flow from each of the two specimens during the 3.27 M NaCl permeation stage, the ratio of the effluent EC of the effluent, EC_f , to the EC of the source NaCl solution, EC_o , (i.e., EC_f / EC_o) was 0.59 for specimen FW-1 and 0.48 for specimen FW-2. The results for EC_f / EC_o thus were not in accordance with the termination criteria established by ASTM D7100, which require values for EC_f / EC_o between 0.90 and 1.10 and no significant upward or downward trend over time. Therefore, the measured k for the 640 mM KCl and 3.27 M NaCl permeation stages should only be considered estimates, since terminating k -tests prior to establishing chemical equilibrium may result in unconservatively low k (Shackelford et al. 2000).

2.3.2 Membrane Testing

The stages of membrane and diffusion testing conducted in this study ($C_{ot} \geq 160$ mM) were a continuation of the multiple-stage membrane testing for the study by Meier (2016). Therefore, the results from both studies are summarized in Table 2.2. Note that the two sets of results ($5 \leq C_{ot} \leq 80$ mM and $C_{ot} \geq 160$ mM) are based on different methods (i.e. use of the van't Hoff expression versus the activity method, as discussed in Section 2.2.5.1.3) with the exception of the measured ΔP values. The effect of the chosen method on the membrane testing results is discussed in greater detail in Section 2.3.2.6.

2.3.2.1 Boundary Electrical Conductivities and Solute Concentrations

Electrical conductivity (EC) for effluent samples from the top and bottom specimen boundaries were measured at the end of each 48-h circulation cycle and are presented in Fig. 2.16. Steady-state values of EC for each testing stage, for both the top and bottom boundary outflows, were calculated as the average of the measured EC for samples collected from the final four circulation cycles of each stage. The steady-state EC for the circulation outflow from the top boundary, EC_t , increased from 2.135 S/m for the 160 mM KCl stage to 20.57 S/m for the 3.27 M NaCl stage for specimen RW-1, and from 2.106 S/m to 20.40 S/m for specimen RW-2. The steady-state EC for the circulation outflow from the bottom boundary, EC_b , increased from 0.1373 S/m for the 160 mM KCl stage to 1.745 S/m for the 3.27 M NaCl stage for specimen RW-1, and from 0.1630 S/m to 1.801 S/m for specimen RW-2. These results follow the expected trend in EC with increasing concentration, i.e., EC increases with increasing solute concentration. For each stage, the EC_t for both specimens were slightly lower than the EC of the source solution circulated across the top boundary, EC_{ot} , which ranged from 2.243 S/m (160 mM KCl) to 21.13 S/m (3.27 M NaCl), whereas EC_b for both specimens during all stages of testing were significantly higher than the baseline EC of the TW, i.e., $EC_{ob} = 0.0119$ S/m, used as the source liquid for circulation across the bottom boundary (i.e. $EC_t < EC_{ot}$ and $EC_b > EC_{ob}$). Changes in EC are indicative of solute transport (diffusion) through the specimen from the top to the bottom boundary in response to the imposed concentration gradient, whereby the number of charged solutes contributing to the EC of the top boundary solution decreases as the number of charged solutes contributing to the EC of the bottom boundary simultaneously increases. By the time of the 3.27 M NaCl stage, the high rate of diffusion (see Section 2.3.3) due to the combination of the suppression of diffuse double layers (DDLs) associated with the bentonite

particles and the high imposed concentration gradient across the specimen resulted in an EC_b that was within 22 % of the EC_t of approximately 2.1 S/m for the 160 mM KCl stage.

A final or flushing stage, consisting of the simultaneous circulation of TW across both boundaries of the specimen, was conducted with the primary purpose of determining whether the baseline pressure difference across the specimen (i.e. ΔP_{TW}) would be re-established after membrane behavior had been eliminated, the results of which are discussed in Section 2.3.2.2. Values of EC_t and EC_b for both specimens RW-1 and RW-2 quickly decreased during this stage as a result of the change of the top boundary source liquid from 3.27 M NaCl to TW. Because of the higher starting value of EC_t relative to EC_b , EC_t initially dropped more rapidly than EC_b until the two values eventually became similar after approximately four circulation cycles, although EC_t remained slightly higher (~ 0.015 S/m) than EC_b and EC_b approached (though remained slightly above) the baseline value for the EC of the TW. Because of the higher concentration in the pores near the top boundary, a higher concentration gradient was established between those tributary pores and the top boundary circulation liquid than was established between the bottom boundary circulation liquid and the tributary pores. Thus, the higher EC_t relative to EC_b during this last or flushing stage of testing can be attributed to a higher diffusive mass flux from the top of the specimen relative to that at the bottom.

Boundary solute concentrations for both specimens were determined for each circulation cycle (see Section 2.2.5.1.2) and are presented in Fig. 2.17. Actual C_{ot} also were estimated for each stage of testing in this study based on the concentration- EC calibration curves in Fig. 2.7 and are listed in Tables 2.2 and 2.3. Note that C_{ot} was directly measured by Meier (2016) for the stages corresponding to C_{ot} ranging from 5 to 80 mM KCl. As previously discussed, all predicted KCl and NaCl concentrations are assumed to be equal to the concentration of the chloride (Cl^-)

anion due to the nonreactive (nonadsorbing) nature of Cl^- in the sand-bentonite system and the requirement for electroneutrality in solution.

Because the concentrations (C) are directly based on the EC , the plots of concentration versus time (Fig. 2.17) exhibit trends identical to those apparent in the EC versus time plots (Fig. 2.16). Steady-state C for each stage were calculated in the same manner as the steady-state EC , i.e., as the average of the C for the final four circulation cycles within each testing stage. For specimen RW-1, C_t increased from 164.5 mM to 3059 mM as C_{ot} increased from 174 mM to 3229 mM, and C_b increased from 8.0 mM to 160.8 mM while C_{ob} remained steady at approximately 0.135 mM, which represents the average of the bottom boundary Cl^- concentrations measured by Meier (2016). For specimen RW-2, and for the same C_{ot} and C_{ob} values, C_t increased from 162.0 mM to 3028 mM and C_b increased from 9.6 mM to 168.0 mM. Similar to the EC results, top boundary effluent concentrations decreased relative to the source concentration (i.e. $C_t < C_{ot}$), whereas bottom boundary effluent concentrations increased relative to the source concentration (i.e. $C_b > C_{ob}$).

Specimens RW-1 and RW-2 exhibited identical trends for both EC and boundary concentrations, although the magnitudes of the results were slightly different for each specimen. The EC_t for specimen RW-2 on average was approximately 1.6 % lower than that for specimen RW-1, whereas the EC_b for specimen RW-2 were about 13.2 % higher relative to those for specimen RW-1. Similarly, the C_t for specimen RW-2 were an average of 2.0 % lower than those for specimen RW-1, whereas the C_b for specimen RW-2 were 14.3 % higher than those for specimen RW-1, indicating a higher rate of diffusion through specimen RW-2 than specimen RW-1. The reasons for these differences are discussed with the results from diffusion testing in Section 2.3.3.1.

2.3.2.2 Maximum Chemico-Osmotic Pressure Differences

Although the $\Delta\pi_o$ and $\Delta\pi_{ave}$ used to determine the final ω values for this study were based on water activity, a_w , via Eqs. 2.4 and 2.5, these parameters also were calculated for each stage of testing using the van't Hoff expression (Eq. 2.3) to allow a comparison of the ω values based on the two methods, as summarized in Table 2.2. Values of $\Delta\pi_o$ were calculated for each testing stage based on the difference in water activities, i.e., $a_{w,ot}$ and $a_{w,ob}$, via Eq. 2.4 and corresponding differences in source solute concentrations, i.e., C_{ot} and C_{ob} , via Eq. 2.3, whereas $\Delta\pi_{ave}$ was calculated via Eq. 2.5 based on the differences between the average boundary water activities calculated via Eqs. 2.6 and 2.7 and the average boundary solute concentrations via Eq. 2.3, as previously described (Section 2.2.5.1). Because steady-state C_t and C_b were used to calculate average boundary concentrations, and because source concentrations remained unchanged throughout each testing stage, a single $\Delta\pi$ was reported for each stage for both $\Delta\pi_o$ and $\Delta\pi_{ave}$. As a result, $\Delta\pi$ obtained using the van't Hoff expression ($\Delta\pi_{C,o}$ and $\Delta\pi_{C,ave}$) were directly compared to those obtained using the activity method ($\Delta\pi_{aw,o}$ and $\Delta\pi_{aw,ave}$) for both test specimens over the range of source concentrations (Figs. 2.18-2.21). Results also were included from Meier (2016), though $\Delta\pi_C$ was assumed to be equal to $\Delta\pi_{aw}$, since the solutions used in that study were assumed to be ideal and dilute with water activities equal to unity (i.e. $a_w = 1$), such that the activity method always would result in values equal to zero [e.g., because $\ln(1/1) = 0$] and, therefore, was assumed to not be applicable for calculating $\Delta\pi$.

Values of $\Delta\pi$ for both specimens RW-1 and RW-2 ranged from approximately 21 kPa to 18.500 MPa (Table 2.2, Figs. 2.18-2.21) as the source Cl⁻ concentration increased from 5 mM KCl to 3.27 M NaCl, respectively. The results followed the expected trend that $\Delta\pi$ increases in response to increasing concentration gradients across the specimen, since a greater chemico-

osmotic pressure is required on the concentrated side of the membrane (specimen) to counteract the increased tendency for osmotic flow (Katchalsky and Curran 1965; Tinoco et al. 1995; Malusis et al. 2001; Shackelford 2013). For the 160 mM, 320 mM, and 640 mM KCl stages, $\Delta\pi_C$ was greater than $\Delta\pi_{aw}$, whereas the opposite (i.e. $\Delta\pi_{aw} > \Delta\pi_C$) was true for the 1.63 M and 3.27 M NaCl stages. The reason for this difference is evident in Fig. 2.5, which illustrates that the linearity of the van't Hoff expression and nonlinearity of the expressions used in the activity method result in higher $\Delta\pi_C$ relative to $\Delta\pi_{aw}$ at lower salt (either KCl or NaCl) concentrations and vice versa at higher salt concentrations, with the intersection of the curves occurring at 1.67 M NaCl and 2.34 M KCl. Note that the C_{ot} used to calculate $\Delta\pi$ for the 1.63 M stage was approximately 1.87 M and, therefore, higher than the threshold value of 1.67 M NaCl, such that $\Delta\pi_{aw} > \Delta\pi_C$ for that stage. Greater differences between $\Delta\pi_{aw}$ and $\Delta\pi_C$ occurred at concentrations higher than the aforementioned threshold values, with the differences increasing at a greater rate for NaCl than for KCl due to differences in the relationships between a_w and C for each salt shown in Fig. 2.4.

One possible explanation for the difference between the NaCl and KCl curves in Fig. 2.5 (resulting from the differing a_w -vs.- C relationships) is the larger hydrated radius of Na^+ compared to that of K^+ , as indicated by the lyotropic series (e.g., Malusis and Shackelford 2002a). A larger hydrated radius is a product of a greater number of water molecules electrostatically held in hydration shells around the dissociated ions, resulting in a lower total water potential (i.e. lower activity) (Essington 2004). Accordingly, more water molecules will be immobilized for hydrated Na^+ ions in a solution of a given concentration than for hydrated K^+ ions, resulting in a lower activity for a NaCl solution relative to a KCl solution, such that a

higher $\Delta\pi$ is required to balance the decrease in chemical potential and maintain equilibrium across the membrane.

In this study, the greatest difference between $\Delta\pi_{aw}$ and $\Delta\pi_C$ (~ 3 MPa) was observed during the 3.27 M NaCl stage due to the deviation from ideal and dilute conditions at high solute concentrations, as shown by water activities decreasing to as low as 0.85 as the NaCl concentration approaches 4 M (Fig. 2.4). Because the van't Hoff approximation is only valid for ideal and dilute solutions (Fritz 1986; Malusis et al. 2001), whereas the activity method accounts for nonideal and concentrated conditions based on the water (H_2O) activity, which is a direct measurement of the total energy for any aqueous solution (Robinson and Stokes 1959), $\Delta\pi_C$ at such high concentrations would be expected to deviate from $\Delta\pi_{aw}$ in a manner similar to that observed in Figs. 2.18 through 2.21.

In the case of both $\Delta\pi_{aw}$ and $\Delta\pi_C$, $\Delta\pi_o$ consistently was higher for a given concentration (Figs. 2.18 and 2.20) than $\Delta\pi_{ave}$ (Figs. 2.19 and 2.21) in accordance with expected trends. Because $\Delta\pi_{ave}$ is based on average boundary concentrations that account for solute diffusion through the specimen, the concentration difference across the specimen (as well as the ratio of water activities) and, therefore, $\Delta\pi$ typically are lower than for the case where only source concentrations are considered.

Three additional methods of comparing $\Delta\pi_{aw}$ and $\Delta\pi_C$ for each testing stage are presented in Figs. 2.22 through 2.24, viz., $\Delta\pi_C$ versus $\Delta\pi_{aw}$ on a one-to-one (1:1) scale, the ratio of $\Delta\pi_{aw}$ relative to $\Delta\pi_C$, and the percent error of $\Delta\pi_C$ relative to $\Delta\pi_{aw}$. The differences between $\Delta\pi_{aw}$ and $\Delta\pi_C$ in Fig. 2.22 are obfuscated primarily due to the values of $\Delta\pi$ associated with the high-concentration stages masking any differences when viewed on a 1:1 plot of this scale. However, the differences in the two methods for determining $\Delta\pi$ are more evident in Fig. 2.23 where

$\Delta\pi_{aw}/\Delta\pi_C$ is shown versus solute concentration, and the trends follow those previously discussed for Figs. 2.18 through 2.21. For the 160 mM through 640 mM KCl stages, $\Delta\pi_{aw,o}$ was approximately 91 to 95 % of $\Delta\pi_{C,o}$ whereas $\Delta\pi_{aw,ave}$ was approximately 94 to 99 % of $\Delta\pi_{C,ave}$. For the 1.63 M and 3.27 M NaCl stages, $\Delta\pi_{aw,o}$ was approximately 102 % and 116 % of $\Delta\pi_{C,o}$, respectively, whereas $\Delta\pi_{aw,ave}$ was approximately 103 % and 118 % of $\Delta\pi_{C,ave}$, respectively. Although $\Delta\pi_{aw,o}/\Delta\pi_{C,o}$ were the same for both specimen RW-1 and RW-2 (because the same source solutions were used for each specimen), $\Delta\pi_{aw,ave}/\Delta\pi_{C,ave}$ for specimen RW-1 were about one percentage point lower than those for specimen RW-2 for the KCl stages, and were nearly identical for the NaCl stages, indicating repeatability of the results between the two test specimens. The error for results obtained using the van't Hoff expression (Fig. 2.24) followed the same trends as those shown in Fig. 2.23, with values for the KCl stages ranging from -5 % to -10 % for $\Delta\pi_o$ and from approximately -2 % to -7 % for $\Delta\pi_{ave}$. For the 1.63 M and 3.27 M NaCl stages, the errors for $\Delta\pi_o$ were about 2 % and 14 %, respectively, and for $\Delta\pi_{ave}$ were approximately 4 % and 15 %, respectively. Errors based on average boundary concentrations for specimen RW-1 were about one percentage point lower than those for specimen RW-2 during the KCl stages while remaining indistinguishable for the NaCl stages. Errors as high as 10 % for the KCl stages and 15 % for the NaCl stages confirmed that the van't Hoff expression may not be appropriate for calculating $\Delta\pi$ in the case of a membrane exposed to solutions with concentrations greater than 0.1 M (i.e. nonideal, concentrated solutions).

2.3.2.3 Boundary Water Pressures

Water pressures were monitored at both the top and bottom boundaries of the specimens (e.g. u_{top} and u_{bottom}) throughout all stages of testing via inline (gage) pressure transducers, the

results of which are shown in Fig. 2.25. Note that results for the 5 through 80 mM KCl stages are not included, but can be found in Meier (2016). The accuracy of the transducers used for specimen RW-2 was greater than those used for specimen RW-1 (0.25 % versus 1 % of the pressure range, i.e., ± 0.4 kPa versus ± 1 kPa, respectively), resulting in greater scatter in the observed pressure readings for specimen RW-1 than for specimen RW-2. As a result, the recurring pressure drops at the end of each 48-h circulation cycle are more apparent for specimen RW-2 compared to specimen RW-1. As previously noted, these pressure drops are a result of the temporary pause in circulation during sampling when the specimen boundaries are not flushed, causing a temporary relief in u_{top} . Once the flow pumps are restarted and the subsequent circulation cycle begins, the concentration gradient again is maintained constant such that the pressure gradually begins to increase towards equilibrium during the remainder of the cycle. Note that the pressure drops are much greater for u_{top} compared to u_{bottom} since the osmotic pressure develops along the top boundary of the specimen, whereas the perpetual circulation of TW along the bottom maintains relatively low and generally constant pressures.

Slight differences in the baseline values of u_{top} and u_{bottom} were observed during the initial TW circulation stage performed by Meier (2016) (shown before the break in the x-axis for each plot in Fig. 2.25), although minor differences are expected as a result of mechanical imperfections within the testing apparatus (see Section 2.2.5.1.1). As higher concentrations of KCl or NaCl were introduced to the top boundary during later stages of testing, u_{top} increased relative to u_{bottom} because, as previously discussed, an osmotic pressure developed on the concentrated side of the semipermeable membrane to counteract the tendency for osmotic flow resulting from the imposed concentration gradient. However, by the end of the 160 mM KCl stage, values of u_{top} reached a maximum and then generally remained steady throughout the 320

mM KCl stage before steadily declining for the remainder of testing. Upon exposure of the specimens to 3.27 M NaCl solutions, u_{top} abruptly dropped to the same baseline pressure measured during the initial TW circulation stage. This sudden return to baseline pressure was believed to coincide with the destruction of membrane behavior within the specimen. Because the specimen no longer behaved as a semipermeable membrane, the tendency for osmotic flow no longer existed and no osmotic pressure developed on the concentrated side of the specimen (Malusis and Shackelford 2002a).

Values of u_{bottom} remained relatively steady through the 320 mM KCl stage before beginning to exhibit additional scatter during the 640 mM KCl stage. Slight increases then were observed during the 640 mM KCl and 1.63 M NaCl stages and were followed by even greater increases (~ 4 kPa for both specimens) during the 3.27 M NaCl stage. The steady values during earlier testing stages can be attributed to the continual circulation of TW along the bottom, even as the top boundary source concentration was increased, resulting in the development of an osmotic pressure at the top boundary but not at the bottom boundary, as previously discussed. Increases in u_{bottom} first were observed approximately at the same time that u_{top} began to decrease, suggesting a correlation between the increased diffusive mass flux through the specimen (see Section 2.3.3.1) and the development of slightly higher pressures along the bottom boundary. For specimen RW-2, this pressure increase along the bottom boundary translated to a higher u_{bottom} than u_{top} during the 3.27 M NaCl stage. In contrast, u_{top} remained about 2 kPa higher than u_{bottom} for specimen RW-1, which was greater than the difference of 0.30 kPa observed by Meier (2016) during the initial TW stage. However, differences between u_{bottom} and u_{top} further decreased during the final flushing circulation stage as both u_{bottom} and u_{top} effectively returned to the initial baseline values. Although u_{bottom} and u_{top} were similar between the initial and final TW stages,

greater scatter and oscillation of the results were observed during the final stage compared to the initial stage, possibly due to the unsteady, outward diffusion of residual salts from the final stages of membrane testing that had yet to be flushed from the specimens.

2.3.2.4 Possible Effect of Diffusion Osmosis on Boundary Water Pressures

One hypothesized mechanism for the increase in u_{bottom} at higher concentrations is diffusion osmosis (Olsen et al. 1990), wherein osmotic flow occurs through a membrane in the direction opposite of that typically seen for chemico-osmosis, i.e., from the more concentrated solution towards the more dilute solution due to the drag of bulk pore fluid by diffusing solutes. Diffusion osmosis typically is noteworthy for materials with a low degree of ion exclusion, either due to a low exchange capacity (e.g. kaolinite) or because of relatively high solute concentrations within the pore fluid, such that the amount of diffusion through the material is sufficiently large to exert enough drag on the fluid to overcome the tendency for chemico-osmotic flow (Olsen et al. 1990). Although this phenomenon is expected to be prevalent in a lower-plasticity clay such as kaolin because of the lack of membrane characteristics, the possibility exists for such behavior to occur in materials containing higher-plasticity clays (such as the sand-bentonite specimens tested in this study) assuming that ion exclusion is sufficiently low. For example, Keijzer et al. (1999) observed a reversal in flow direction in an open-system testing apparatus and an associated pressure increase on the side of low concentration for compacted Na-bentonite specimens with membrane efficiency coefficients of 0.003 and 0.001, which were similar to the coefficients determined for the later stages of testing in this study. The change in the direction of the pressure gradient was attributed to possible diffusion osmosis resulting from the relatively

high porosity (e.g., $n = 0.65$ vs. $n = 0.34$ for specimens RW-1 and RW-2) of the bentonite specimens (Keijzer et al. 1999).

Because of the closed system implemented in this study, flow through the specimen was prevented such that diffusion osmosis could not have occurred. However, conditions near and at the end of membrane testing were similar to those described by Elrick et al. (1976) and Olsen et al. (1990) as being conducive to establishing the driving force behind diffusion osmosis. For example, the low degree of membrane efficiency ($< 1\%$; see Section 2.3.2.6) measured during the final three stages of testing (640 mM KCl, 1.63 M NaCl, and 3.27 M NaCl), coupled with the relatively high concentration gradients imposed during those stages, suggests that diffusion of solutes may have been of a sufficiently high magnitude to exert a significant drag force on the bulk pore fluid and create a tendency for flow towards the bottom boundary of the specimen. Thus, the increase in u_{bottom} could be the result of the development of an upward hydraulic pressure at the bottom boundary to counteract the resultant downward drag force and maintain equilibrium within the closed system. Similarities in both the timing and magnitudes of the observed increases in u_{bottom} for both specimens RW-1 and RW-2 supports the diffusion osmosis hypothesis.

2.3.2.5 Measured Chemico-Osmotic Pressure Differences

Similar to the boundary pressure results, values of $-\Delta P$ (> 0) measured with the differential pressure transducers for both specimens RW-1 and RW-2 peaked during the 160 mM and 320 mM KCl stages before steadily declining for the remainder of membrane testing. The peak and subsequent decrease in $-\Delta P$ as C_{ot} continued to increase beyond 160 mM KCl was indicative of reduced membrane behavior due to compression of the DDLs surrounding the

individual bentonite clay particles, resulting in an increase in the size of the pores as the pore fluid became increasingly concentrated (Fritz 1986). Thus, diffusion of solutes through the bentonite resulted in diminishing, and ultimately elimination, of the exclusionary capabilities of the pores such that only a small fraction (or zero in the case of the 3.27 M NaCl stage) of $\Delta\pi$ developed across the specimen.

The steady-state values of $-\Delta P$ at the end of each 48-h circulation cycle, $-\Delta P_c$, are presented in Fig. 2.27. Note that $-\Delta P_c$ is not necessarily the true steady-state value for each cycle, since $-\Delta P$ generally continued to increase and failed to stabilize by the time of sample collection and resetting of the flow pumps, a trend which also has been reported for previous rigid-wall membrane tests with a similar flow pump circulation rate (i.e. $Q = 2.3 \times 10^{-10} \text{ m}^3/\text{s}$) (e.g. Bohnhoff 2012; Meier 2016). The failure of the measured $-\Delta P$ values to reach a true steady state may have been a result of the greater thickness and higher bentonite contents of the specimens used in this study relative to past studies where pressures did stabilize. For example, Malusis and Shackelford (2002a) tested GCL specimens that, although consisting of 100 % bentonite, were thinner than the sand-bentonite specimens tested in this study (10 mm vs. 29.1 mm). Additionally, Kang and Shackelford (2010) tested bentonite-amended clays also with a thickness of 29.1 mm, but that contained a bentonite content of only 5 % versus the value of 15 % associated with the specimens in this study.

Meier (2016) explored two approaches for determining values of $-\Delta P_c$ for a given circulation cycle, the first of which was used for specimen RW-1 and the second of which was used for specimen RW-2. The two approaches also were applied to the test data for the same respective specimen in this study. For the first approach, $-\Delta P_c$ was determined as the geometric mean, or central tendency, of the data recorded for the second day of the circulation cycle,

whereas for the second approach $-\Delta P_c$ was determined as the maximum value of the same range of data. Meier (2016) applied both methods to the $-\Delta P$ results for each specimen and determined that the central tendency approach was more appropriate for specimen RW-1, whereas the maximum value approach was more appropriate for specimen RW-2. Because of the scatter in the results obtained from the pressure transducer used to measure $-\Delta P$ for specimen RW-1, the maximum-value approach resulted in values that were both unconservatively high and not representative of the actual $-\Delta P_c$ (Meier 2016). However, the central tendency approach was effective at normalizing the scatter such that the range of $-\Delta P$ values did not have a calculable effect on the average value. Conversely, results obtained from the more accurate transducer used for specimen RW-2 exhibited steady increases in $-\Delta P$ throughout each cycle, with little scatter, such that the maximum (and often final) value of $-\Delta P$ was most representative of $-\Delta P_c$. Although the application of the central tendency approach to specimen RW-2 would result in conservatively low values of $-\Delta P_c$, use of this method was deemed unnecessary since scatter was sufficiently limited that the maximum value of $-\Delta P$ was considered to be a more accurate representation of the steady-state value (Meier 2016). Although neither approach provided the true steady-state $-\Delta P$ for each cycle because pressures did not fully stabilize, the values of $-\Delta P_c$ derived from the two aforementioned methods are believed to be conservative since lower values of $-\Delta P$ result in lower, and thus more conservative, values of ω (see Eq. 2.8).

The steady-state chemico-osmotic pressure difference, $-\Delta P_{ss}$, for each testing stage was calculated as the average of the final four $-\Delta P_c$ values once the pressures were stable, defined as having a value within $\pm 3\%$ of the average of those same four values and showing no visible upward or downward trend (Meier 2016). One exception was the 160 mM KCl stage for specimen RW-2, in which an erratic response was observed during the final 10 to 12 circulation

cycles. The irregular results were characterized by oscillating $-\Delta P_c$ values originating from oscillating pressures only along the top boundary of the specimen (i.e., u_{top} as shown in Fig. 2.25b). Both the inline and differential pressure transducers recorded the oscillation, therefore, the oscillation is interpreted to have occurred within the rigid wall cell or flow pump system, as opposed to measurement error by the pressure transducers. However, there was no observed oscillation of other variables such as top boundary EC or concentration, thus the source of error, whether mechanical (in terms of the test apparatus) or behavioral in nature, remains unknown. Because the $-\Delta P_c$ values appeared to oscillate around a relatively constant average value with no significant upward or downward trend, steady state was assumed to have been attained and $-\Delta P_{ss}$ was calculated as the average of the final $-\Delta P_c$ values.

Results for $-\Delta P_{ss}$ from all stages of membrane testing ($5 \text{ mM KCl} \leq C_{ot} \leq 3.27 \text{ M NaCl}$) conducted on the sand-bentonite specimens are listed in Table 2.3 as well as plotted versus C_{ot} in Fig. 2.28. For specimen RW-1, $-\Delta P_{ss}$ increased from 9.7 kPa for the 5 mM KCl stage to a maximum of 26.3 kPa for the 160 mM KCl stage before dropping to a minimum value of 2.5 kPa for the 3.27 M NaCl stage. For specimen RW-2, $-\Delta P_{ss}$ increased from 6.9 kPa for the 5 mM KCl stage to 24.2 kPa for the 320 mM KCl stage, then decreased to -7.7 kPa for the 3.27 M NaCl stage. Although a true value of $-\Delta P_{ss}$ for the final TW circulation stage was not determined, values of $-\Delta P_c$ approached $-\Delta P_{TW}$, indicating that steady-state conditions most likely would be equivalent to the baseline conditions measured by Meier (2016) upon eventual removal of all residual salts from the system. Values of $-\Delta P_{ss}$ calculated for specimen RW-1 were higher than those reported for specimen RW-2 for all stages of membrane testing, possibly because specimen RW-2 was better flushed of soluble salts prior to membrane testing (Meier 2016). Consistently smaller concentration gradients were observed for specimen RW-2 relative to specimen RW-1,

as shown by comparatively lower values of C_t and higher values of C_b (see Fig. 2.17), resulting in a lower tendency for osmotic flow and lower osmotic pressures developed within the system.

Table 2.3 also includes the effective chemico-osmotic pressure differences, $-\Delta P_e$, used to calculate ω for each stage in accordance with Eq. 2.8. As previously discussed, values of $-\Delta P_e$ were calculated as the difference between $-\Delta P_{ss}$ and $-\Delta P_{TW}$ to account for non-zero baseline pressures during the initial TW circulation stage. Therefore, the resulting values of ω were a measurement of only chemico-osmotic effects.

Membrane behavior was completely eliminated within the specimens after introduction of 3.27 M NaCl solution to the top boundary, resulting in values of $-\Delta P$ quickly decreasing by about 12-15 kPa in response to the complete loss of solute restriction. However, values of $-\Delta P$ during this stage for specimen RW-2 unexpectedly decreased to less than the initial baseline value ($-\Delta P_{TW} = -1.45$ kPa), indicating a pressure difference in the opposite direction of that observed during previous stages of membrane testing. Initially, this occurrence was thought to be a result of clogging within the porous stones at the specimen boundaries, potentially resulting from precipitation of salts in the highly concentrated NaCl solutions. However, this hypothesis was refuted based on consideration of the boundary water pressures in Fig. 2.25, because clogging only would have been a concern for the top boundary porous stone since this is where the high-concentration solutions were circulated, and u_{top} would have been expected to increase due to the increased resistance to flow of the top stone when clogged. According to Darcy's law for flow through porous media, greater hydraulic resistance (i.e., lower k) will result in an increased hydraulic gradient to maintain a constant flow rate. Therefore, a decrease in k for the porous stone should result in an increase in the water pressure measured at the center of the stone (i.e., u_{top}), assuming a constant flow rate is maintained by the flow pump. In actuality, u_{top}

decreased to baseline levels while u_{bottom} increased to approximately 3 kPa above baseline levels, suggesting that the occurrence may be due to the previously discussed hypothesis related to diffusion osmosis (see Section 2.3.2.4). Values of $-\Delta P$ during the final TW circulation stage eventually returned to the same baseline values that were measured during the initial TW stage for both. This closure on $-\Delta P$ provides additional support for the hypothesis that increased values of u_{bottom} during the 3.27 M NaCl stage resulted from measurable behavior within the system and not pressure transducer error.

However, this hypothesis does not account for u_{bottom} lesser than u_{top} during the 3.27 M NaCl stage for specimen RW-1 and yet greater than u_{top} during the same stage for specimen RW-2. Therefore, to clarify this inconsistency in the results, the reliability of the inline pressure transducers (also see Appendix C) was explored by comparing values for the pressure differences across the specimen, ΔP , directly measured using the differential pressure transducers versus those based on the difference in the measured boundary water pressures (i.e., $\Delta u = u_{bottom} - u_{top}$). No specific evidence was found supporting the difference in the relationship between u_{bottom} and u_{top} observed for the two test specimens during the 3.27 M NaCl stage.

2.3.2.6 Membrane Efficiency Coefficients

Membrane efficiency coefficients (ω_C and ω_{aw}) were calculated based on both $\Delta\pi_C$ and $\Delta\pi_{aw}$ to further examine the implications of basing the analysis on solute concentrations instead of the more thermodynamically accurate water activities; values of ω_C and ω_{aw} for each testing stage are listed in Table 2.3. Direct comparisons between ω_C and ω_{aw} via 1:1 plots based on both initial and average boundary concentrations are presented in Figs. 2.29 and 2.30, respectively. Similar to Fig. 2.22, differences between the two methods appear minor in the 1:1 plots,

especially due to the very small magnitudes (< 0.01) of the coefficients for the 640 mM KCl, 1.63 M NaCl, and 3.27 M NaCl stages. However, the inaccuracy of the van't Hoff expression (Eq. 2.3) at high concentrations becomes more apparent in terms of the ratio of ω_C to ω_{aw} and the error in ω_C relative to ω_{aw} versus solute concentration (Figs. 2.31 and 2.32). Because ω is inversely proportional to $\Delta\pi$ (Eq. 2.8), and because the same values of $-\Delta P_e$ were used to calculate ω_C and ω_{aw} , the values and trends shown in Figs. 2.31 and 2.32 are the inverse of those shown in Figs. 2.23 and 2.24. As previously concluded based on the analysis of $\Delta\pi_C$ compared to $\Delta\pi_{aw}$, results based on the activity method are more accurate for source concentrations greater than 0.1 M. Therefore, the values of ω reported and discussed hereafter were all based on water activities (i.e., $\omega = \omega_{aw}$).

Values of ω_{aw} for all stages of membrane testing conducted on the sand-bentonite specimens are presented in Table 2.3 and shown as a function of C_{ot} in Fig. 2.33. For the testing stages in this study (i.e., $C_{ot} \geq 160$ mM KCl), ω ranged from 0.000 to 0.032 for specimen RW-1 and from 0.000 to 0.031 for specimen RW-2. Values of ω were calculated for specimens RW-1 and RW-2 based on both source water activities (ω_o) and average boundary water activities (ω_{ave}). Although ω_o generally is more conservative than ω_{ave} , ω_{ave} is considered a more accurate assessment for cases where the specimen boundaries are not “perfectly flushed” (Malusis et al. 2001).

Membrane efficiency decreased as solutions of higher source concentrations were introduced to the top boundaries of the specimens and the thickness of the clay particle DDLs gradually were reduced, which was consistent with the expected trends based on previous studies (e.g., Kemper and Rollins 1966; Malusis and Shackelford 2002a; Kang and Shackelford 2010; Meier et al. 2014). The decrease in ω was nonlinear on a semi-log scale, similar to the trend

reported by Shackelford et al. (2016), with measurable membrane behavior (i.e. $\omega > 0.000$; Shackelford et al. 2016) persisting for source concentrations as high as 1.63 M NaCl. Note that despite that the ω for the 3.27 M NaCl stage for specimen RW-2 was negative due to the reversal in the direction of the measured pressure difference across the specimen (i.e. $-\Delta P_e < 0$), the ω was zero when rounded to three decimal places, and thus was plotted in Fig. 2.33 as zero.

Values of ω for specimens RW-1 and RW-2 generally were similar for the testing stages in this study, as shown in Fig. 2.34, with the magnitude of the difference between ω_{RW-1} and ω_{RW-2} , $\Delta\omega$, approaching zero for the later stages. However, this trend is the result of the small ω associated with high concentrations since the relative difference (percent error) between ω_{RW-1} and ω_{RW-2} was variable from one stage to the next and did not exhibit a distinct trend. Percent error ranged from about 0 % to 30 % with the exception of the 3.27 M NaCl stage, in which the error was nearly 400 % due to the larger relative difference between the positive ω_{RW-1} and the negative ω_{RW-2} . Nonetheless, the relatively small error reported for most testing stages is indicative of repeatable and reliable results. In addition, observed differences had little to no effect on the significance of the membrane behavior for low values of ω (e.g. $\omega \leq 0.03$). Note that the percent error was calculated based on unrounded values of ω , whereas the ω values listed in Tables 2.3 and 2.4 have been rounded to three decimal places such that small differences resulting from the use of distinct calculation methods (e.g., van't Hoff vs. activity method; initial concentration vs. average concentrations) may not be evident. Thus, the reported percent errors may be conservatively high due to the use of potentially insignificant digits in the calculations.

Results for ω again are presented in Fig. 2.35 to compare values calculated based on concentrations of the source solutions (ω_o) with those calculated based on average boundary concentrations (ω_{ave}). Values of ω_{ave} consistently were higher than values of ω_o , except for the 5

mM KCl stage for specimen RW-2; because specimen RW-2 was less flushed of soluble salts than specimen RW-1 prior to membrane testing, outward diffusion resulted in $C_t > C_{ot}$ such that, initially, $\Delta\pi_{ave} > \Delta\pi_o$, and thus $\omega_{ave} > \omega_o$ (Meier 2016). As C_{ot} increased, the difference between ω_o and ω_{ave} , $\Delta\omega$ ($= \omega_{ave} - \omega_o$), steadily decreased before becoming essentially zero for $C_{ot} \geq 160$ mM as shown in Fig. 2.36. Furthermore, whereas the percent error of ω_o relative to ω_{ave} was as high as 18 % for the 5-80 mM KCl stages conducted by Meier (2016), less than 8 % error was observed for both specimens for the stages conducted during this study ($C_{ot} \geq 160$ mM). The negligible difference between ω_o and ω_{ave} at high concentrations is even more apparent when the ω versus C_{ot} relationship is viewed on a log-log scale, as in Fig. 2.37 for the results from specimen RW-1. Although the values for specimen RW-2 could not be plotted in similar fashion (because $\omega < 0$ for the 3.27 M NaCl stage), a similar result can be expected based on the similarities in the values listed in Table 2.3.

For the 5 to 80 mM KCl stages, the use of TW instead of DIW as the bottom boundary circulation liquid was a contributing factor to the closeness of values reported for ω_o and ω_{ave} , since smaller differences between ΔC_o and ΔC_{ave} resulted from the presence of nonzero concentrations along the bottom boundary (i.e. $C_{ob} > 0$) (Meier 2016). However, such differences between ΔC_o and ΔC_{ave} are negligible relative to the large concentration gradients imposed in this study and thus are believed to have had no measurable effect on the resulting values of ω reported for the 160 mM KCl – 3.27 M NaCl stages.

2.3.3 Diffusion

2.3.3.1 Diffusive Mass Flux

Steady-state diffusion of the nonreactive solute (Cl⁻) was evaluated for specimens RW-1 and RW-2 for all testing stages in accordance with the procedure described in Section 2.2.5.2. Diffusive mass flux was characterized by inward diffusion of solutes at the top boundary of the specimen and outward diffusion at the bottom boundary, consistent with the direction of the concentration gradient imposed across the specimen. Therefore, the solute mass flux through the specimen was measured based on the concentrations (calculated based on the measured *EC*) of samples collected from the bottom boundary circulation outflow (C_b). Meier (2016) measured a relatively low background Cl⁻ concentration of 0.11 mM in the tap water circulated across the bottom boundary, which was subtracted from C_b to determine the increase in the concentration attributable to solute mass flux through the specimen. Failure to account for the background concentration would result in slightly higher, and thus more conservative, values of the accumulated solute mass per unit area, Q_t . However, because the magnitude of the background concentration was only 1.4 % of the lowest steady-state C_b value reported for this study (e.g. $C_b = 8.0$ mM, for $C_{ot} = 160$ mM KCl) differences between membrane testing and diffusion results obtained with or without having accounted for background Cl⁻ concentrations were negligible.

Values of Q_t for specimen RW-1 following each two-day circulation cycle are plotted versus the cumulative time, t , in Fig. 2.38, including results from the beginning of the 160 mM KCl stage and onward. Cumulative solute mass fluxes were not available for specimen RW-2 because bottom boundary effluent samples were not continuously collected for this specimen during the 5-80 mM KCl stages conducted by Meier (2016). Therefore, no results for Q_t for specimen RW-2 are reported in this document, although a similar trend in Q_t as that observed

with specimen RW-1 would be expected. Values of Q_t consistently increased from one circulation cycle to the next due to the continual diffusion of solutes into the bottom boundary circulation liquid, ranging from approximately 60 g/m^2 at the start of the 160 mM KCl stage to greater than 3000 g/m^2 by the end of the 3.27 M NaCl stage. After slowly increasing throughout the 160-640 mM KCl stages, Q_t increased at a distinctly higher rate for the final two testing stages for two primary reasons, i.e., the greater imposed concentration gradients driving solute diffusion through the specimen as well as reduced DDL thicknesses resulting from the introduction of the highly concentrated NaCl solutions to the system.

To evaluate and compare diffusion behavior for each individual testing stage, Q_t and t were separated into a series of net cumulative values relative to the beginning of the given stage, Q_t' and t' , calculated as follows (e.g. Bohnhoff and Shackelford 2015; Meier 2016):

$$Q_t' = Q_{t,x+1} - Q_{t,x} \quad (2.21)$$

$$t' = t_{x+1} - t_x \quad (2.22)$$

where $Q_{t,x}$ represents the value of Q_t at the end of the previous stage, $Q_{t,x+1}$ represents the value of Q_t at the end of a given time increment during the current stage, t_x represents the total elapsed time prior to the start of the current stage, and t_{x+1} represents the total elapsed time to the end of a given time increment within the current stage. By converting Q_t and t to net values, the diffusion analysis is limited to a single stage such that a distinct D^* can be determined on the basis of the solute flux accumulated within the time frame of a specific stage. The resulting plots of Q_t' versus t' are presented for the 160 mM KCl through 3.27 M NaCl stages in Fig. 2.39 (specimen RW-1) and Fig. 2.40 (specimen RW-2). Values of Q_t' quickly achieved steady state (e.g. within

approximately three to four circulation cycles) due to the nonreactive nature of the Cl^- anions. In the case of the reactive solute (e.g. K^+ or Na^+), a longer period of transient diffusion generally would be expected relative to that observed for the nonreactive solute due to interactions with the negatively charged clay particle surfaces (e.g. Malusis and Shackelford 2002b; Bohnhoff and Shackelford 2015).

The slope of the steady-state portion of the Q_t' versus t' data (i.e. $\Delta Q_t'/\Delta t'$) increased as the concentration difference across the specimen, $-\Delta C_{\text{Cl}^-}$ (> 0), was increased with each successive testing stage, as shown for both specimens in Fig. 2.41 (also see Table 2.4). Higher imposed concentration differences generally are expected to result in higher values of $\Delta Q_t'/\Delta t'$ because of the corresponding increase in the “driving force” behind diffusion (i.e., the concentration gradient), which leads to a faster rate of transport and thus a greater amount of solutes migrating through the specimen during a given time increment. The rate of the increase in values of $\Delta Q_t'/\Delta t'$ (i.e., the slope of $\Delta Q_t'/\Delta t'$ vs. $-\Delta C_{\text{Cl}^-}$) for specimen RW-1 gradually decreased throughout the 5-80 mM KCl stages before maintaining a steady state for the remainder of testing. A similar, relatively steady increase in $\Delta Q_t'/\Delta t'$ was observed for specimen RW-2, though the trend at lower concentrations remains unknown because diffusion behavior was not evaluated for that specimen during the testing stages conducted by Meier (2016). Because the observed increase in $\Delta Q_t'/\Delta t'$ with respect to $-\Delta C_{\text{Cl}^-}$ is linear at higher concentrations, changes in the restrictive capacity of the clay (i.e., changes in the degree of membrane behavior) resulting from compression of DDLs at low values of ω appear to have no measurable influence on the diffusive mass flux through the specimens. Therefore, changes in $\Delta Q_t'/\Delta t'$ likely were only dependent on changes in the boundary conditions since changes within the clay pores essentially were negligible.

The aforementioned trends in $\Delta Q_t'/\Delta t'$ are the same when plotted as a function of the difference in source Cl^- concentrations ($-\Delta C_{o,\text{Cl}^-}$) or as the difference in the average Cl^- concentrations at the specimen boundaries ($-\Delta C_{\text{ave},\text{Cl}^-}$). Additionally, as shown in Fig. 2.42, $\Delta Q_t'/\Delta t'$ increased at nearly the same rate during the steady-state period for both specimens RW-1 and RW-2. However, $\Delta Q_t'/\Delta t'$ for specimen RW-2 consistently was slightly higher than $\Delta Q_t'/\Delta t'$ for specimen RW-1, with the percent difference ranging from about 24 % for the 160 mM KCl stage to 9.4 % for the 3.27 M NaCl stage. The higher values of $\Delta Q_t'/\Delta t'$ for specimen RW-2 compared to specimen RW-1 were consistent with a lower degree of solute restriction, as shown by the slightly lower values of ω measured for specimen RW-2 than for specimen RW-1 (see Table 2.3), in addition to the greater increase in C_b relative to C_{ob} measured for specimen RW-2 than for specimen RW-1 (see Fig. 2.17).

2.3.3.2 Effective Diffusion Coefficients

The D^* from each testing stage calculated based on the steady-state portion of the Q_t' versus t' relationship and Eq. 2.15 are presented as a function of C_{ot} in Fig. 2.43. For specimen RW-1, D^* initially increased from about $6 \times 10^{-11} \text{ m}^2/\text{s}$ to about $2.5 \times 10^{-10} \text{ m}^2/\text{s}$ as C_{ot} increased from 5 mM to 80 mM KCl, after which D^* remained relatively constant for the remaining membrane testing stages. Steady values of D^* also were observed for specimen RW-2 for the same values of $C_{ot} \geq 160 \text{ mM KCl}$. The rate of increase in D^* lessened over the course of the 5-80 mM KCl stages (Meier 2016) and abruptly transitioned to steady values of D^* during this study. This abrupt transition was not the result of differences in the methods used to obtain boundary Cl^- concentrations [e.g., the use of ion chromatography (IC) testing by Meier (2016) as opposed to the use of *EC* calibration curves in this study] because predicted concentrations for

the 80 mM KCl stage were slightly higher than the measured concentrations obtained from IC testing (e.g., see Fig. 2.7). Higher predicted concentrations would result in higher D^* than those shown in Fig. 2.43a such that the transition would appear even more sudden. Therefore, the lack of a smooth transition is hypothesized to be the result of sensitivity to measurement error, especially given the small magnitude of the difference ($\leq 0.2 \times 10^{-10} \text{ m}^2/\text{s}$) between the D^* values measured for the 80 mM and 160 mM KCl stages. Values of D^* calculated based on source Cl⁻ concentrations (D^*_{o}) were similar to those calculated based on average boundary Cl⁻ concentrations (D^*_{ave}), with a maximum difference of $0.3 \times 10^{-10} \text{ m}^2/\text{s}$ for any given stage. Similar values of D^*_{o} and D^*_{ave} are expected at higher concentrations since changes in the concentrations of the circulating liquids along each specimen boundary resulting from solute diffusion are relatively small compared to the much larger concentration differences imposed across the entire specimen.

Additionally, a comparison of the results for specimens RW-1 and RW-2 (Fig. 2.44) shows small differences ($\leq 0.6 \times 10^{-10} \text{ m}^2/\text{s}$) in the D^* values calculated for each specimen. However, consistently higher values are observed for specimen RW-2 than for specimen RW-1 because of the greater diffusive mass flux measured for specimen RW-2, which may have been due to specimen RW-2 being more flushed of soluble salts than specimen RW-1 was prior to the start of membrane testing (Meier 2016). A slight decrease (between 0.2 and $0.4 \times 10^{-10} \text{ m}^2/\text{s}$) in D^* between the 640 mM KCl and 1.63 M NaCl stages was observed for both specimens, hypothesized to be due to the larger hydrated radius (and thus increased possibility of restriction) of Na⁺ relative to K⁺.

Values of D^* also are plotted as a function of ω for both specimens in Figs. 2.45 and 2.46. For specimen RW-1, ω greater than approximately 0.06 corresponded to lower D^* , consistent

with the expected trend of decreased solute restriction for a material with a higher membrane efficiency and increased solute restriction for a material with a lower membrane efficiency. However, instead of a continual increase in D^* in conjunction with the gradual destruction of membrane behavior within the specimen, D^* remained unchanged as ω decreased from approximately 0.06 to the limiting value (~ 0.000), suggesting that additional decreases in the membrane efficiency of a material that already exhibits a low degree of membrane behavior may have a negligible effect on the transport of charged solutes through the material. Values of D^* for specimen RW-2 also were relatively constant for values of ω less than approximately 0.03 (the maximum measured ω for that specimen), with the exception of the previously noted decrease in D^* for the 1.63 M NaCl stage, thus providing further support for the hypothesis that changes in low ω values (e.g. $\omega \sim 0.06$ or less) have no measurable effect on diffusion behavior.

Extrapolated pore diffusion coefficients, D_p , determined by Meier (2016) based on both the D_o^* versus ω_o and D_{ave}^* versus ω_{ave} data (i.e. $D_{p,o}$ and $D_{p,ave}$, respectively) also are shown in Fig. 2.45. The extrapolation was a linear extension of the line between the final two data points from that study (i.e. the 40 mM and 80 mM KCl stages) and thus was created under the assumption that D^* would continue to increase at a steady rate until membrane behavior was eliminated. However, deviation from this expected trend is evident at the low ω values (< 0.05) reported for this study, represented by the open symbols in Fig. 2.45a. The end result was measured values of $D_{p,o}$ and $D_{p,ave}$ 1.0×10^{-10} m²/s lower than the respective extrapolated values for specimen RW-1.

Because diffusion coefficients are not only a function of the material properties, but also of the diffusing chemical species (Shackelford and Daniel 1991), distinct $D_{p,o}$ and $D_{p,ave}$ were determined based on the diffusing salt for different periods of membrane testing in this study.

Fig. 2.46 consists of linear-scale D^* versus ω plots for both specimens used to determine $D_{p,o}$ and $D_{p,ave}$ based on both KCl and NaCl solutions, which then could be used in conjunction with the appropriate D^* and D_o values to accurately calculate the tortuosity factors for each testing stage using Eq. 2.19. Whereas $D_{p,o}$ and $D_{p,ave}$ for NaCl were directly measured in this study since membrane behavior was eliminated during exposure of the specimens to NaCl solutions, $D_{p,o}$ and $D_{p,ave}$ for KCl were estimated using the same approach implemented by Meier (2016), i.e., by extrapolating the line between the final two data points from the period of KCl circulation (i.e., between the 320 mM and 640 mM KCl stages). For specimen RW-1, extrapolated $D_{p,o}$ and $D_{p,ave}$ for KCl were the same as those measured for NaCl. However, for specimen RW-2, extrapolated $D_{p,o}$ and $D_{p,ave}$ for KCl were larger than the measured values for NaCl by $0.2 \times 10^{-10} \text{ m}^2/\text{s}$.

2.3.3.3 Tortuosity Factors

Apparent tortuosity factors, τ_a , were calculated by Eq. 2.16 as the ratio of the measured D^* for Cl^- (i.e. the nonreactive solute) to the free-solution diffusion coefficient for the salt species in aqueous solution, D_o . Accordingly, τ_a is a measure of the effectiveness of a porous medium at reducing the diffusive solute mass flux relative to that which would exist in the absence of the porous medium (Shackelford and Moore 2013). Values of τ_a range from 0 to unity (i.e. $0 \leq \tau_a \leq 1$) with lower values representing a more tortuous pathway and lower rates of solute diffusion, and higher values representing a less tortuous pathway allowing for higher rates of solute diffusion. Although the D_o corresponding to the self-diffusion coefficient of the nonreactive tracer (e.g. $2.03 \times 10^{-9} \text{ m}^2/\text{s}$ for Cl^-) commonly has been used in place of the D_o for the salt (e.g., $1.993 \times 10^{-9} \text{ m}^2/\text{s}$ for KCl; $1.610 \times 10^{-9} \text{ m}^2/\text{s}$ for NaCl) for calculating τ_a , this approach assumes a scenario of infinite dilution characterized by the lack of interaction between co-diffusing anions

and cations (Shackelford and Daniel 1991). Because the solutions used in this study were neither ideal nor infinitely dilute, consideration of electroneutrality was required to account for the drag exerted on the Cl^- anion by the more slowly diffusing cation. Therefore, calculations of tortuosity factors for each testing stage, including the matrix and restrictive tortuosities (τ_m and τ_r , respectively), were performed using the D_o for the salt solution used in the given stage, i.e., $19.93 \times 10^{-10} \text{ m}^2/\text{s}$ for the 160-640 mM KCl stages and $16.10 \times 10^{-10} \text{ m}^2/\text{s}$ for the 1.63 M and 3.27 M NaCl stages (Shackelford and Daniel 1991).

The resulting τ_a , including those based on both D_o^* and D_{ave}^* (i.e., $\tau_{a,o}$ and $\tau_{a,ave}$ respectively) are summarized in Table 2.4. For specimen RW-1, $\tau_{a,o}$ and $\tau_{a,ave}$ increased from 0.03 to 0.15 and from 0.03 to 0.16, respectively, as C_{ot} increased from 5 mM KCl to 3.27 M NaCl, which was consistent with the trends observed in previous studies (e.g., Shackelford et al. 2016). However, the results were nearly constant for C_{ot} greater than 80 mM KCl, with slightly higher (e.g., by magnitudes of 0.01-0.02) τ_a reported for the 1.63-3.27 M NaCl stages relative to the 160-640 mM KCl stages. This trend is directly related to the trends previously noted for the calculated D^* values with increasing C_{ot} (see Fig. 2.43). Similar results were reported for specimen RW-2, as values of $\tau_{a,o}$ and $\tau_{a,ave}$ remained steady for an increase in C_{ot} from 160-640 mM KCl and were slightly higher (e.g., by 0.01-0.02) for the 1.63-3.27 M NaCl stages.

The apparent tortuosity factor, τ_a , also can be defined as the product of the matrix tortuosity factor, τ_m , and the restrictive tortuosity factor, τ_r , as defined in Eq. 2.17 (Malusis and Shackelford 2002b; Shackelford and Moore 2013; Shackelford 2014). The matrix tortuosity factor, which only accounts for the reduction in the diffusive mass flux based on the geometry and interconnectedness of pores within the porous medium, can be calculated in accordance with Eq. 2.19 as the ratio of D_p to D_o . Contrary to τ_a , τ_m generally is hypothesized to be unique for a

given porous medium and thus independent of changes in C_{or} and ω (Shackelford et al. 2016). However, five distinct τ_m (summarized in Table 2.4) were determined for the sand-bentonite tested in this study, including three values for specimen RW-1 and two for specimen RW-2.

Because the $D_{p,o}$ and $D_{p,ave}$ values predicted in the study by Meier (2016) based on extrapolating the KCl data for specimen RW-1 were higher than those determined in this (e.g. $3.4 \times 10^{-10} \text{ m}^2/\text{s}$ and $3.5 \times 10^{-10} \text{ m}^2/\text{s}$ vs. $2.4 \times 10^{-10} \text{ m}^2/\text{s}$ and $2.5 \times 10^{-10} \text{ m}^2/\text{s}$, respectively), the resulting $\tau_{m,o}$ and $\tau_{m,ave}$ values reported by Meier (2016) also were higher than those reported in this study (e.g. 0.17 and 0.18 vs. 0.12 and 0.13, respectively). Ultimately, the $D_{p,o}$ and $D_{p,ave}$ (and thus the associated $\tau_{m,o}$ and $\tau_{m,ave}$) determined in this study likely are more representative than those determined by Meier (2016) since the ω values are much closer to the limiting value ($\omega = 0$), such that potential error associated with extrapolation of the D^* versus ω curve likely is lower. An additional set of $\tau_{m,o}$ and $\tau_{m,ave}$ values reported for specimen RW-1 resulted from the use of NaCl solutions instead of KCl solutions during the final two testing stages. Although the measured $D_{p,o}$ and $D_{p,ave}$ values at $\omega = 0$ for the 3.27 M NaCl stage were the same as those extrapolated from the KCl data (see Fig. 2.46a), the lower value of D_o for NaCl relative to KCl ($16.10 \times 10^{-10} \text{ m}^2/\text{s}$ vs. $19.93 \times 10^{-10} \text{ m}^2/\text{s}$) resulted in higher calculated values of $\tau_{m,o}$ and $\tau_{m,ave}$ (0.15 and 0.16 vs. 0.12 and 0.13, respectively). Unlike specimen RW-1, measured values of $D_{p,o}$ and $D_{p,ave}$ for specimen RW-2 were lower for NaCl than for KCl (e.g. $2.6 \times 10^{-10} \text{ m}^2/\text{s}$ and $2.8 \times 10^{-10} \text{ m}^2/\text{s}$ vs. $2.8 \times 10^{-10} \text{ m}^2/\text{s}$ and $3.0 \times 10^{-10} \text{ m}^2/\text{s}$, respectively). However, the measured decrease in D_p was not sufficiently large to offset the difference in the D_o values for KCl and NaCl and maintain a constant ratio of D_p to D_o (i.e. constant τ_m). Similar increases in $\tau_{m,o}$ and $\tau_{m,ave}$ were observed following the switch to NaCl for specimen RW-2 as were observed for specimen RW-1, with $D_{p,o}$ and $D_{p,ave}$ increasing from 0.14 to 0.16 and from 0.15 to 0.17, respectively.

Restrictive tortuosity factors, τ_r ($0 \leq \tau_r \leq 1$), which represent the effect of all factors other than pore geometry and interconnectivity that may act to limit solute diffusion through a porous medium, such as semipermeable membrane behavior or ion sorption (Malusis and Shackelford 2002c; Shackelford and Moore 2013; Shackelford 2014), were calculated in accordance with Eq. 2.19 and are summarized in Table 2.4. The $\tau_{r,o}$ and $\tau_{r,ave}$ calculated based on D_o^* and D_{ave}^* , respectively, for specimen RW-1 both increased from 0.19 to 1.00 as C_{ot} increased from 5 mM KCl to 3.27 M NaCl. This trend is consistent with the gradual destruction of membrane behavior within the specimen, as indicated by the observed decrease in ω with increasing C_{ot} , resulting in the pathways for diffusion becoming less restrictive as the ion exclusion effects of the electrostatic DDLs became negligible at higher concentrations. In accordance with the observed trends in D_o^* and D_{ave}^* , $\tau_{r,o}$ and $\tau_{r,ave}$ were relatively constant for C_{ot} greater than 80 mM, apart from a slight decrease during the 1.63 M NaCl stage which can be attributed in part to the lower D_o for NaCl compared to that of KCl. Similar trends in the results for $\tau_{r,o}$ and $\tau_{r,ave}$ were observed for specimen RW-2, as indicated by values equal to the limiting condition (i.e. $\tau_r = 1$) for all testing stages other than the 1.63 M NaCl stage, in which $\tau_{r,o}$ and $\tau_{r,ave}$ decreased to 0.94 and 0.97, respectively.

Results for τ_r also were plotted versus calculated ω , as shown in Figs. 2.48 and 2.49. In contrast to the linear relationship (i.e. $\tau_r = 1 - \omega$) proposed by Manassero and Dominijanni (2003) for GCL specimens, values of τ_r for specimen RW-1 reported by Meier (2016) exhibited a nonlinear trend with increasing ω and were significantly lower than the expected values of τ_r based on the $\tau_r = 1 - \omega$ function. Values of $\tau_{r,o}$ and $\tau_{r,ave}$ for specimen RW-1 for the testing stages in this study also were lower than expected, yet did appear to more closely follow the expected linear relationship, with the exception of the reported values for the 1.63 M NaCl stage which

exhibited a deviation from the apparent trend in the results observed for the other four stages (see Fig. 2.48b). Alternatively, most of the τ_r calculated for specimen RW-2 (see Fig. 2.49b) plotted above expected values as a result of the constant values of τ_r ($= 1$) reported for all stages not including the 1.63 M NaCl stage, in which τ_r were lower than expected in a manner similar to results for specimen RW-1.

Meier (2016) attributed the lower than anticipated τ_r to the lingering presence of unflushed soluble metals (other than K^+) in the pore fluid during the earlier testing stages (i.e. for $C_{ot} \leq 40$ mM KCl), such that diffusion of Cl^- through the sand-bentonite specimens was suppressed due to the charge contribution of the additional ions and the associated electroneutrality constraint. Furthermore, the use of tap water as the circulating solution along the bottom boundary of the specimen may have resulted in the diffusion of additional ions into the specimen pores that further contributed to the electroneutrality constraint (Meier 2016). GCL specimens tested for membrane and diffusion behavior by Shackelford et al. (2016) also were not fully flushed of soluble salts and exhibited similar trends in τ_r versus ω (see Figs. 2.50 and 2.51), providing further evidence of the effect of relatively uncontrolled pore water and boundary chemistry on measured τ_r (Meier 2016). In contrast to Meier (2016) and Shackelford et al. (2016), Malusis et al. (2015) reported results for diffusion of KCl that generally were in good agreement with the expected $\tau_r = 1 - \omega$ relationship. However, that study involved the use of a GCL specimen that was fully flushed of soluble salts via permeation with DIW as well as the use of DIW as the liquid circulated along the lower boundary, thus suggesting that the lack of complicated pore water chemistry likely was a key factor to the observed τ_r versus ω relationship.

Shackelford (2016) also attributed the lower than anticipated values of τ_r to possible increases in τ_m resulting from changes in the micro-fabric of the interconnected pores at relatively high concentrations, contrary to the typical assumption that τ_m is unique and independent of solute concentration for diffusion through a given porous medium. Increased τ_a with increasing C_{ot} thus could be attributed to higher τ_m rather than the lower τ_r associated with the observed nonlinear trend (Shackelford 2016). The possibility of such changes in τ_m also was proposed by Malusis and Shackelford (2002a) to explain measured increases in D^* with increasing C_{ot} in the absence of any solute exclusion due to membrane behavior as reported by Lake and Rowe (2000). The observed increase in τ_m from this study, which was evident in both specimens subjected to membrane and diffusion testing, also supports the hypothesis that the typical assumption of a constant τ_m (e.g., Shackelford and Moore 2013; Shackelford 2014) may not necessarily be true.

The better agreement between measured and expected τ_r observed during the testing stages for specimen RW-1 in this study compared to Meier (2016) may be a result of the negligible effects of using TW instead of DIW as the bottom boundary solution when C_{ot} is relatively high, as previously discussed in Section 2.3.2.6. Whereas additional electroneutrality constraints may have had a sufficiently large effect to alter the pore water chemistry and suppress Cl^- diffusion through the sand-bentonite specimens during the testing stages conducted by Meier (2016), such factors likely would have had a negligible effect on Cl^- diffusion through the same specimens at the concentrations used in this study due to the dominant presence of K^+ and Na^+ in the pore water. The same general agreement with expected values observed for specimen RW-1 in this study was not observed for specimen RW-2, since τ_r were equal to 1 for all stages aside from the 1.63 M NaCl stage, as previously discussed. Nearly constant values of τ_r

with a continued decrease in ω were unexpected, since the measurement of some degree of membrane efficiency is assumed to be representative of a comparable degree of solute exclusion within the pore space, which then should be accounted for in τ_r . The results provide inconclusive evidence that membrane efficiencies less than approximately 3 % may have no effect on the resulting diffusive solute flux, which is inconsistent with results reported for specimen RW-1 in this study (e.g., $\tau_{r,o} = 0.96$ for $\omega_o = 3.1$ %) as well as results reported by Shackelford et al. (2016) (e.g., $\tau_{r,o} = 0.82$ for $\omega_o = 3.4$ %). Therefore, the reliability of the results for specimen RW-2 remains uncertain.

2.3.4 *Effect of NaCl versus KCl*

Multiple-stage membrane and diffusion testing typically is conducted by exposing test specimens to aqueous solutions with increasing concentrations of the same chemical species (Malusis and Shakelford 2002a; Kang and Shackelford 2009; Shackelford and Scalia 2016). The change in the salt solutions introduced to the specimens in this study from KCl to NaCl during the final two testing stages, which occurred due to human error in the laboratory, thus was atypical compared to previous studies consisting of multiple-stage membrane and/or diffusion testing (e.g., Kemper and Rollins 1966; Malusis and Shakelford 2002a,c; Kang and Shackelford 2010b; Bohnhoff 2012; Meier et al. 2014; Bohnhoff and Shackelford 2015; Meier 2016; Shackelford et al. 2016). However, this error is not believed to have had a compromising effect on the overall results of the study.

Because both KCl and NaCl solutions contain monovalent cations (K^+ and Na^+ , respectively), the relative contribution of ion valence effects to changes in the thickness of the DDLs surrounding the individual bentonite particles likely remained unchanged following the

switch to NaCl in this study. Thus, the potential for observable membrane behavior existed at a similar level for NaCl solutions as for KCl. However, effects were observed in the diffusion results that may have been attributable to characteristic differences between K^+ and Na^+ .

The observed decrease in D^* between the 640 mM KCl stage and the 1.63 M NaCl stage for both specimens RW-1 and RW-2 (see Fig. 2.43) may have been a result of the larger hydrated radius of Na^+ relative to that of K^+ , as indicated by the lyotropic series, since movement of ions with larger hydrated radii generally will be restricted to a greater extent for a given pore size (Malusis and Shackelford 2002a). The increased restriction of Na^+ compared to K^+ is evident in the lower D_o for NaCl relative to D_o for KCl ($16.10 \times 10^{-10} \text{ m}^2/\text{s}$ vs. $19.93 \times 10^{-10} \text{ m}^2/\text{s}$), which accounts for the greater drag exerted by diffusing Na^+ ions on the codiffusing Cl^- ions than would be exerted by K^+ (Shackelford and Daniel 1991). Given this hypothesis, and assuming the relatively steady trend in D^* observed for the 160-640 mM KCl stages would have continued through the 1.63 M stage prior to increasing upon destruction of membrane behavior, then the measured D^* for the 1.63 M and 3.27 M NaCl stages can be shifted upward by an amount corresponding to the magnitude of the decrease observed following the 640 mM KCl stage to estimate the D^* values that might have resulted in the absence of the switch from KCl to NaCl. As shown in Fig. 2.52, the resulting trend in D^* versus ω would more closely resemble that observed by Shackelford et al. (2016), since the increase in D^* at the limiting value for each set of data shown in Fig. 2.52 is consistent with the observation by Shackelford et al. (2016) that estimates of D_p based on extrapolation of the trend in D^* versus ω (e.g., see Section 2.3.3.2) are unconservatively low relative to the true D_p .

The degree of observed membrane behavior in a porous material also can be affected by the hydrated radius of the diffusing salt species. According to Malusis and Shackelford (2002a),

ω generally tends to increase for bentonite specimens with the use of NaCl solutions relative to the use of KCl solutions in accordance with the greater restriction of Na^+ compared to K^+ , assuming all other factors are the same. Therefore, the use of NaCl solutions for the final two testing stages in this study may have resulted in greater persistence of membrane behavior than would have occurred with the use of KCl solutions, though such an effect was not measured within the accuracy of this study. Although this would result in an unconservatively high ω for the 1.63 M NaCl stage, as well as an unconservatively high threshold concentration associated with the limiting value of ω (i.e., $\omega = 0$), the results from membrane testing in this study nonetheless indicate that measurable membrane behavior can persist for bentonite-based materials in the presence of monovalent salt solutions at much higher concentrations than previously thought.

2.3.5 Comparison with Previous Research on Limiting Membrane Behavior

Only one previous study has provided experimental evidence quantifying the limiting membrane and diffusion behavior of bentonite-based materials with a monovalent salt (e.g., Shackelford et al. 2016); consequently, limited data was available for comparison with results from this study. The data shown in Fig. 2.53 have similar trends in ω with increasing C_{ot} for the two studies, i.e., a nonlinear decrease as C_{ot} approaches the threshold value, which is consistent with trends reported by previous studies (e.g., Kemper and Rollins 1966; Dominijanni et al. 2013) for low values of ω (e.g., ω less than approximately 0.1 – 0.2) corresponding to concentrations near the threshold value. Although ω decreased at a similar rate for each set of data in Fig. 2.53, ω_o and ω_{ave} measured by Shackelford et al. (2016) consistently were lower than ω_o and ω_{ave} measured in this study such that the resulting threshold salt concentration for limiting

membrane behavior also was much lower than that observed in this study (i.e., 400 mM KCl vs. 3.27 M NaCl). As a result, membrane behavior may be more relevant in waste containment applications than previously expected. However, additional research is needed to determine the persistence and relevance of membrane behavior for sand-bentonite mixtures exposed to more aggressive (and potentially more realistic) solutions, such as those containing chemical species with multivalent ions, similar to those that may be encountered in many practical waste containment applications.

This relatively large difference in the observed threshold concentrations likely was a direct result of the different materials tested for each study; whereas compacted sand-bentonite specimens were tested in this study, Shackelford et al. (2016) conducted membrane and diffusion testing on a GCL specimen with a distinctly different porosity and bentonite content than the specimens in this study. Materials with lower porosities have been shown to result in higher membrane efficiencies due to the reduced void space available for solute migration (Fritz 1986; Malusis and Shackelford 2002a), thus the much lower porosity, n , measured for the sand-bentonite specimens relative to the GCL (e.g., $n = 0.34$ vs. 0.79) likely was a contributing factor to the higher membrane efficiencies reported in this study. However, because materials containing a greater percentage (by dry weight) of bentonite typically exhibit increased membrane behavior (Shackelford 2012, 2013; Shackelford and Moore 2013), the relatively high bentonite content of the GCL specimen compared to the sand-bentonite specimens (e.g., 100 % vs. 15 %) likely offset much of the potential reduction in membrane efficiency resulting from the higher porosity. Overall, similarities in the measured D_o^* and D_{ave}^* for the sand-bentonite and GCL specimens (e.g., Fig. 2.52) may indicate that the bentonite content of 15 % was sufficiently high to dominate the void space between the sand particles, thus reducing the diffusive solute

flux and enhancing membrane behavior within the specimens to a greater extent than has been observed for specimens comprising 100 % bentonite due to the added effect of the inert sand matrix.

2.4 Conclusions

The primary objective of this study was to evaluate the extent to which specimens of a compacted sand-bentonite (SB) mixture comprising 15 % bentonite acted as semipermeable membranes in the presence of increasing salt concentrations. The limit of membrane behavior was determined based on the top boundary source concentration, C_{ot} , that resulted in the complete destruction of the solute exclusion capabilities of the test specimens. Based on the experimental results presented in this study, which are believed to represent the first evaluation of limiting membrane behavior of a compacted sand-bentonite mixture, observable membrane behavior persisted until specimens were exposed to a NaCl concentration of 3.27 M, which is far higher than the threshold concentration of 400 mM KCl previously reported for sodium bentonite-based GCLs exposed to simple, monovalent salt solutions. The membrane efficiency coefficient, ω , decreased as C_{ot} increased, with the trend in ω versus $\log(C_{ot})$ being nonlinear as C_{ot} approached the threshold concentration; this trend previously had been observed, though experimental evidence are limited. As a result, the observed threshold concentration was higher than that which would have been predicted based on extrapolation of the semi-log linear relationship typically observed at lower concentrations, which had been a common practice for estimating the limits of membrane behavior. Therefore, membrane behavior may be more relevant in chemical containment applications than previously thought, since a clay barrier with a higher threshold concentration will restrict solute migration for a broader range of potential

contaminant concentrations compared to a barrier with a lower threshold concentration, for which the existence of membrane behavior would be less likely at a given contaminant concentration.

The ability of the SB specimens to restrict diffusion of the nonreactive solute (Cl^-) was evaluated during membrane testing. Effective diffusion coefficients, D^* , reported for the testing stages consisting of $160 \text{ M KCl} \leq C_{ot} \leq 3.27 \text{ M NaCl}$ were relatively constant for both test specimens, indicating that the corresponding decrease in ω from an average of 0.032 to 0.000 had little to no effect on the diffusive rate of Cl^- . Also, previously observed effects on the diffusion of Cl^- of additional cations (e.g., Ca^{2+} , Mg^{2+}), introduced to the system via the tap water circulated along the bottom of the specimens, were shown to be negligible due to the dominant presence of relatively high concentrations of K^+ and Na^+ cations introduced to the system via the source KCl and NaCl solutions circulated along the top of the specimens.

Whereas the van't Hoff expression was an appropriate method for approximating the theoretical chemico-osmotic pressure difference across the specimen, $\Delta\pi$, for lower concentration gradients ($< 100 \text{ mM}$) imposed during previous studies on membrane behavior, the solutions used to establish the relatively high concentration gradients in this study were not sufficiently dilute to satisfy the conditions required for use of this approximation method (i.e., that the solutions are ideal and dilute). Therefore, an alternative method (designated as the activity method) was used in which $\Delta\pi$ was calculated based on the difference in the water activities of the solutions separated by the specimens. A comparison of $\Delta\pi$ calculated using the van't Hoff expression ($\Delta\pi_C$) with $\Delta\pi$ calculated using the activity method ($\Delta\pi_{aw}$) for each of the testing stages in this study resulted in observed percent differences as high as approximately 15%. As a result, ω was reported for each stage based on $\Delta\pi_{aw}$. However, because the resulting

values of ω in this study were small (≤ 0.032), the aforementioned error in $\Delta\pi_C$ compared to $\Delta\pi_{aw}$ appeared to have a negligible effect on the calculated ω . The observed percent difference likely would have a greater effect for a material that exhibited an enhanced degree of membrane behavior at concentrations similar to those in this study. For example, bentonites that have either been treated with additives to increase chemical resistance (e.g., polymerized bentonites) or compressed to higher densities may exhibit membrane efficiencies much closer to 100 % when exposed to a similar range of chemical concentrations as that in this study, such that a percent error of 15 % could result in calculated ω varying by as much as 0.15.

This study is at the forefront of efforts to quantify limiting membrane behavior for bentonite-based materials used in chemical containment applications. Thus, considerably more research still is required before the extent to which clays act as effective membranes can be fully understood. In particular, limiting membrane behavior of modified bentonites with enhanced membrane capabilities (e.g., due to polymerization or low void ratios) should be further explored, since these types of materials would be more likely to exhibit membrane efficiencies that are more relevant for waste containment applications involving more aggressive contaminants, such as those containing multivalent ions, that may thus represent a more realistic containment scenario than the monovalent chemical species used in this study.

Table 2.1. Chemical properties of tap water used in this study.

Chemical Property	Value	
pH	6.9	
Electrical Conductivity, EC (S/m)	0.0119	
*Anion Concentrations ^a [mg/L (mM)]	Cl ⁻	3.7 (0.10)
	F ⁻	0.7 (0.04)
	HCO ₃ ⁻	24.4 (0.40)
	SO ₄ ²⁻	11.7 (0.12)
*Cation Concentrations ^b [mg/L(mM)]	Ca ²⁺	16.1 (0.40)
	Mg ²⁺	2.3 (0.095)
	Na ⁺	3.5 (0.15)
	K ⁺	0.7 (0.018)

* Concentrations obtained from Meier (2016).

^a Based on ion chromatography analysis performed by the Soil, Water and Plant Testing Laboratory, CSU, Fort Collins, CO.

^b Based on inductively coupled plasma-atomic emission spectrometry analysis performed by the Soil, Water and Plant Testing Laboratory, CSU, Fort Collins, CO.

Table 2.2. Summary of results obtained using the van't Hoff method ($\Delta\pi_C$, ω_C) and using the activity method ($\Delta\pi_{aw}$, ω_{aw}).

Specimen Designation	Solute	Source Concentration, C_{or} (mM)		Maximum Chemico-Osmotic Pressure Difference, $\Delta\pi_o$ (kPa)		Maximum Chemico-Osmotic Pressure Difference, $\Delta\pi_{ave}$ (kPa)		Membrane Efficiency Coefficient, ω_o		Membrane Efficiency Coefficient, ω_{ave}	
		Target	Measured or Predicted ^a	$\Delta\pi_{C,o}$	$\Delta\pi_{aw,o}$	$\Delta\pi_{C,ave}$	$\Delta\pi_{aw,ave}$	$\omega_{C,o}$	$\omega_{aw,o}$	$\omega_{C,ave}$	$\omega_{aw,ave}$
RW-1	KCl	5	5.02	22.2	22.2	21.0	21.0	0.423	0.423	0.448	0.448
		10	10.2	47.3	47.3	42.1	42.1	0.258	0.258	0.290	0.290
		20	20.4	94.1	94.1	82.4	82.4	0.163	0.163	0.186	0.186
		40	42.2	203	203	172	172	0.102	0.102	0.120	0.120
		80	82.1	399	399	339	339	0.064	0.064	0.075	0.075
		160	174	861	822	819	802	0.030	0.032	0.032	0.032
		320	329	1628	1491	1538	1444	0.015	0.017	0.016	0.017
		640	681	3378	3070	3182	2966	0.006	0.007	0.007	0.007
	NaCl	1630	1872	9278	9449	8719	9030	0.002	0.002	0.002	0.002
		3270	3229	16005	18538	15186	17904	0.000	0.000	0.000	0.000
RW-2	KCl	5	4.9	21.4	21.4	24.4	24.4	0.391	0.391	0.342	0.342
		10	10.2	47.4	47.4	41.6	41.6	0.244	0.244	0.277	0.277
		20	21.2	101	101	83.4	83.4	0.141	0.141	0.171	0.171
		40	42.3	204	204	174	174	0.081	0.081	0.095	0.095
		80	82.1	399	399	345	345	0.044	0.044	0.051	0.051
		160	174	861	822	808	796	0.029	0.031	0.031	0.032
		320	329	1628	1491	1517	1433	0.016	0.017	0.017	0.018
		640	681	3378	3070	3161	2957	0.005	0.006	0.006	0.006
	NaCl	1630	1872	9278	9449	8473	8771	0.001	0.001	0.001	0.001
		3270	3229	16005	18538	15092	17790	0.000	0.000	0.000	0.000

^a C_{or} for the 5-80 mM KCl stages was measured by Meier (2016), whereas values were predicted based on *EC* for the 160 mM KCl to 3270 mM NaCl stages.

Table 2.3. Summary of results from membrane efficiency testing.

Specimen Designation	Solute	Source Concentration, C_{or} (mM)		Steady-State Chemico-Osmotic Pressure Difference, $-\Delta P_{ss}$ (kPa)	Effective Chemico-Osmotic Pressure Difference, $-\Delta P_e$ (kPa)	Maximum Chemico-Osmotic Pressure Difference, $\Delta\pi_{aw}$ (kPa) ^b		Membrane Efficiency Coefficient, ω_{aw} ($= -\Delta P_e / \Delta\pi_{aw}$) ^b	
		Target	Measured or Predicted ^a			$\Delta\pi_{aw,o}$	$\Delta\pi_{aw,ave}$	$\omega_{aw,o}$	$\omega_{aw,ave}$
RW-1	KCl	5	5.02	9.6	9.4	22.2	21.0	0.423	0.448
		10	10.2	12.5	12.2	47.3	42.1	0.258	0.290
		20	20.4	15.6	15.3	94.1	82.4	0.163	0.186
		40	42.2	21.0	20.7	203	172	0.102	0.120
		80	82.1	25.7	25.4	399	339	0.064	0.075
		160	174	26.3	26.0	822	802	0.032	0.032
		320	329	25.3	25.0	1491	1444	0.017	0.017
	NaCl	640	681	21.2	20.9	3070	2966	0.007	0.007
		1630	1872	14.9	14.6	9449	9030	0.002	0.002
RW-2	KCl	5	4.9	6.9	8.3	21.4	24.4	0.391	0.342
		10	10.2	10.1	11.5	47.4	41.6	0.244	0.277
		20	21.2	12.8	14.3	101	83.4	0.141	0.171
		40	42.3	15.0	16.5	204	174	0.081	0.095
		80	82.1	16.2	17.7	399	345	0.044	0.051
		160	174	24.0	25.4	822	796	0.031	0.032
		320	329	24.2	25.7	1491	1433	0.017	0.018
	NaCl	640	681	16.3	17.7	3070	2957	0.006	0.006
		1630	1872	9.56	11.0	9449	8771	0.001	0.001
		3270	3229	-7.6	-6.2	18538	17790	0.000	0.000

^a C_{or} for the 5-80 mM KCl stages was measured by Meier (2016), whereas values were predicted based on EC for the 160 mM KCl to 3270 mM NaCl stages.

^b $\Delta\pi_{aw}$ and ω_{aw} for the 5-80 mM stages are assumed to be the same as the $\Delta\pi_c$ and ω_c values determined based on the van't Hoff expression by Meier (2016).

Table 2.4. Summary of diffusion results.

Specimen Designation	Salt in Solution	Target Source Concentration, C_{ot} (mM)	Osmotic Efficiency Coefficients, ω		Diffusive Mass Flux, $\Delta Q_i'/\Delta t'$ (mM/m ² *d)	Time Lag, t_L (d)	Effective Diffusion Coefficient, D^* ($\times 10^{-10}$) (m ² /s)		Apparent Tortuosity Factor, τ_a		Restrictive Tortuosity Factor, τ_r		Matrix Tortuosity Factor, τ_m	
			ω_o	ω_{ave}			D_o^*	D_{ave}^*	$\tau_{a,o}$	$\tau_{a,ave}$	$\tau_{r,o}$	$\tau_{r,ave}$	$\tau_{m,o}$	$\tau_{m,ave}$
RW-1	KCl	5	0.423	0.448	0.32	11.8	0.6	0.7	0.03	0.03	0.19	0.19	0.17	0.18
		10	0.258	0.290	1.02	6.3	1.0	1.0	0.05	0.05	0.29	0.30		
		20	0.163	0.186	2.99	3.3	1.5	1.5	0.08	0.08	0.44	0.43		
		40	0.102	0.120	8.07	3.0	1.9	2.0	0.09	0.10	0.55	0.57		
		80	0.064	0.075	20.3	4.5	2.4	2.6	0.12	0.13	0.71	0.74		
		160	0.031	0.032	40.6	1.9	2.3	2.4	0.11	0.12	0.96	0.96		
		320	0.017	0.017	75.7	3.3	2.3	2.4	0.11	0.12	0.94	0.95		
	640	0.007	0.007	162	4.6	2.3	2.5	0.12	0.12	0.98	0.98			
	NaCl	1630	0.002	0.002	403	3.5	2.1	2.2	0.13	0.14	0.88	0.89	0.15	0.16
3270		0.000	0.000	788	4.6	2.4	2.5	0.15	0.16	1.00	1.00			
RW-2 ^a	KCl	160	0.031	0.032	50.2	2.7	2.8	3.0	0.14	0.15	1.00	1.00	0.14	0.15
		320	0.017	0.018	94.5	2.9	2.8	3.0	0.14	0.15	1.00	1.00		
		640	0.006	0.006	196	3.1	2.8	3.0	0.14	0.15	1.00	1.00		
	NaCl	1630	0.001	0.001	469	2.8	2.4	2.7	0.15	0.17	0.94	0.97	0.16	0.17
		3270	0.000	0.000	862	3.1	2.6	2.8	0.16	0.17	1.00	1.00		

^a Diffusion was not analyzed for specimen RW-2 by Meier (2016), thus only results for the 160 – 3270 mM stages are shown.

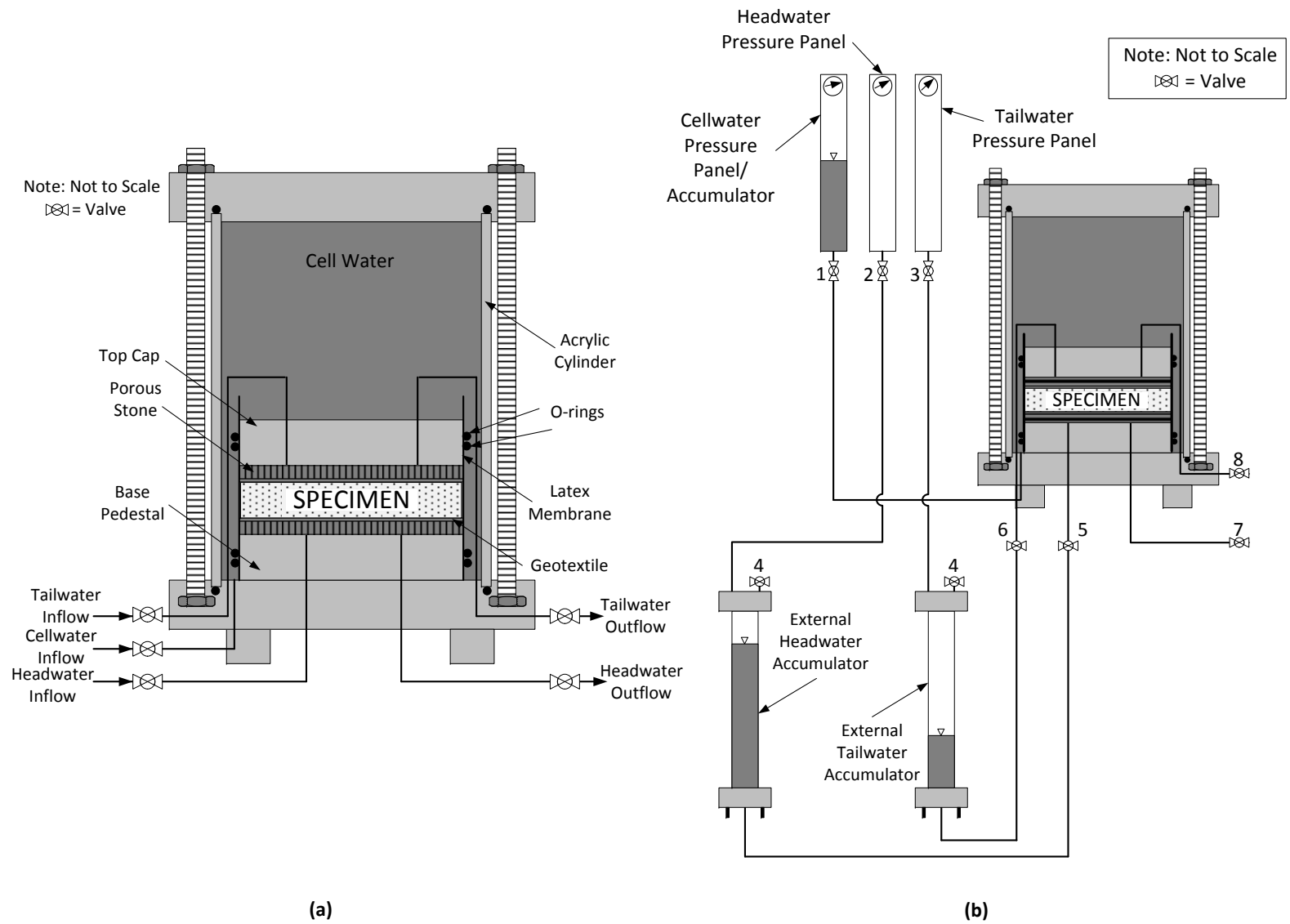


Figure 2.1. Schematics of the (a) flexible-wall (FW) permeameter (after Meier 2016) and (b) k -testing apparatus with FW permeameter.

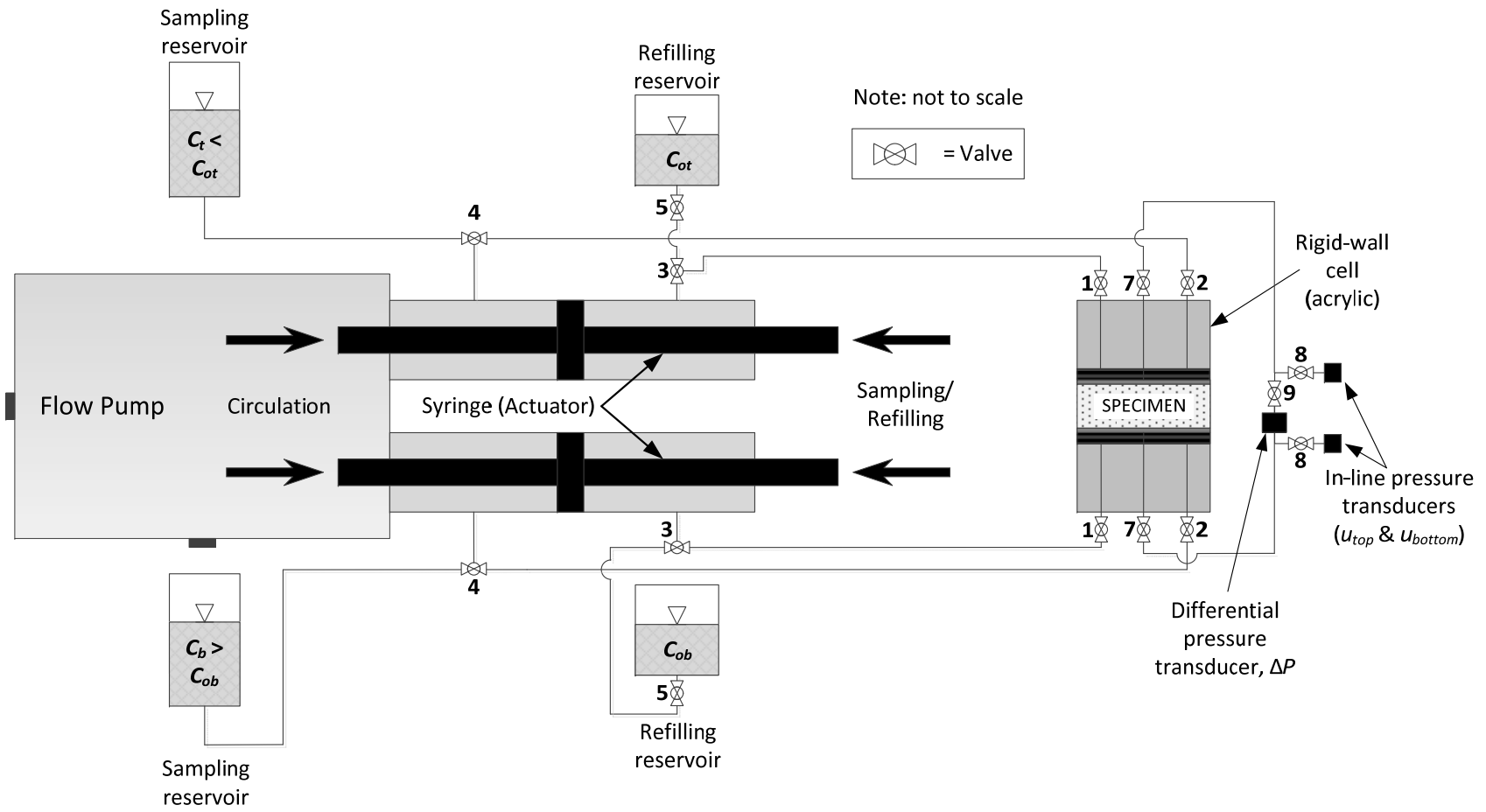


Figure 2.2. Schematic of membrane testing apparatus (after Meier 2016).

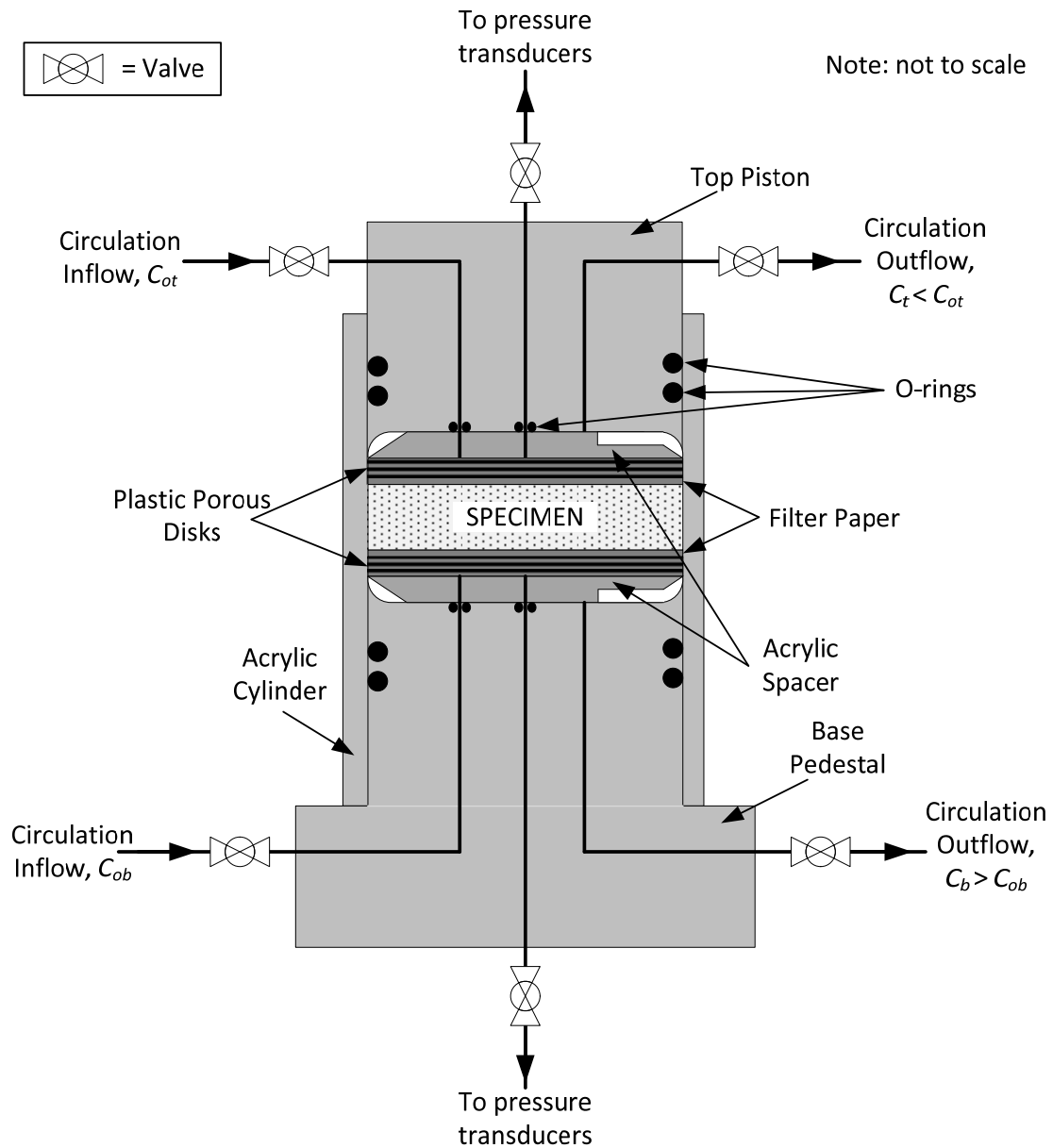


Figure 2.3. Schematic of the rigid-wall membrane testing cell (after Meier 2016).

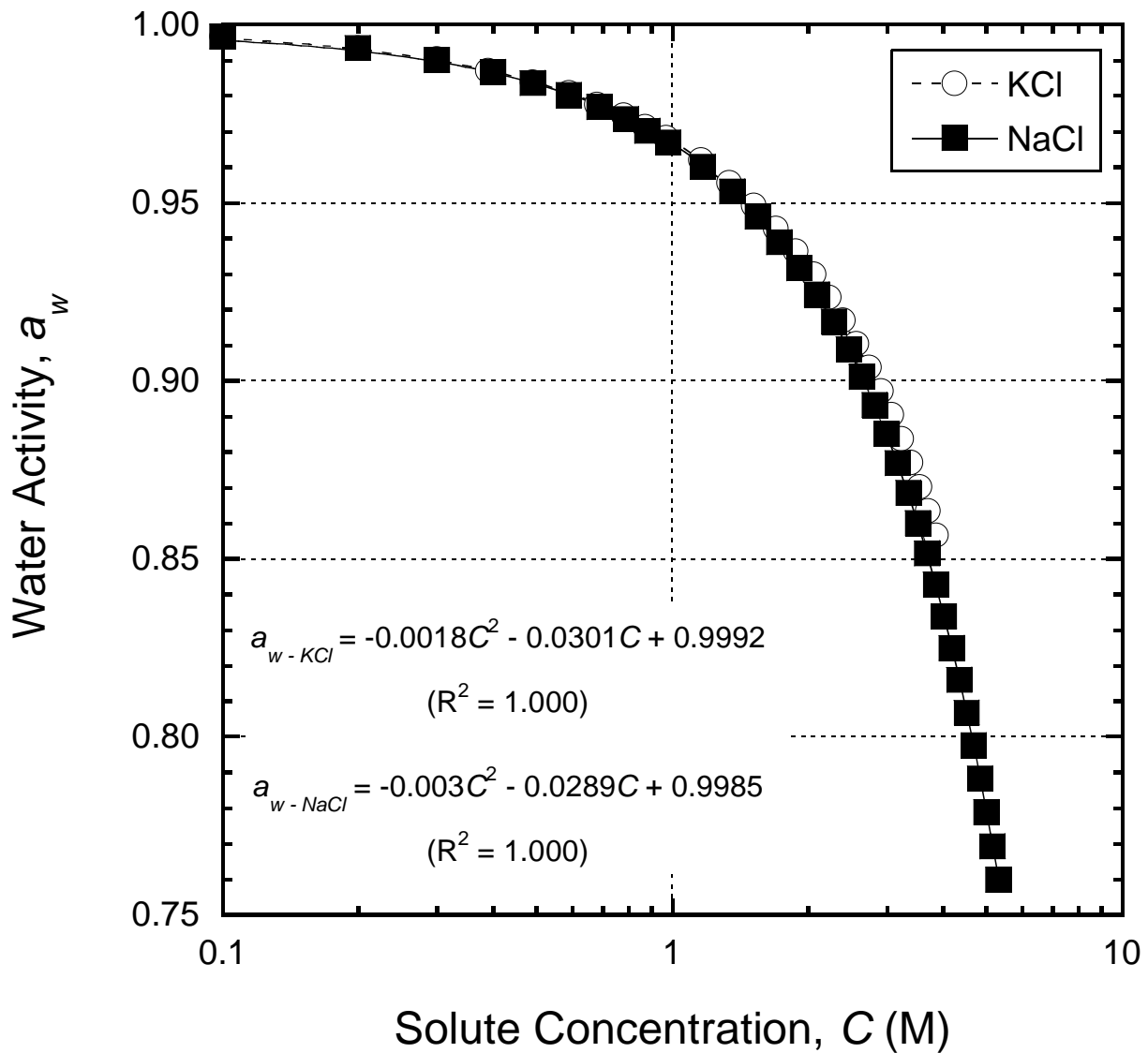


Figure 2.4. Activity of water for varying concentrations of aqueous KCl and NaCl solutions, fitted with second-order polynomial regressions. Based on all available data from Robinson and Stokes (1959).

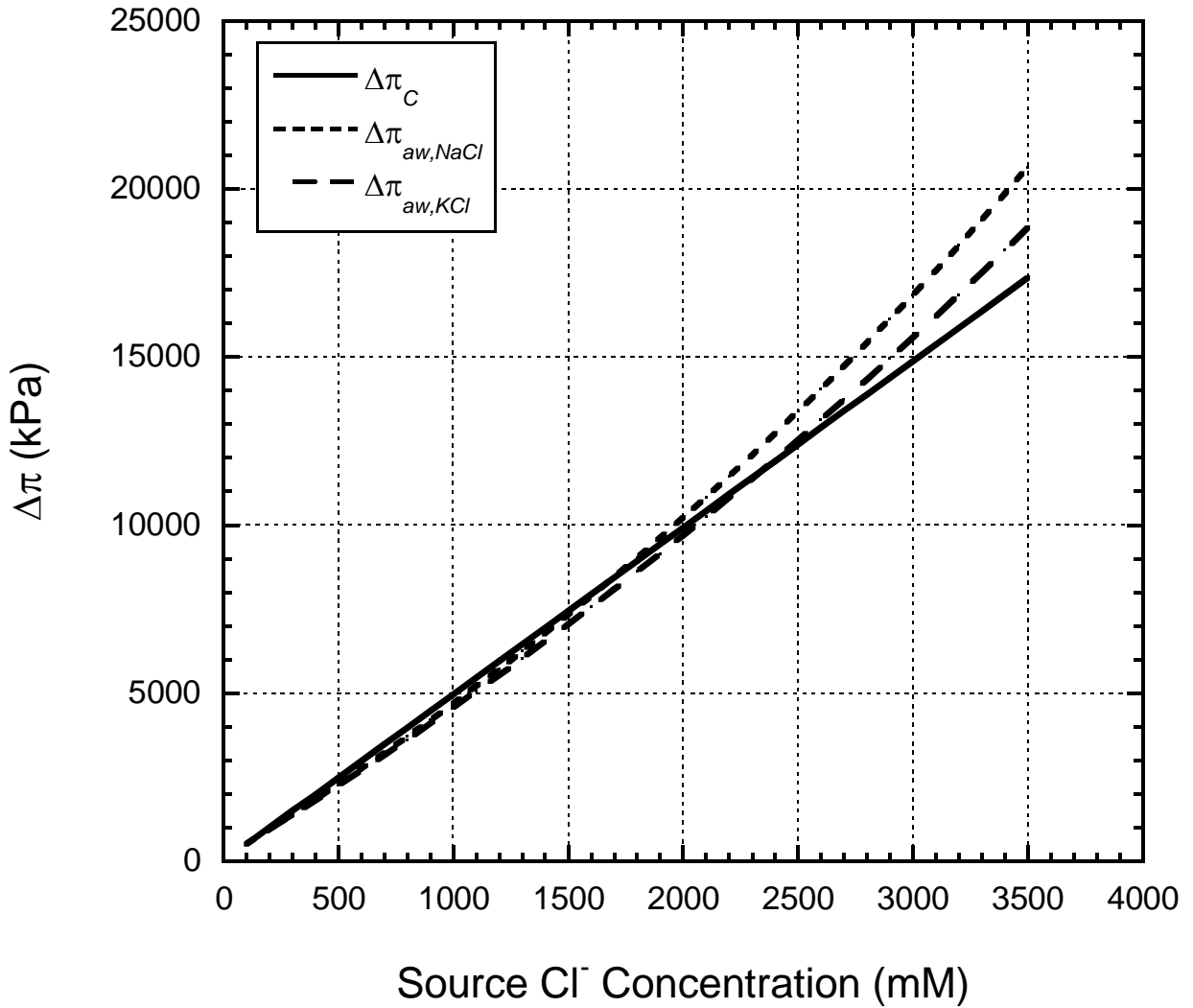


Figure 2.5. Values of the theoretical maximum chemico-osmotic pressure difference for a range of Cl^- concentrations using the van't Hoff approximation ($\Delta\pi_C$) and the activity method ($\Delta\pi_{aw}$). Values of $\Delta\pi_{aw}$ calculated using both NaCl water activity relationship ($\Delta\pi_{aw,NaCl}$) and KCl water activity relationship ($\Delta\pi_{aw,KCl}$).

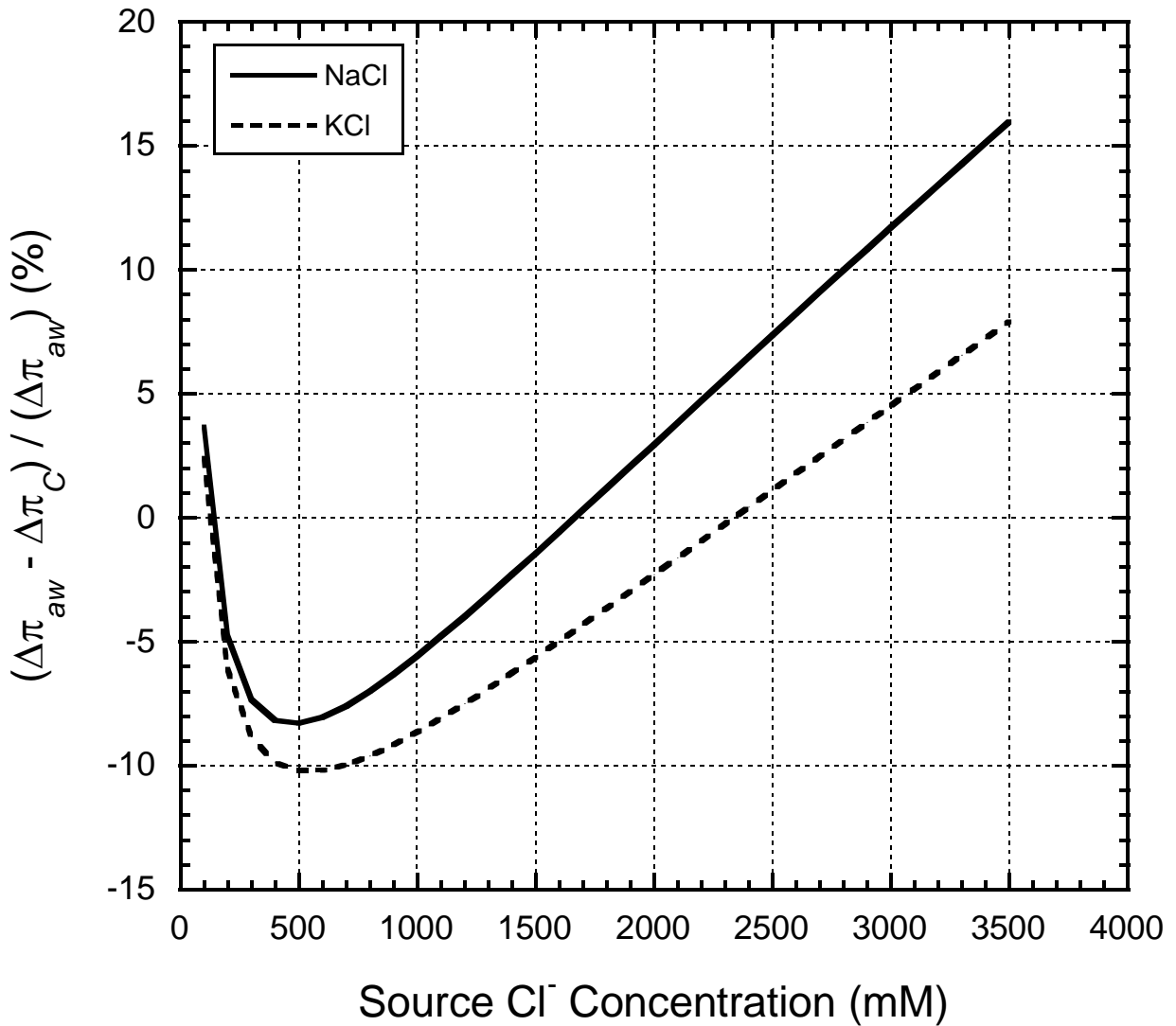


Figure 2.6. Percent error of maximum chemico-osmotic pressure differences calculated using the van't Hoff approximation ($\Delta\pi_C$) relative to those calculated using the activity method ($\Delta\pi_{aw}$) for a range of theoretical NaCl and KCl concentrations.

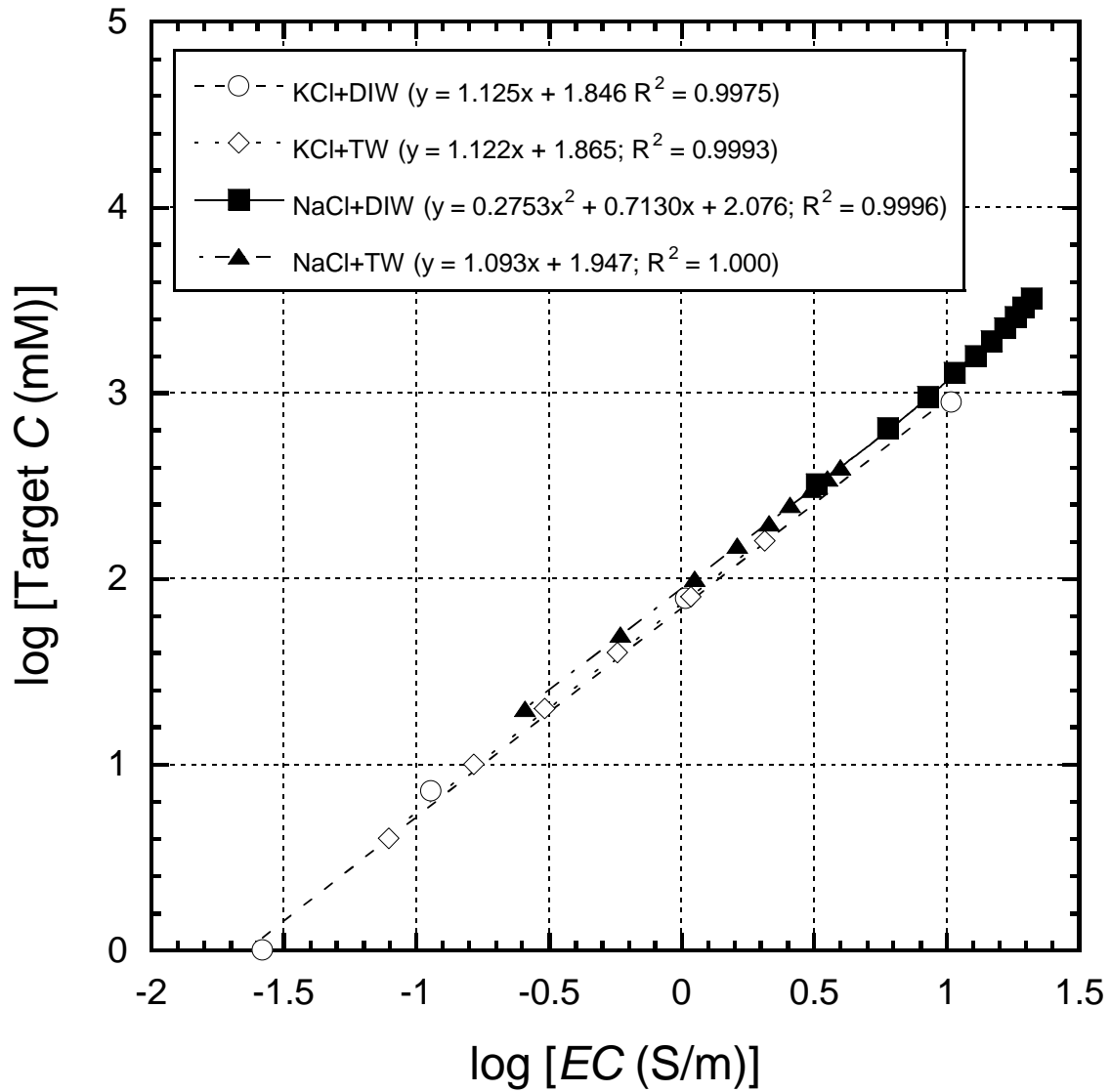


Figure 2.7. Concentration vs. *EC* log-log relationships for KCl and NaCl solutions prepared at varying target concentrations with de-ionized water (DIW) and tap water (TW).

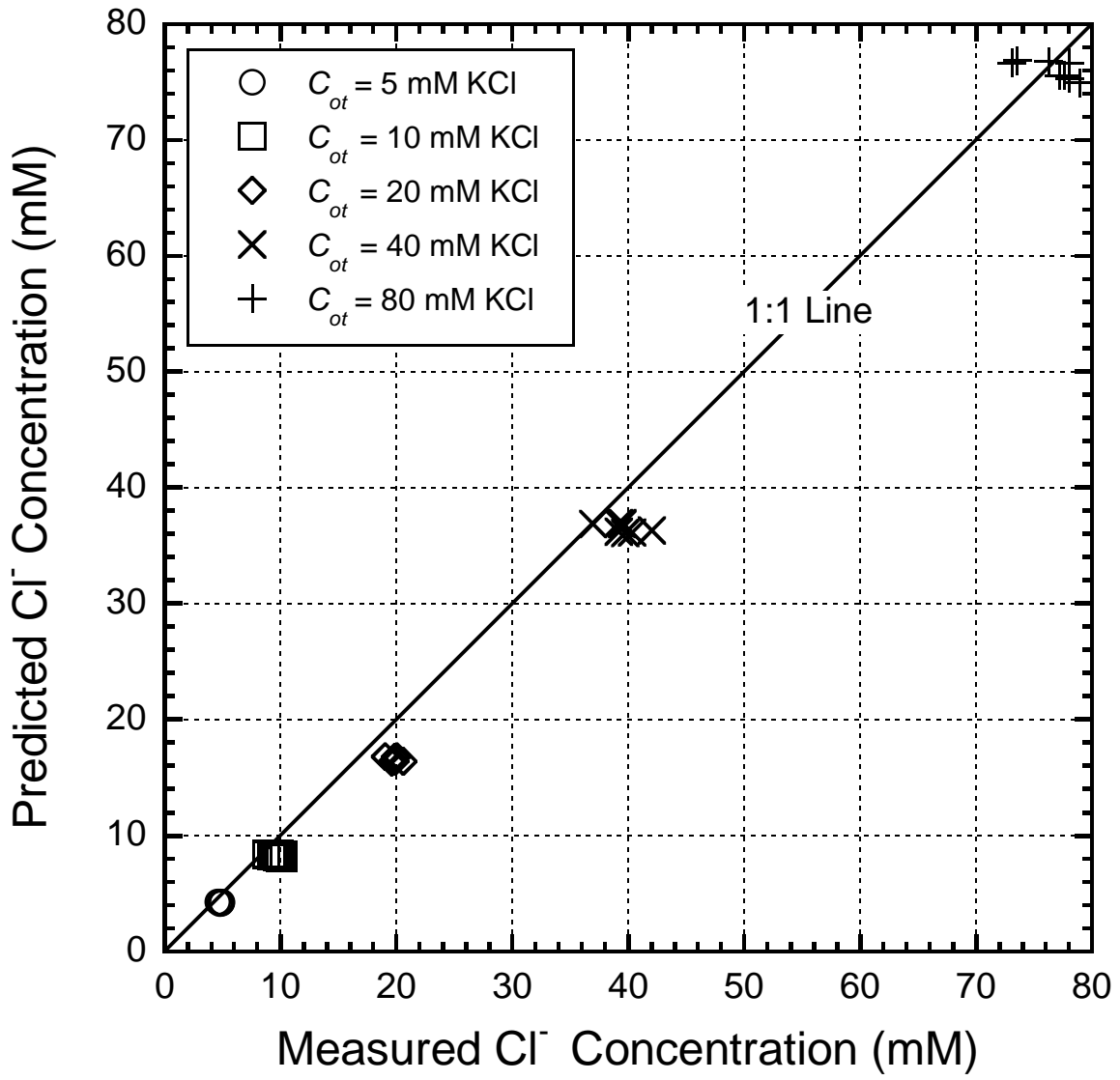


Figure 2.8. Sample Cl⁻ concentrations predicted using calibration curves vs. actual Cl⁻ concentrations measured using ion chromatography (IC). Samples collected from top boundary circulation effluent by Meier (2016).

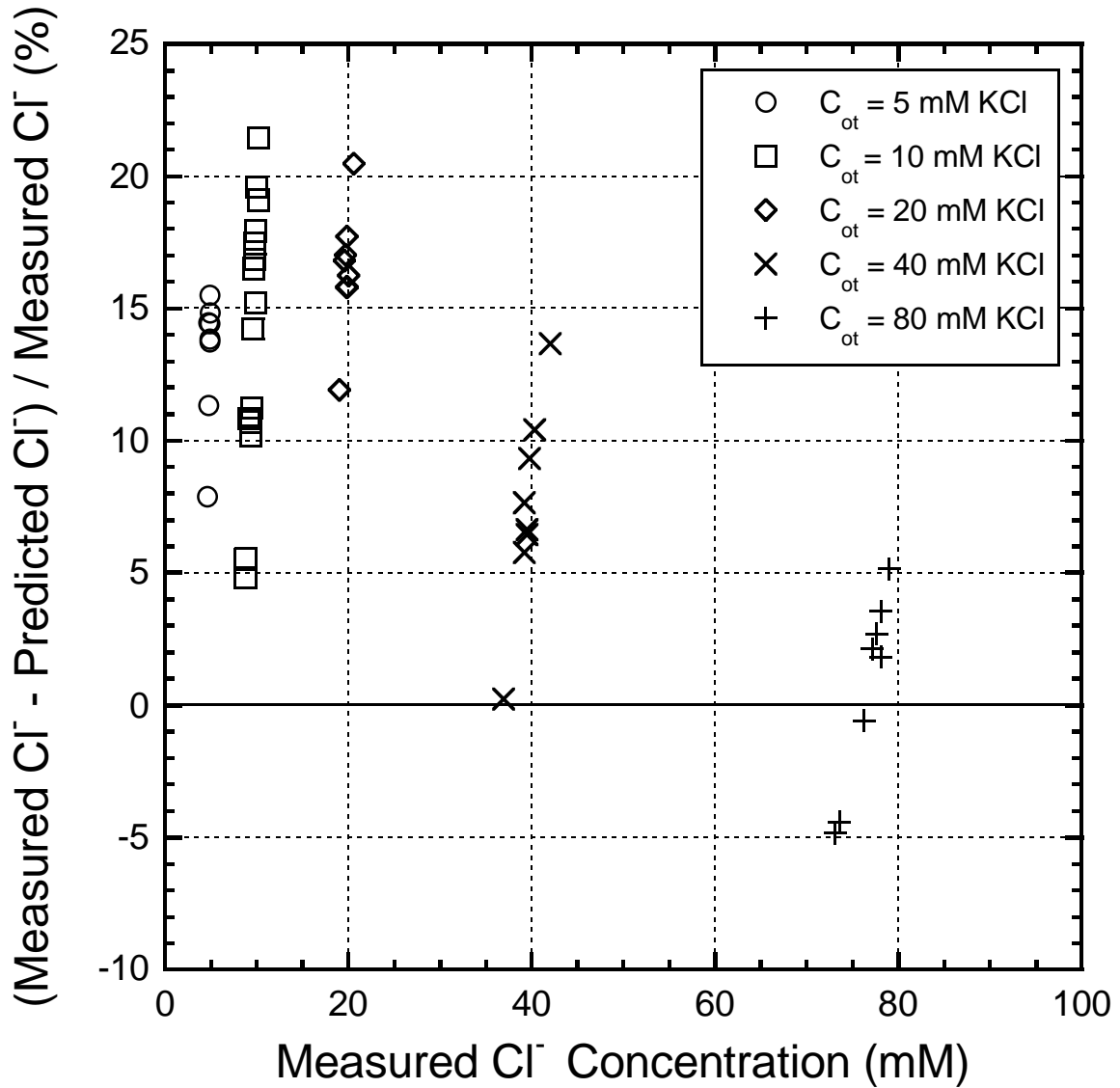


Figure 2.9. Percent error of sample Cl^- concentrations predicted using calibration curves relative to actual Cl^- concentrations measured using ion chromatography (IC). Samples collected from top boundary circulation effluent by Meier (2016).

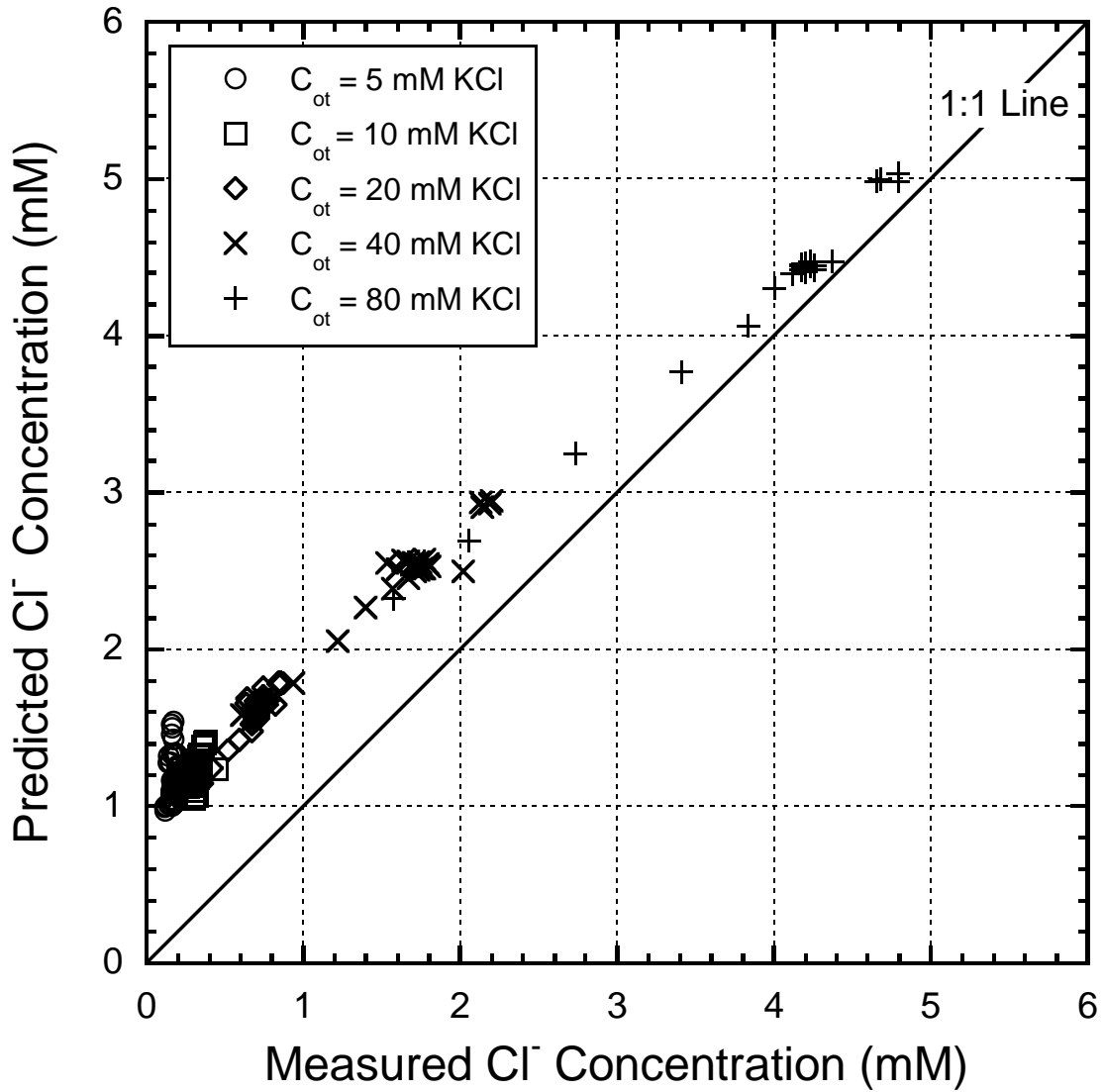


Figure 2.10. Sample Cl^- concentrations predicted using calibration curves vs. actual Cl^- concentrations measured using ion chromatography (IC). Samples collected from bottom boundary circulation effluent by Meier (2016).

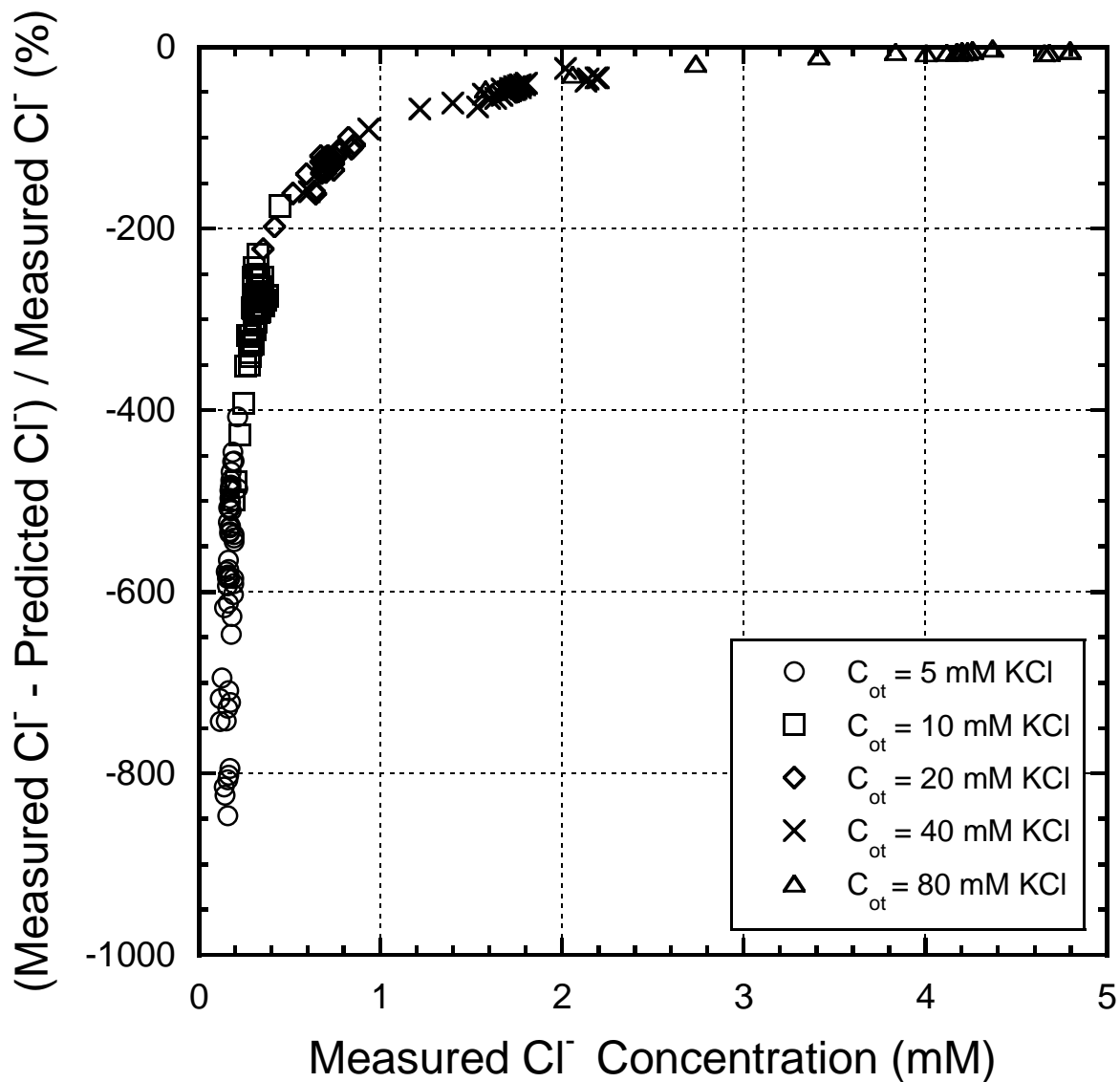


Figure 2.11. Percent error of sample Cl^- concentrations predicted using calibration curves relative to actual Cl^- concentrations measured using ion chromatography (IC). Samples collected from bottom boundary circulation effluent by Meier (2016).

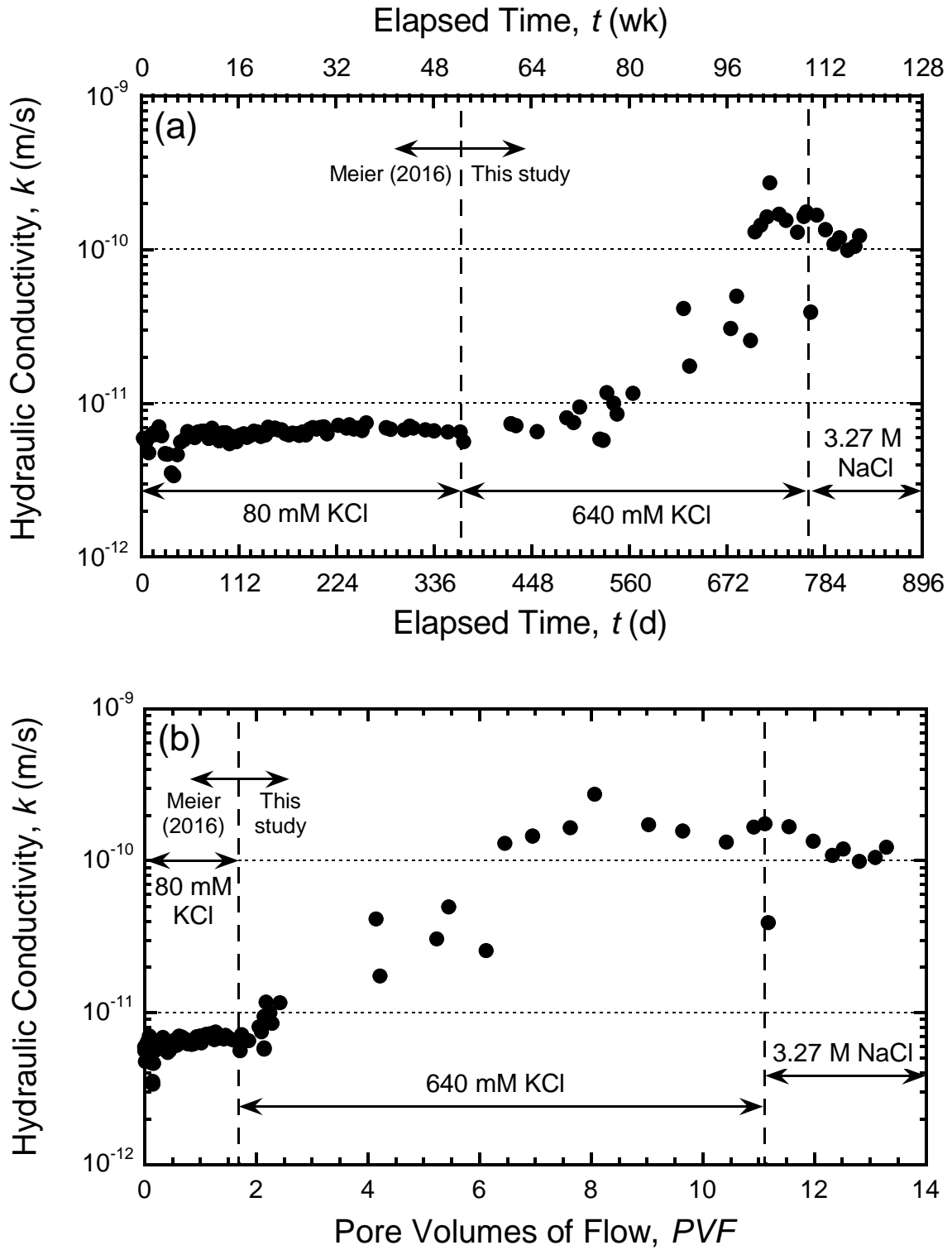


Figure 2.12. Hydraulic conductivity test results for specimen FW-1: (a) k versus time; (b) k versus pore volumes of flow.

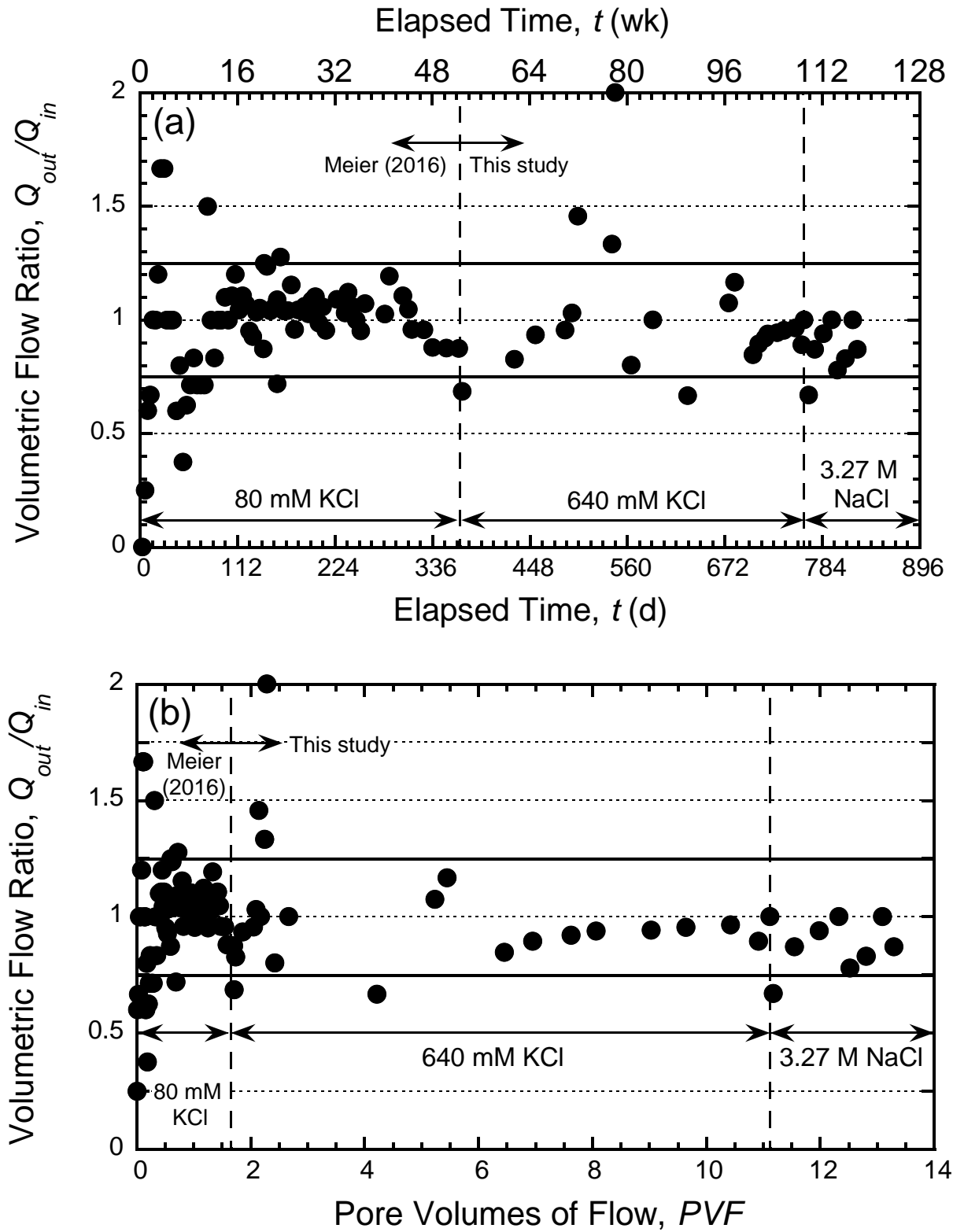


Figure 2.13. Hydraulic conductivity test results for specimen FW-1: (a) Q_{out}/Q_{in} versus time; (b) Q_{out}/Q_{in} versus pore volumes of flow.

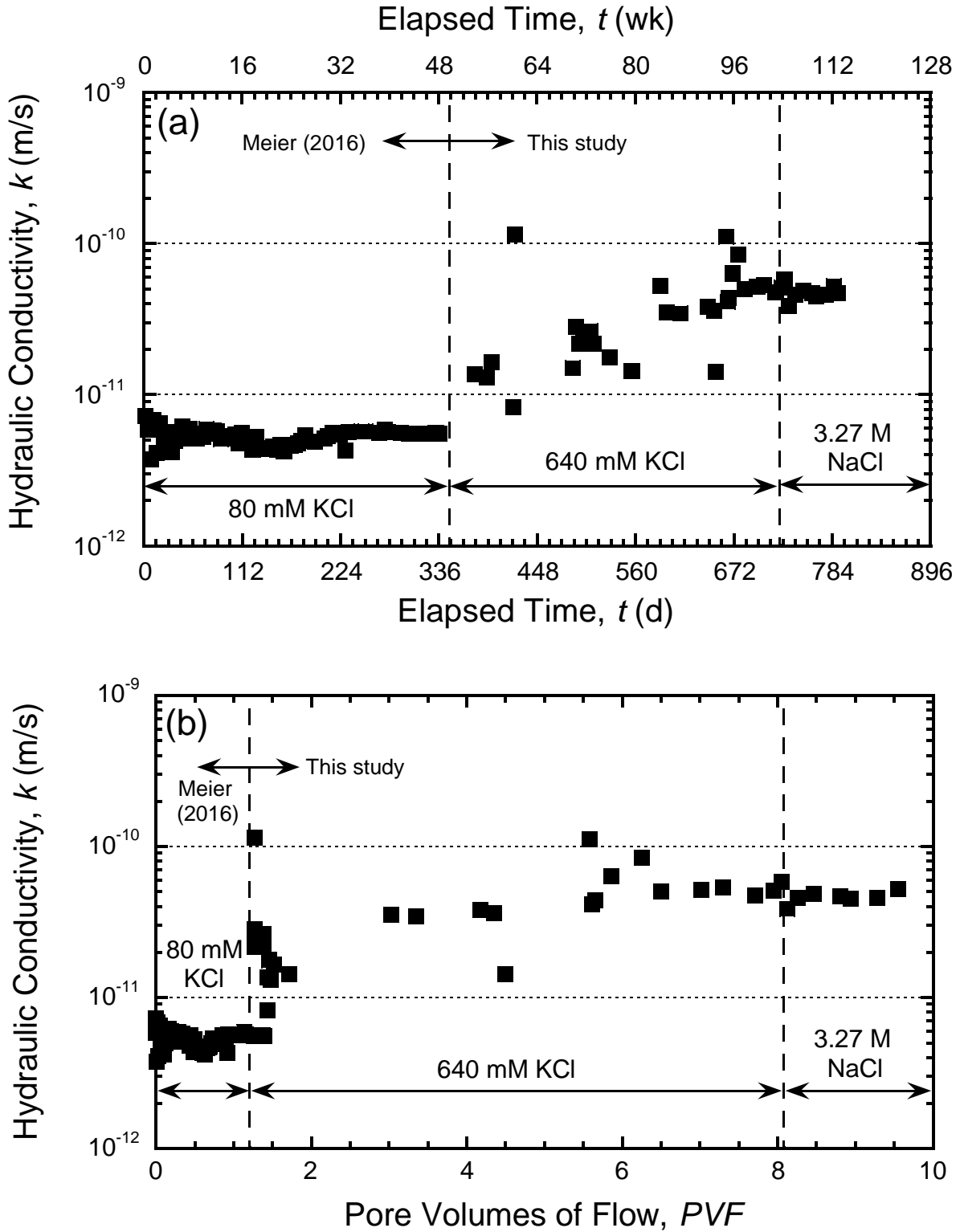


Figure 2.14. Hydraulic conductivity test results for specimen FW-2: (a) k versus time; (b) k versus pore volumes of flow.

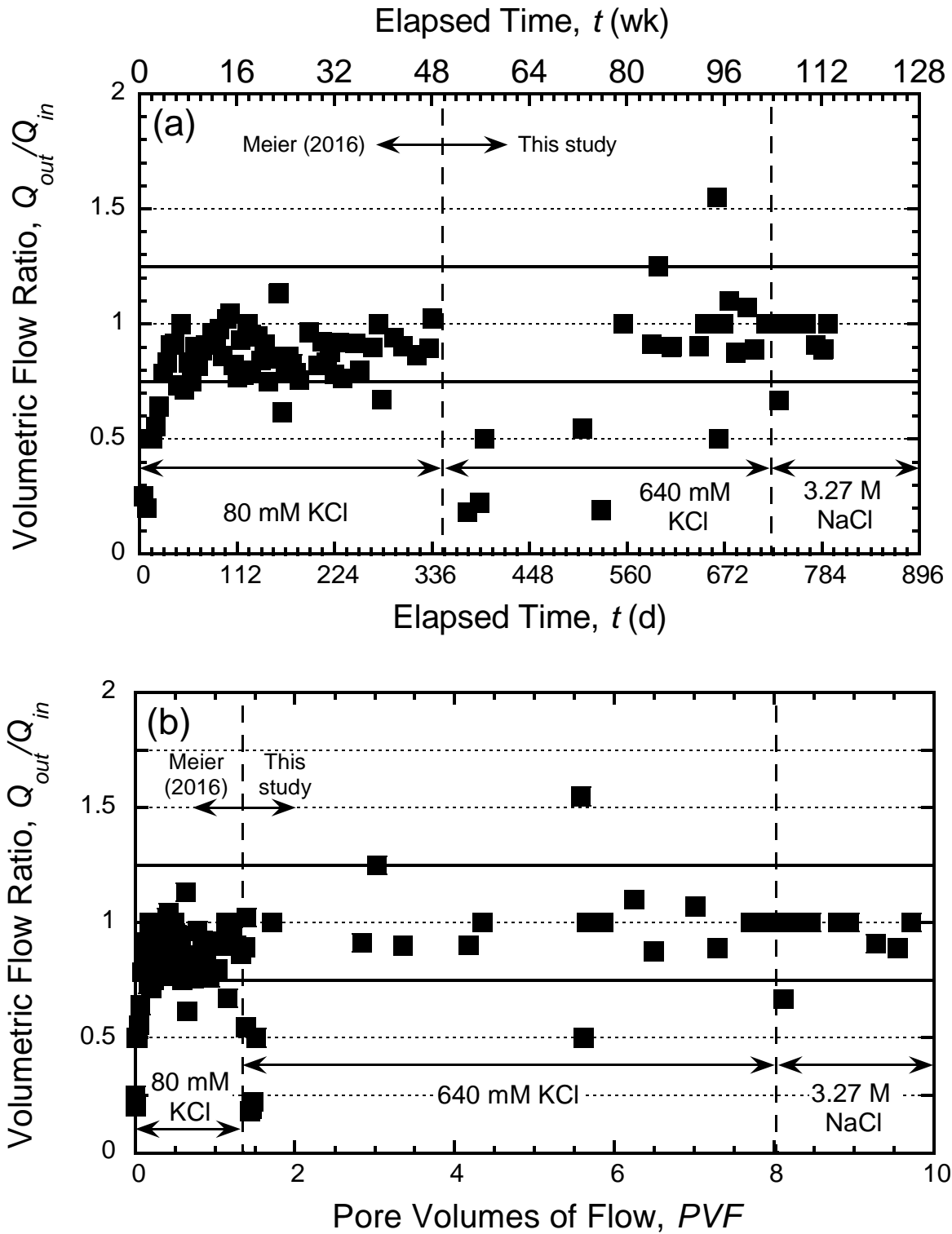


Figure 2.15. Hydraulic conductivity test results for specimen FW-2: (a) Q_{out}/Q_{in} versus time; (b) Q_{out}/Q_{in} versus pore volumes of flow.

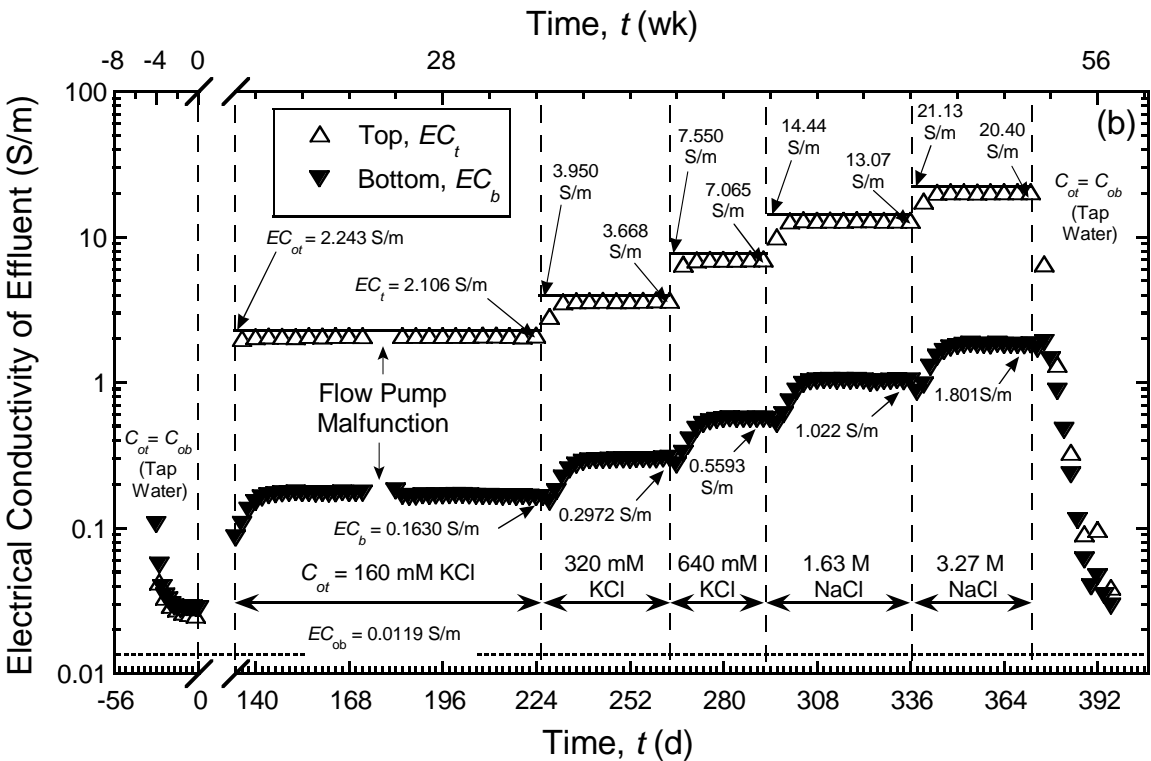
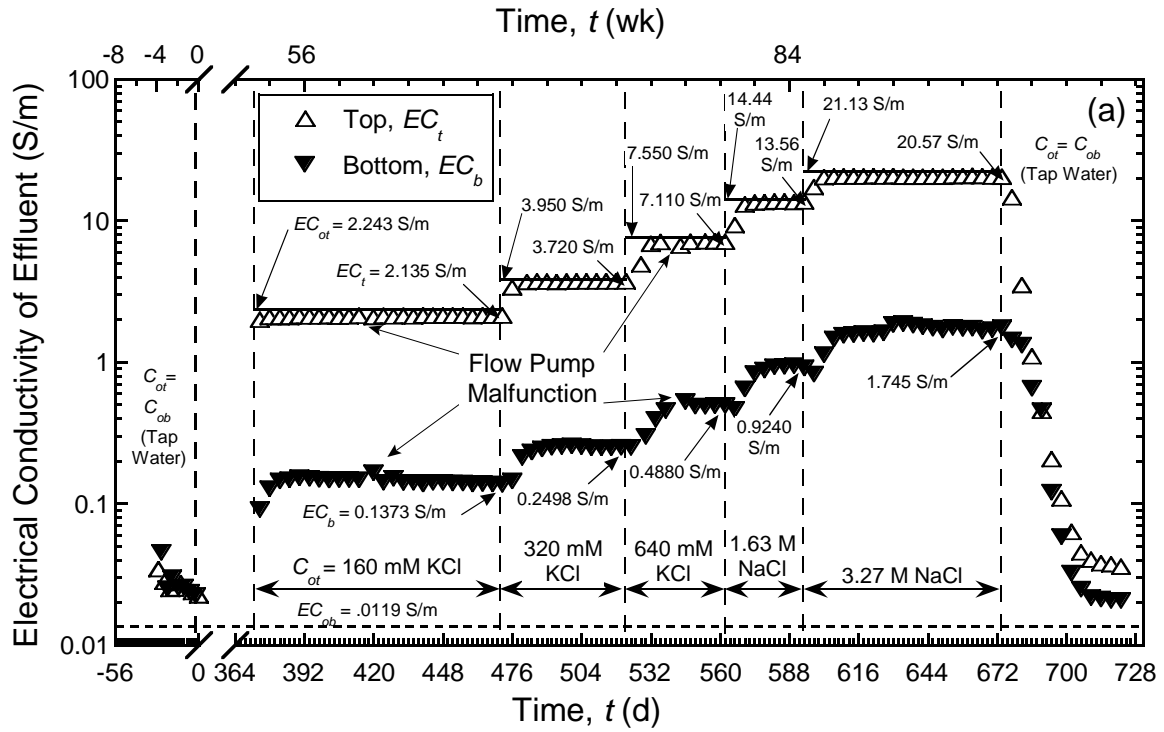


Figure 2.16. Measured electrical conductivity values of the top and bottom boundary circulation outflow liquids: (a) specimen RW-1; (b) specimen RW-2.

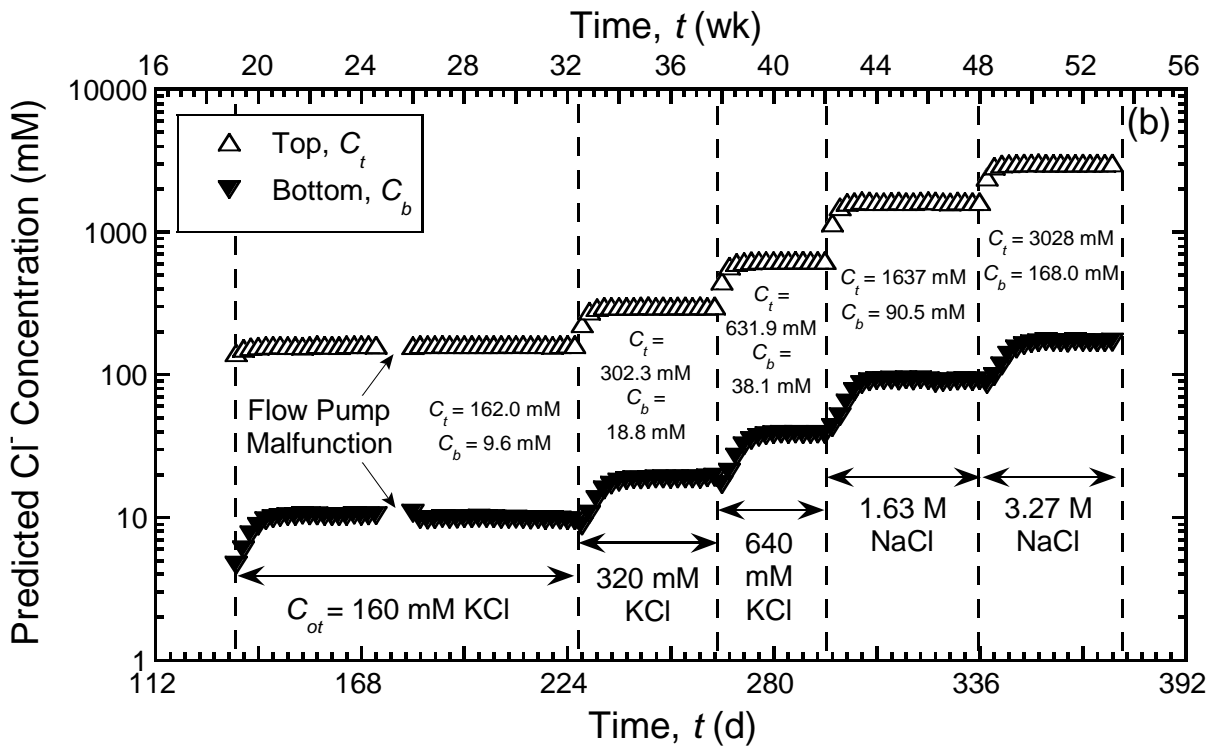
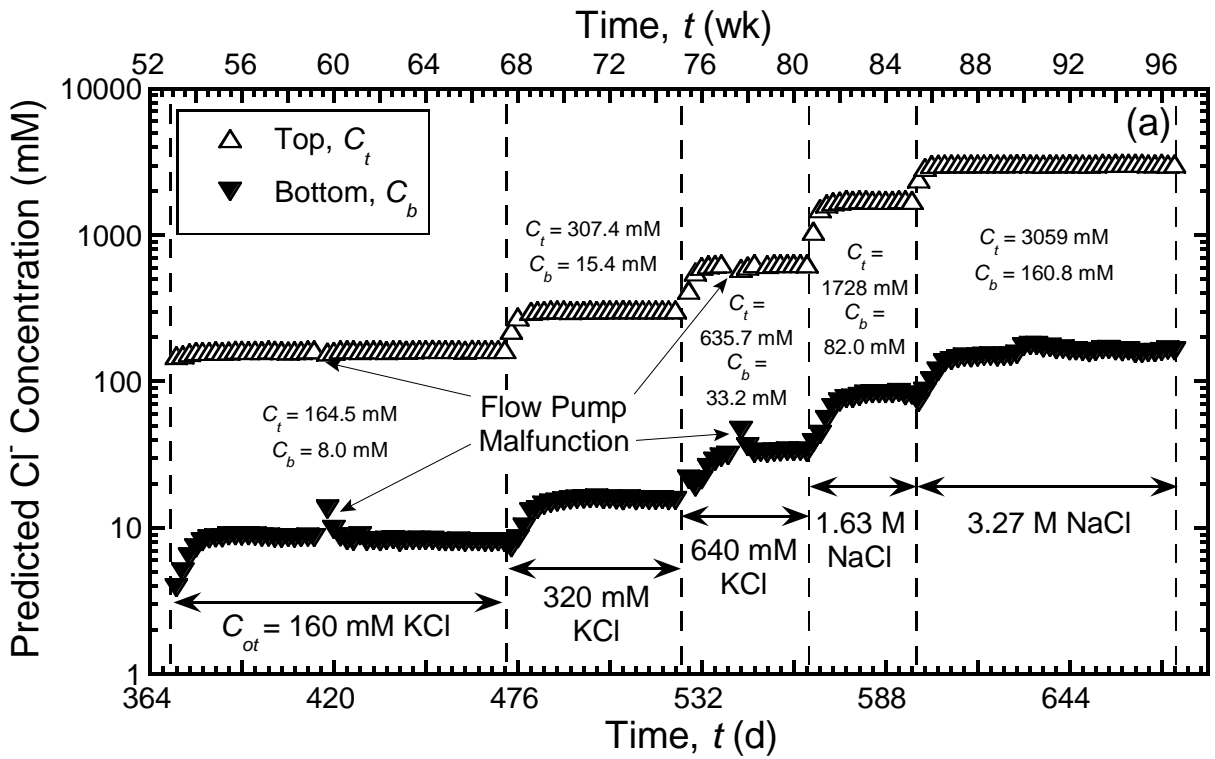


Figure 2.17. Predicted Cl^- concentrations of top and bottom boundary circulation outflow liquids, calculated based on measured EC values: (a) specimen RW-1; (b) specimen RW-2.

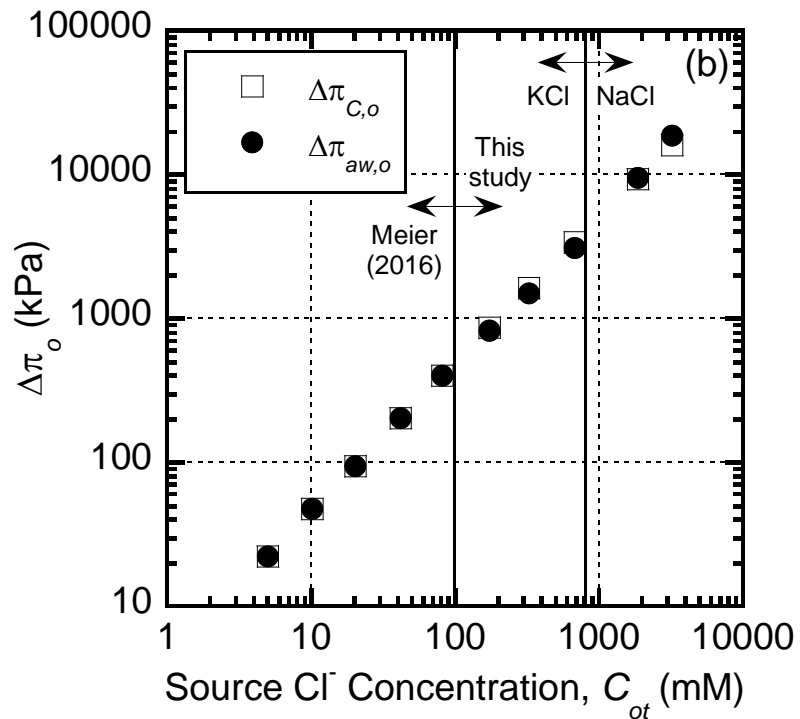
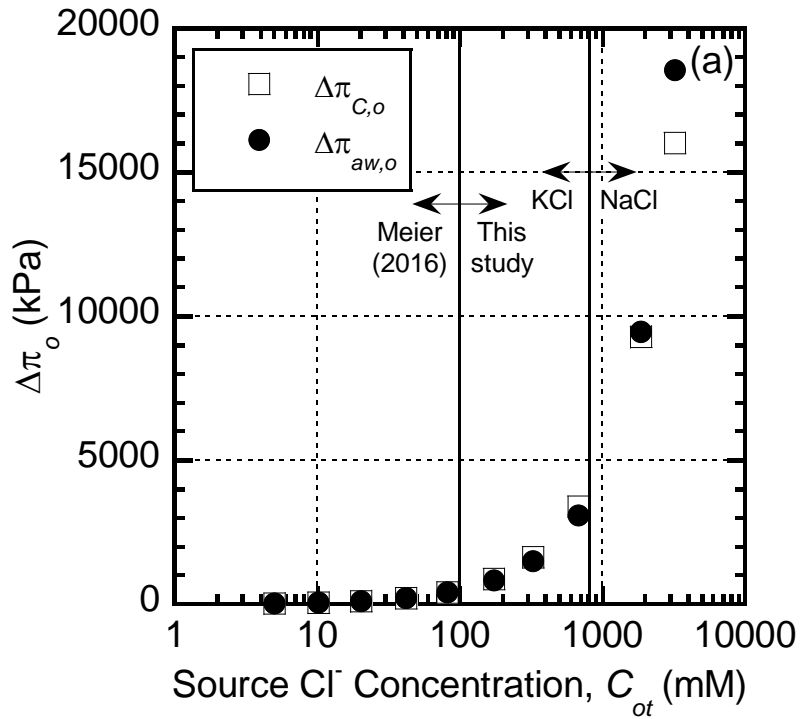


Figure 2.18. Comparison of $\Delta\pi$ calculated based on initial (source) concentrations using the van't Hoff expression ($\Delta\pi_{C,o}$) and the activity method ($\Delta\pi_{aw,o}$) for specimen RW-1: (a) semi-log relationship; (b) log-log relationship.

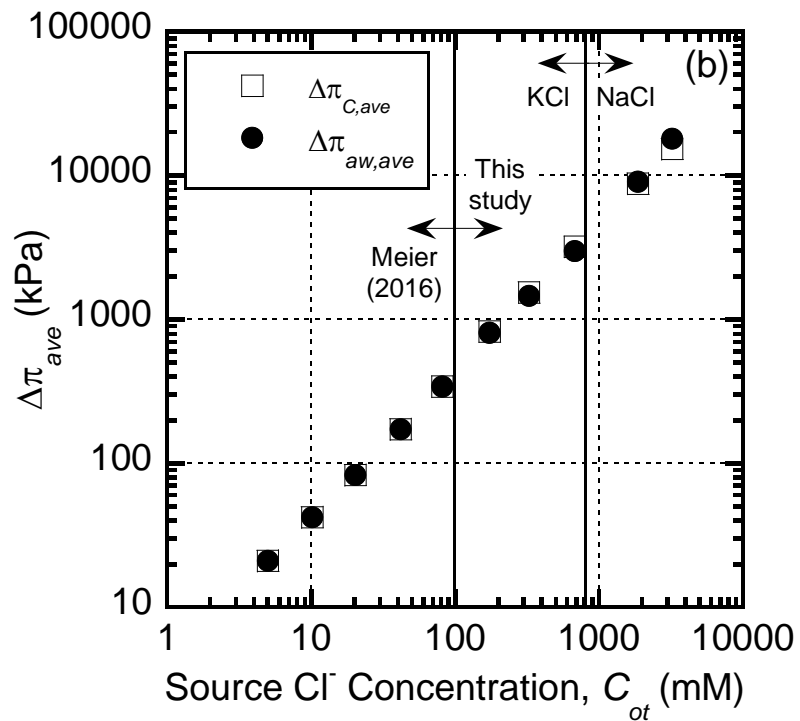
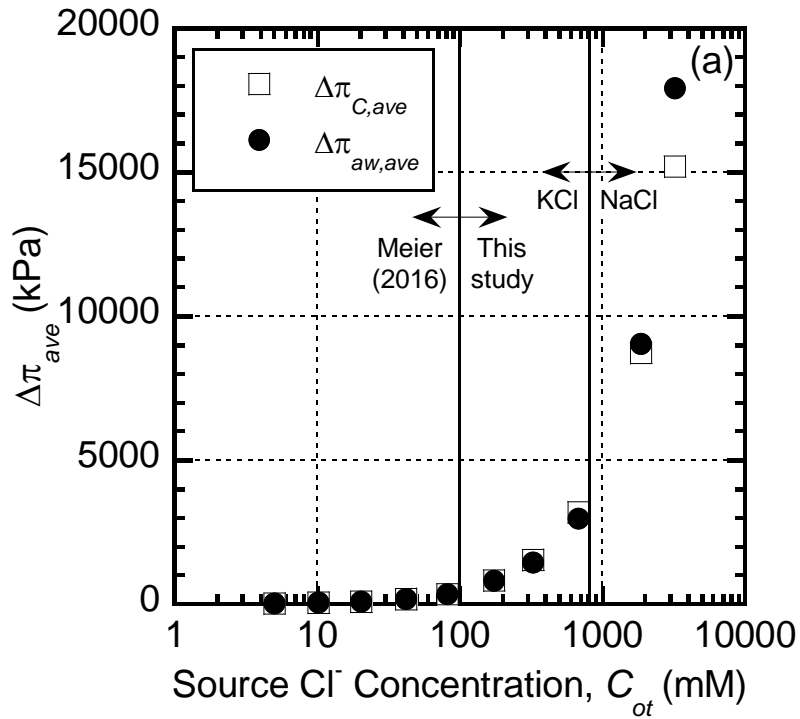


Figure 2.19. Comparison of $\Delta\pi$ calculated based on average concentrations using the van't Hoff expression ($\Delta\pi_{C,o}$) and the activity method ($\Delta\pi_{aw,o}$) for specimen RW-1: (a) semi-log relationship; (b) log-log relationship.

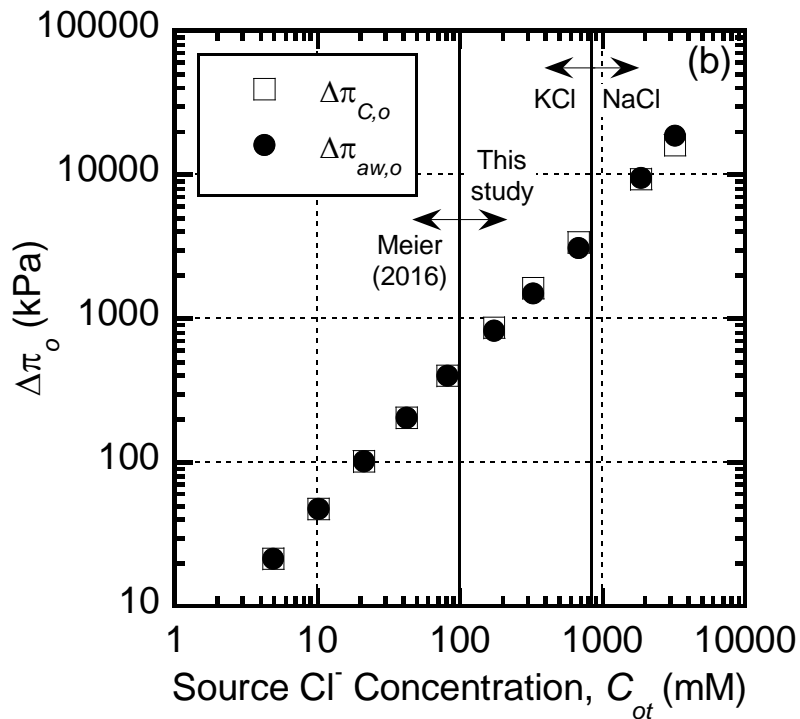
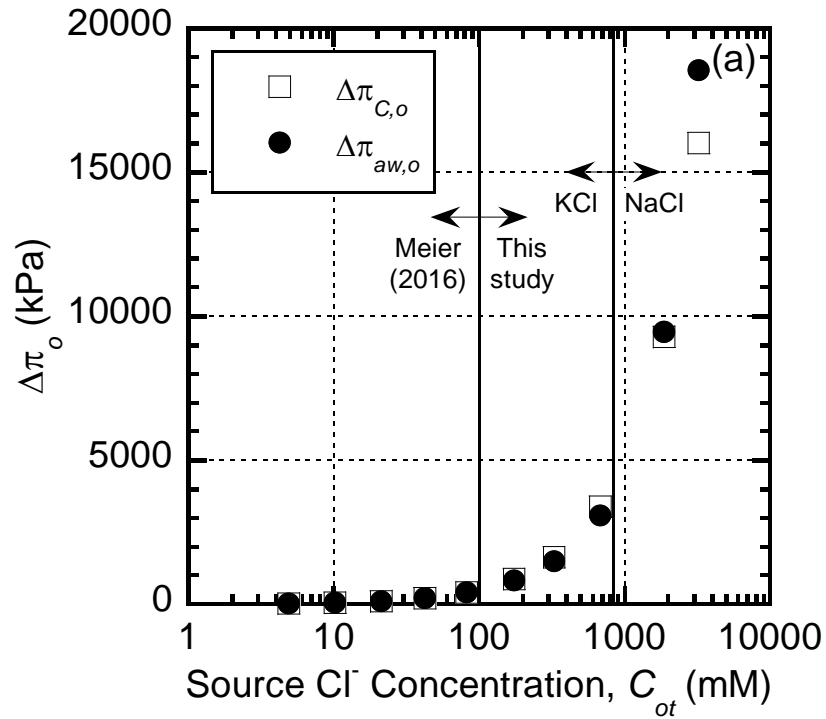


Figure 2.20. Comparison of $\Delta\pi$ calculated based on initial (source) concentrations using the van't Hoff expression ($\Delta\pi_{C,o}$) and the activity method ($\Delta\pi_{aw,o}$) for specimen RW-2: (a) semi-log relationship; (b) log-log relationship.

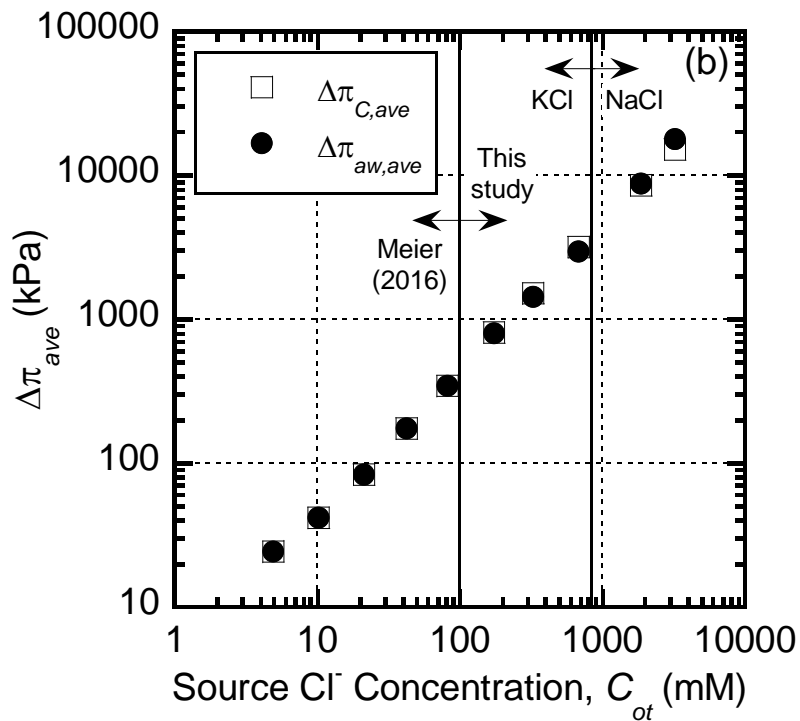
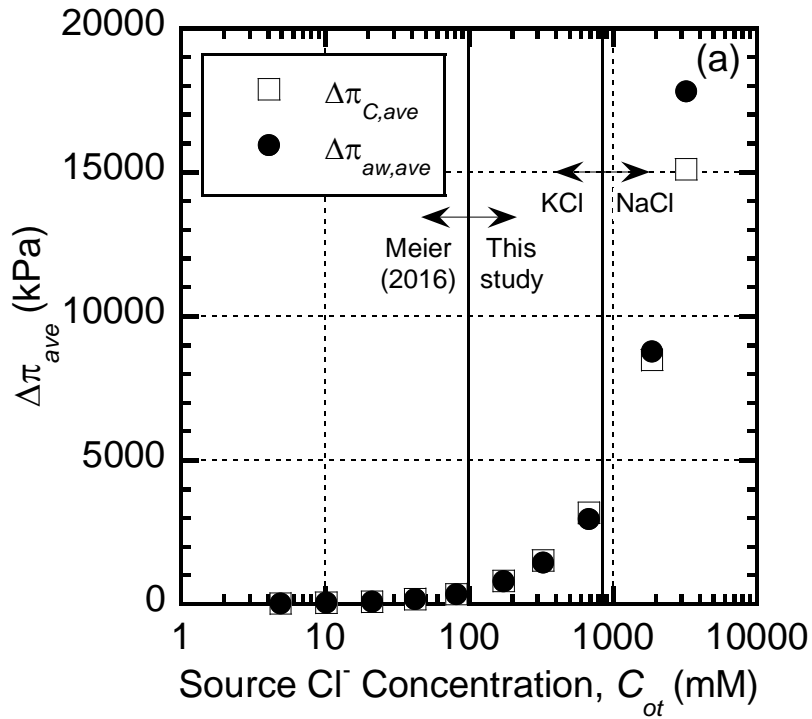


Figure 2.21. Comparison of $\Delta\pi$ calculated based on average concentrations using the van't Hoff expression ($\Delta\pi_{C,o}$) and the activity method ($\Delta\pi_{aw,o}$) for specimen RW-2: (a) semi-log relationship; (b) log-log relationship.

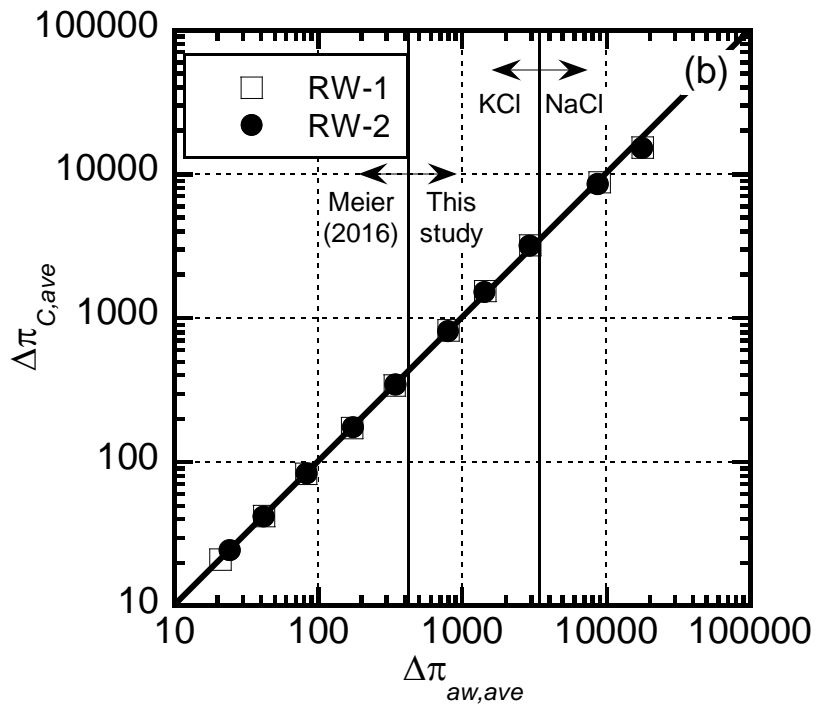
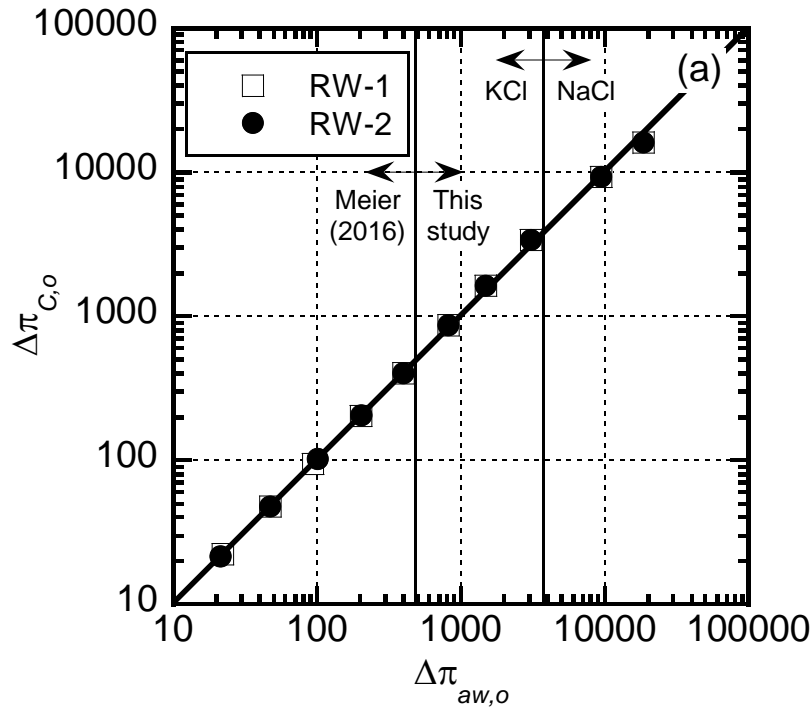


Figure 2.22. 1:1 plot of $\Delta\pi$ calculated using the van't Hoff expression ($\Delta\pi_C$) vs. $\Delta\pi$ calculated using the activity method ($\Delta\pi_{aw}$) for specimens RW-1 and RW-2: (a) based on initial (source) solute concentrations; (b) based on average solute concentrations.

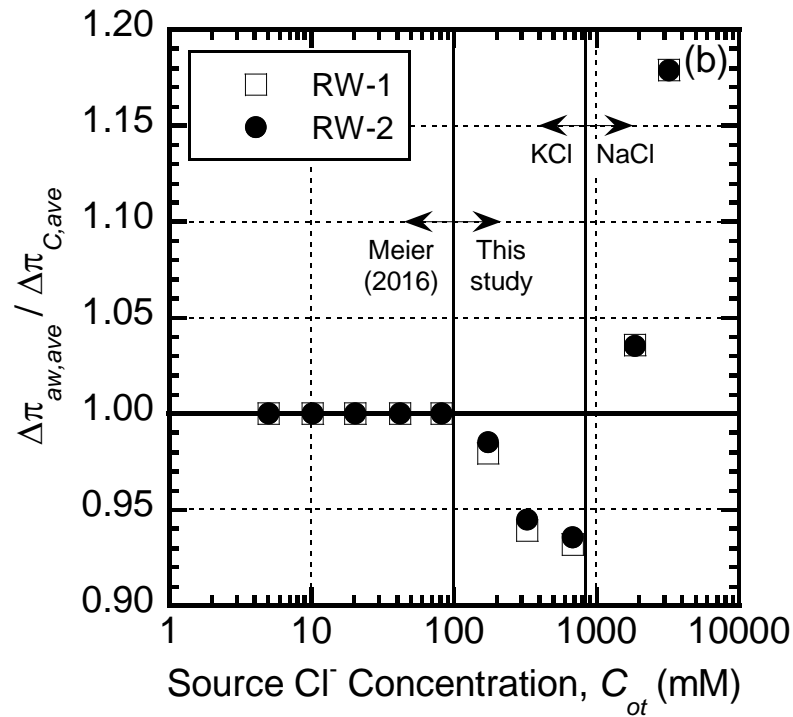
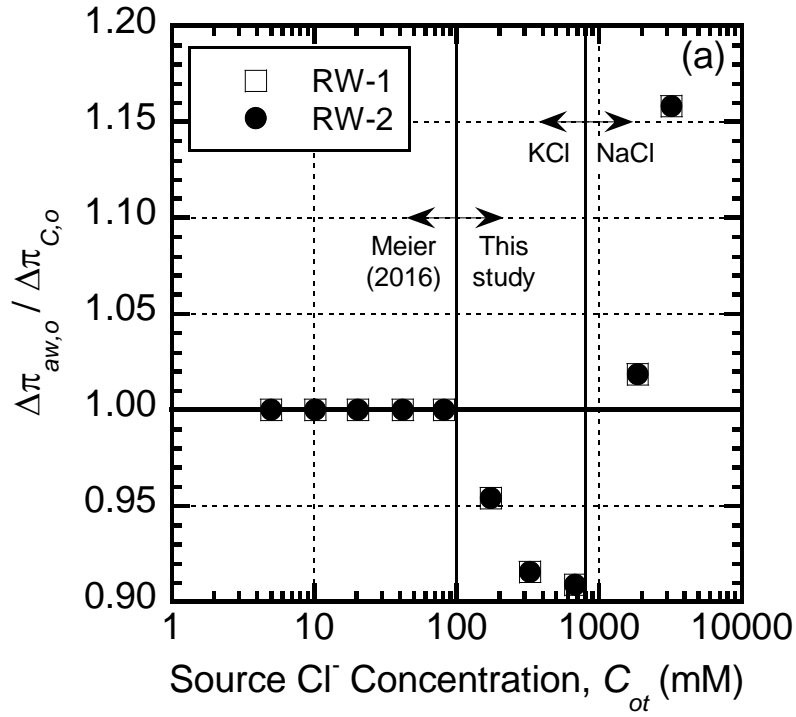


Figure 2.23. Ratio of $\Delta\pi$ calculated using the activity method ($\Delta\pi_{aw}$) to $\Delta\pi$ calculated using the van't Hoff expression ($\Delta\pi_C$) for specimens RW-1 and RW-2: (a) based on initial (source) solute concentrations; (b) based on average solute concentrations.

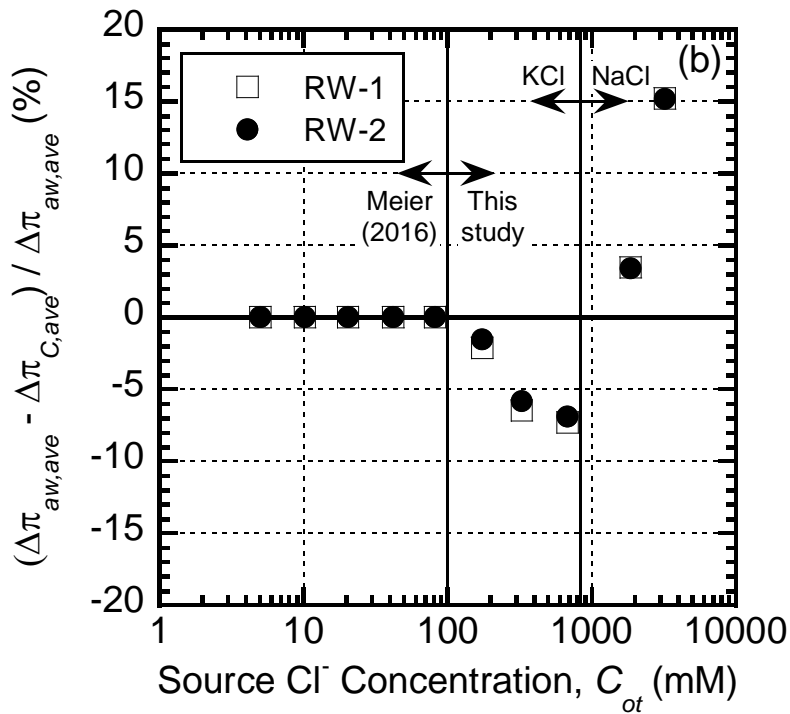
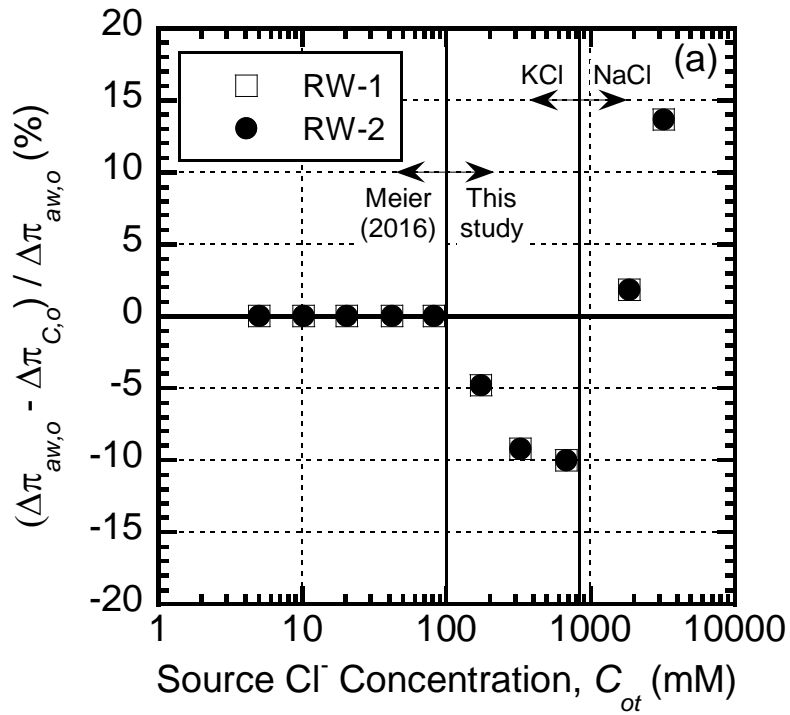


Figure 2.24. Percent error of $\Delta\pi$ calculated using the van't Hoff expression ($\Delta\pi_C$) relative to $\Delta\pi$ calculated using the activity method ($\Delta\pi_{aw}$) for specimens RW-1 and RW-2: (a) based on initial (source) solute concentrations; (b) based on average solute concentrations.

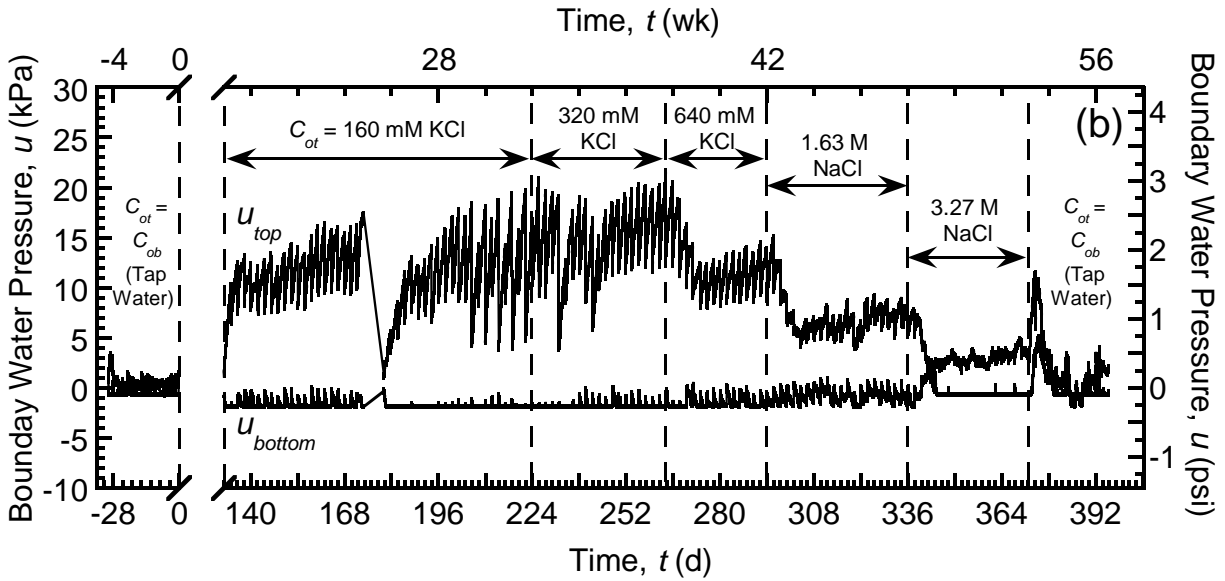
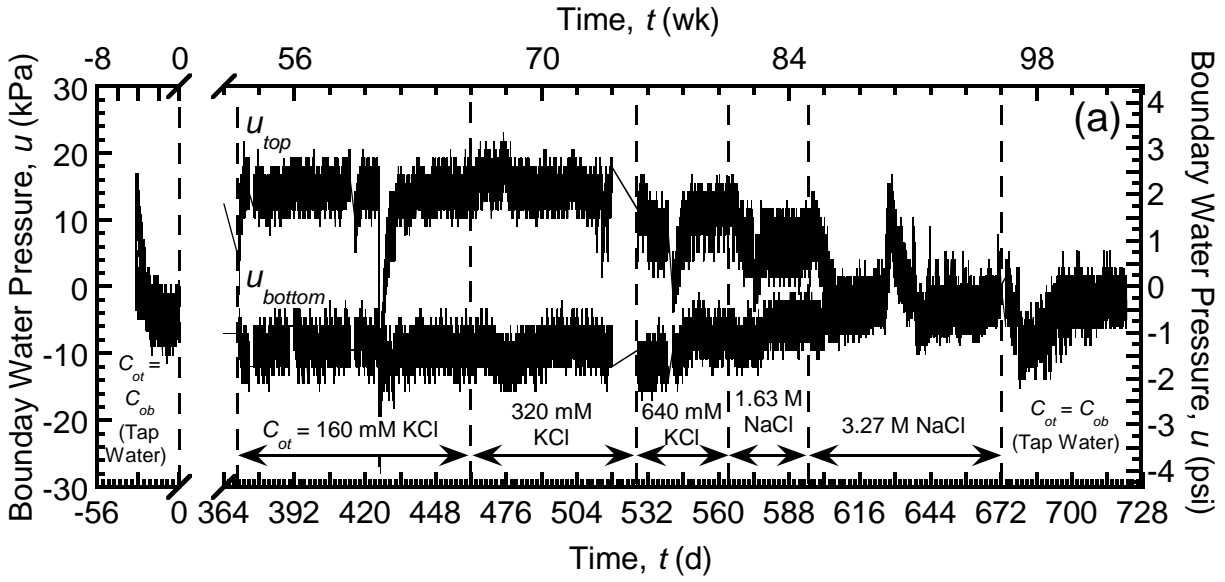


Figure 2.25. Boundary water pressures measured via in-line gage transducers: (a) specimen RW-1; (b) specimen RW-2.

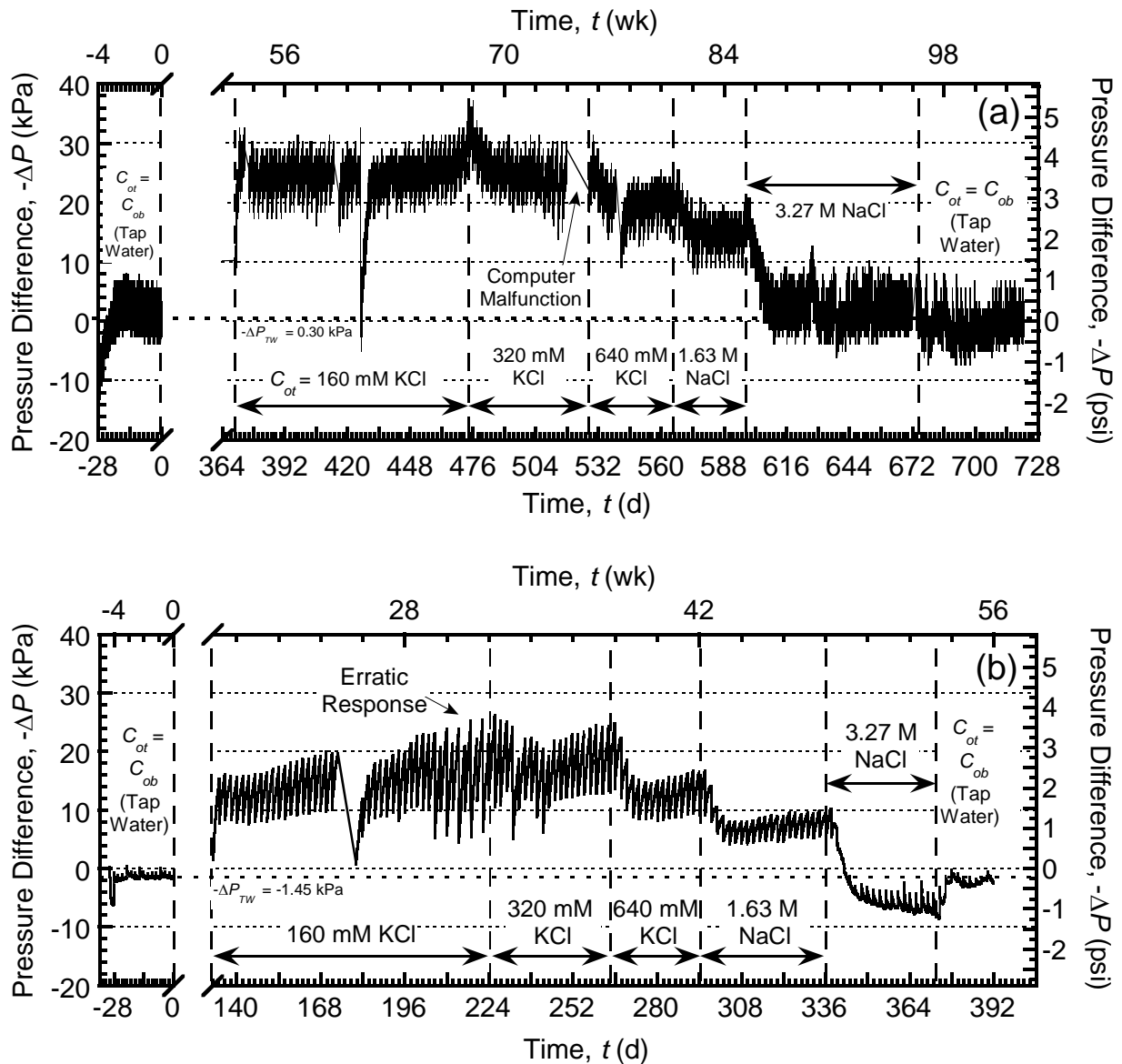


Figure 2.26. Chemico-osmotic pressure differences across the specimen measured via a differential pressure transducer: (a) specimen RW-1; (b) specimen RW-2.

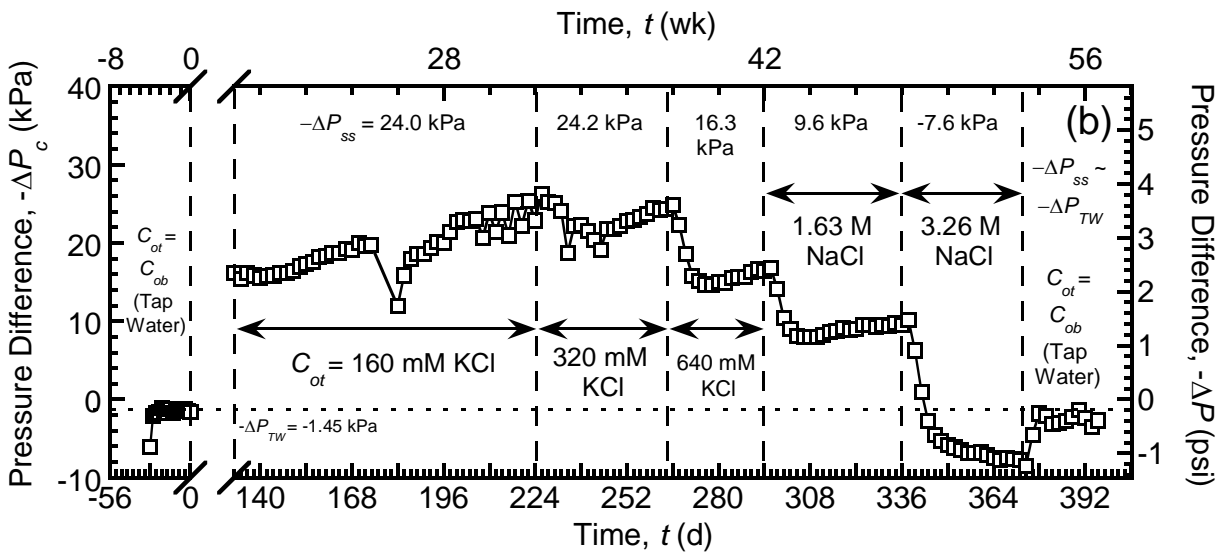
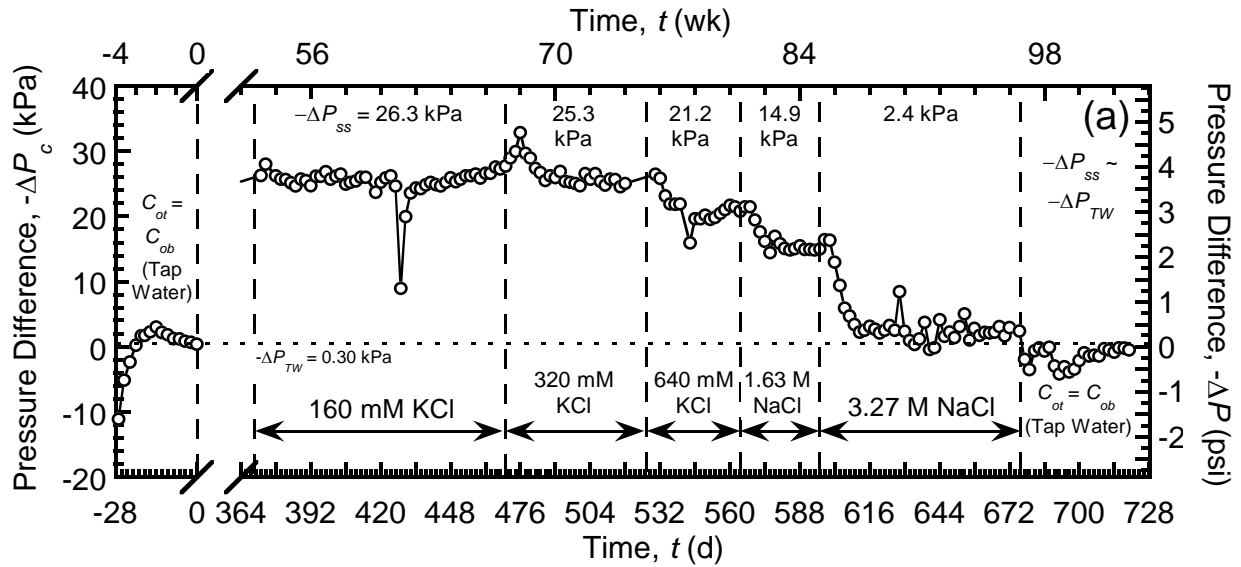


Figure 2.27. Values of the steady-state chemico-osmotic pressure difference for each two-day circulation cycle, $-\Delta P_c$: (a) specimen RW-1, determined as the geometric mean of the $-\Delta P$ values from the second day of the given cycle; (b) specimen RW-2, determined as the final (maximum) $-\Delta P$ value from the second day of the given cycle.

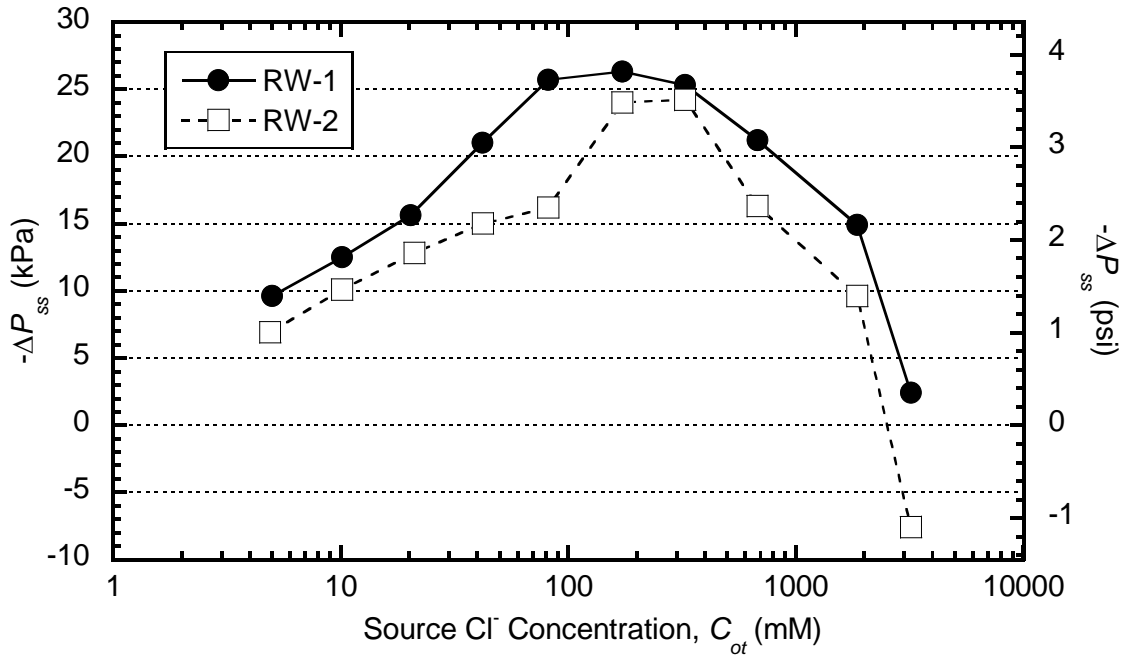


Figure 2.28. Steady-state chemico-osmotic pressures, $-\Delta P_{ss}$, for each stage of membrane testing for specimens RW-1 and RW-2, measured using a differential pressure transducer.

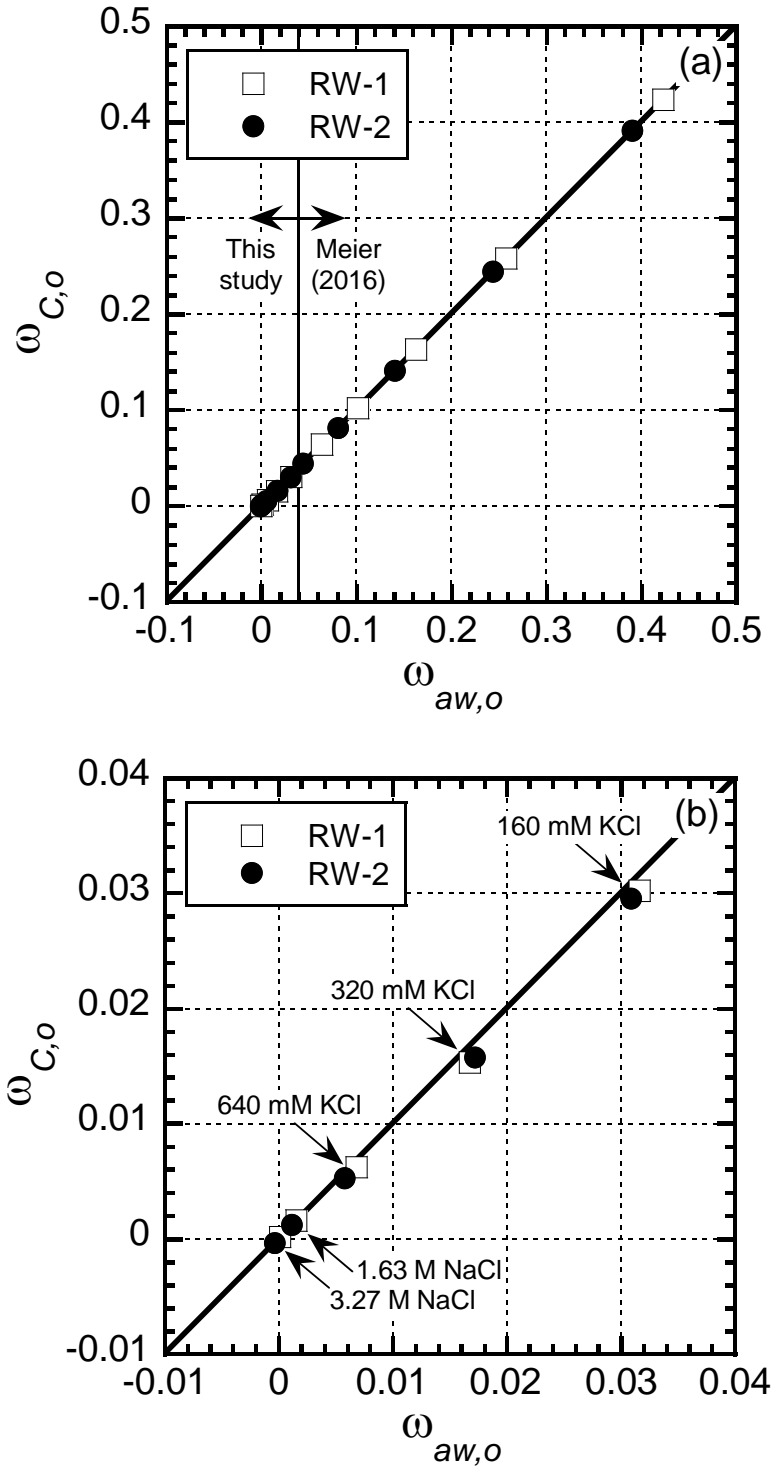


Figure 2.29. 1:1 plot of ω calculated using the van't Hoff expression (ω_C) vs. ω calculated using the activity method (ω_{aw}) for specimens RW-1 and RW-2 based on initial (source) solute concentrations: (a) for all stages of testing (Meier 2016 and this study); (b) for stages of testing conducted during this study.

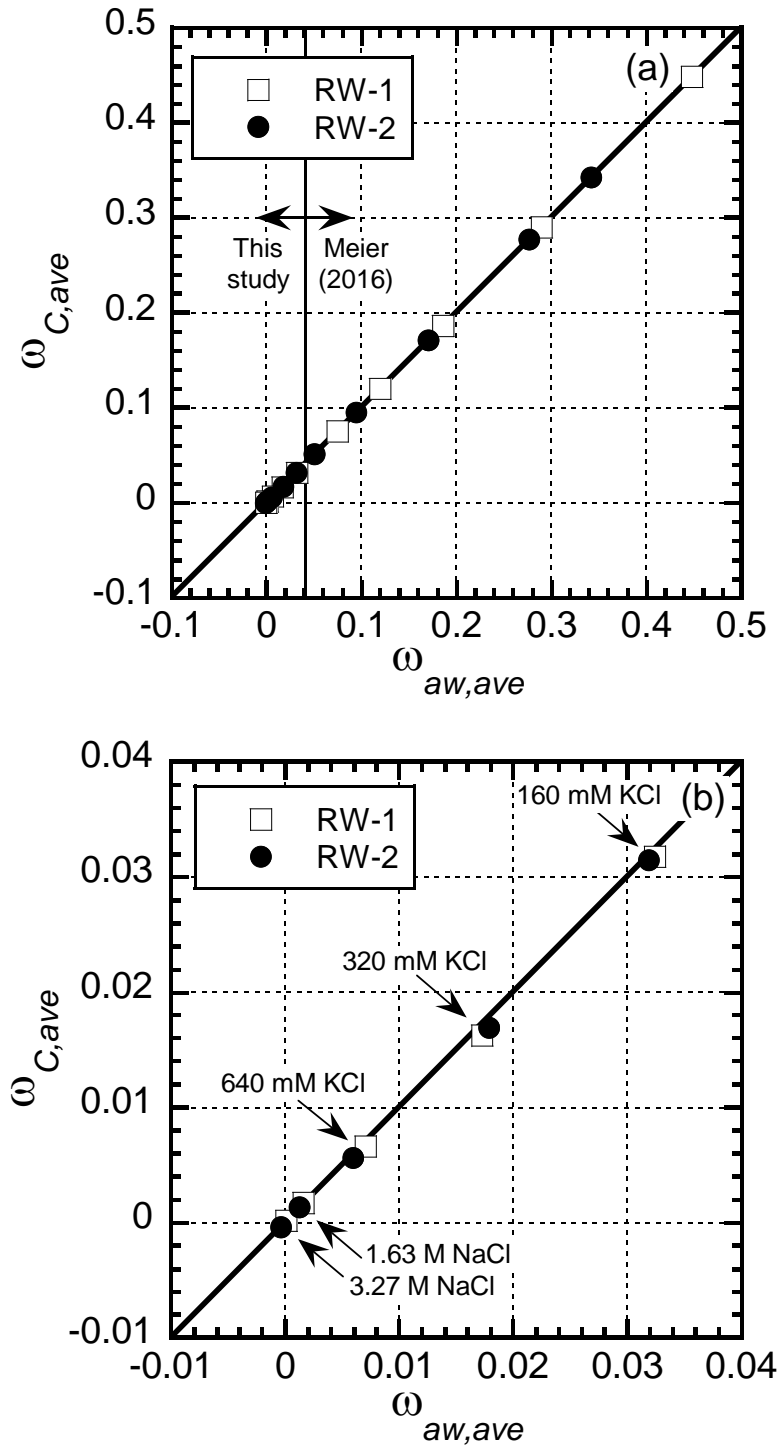


Figure 2.30. 1:1 plot of ω calculated using the van't Hoff expression (ω_C) vs. ω calculated using the activity method (ω_{aw}) for specimens RW-1 and RW-2 based on average solute concentrations: (a) for all stages of testing (Meier 2016 and this study); (b) for stages of testing conducted during this study.

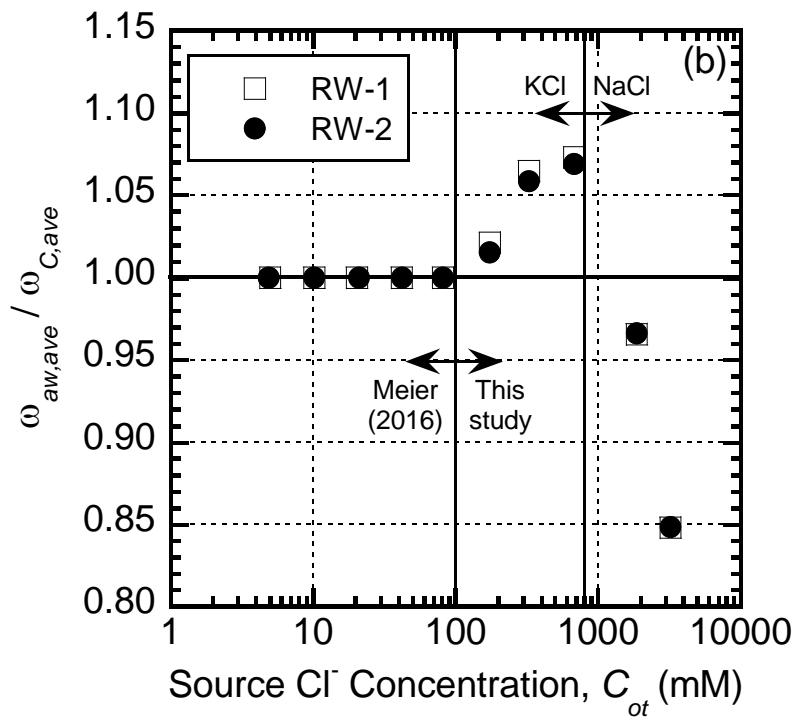
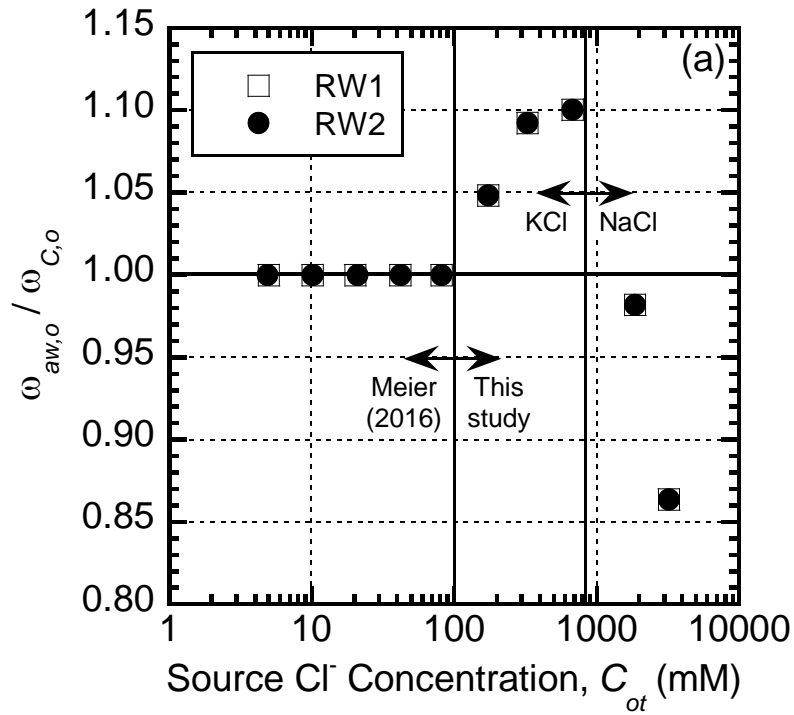


Figure 2.31. Ratio of ω calculated using the activity method (ω_{aw}) to ω calculated using the van't Hoff expression (ω_C) for specimens RW-1 and RW-2: (a) based on initial (source) solute concentrations; (b) based on average solute concentrations.

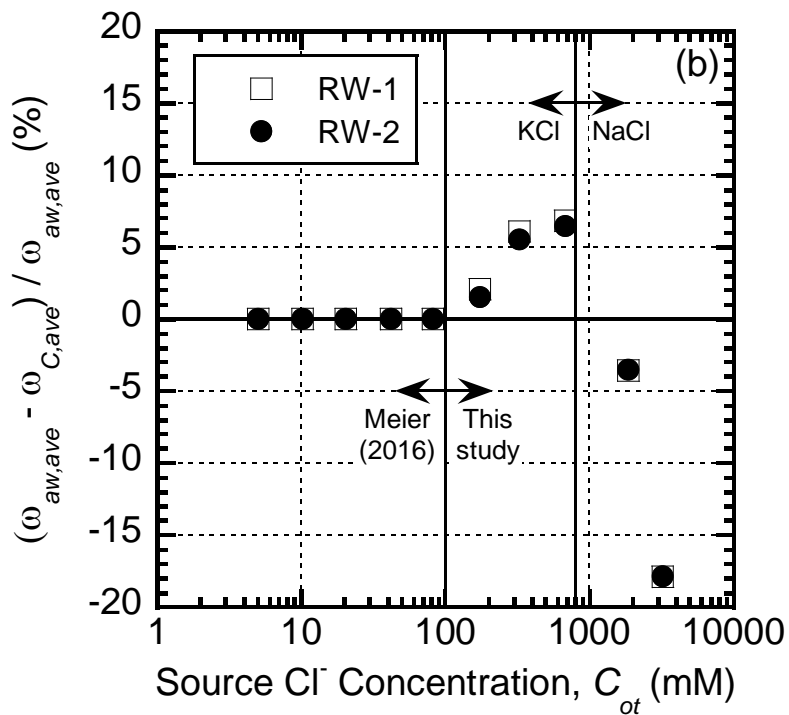
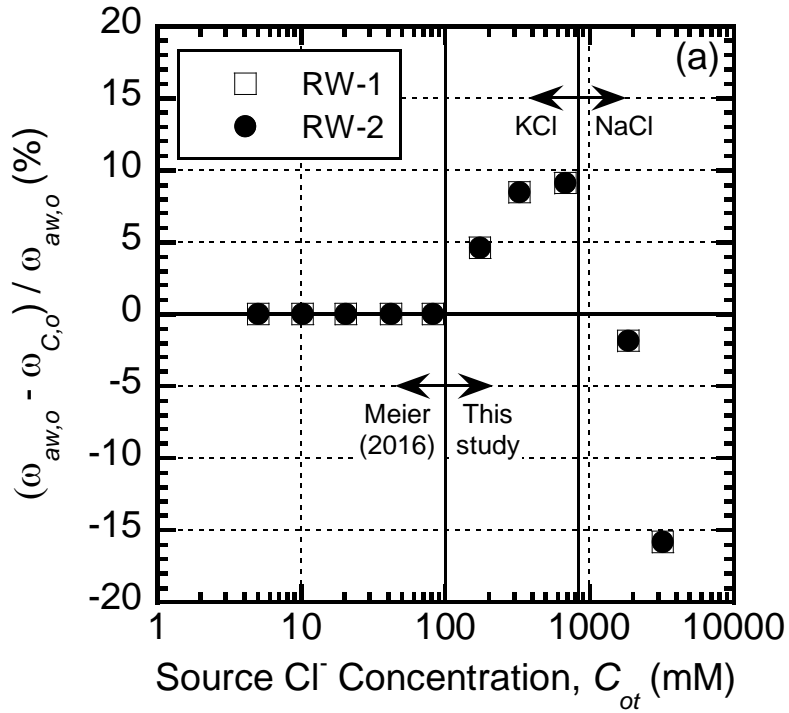


Figure 2.32. Percent error of ω calculated using the van't Hoff expression (ω_C) relative to ω calculated using the activity method (ω_{aw}) to for specimens RW-1 and RW-2: (a) based on initial (source) solute concentrations; (b) based on average solute concentrations.

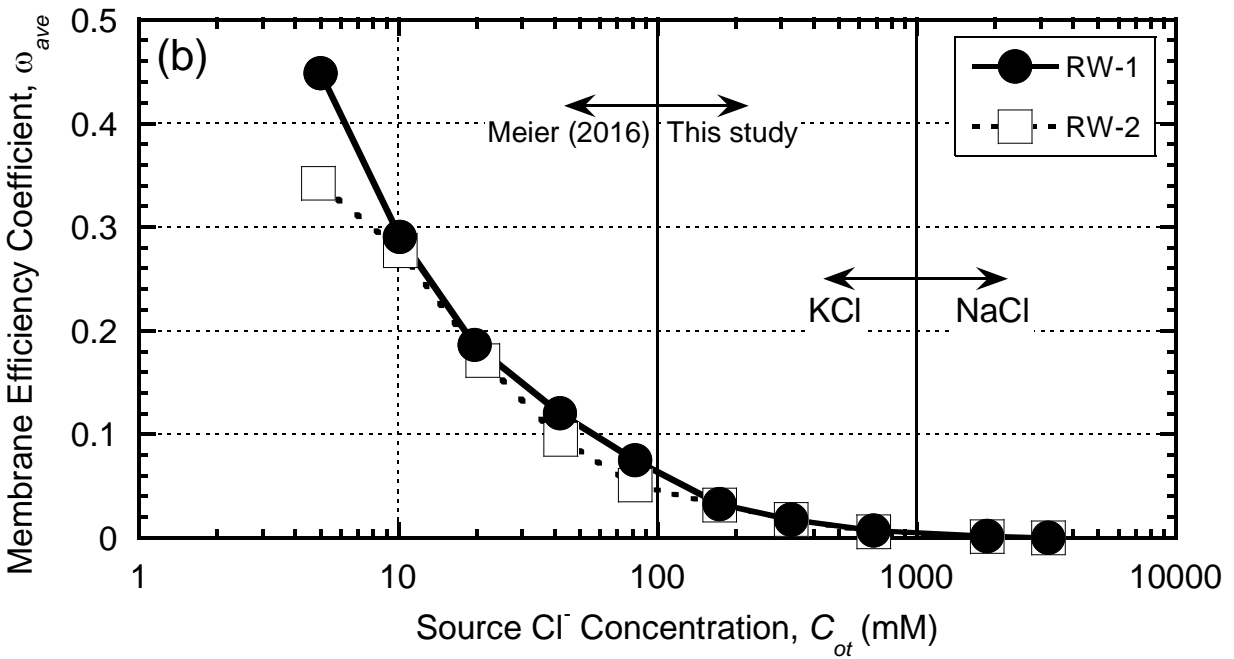
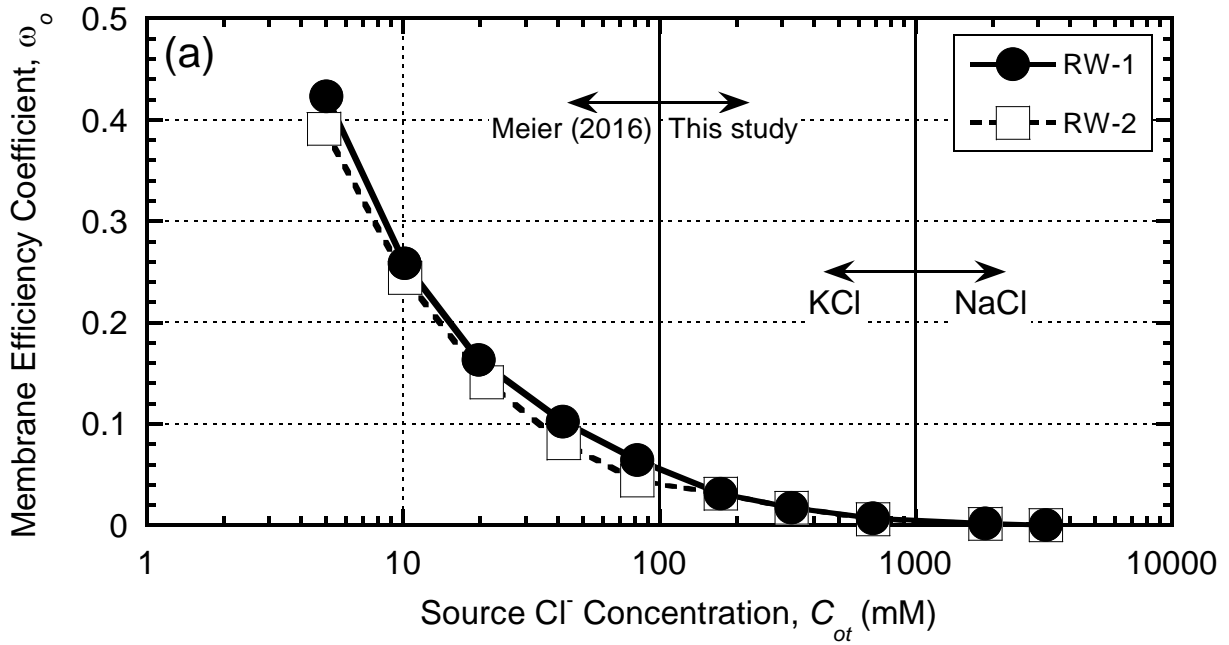


Figure 2.33. Membrane efficiency coefficients calculated for specimens RW-1 and RW-2; (a) based on initial (source) solute concentrations; (b) based on average solute concentrations.

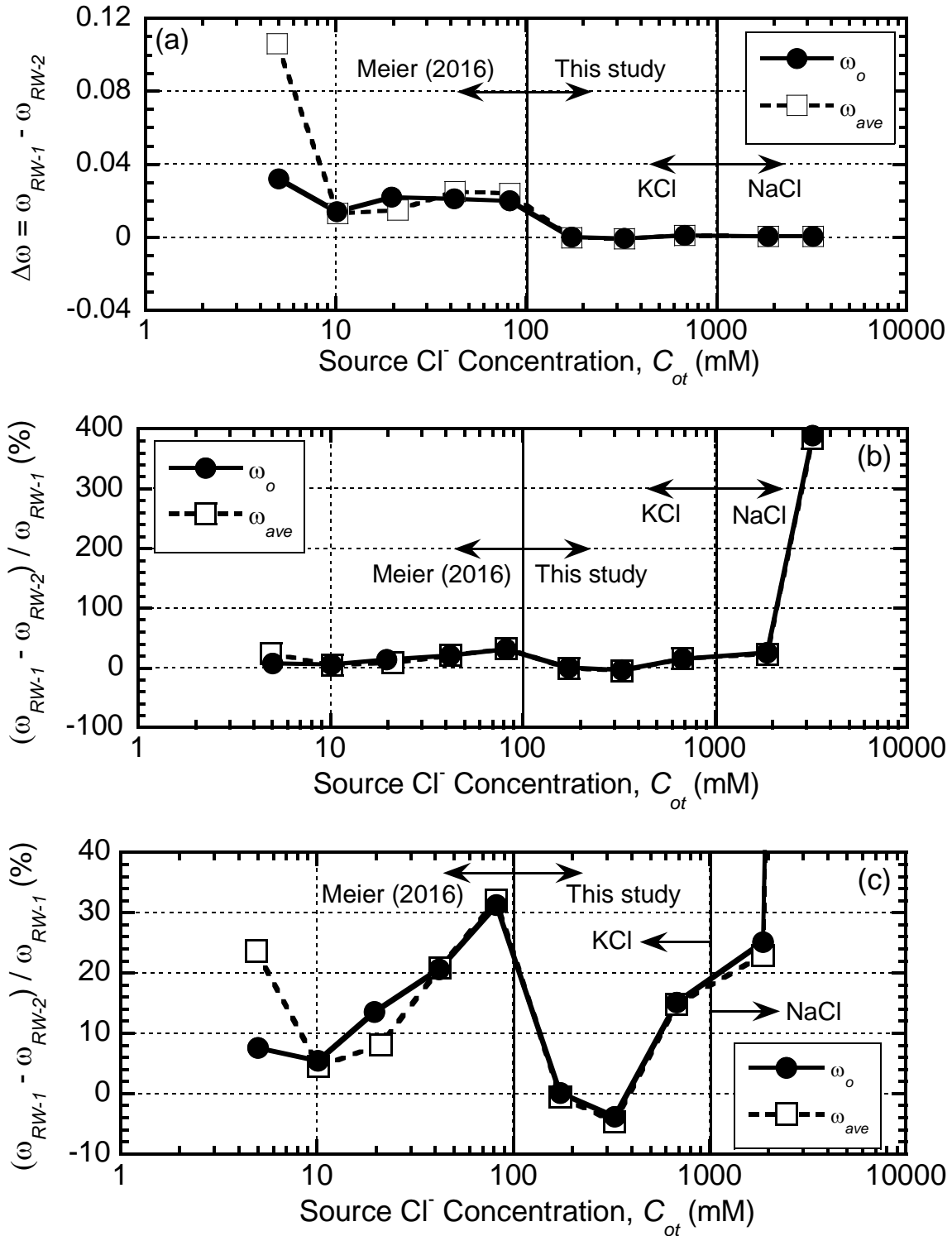


Figure 2.34. Comparison of membrane efficiency coefficients calculated for specimens RW-1 and RW-2 based on initial (source) solute concentrations (ω_o) and average solute concentrations (ω_{ave}): (a) difference ($\Delta\omega$) between ω_{RW-1} and ω_{RW-2} ; (b) percent error of ω_{RW-2} relative to ω_{RW-1} ; (c) reduced range of percent error of ω_{RW-2} relative to ω_{RW-1} .

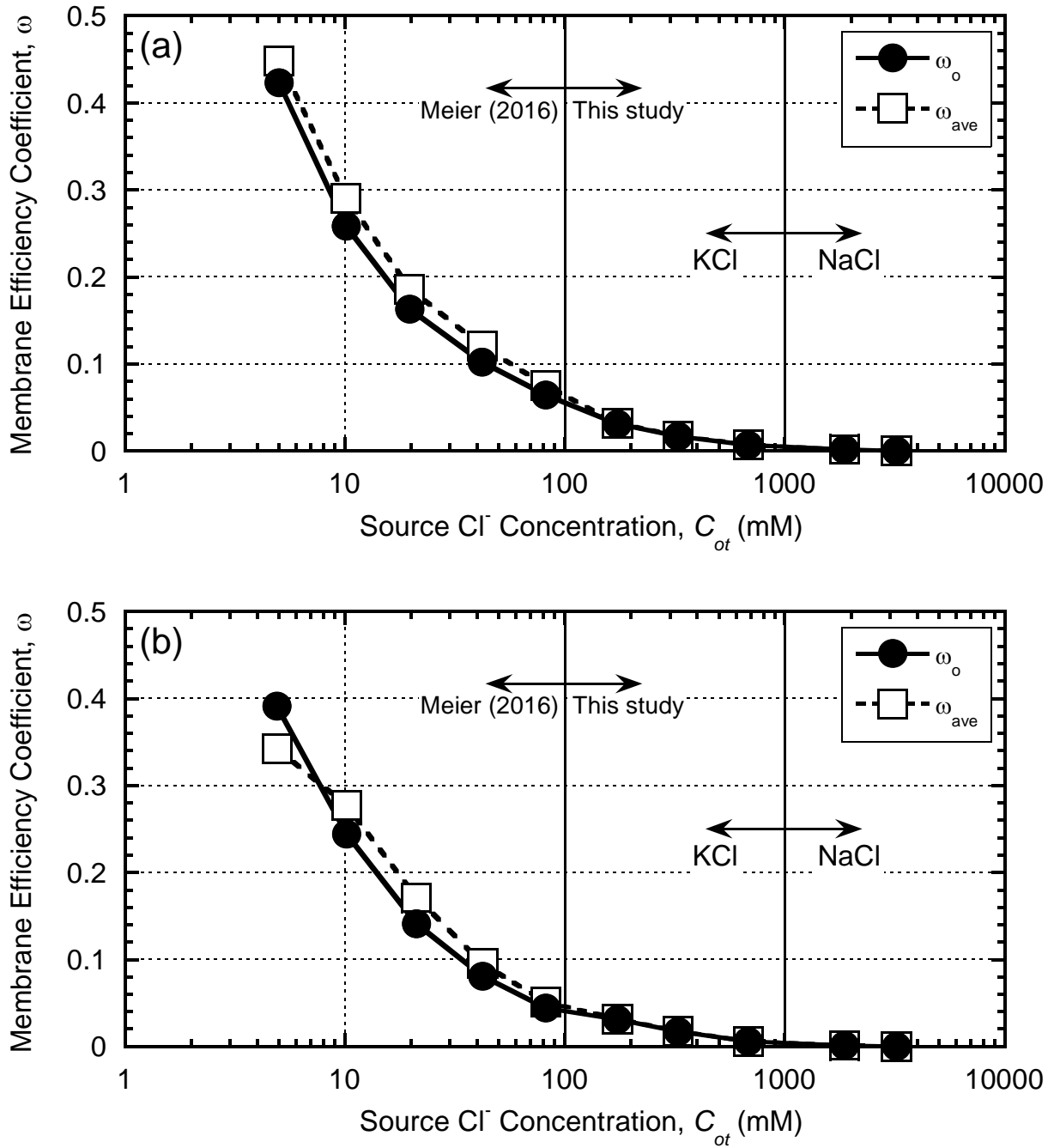


Figure 2.35. Membrane efficiency coefficients calculated based on initial (source) solute concentrations (ω_o) and average solute concentrations (ω_{ave}): (a) specimen RW-1; (b) specimen RW-2.

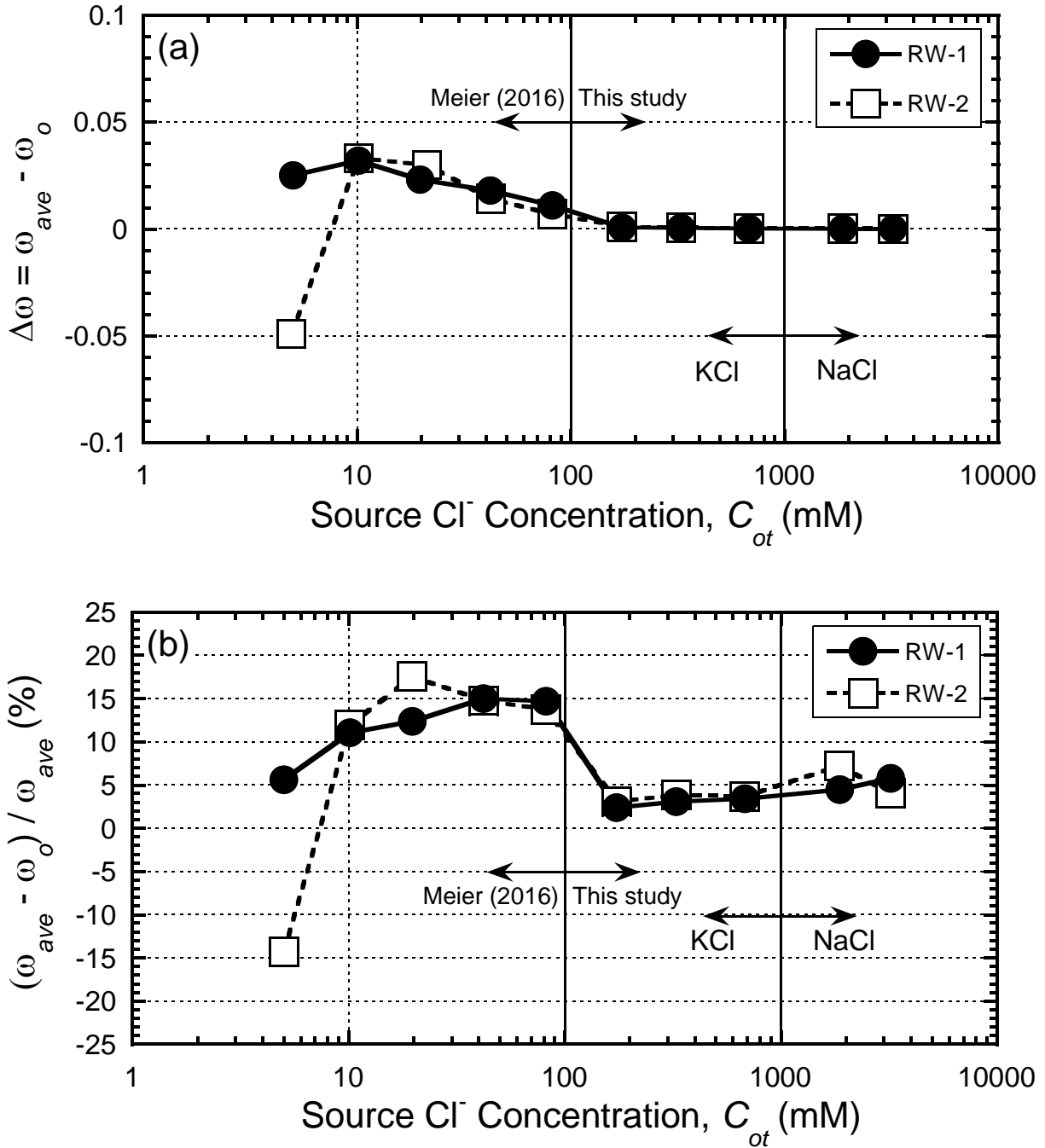


Figure 2.36. Comparison of membrane efficiency coefficients calculated based on initial (source) solute concentrations (ω_o) and average solute concentrations (ω_{ave}) for specimens RW-1 and RW-2: (a) difference ($\Delta\omega$) between ω_o and ω_{ave} ; (b) percent error of ω_o relative to ω_{ave} .

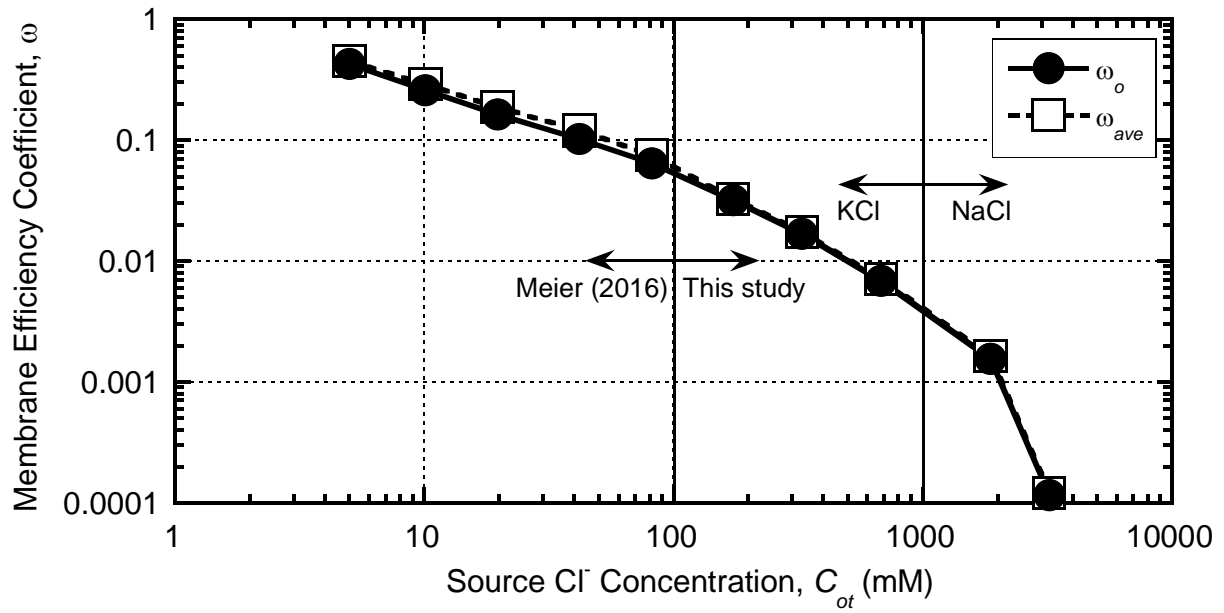


Figure 2.37. Membrane efficiency coefficients calculated for specimen RW-1 based on initial (source) solute concentrations (ω_o) and average solute concentrations (ω_{ave}); plotted on a log-log scale.

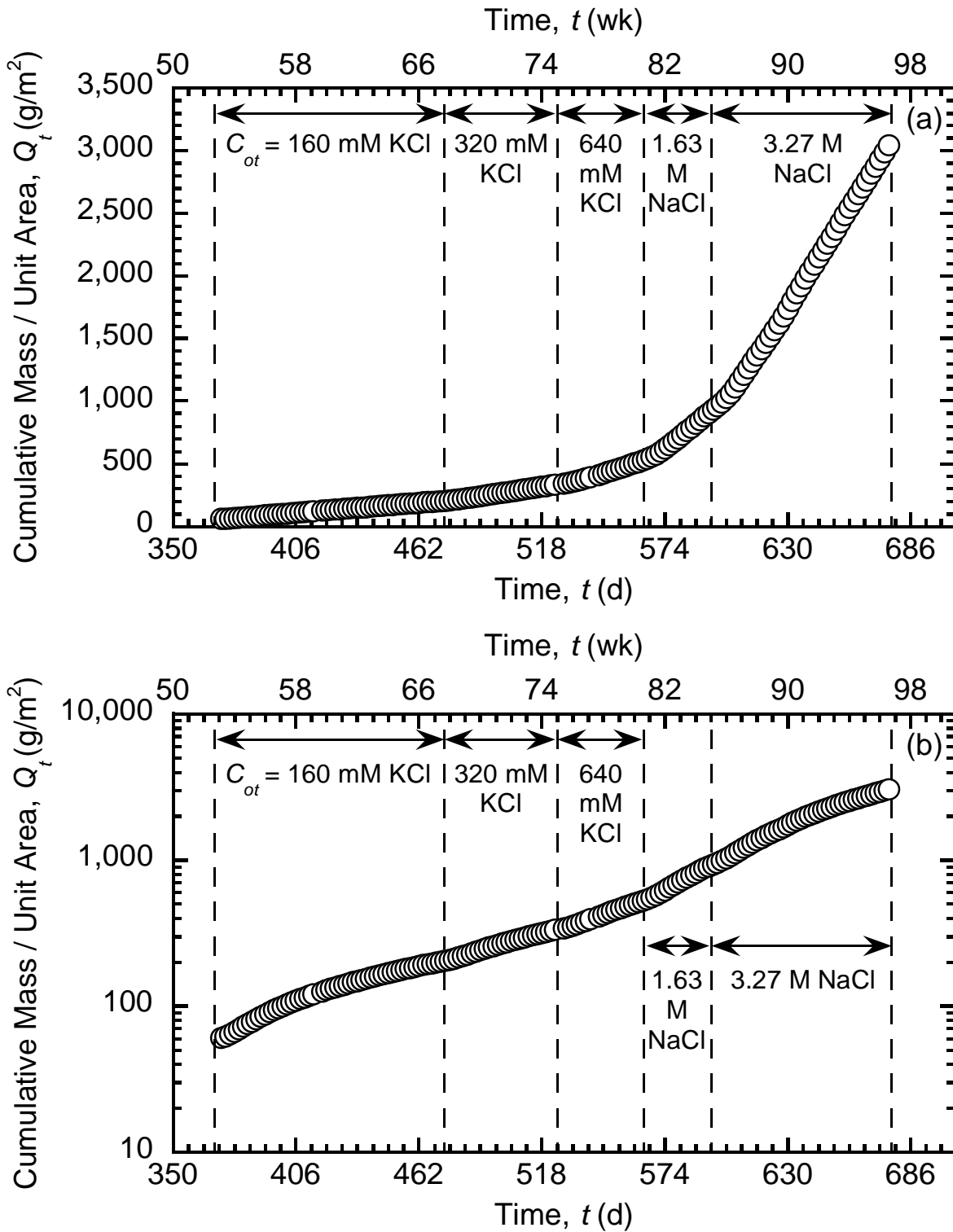


Figure 2.38. Cumulative mass data for chloride (Cl⁻) diffusion through specimen RW-1 for stages of testing conducted in this study: (a) plotted on a linear scale; (b) plotted on a semi-log scale.

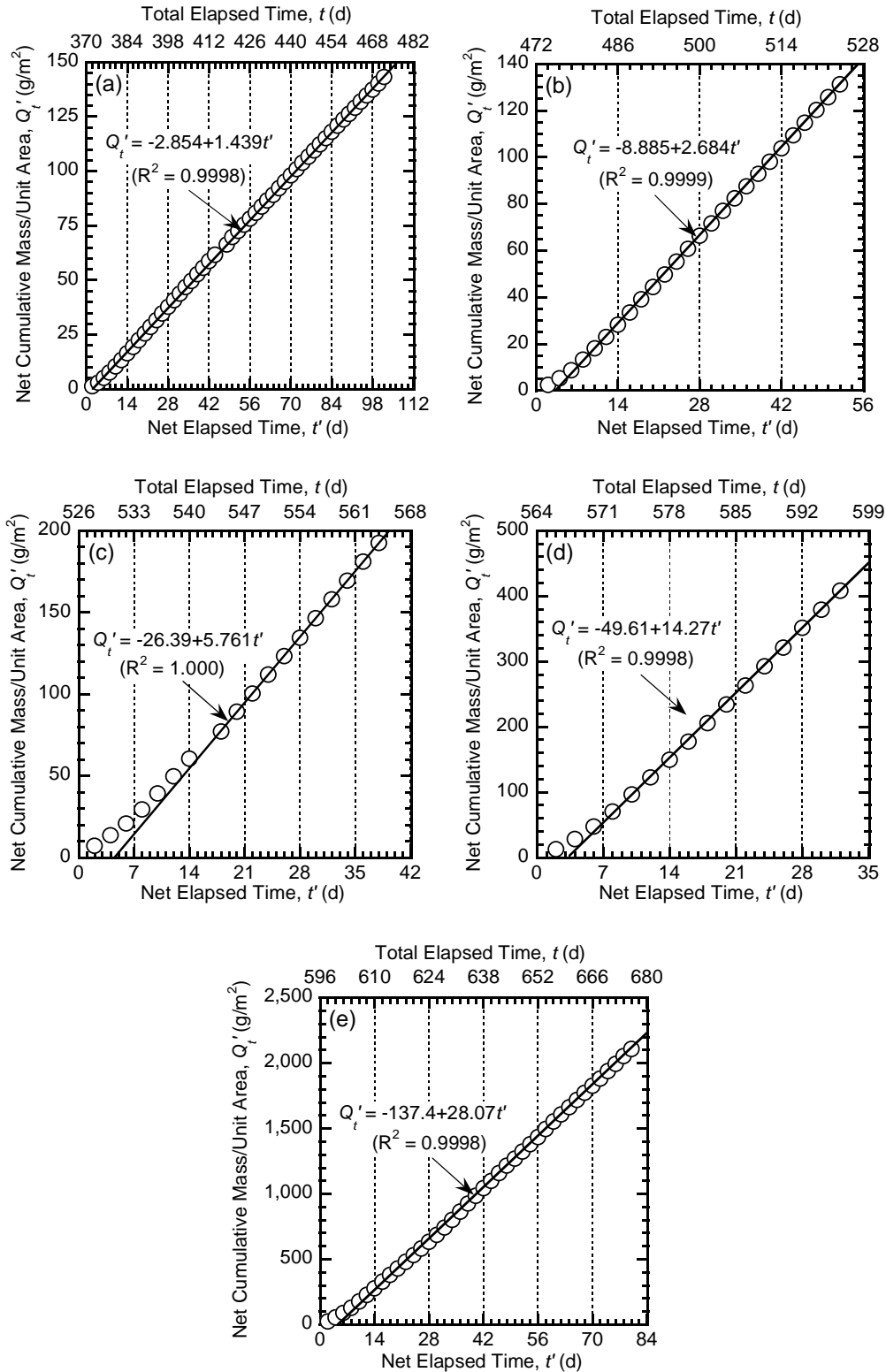


Figure 2.39. Net cumulative mass data for chloride (Cl⁻) diffusion through specimen RW-1 with steady-state linear regressions: (a) $C_{ot} = 160$ mM KCl; (b) 320 mM KCl; (c) 640 mM KCl; (d) 1.63 M NaCl; (e) 3.27 M NaCl.

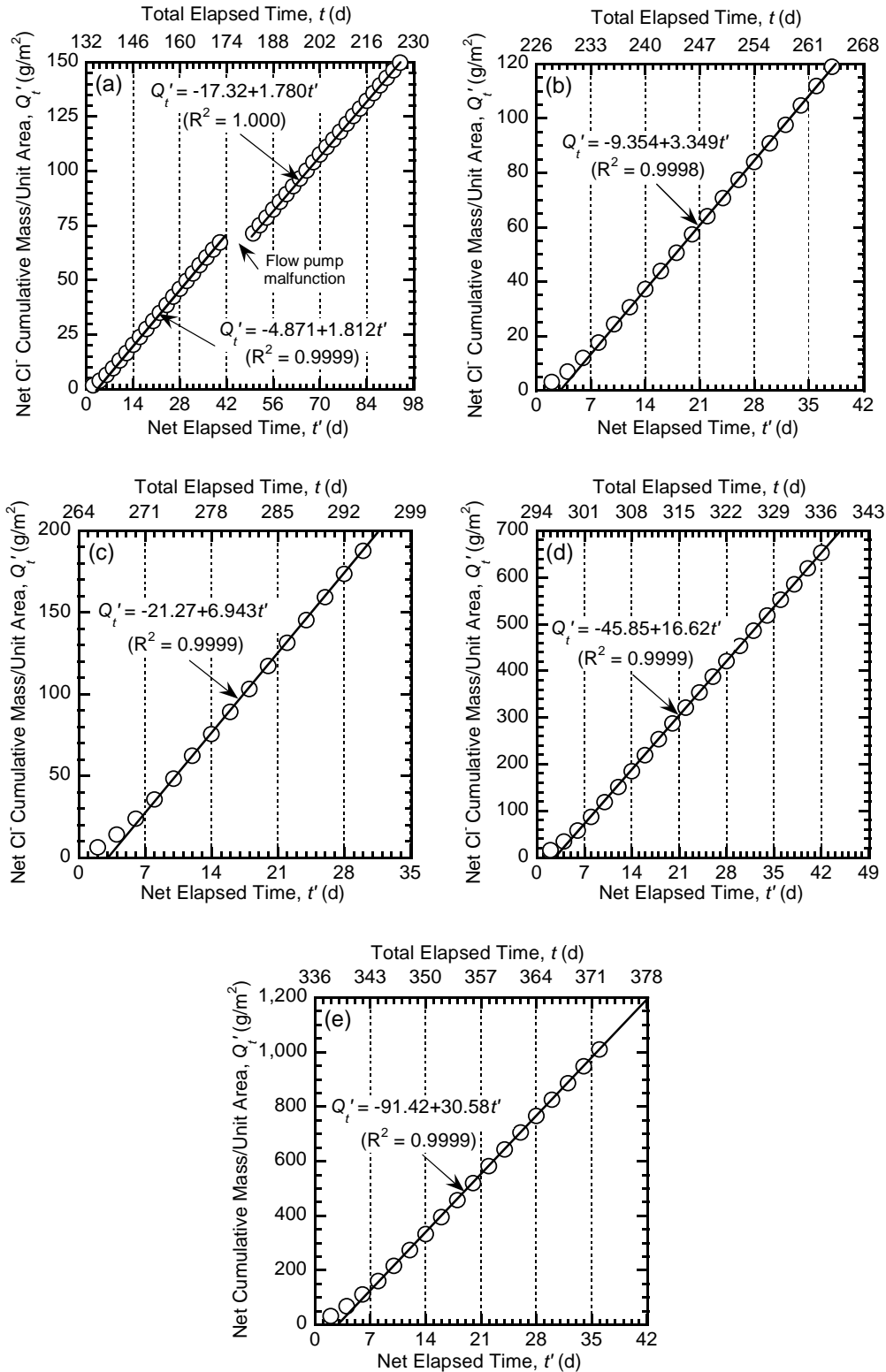


Figure 2.40. Net cumulative mass data for chloride (Cl⁻) diffusion through specimen RW-2 with steady-state linear regressions: (a) $C_{ot} = 160$ mM KCl; (b) 320 mM KCl; (c) 640 mM KCl; (d) 1.63 M NaCl; (e) 3.27 M NaCl.

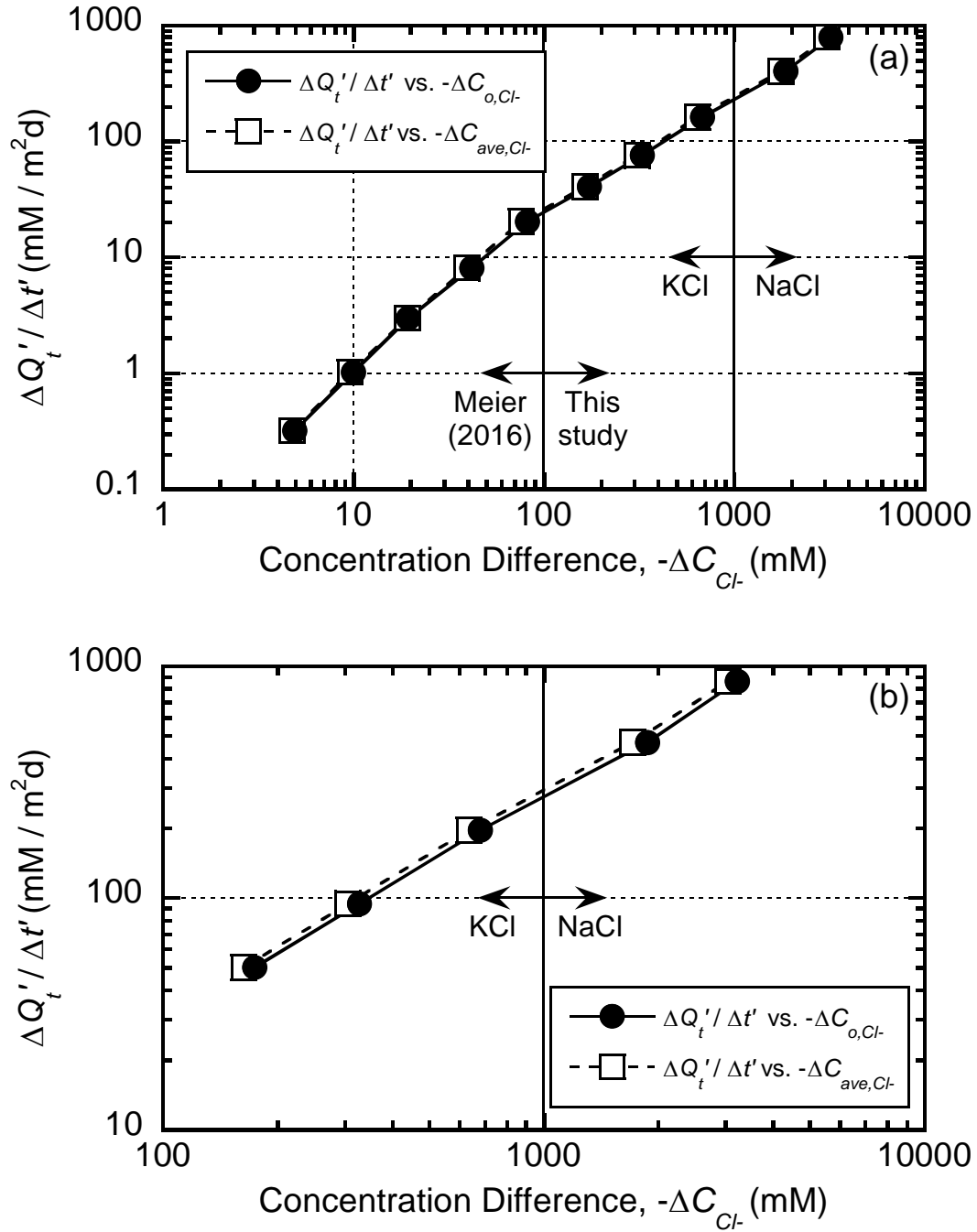


Figure 2.41. Slopes of the net cumulative mass plots, $\Delta Q'_t / \Delta t'$, as a function of the difference in the source ($\Delta C_{o,Cl^-}$) and average ($\Delta C_{ave,Cl^-}$) solute concentrations: (a) specimen RW-1; (b) specimen RW-2.

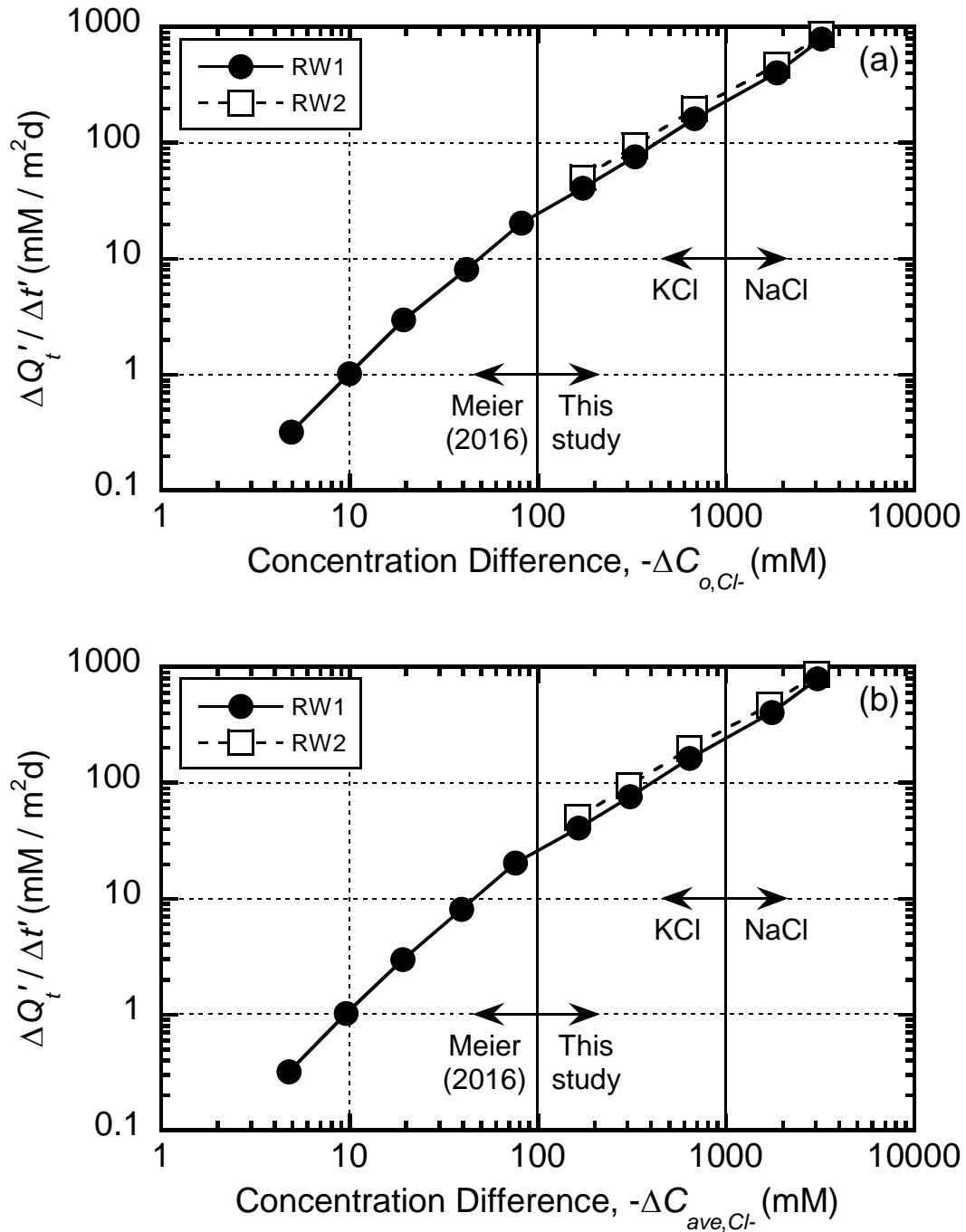


Figure 2.42. Comparison of the slopes of the net cumulative mass plots, $\Delta Q'_t / \Delta t'$, as a function of the concentration difference across specimens RW-1 and RW-2: (a) based on the initial (source) solute concentration difference ($\Delta C_{o,Cl-}$); (b) based on the average solute concentration difference ($\Delta C_{ave,Cl-}$).

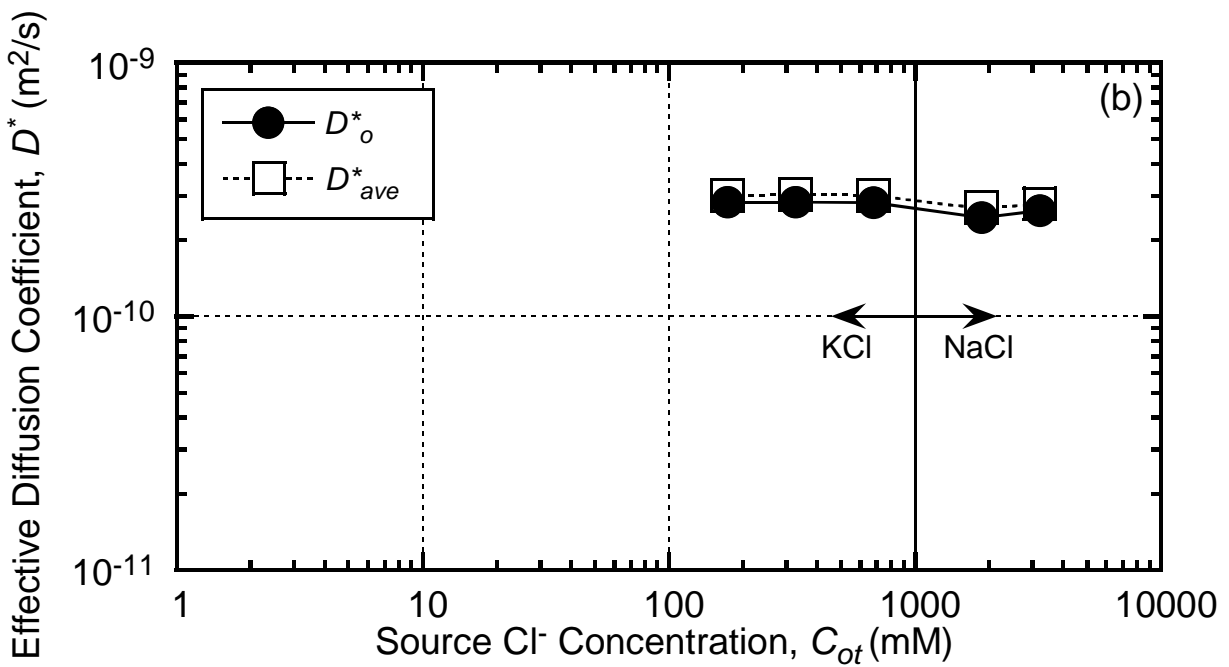
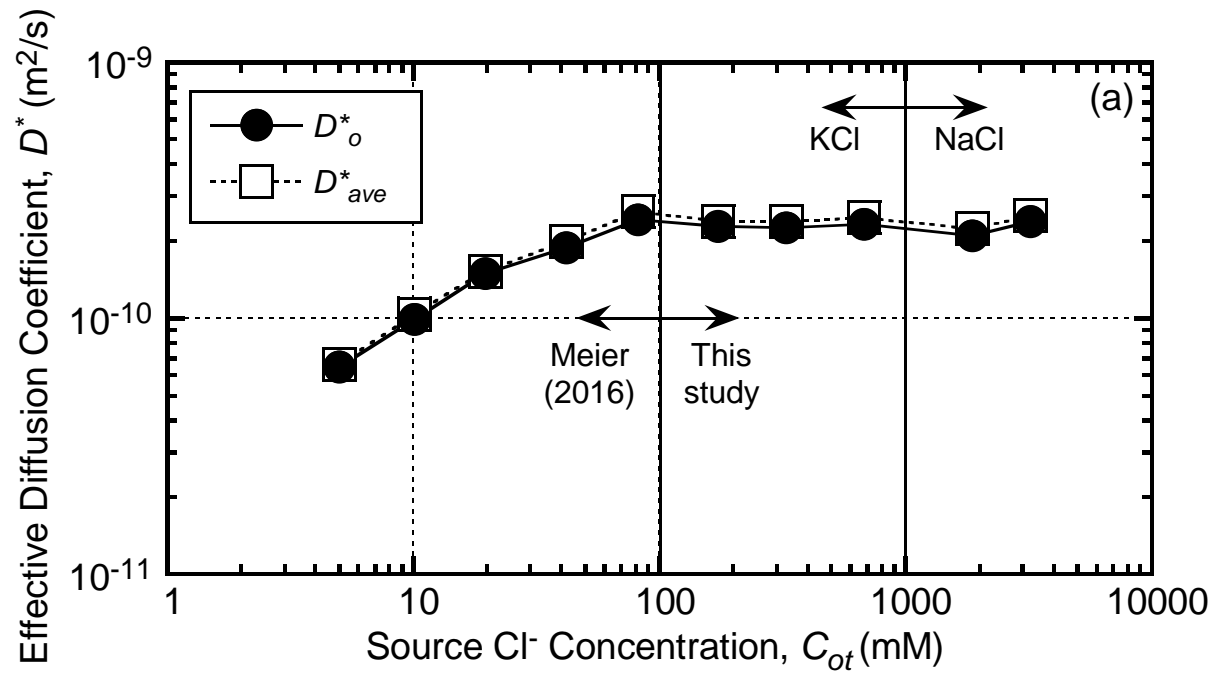


Figure 2.43. Effective diffusion coefficients for Cl⁻ as a function of initial (source) solute concentrations (D_o^*) and average solute concentrations (D_{ave}^*): (a) specimen RW-1; (b) specimen RW-2.

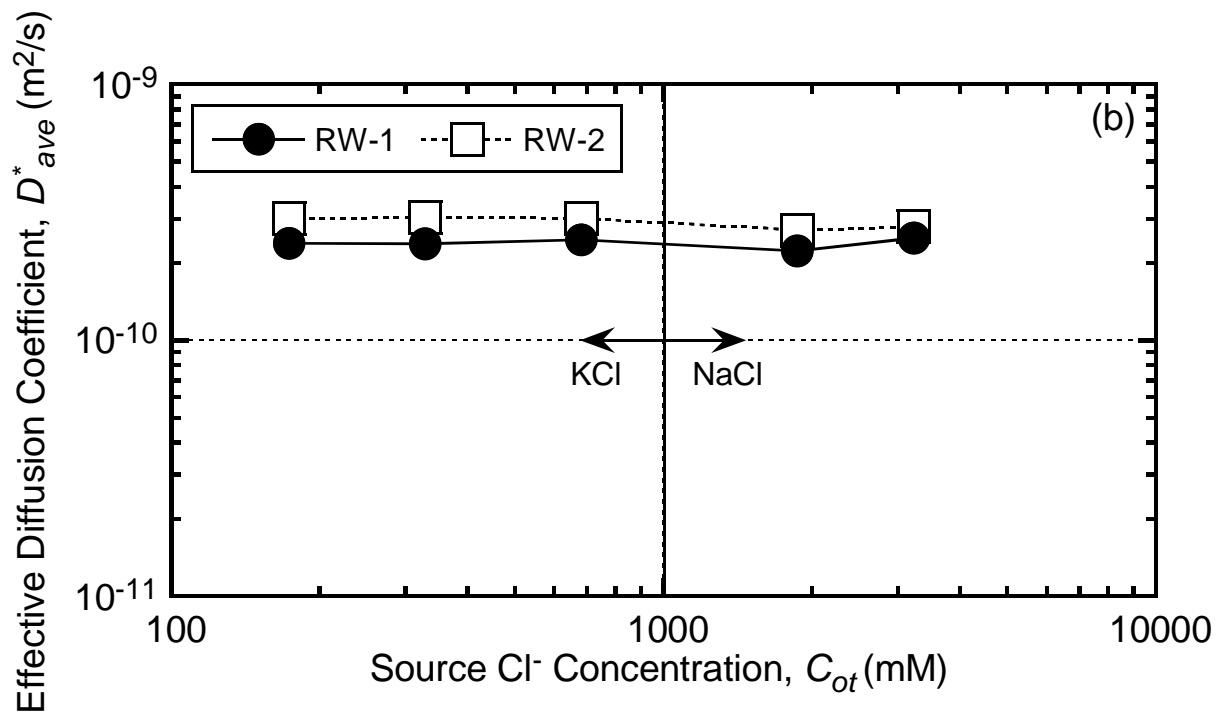
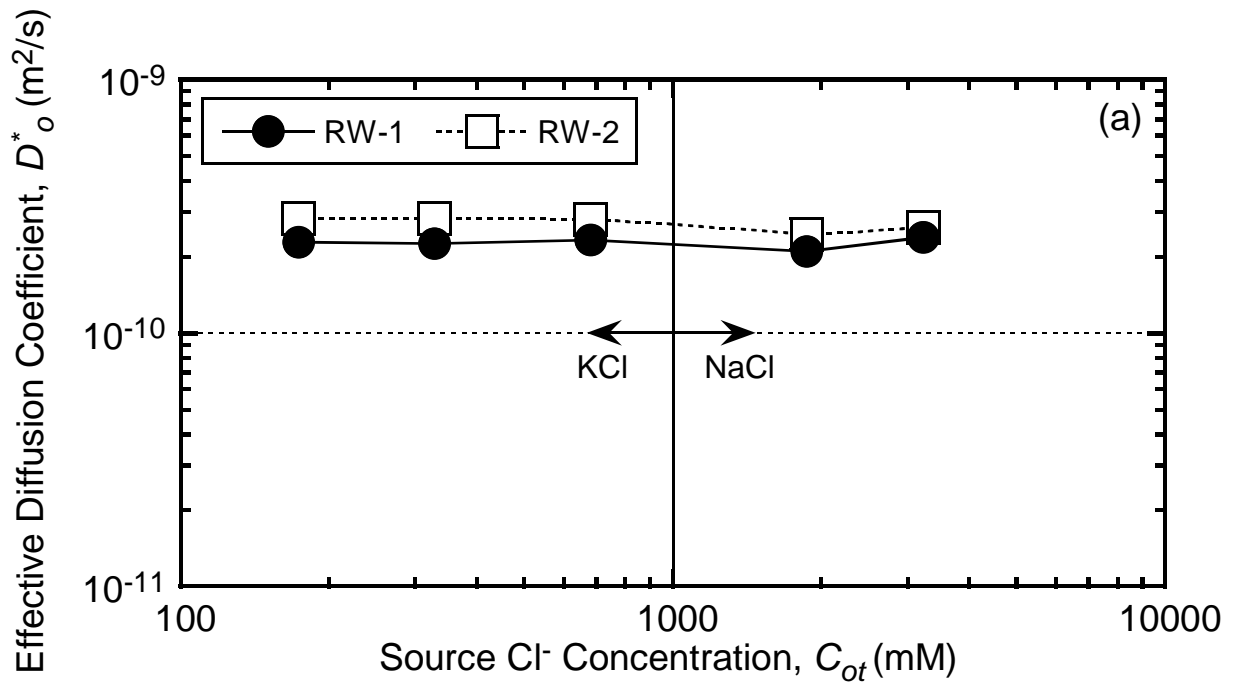


Figure 2.44. Comparison of effective diffusion coefficients for Cl⁻ for specimens RW-1 and RW-2: (a) as a function of initial (source) solute concentrations (D_o^*); (b) as a function of average solute concentrations (D_{ave}^*).

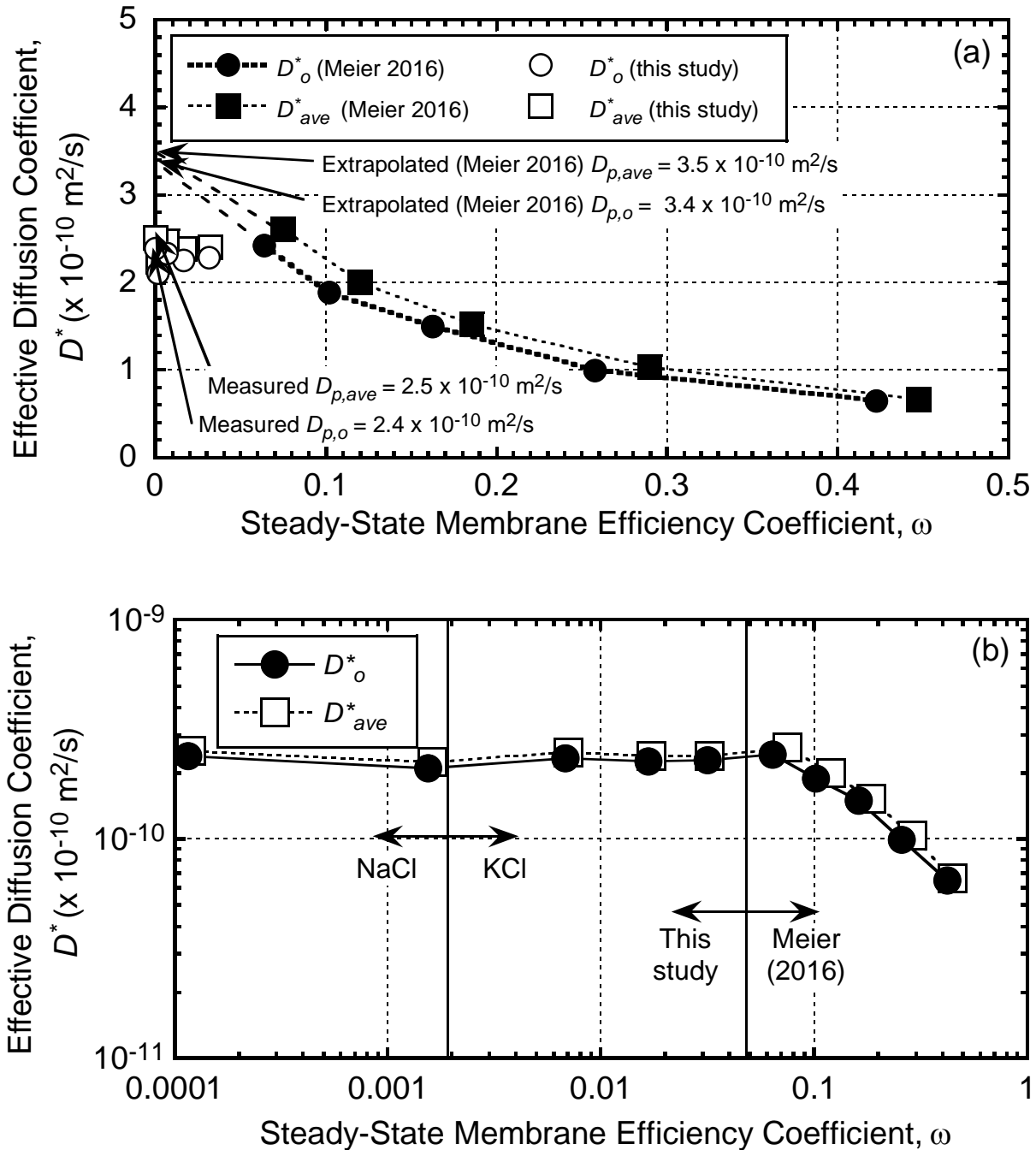


Figure 2.45. Effective diffusion coefficients for Cl^- as a function of the steady-state membrane efficiency coefficients for specimen RW-1, based on initial (source) solute concentrations (D_o^* , ω_o) and average solute concentrations (D_{ave}^* , ω_{ave}): (a) with extrapolated D_p values determined by Meier (2016) and measured D_p values from this study; (b) values plotted on a log-log scale.

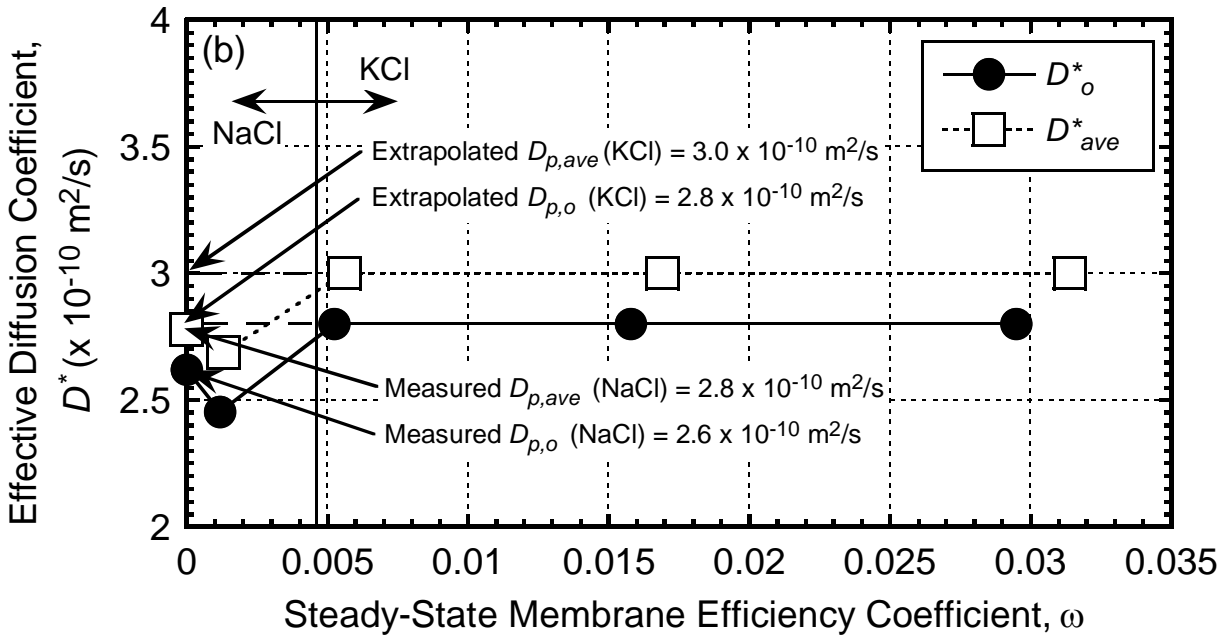
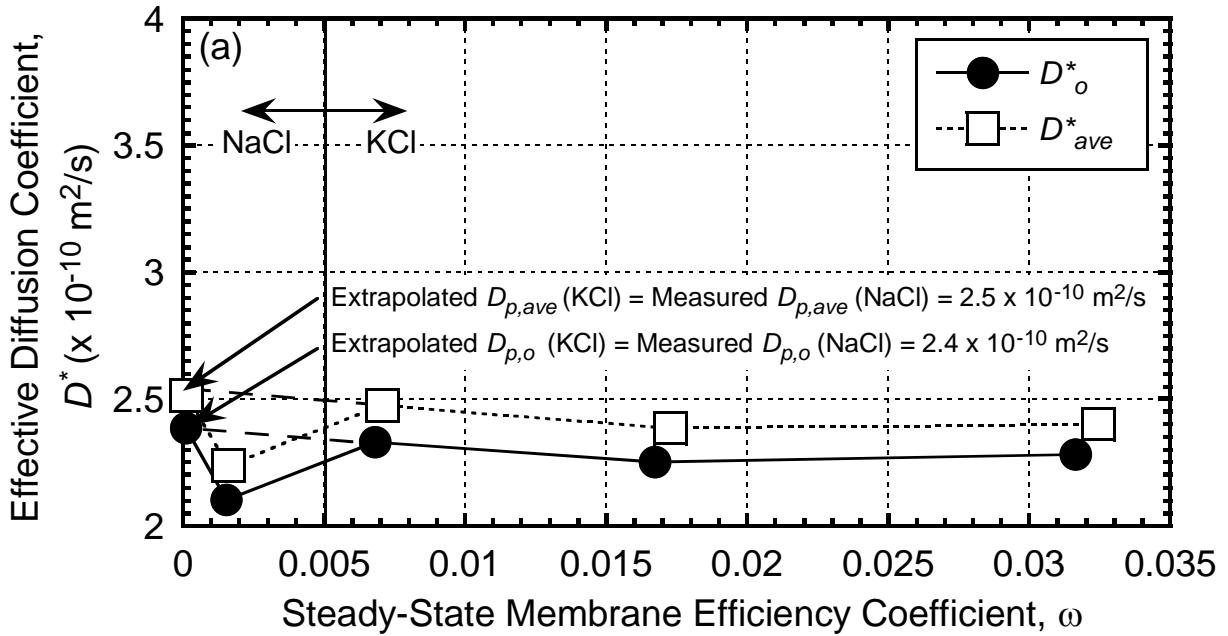


Figure 2.46. Effective diffusion coefficients for Cl^- as a function of the steady-state membrane efficiency coefficients based on initial (source) solute concentrations (D_o^* , ω_o) and average solute concentrations (D_{ave}^* , ω_{ave}): (a) specimen RW-1; (b) specimen RW-2.

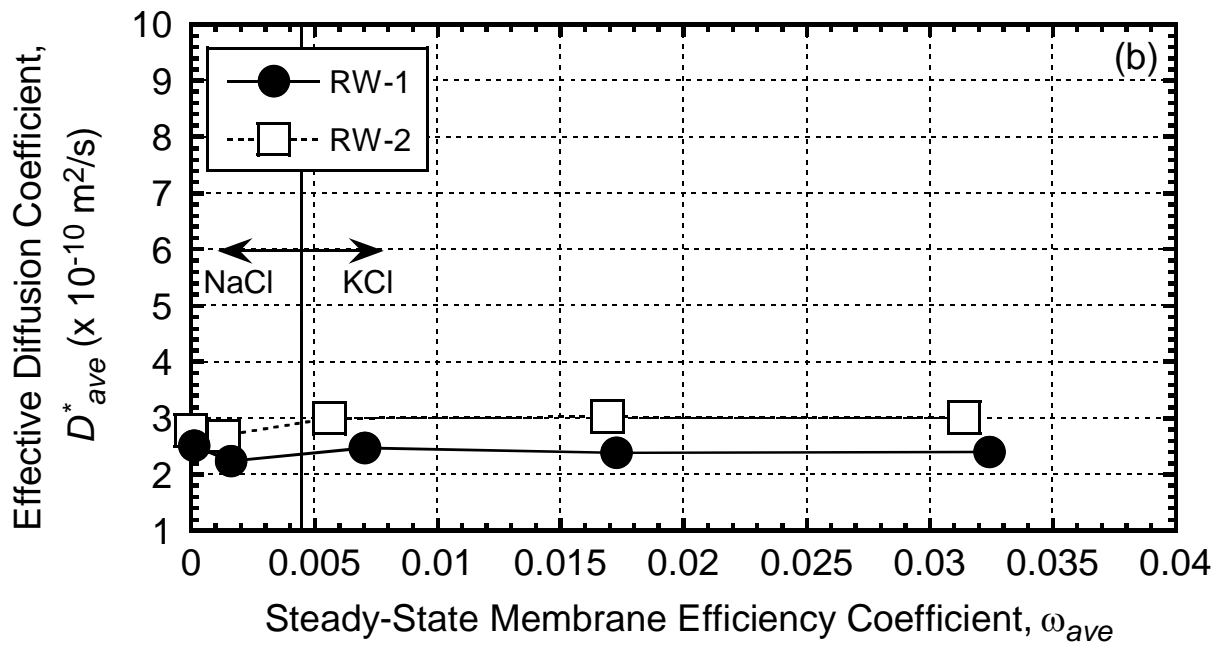
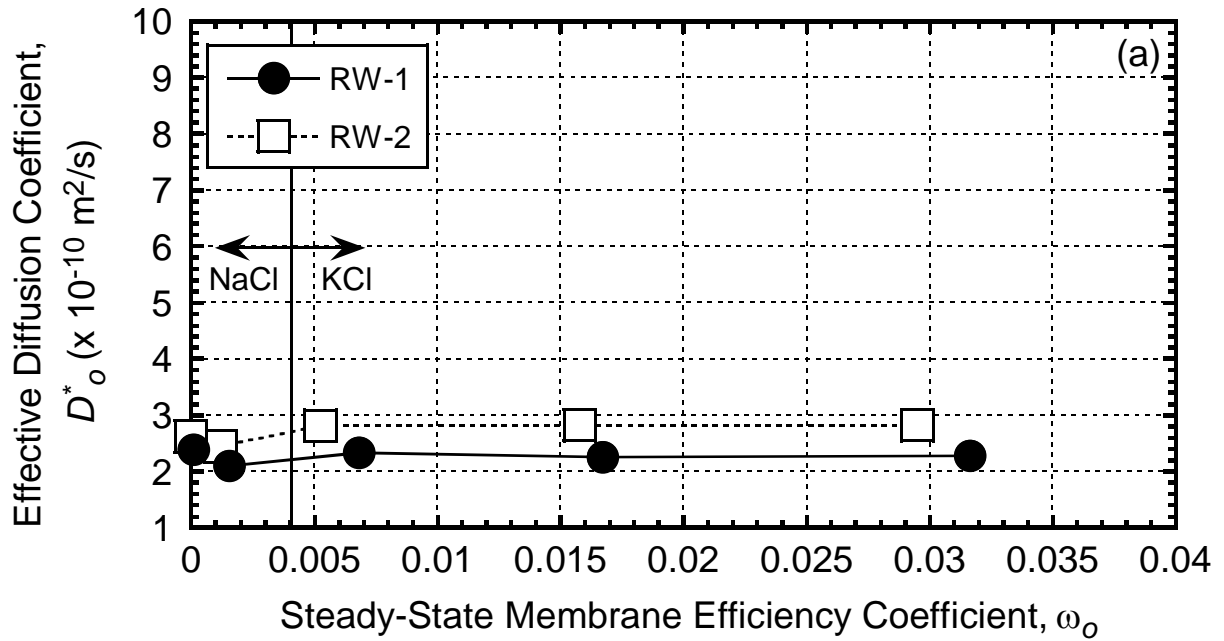


Figure 2.47. Comparison of effective diffusion coefficients for Cl^- as a function of steady-state membrane efficiency coefficients for specimens RW-1 and RW-2: (a) based on initial (source) solute concentrations (D_o^* , ω_o); (b) based on average solute concentrations (D_{ave}^* , ω_{ave}).

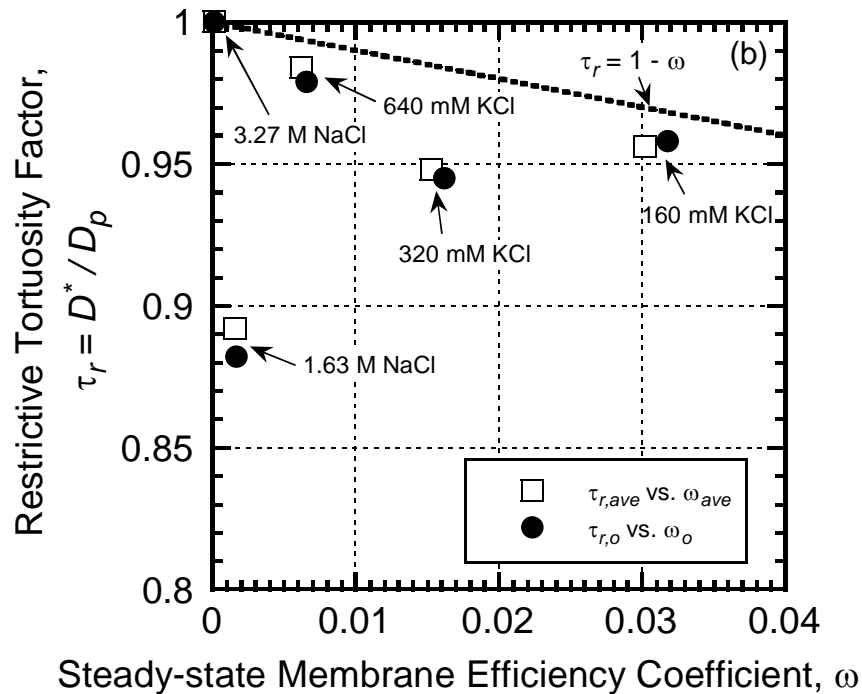
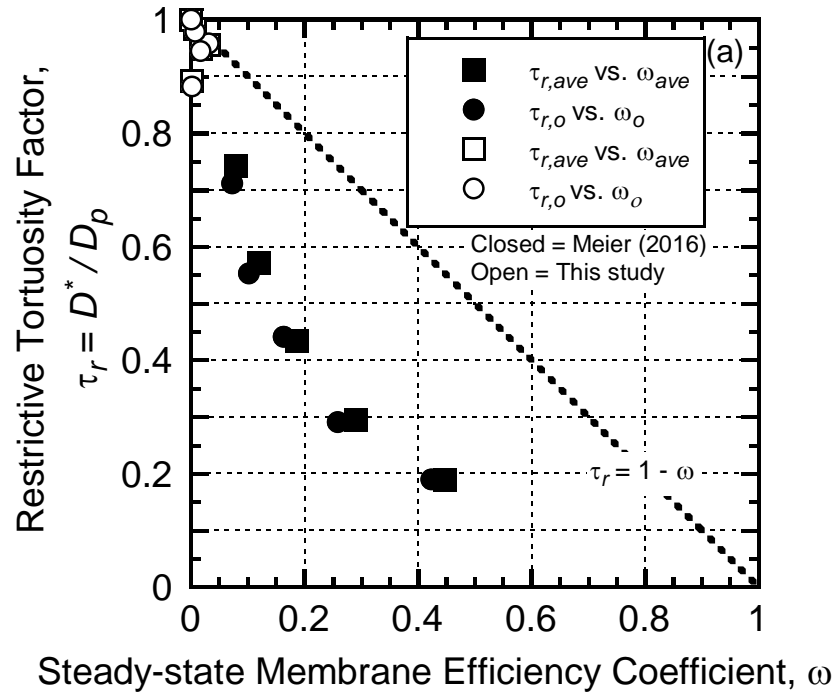


Figure 2.48. Restrictive tortuosity factors for specimen RW-1, based on the measured effective diffusion coefficient, D^* , for Cl^- , as a function of the steady-state membrane efficiency coefficient, ω : (a) including results from Meier (2016) for comparison; (b) reduced range including the results from this study.

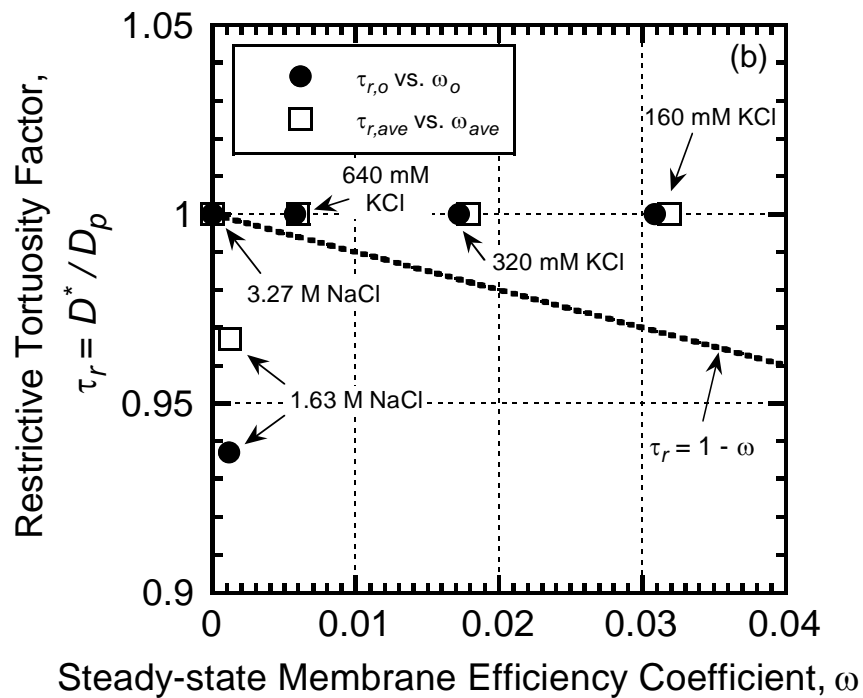
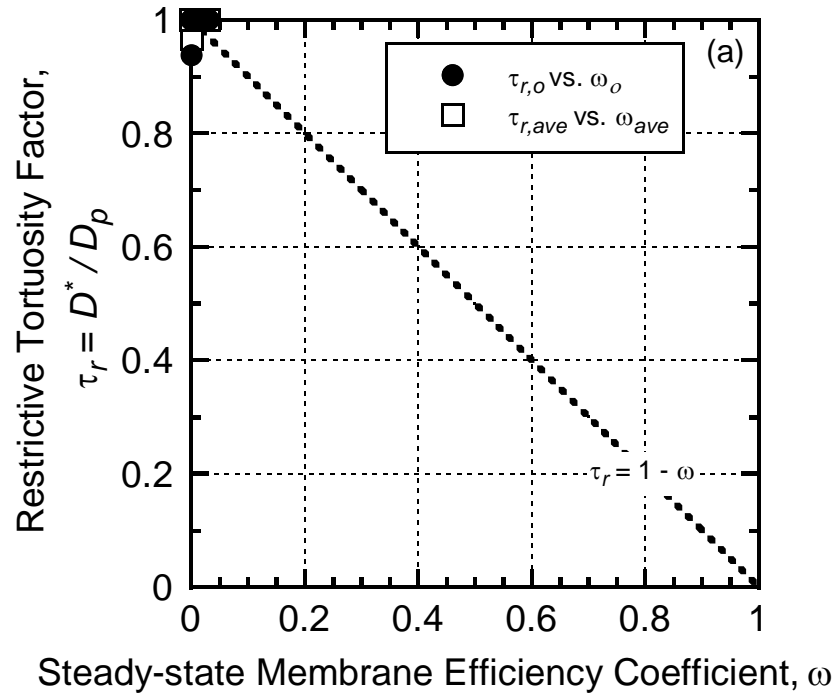


Figure 2.49. Restrictive tortuosity factors for specimen RW-2, based on the measured effective diffusion coefficient, D^* , as a function of the steady-state membrane efficiency coefficient, ω : (a) shown on a 1:1 plot (as typically shown); (b) shown over a reduced range.

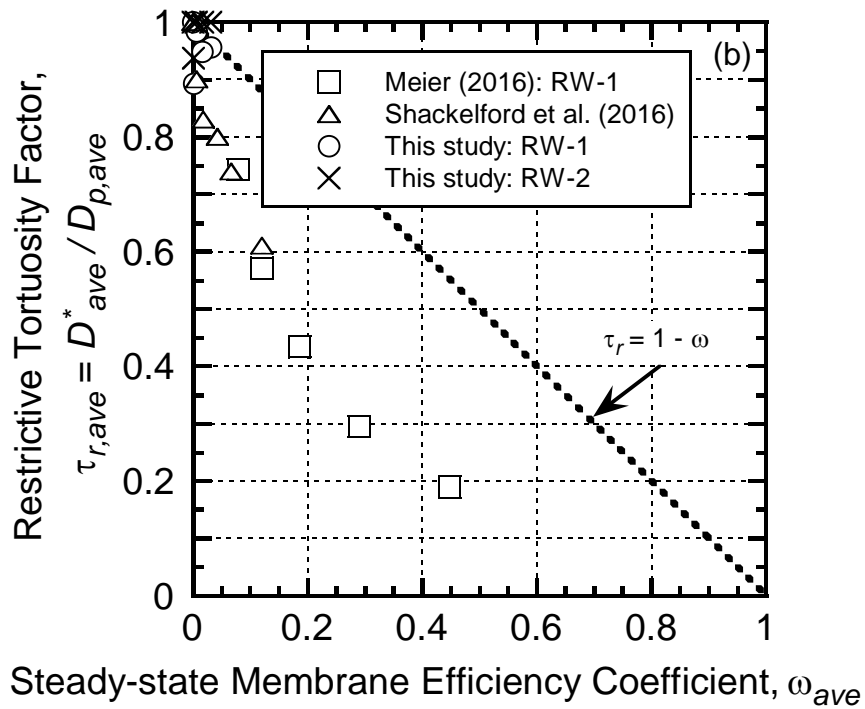
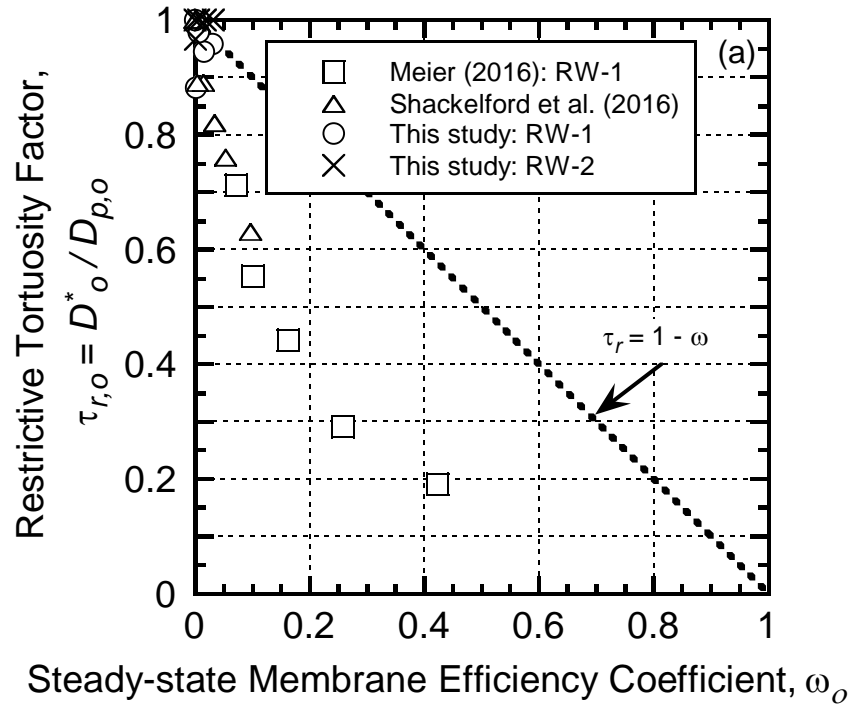


Figure 2.50. Comparison of restrictive tortuosity factors, based on the measured effective diffusion coefficient, D^* , as a function of the steady-state membrane efficiency coefficient, ω : (a) based on initial (source) solute concentrations; (b) based on average solute concentrations across the specimen boundaries.

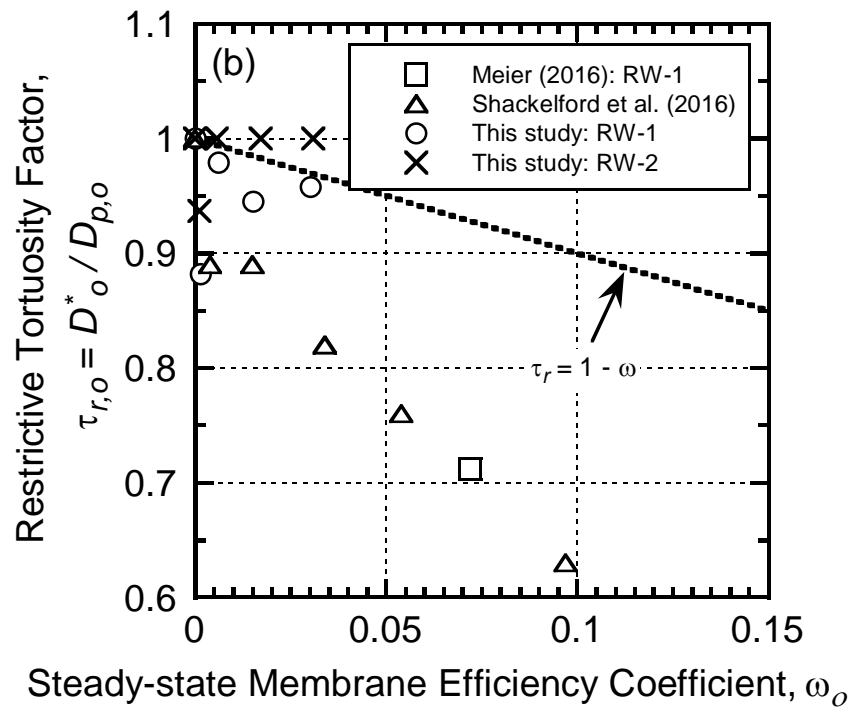
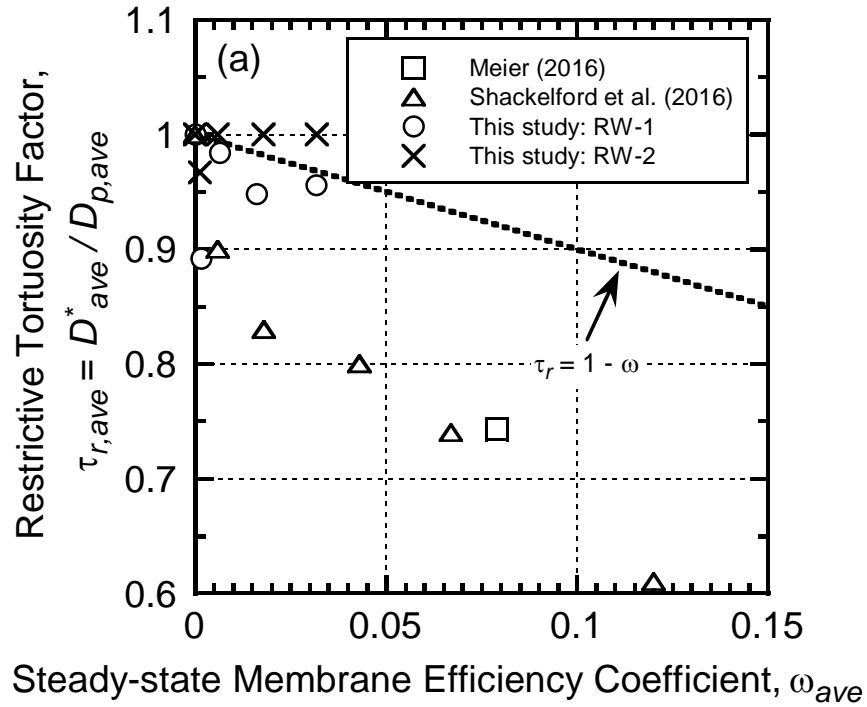


Figure 2.51. Comparison of restrictive tortuosity factors over a reduced range, based on the measured effective diffusion coefficient, D^* , as a function of the steady-state membrane efficiency coefficient, ω : (a) based on initial (source) solute concentrations; (b) based on average solute concentrations across the specimen boundaries.

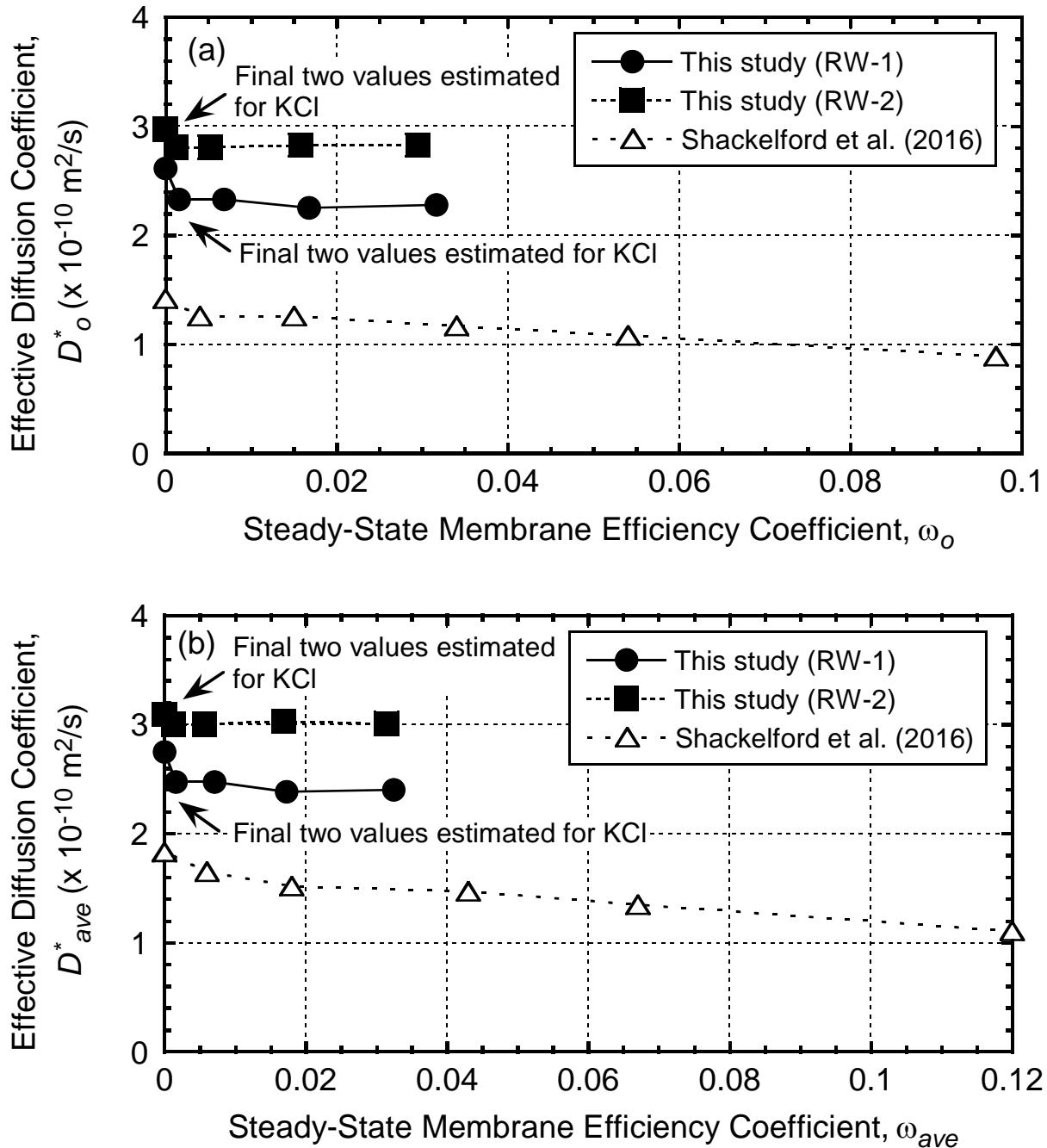


Figure 2.52. Comparison of D^* for specimens RW-1 and RW-2 with D^* for a GCL specimen tested by Shackelford et al. (2016), where D^* for the two lowest ω values for specimens RW-1 and RW-2 are estimates of the D^* that would result in the absence of the switch from KCl to NaCl for those two stages; (a) based on initial (source) solute concentrations; (b) based on average solute concentrations across the specimen boundaries.

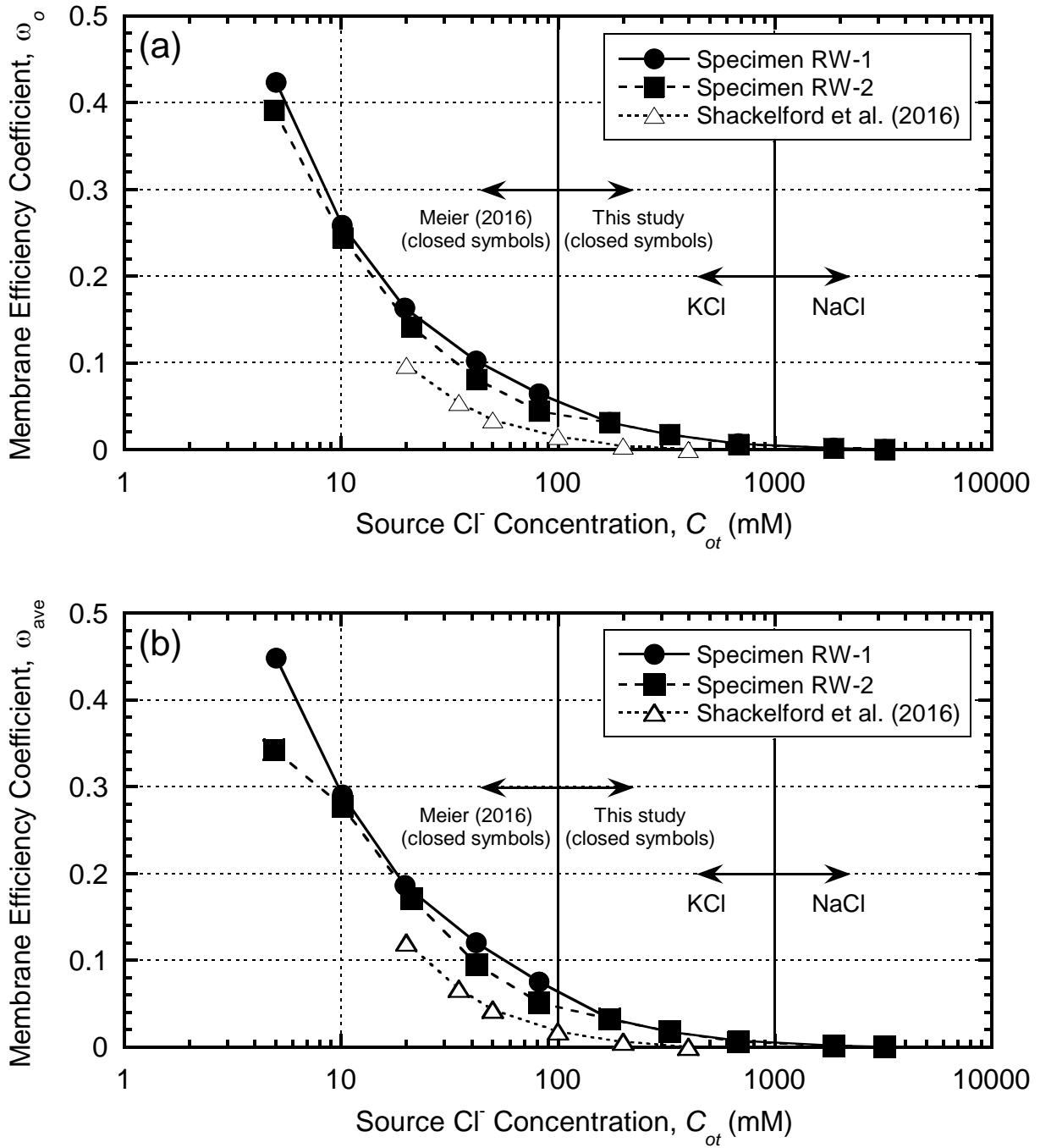


Figure 2.53. Comparison of steady-state membrane efficiency coefficients, ω : (a) based on initial (source) solute concentrations; (b) based on average solute concentrations across the specimen boundaries.

REFERENCES

- Akgün, H., Ada, M., and Koçkar, M.K., 2015. "Performance Assessment of a Bentonite-Sand Mixture for Nuclear Waste Isolation at the Potential Akkuyu Nuclear Waste Disposal Site, Southern Turkey." *Environmental Earth Sciences*, 73, 6101-6116.
- Alston, C., Daniel, D.E., and Devroy, D.J., 1997. "Design and Construction of Sand-Bentonite Liner for Effluent Treatment Lagoon, Marathon, Ontario." *Canadian Geotechnical Journal*, 34(6), 841-852.
- ASTM D422-63, 2007: Standard Test Method for Particle-Size Analysis of Soils, *Annual Book of ASTM Standards*, ASTM International, West Conshohocken, PA.
- ASTM D5084-10, 2010: Standard Test Methods for Measurement of Hydraulic Conductivity of Saturated Porous Materials Using a Flexible Wall Permeameter, *Annual Book of ASTM Standards*, ASTM International, West Conshohocken, PA.
- ASTM D7100-11, 2012: Standard Test Method for Hydraulic Conductivity Compatibility Testing of Soils with Aqueous Solutions, *Annual Book of ASTM Standards*, ASTM International, West Conshohocken, PA.
- ASTM D2487-11, 2011: Standard Practice for Classification of Soils for Engineering Purposes (Unified Soil Classification System), *Annual Book of ASTM Standards*, ASTM International, West Conshohocken, PA.
- ASTM D698-12, 2012: Standard Test Methods for Laboratory Compaction Characteristics of Soil Using Standard Effort (12400 ft-lbf/ft³ (600 kN-m/m³)), *Annual Book of ASTM Standards*, ASTM International, West Conshohocken, PA.
- Barbour, S., and Fredlund, D., 1989. "Mechanisms of Osmotic Flow and Volume Change in Clay Soils." *Canadian Geotechnical Journal*, 26(4), 551-562.

- Benson, C.H., Zhai, H., and Wang, X., 1994. "Estimating Hydraulic Conductivity of Compacted Clay Liners." *Journal of Geotechnical Engineering*, 120(2), 366–387.
- Benson, C.H., Daniel, D.E., and Boutwell, G.P. 1999. "Field Performance of Compacted Clay Liners." *Journal of Geotechnical and Geoenvironmental Engineering*, 125(5), 390-403.
- Bohnhoff, G., 2012. *Membrane Behavior, Diffusion, and Compatibility of a Polymerized Bentonite for Containment Barrier Applications*. PhD Dissertation, Colorado State University, Fort Collins, CO.
- Bohnhoff, G.L., and Shackelford, C.D., 2013. "Improving Membrane Performance via Bentonite Polymer Nanocomposite." *Applied Clay Science*, 86, 83-98.
- Bohnhoff, G.L., and Shackelford, C.D., 2015. "Salt Diffusion through a Bentonite-Polymer Composite." *Clays and Clay Minerals, Clay Minerals Society*, 63(3), 172-189.
- Daniel, D.E., 1987. "Earthen Liners for Land Disposal Facilities." *Geotechnical Practice for Waste disposal '87*, Woods. R.D. eds., GSP 13, ASCE, 21-39.
- Daniel, D. E., 1993. "Clay Liners." *Geotechnical Practice for Waste Disposal*, Daniel, D.E., eds., Chapman & Hall, London, England, 137- 163.
- Dominijanni, A. and Manassero, M., 2008. "Influence of Membrane Behavior on Contaminant Transport through Geosynthetic Clay Liners." *Characterization, Monitoring, and Modeling of GeoSystems*, Alshawabkeh, A.N. Reddy, K.R., and Khire, M.V. Eds., GeoCongress 2008, ASCE, Reston, Virginia, USA, 814-821.
- Dominijanni, A., Manassero, M, and Puma, S., 2013. "Coupled Chemical-Hydraulic-Mechanical Behavior of Bentonites." *Gèotechnique*, 63(3), 191-205.
- Dow Chemical Company, 2000. "DOWICIL QK-20 Antimicrobial." Product Information, Form No. 253-01184-0100X/GW, Dow Chemical Company, Midland, MI.

- Essington, M.E., 2004. *Soil and Water Chemistry: An Integrative Approach*. CRC Press LLC, Boca Raton, FL.
- Fritz, S., 1986. "Ideality of Clay Membranes in Osmotic Processes: A Review." *Clays and Clay Minerals*, 34(2), 214-223.
- Garlanger, J.E., Cheung, F.K., and Bishar, S.T. 1987. "Quality Control Testing for a Sand-Bentonite Liner." *Geotechnical Practice for Waste Disposal '87*, Woods, R.D., ed., ASCE, New York, NY, 488-499.
- Groenevelt, P., and Elrick, D., 1976. "Coupling Phenomena in Saturated Homo-Ionic Montmorillonite: II. Theoretical." *Soil Science Society of America Journal*, 40(6), 820-823.
- Henning, J., Evans, J., and Shackelford, C., 2006. "Membrane Behavior of Two Backfills from Field-Constructed Soil-Bentonite Cutoff Walls." *Journal of Geotechnical and Geoenvironmental Engineering*, 132(10), 1243-1249.
- Kang, J., and Shackelford, C., 2009. "Clay Membrane Testing Using a Flexible-Wall Cell under Closed-System Boundary Conditions." *Applied Clay Science*, 44(1-2), 43-58.
- Kang, J., and Shackelford, C., 2010. "Membrane Behavior of Compacted Clay Liners." *Journal of Geotechnical and Geoenvironmental Engineering*, 136(10), 1368-1382.
- Kang, J., and Shackelford, C., 2011. "Consolidation Enhanced Membrane Behavior of a Geosynthetic Clay Liner." *Geotextiles and Geomembranes*, 29, 544-556.
- Katchalsky, A., and Curran, P.F., 1965. *Nonequilibrium thermodynamics in biophysics*, Harvard University Press, Cambridge, MA.
- Keijzer, T., Kleingeld, P., and Loch, J., 1999. "Chemical Osmosis in Compacted Clayey Material and the Prediction of Water Transport." *Engineering Geology*, 53(2), 151-159.

- Kemper, W., and Maasland, D., 1964. "Reduction in Salt Content of Solution Passing through Thin Films Adjacent to Charged Surfaces." *Proceedings of the Soil Science Society of America*, 28(3), 318-323.
- Kemper, W. and Rollins, J., 1966. "Osmotic Efficiency Coefficients across Compacted Clays." *Proceedings of the Soil Science Society of America*, 30(5), 529-534.
- Kenney, T.C., van Veen, W.A., Swallow, M.A., and Sungaila, M.A. 1992. "Hydraulic Conductivity of Compacted Bentonite-Sand Mixtures." *Canadian Geotechnical Journal*, 29(3), 364-374.
- Lake, C.B., and Rowe, R.K., 2000. "Diffusion of Sodium and Chloride through Geosynthetic Clay Liners." *Geotextiles and Geomembranes*, 18, 103-131.
- Lundgren, T.A. 1981. "Some Bentonite Sealants in Soil Mixed Blankets." *Proceedings, 10th International Conference on Soil Mechanics and Foundation Engineering*, Stockholm, Sweden, June 15-19, Balkema, A. A. eds., Rotterdam, The Netherlands, Vol. 2, 349-354.
- Malusis, M.A., and Daniyarov, A.S., 2016. "Membrane Efficiency and Diffusive Tortuosity of a Dense Prehydrated Geosynthetic Clay Liner." *Geotextiles and Geomembranes*, 44(5), 719-730.
- Malusis, M., and Shackelford, C., 2002a. "Chemico-Osmotic Efficiency of a Geosynthetic Clay Liner." *Journal of Geotechnical and Geoenvironmental Engineering*, 128(2), 97-106.
- Malusis, M., and Shackelford, C., 2002b. "Theory for Reactive Solute Transport through Clay Membrane Barriers." *Journal of Contaminant Hydrology*, 59(4), 291-316.
- Malusis, M., and Shackelford, C., 2002c. "Coupling Effects during Steady-State Solute Diffusion through a Semipermeable Clay Membrane." *Environmental Science and Technology*, 36(6), 1312-1319.

- Malusis, M.A., Kang, J.-B., and Shackelford, C.D., 2015. "Restricted Salt Diffusion in a Geosynthetic Clay Liner." *Environmental Geotechnics*, ICE, Thomas Telford Ltd., London, 2(2), 68-77.
- Malusis, M., Shackelford, C., and Olsen, H., 2001. "Flow and Transport through Clay Membrane Barriers." *Geoenvironmental Engineering, Geoenvironmental Impact Management*, R. Yong and H. Thomas, Eds., *Thomas Telford Publ.*, London, UK, 334-341.
- Manassero, M. and Dominijanni, A., 2003. "Modelling the Osmosis Effect on Solute Migration through Porous Media." *Géotechnique*, 53(5), 481-492.
- Mazzieri, F., Di Emidio, G., and Van Impe, P., 2010. "Diffusion of Calcium Chloride in a Modified Bentonite: Impact on Osmotic Efficiency and Hydraulic Conductivity." *Clays and Clay Minerals*; 58(3), 351-363.
- Meier, A., 2016. "Membrane and Diffusion Behavior of a Compacted Sand-Bentonite Mixture for Hydraulic and Chemical Containment Applications." MS Thesis, Colorado State University, Fort Collins, CO.
- Meier, A.J. and Shackelford, C.D. (2017). "Membrane behavior of compacted sand-bentonite mixture." *Canadian Geotechnical Journal*, in press.
- Meier, A., Sample-Lord, K., Castelbaum, D., Kallase, S., Moran, B., Ray, T., and Shackelford, C., 2014. "Persistence of Semipermeable Membrane Behavior for a Geosynthetic Clay Liner." *Proceedings, 7th International Conference on Environmental Geotechnics*, A. Bouazza, S. Yuen, and B. Brown, Eds., Nov. 10-14, 2014, Melbourne, Australia (ISBN 978-1-922107-23-7), 496-503.

- Olsen, H. W., Yearsley, E. N., and Nelson, K. R., 1990. "Chemico-Osmosis Versus Diffusion-Osmosis." *Transportation Research Record 1288*, Transportation Research board, Washington D.C., 15-22.
- O'Sadnick, D.L., Simpson, B.E., and Kasel, G.K. 1995. "Evaluation and Performance of a Sand/Bentonite Liner." *Geoenvironment 2000*, Y. B. Acar and D. E. Daniel, eds., ASCE, New York, NY, 688-701.
- Robinson, R.A., and Stokes, R.H., 1959. *Electrolyte Solutions*, Dover Publications, Inc., Mineola, NY.
- Romankiw, L.A., and Chou, I., 1983. "Densities of Aqueous NaCl, KCl, MgCl₂ and CaCl₂ Binary Solutions in the Concentration Range 0.5-6.1 *m* at 25, 30, 35, 40, and 45 °C." *Journal of Chemical Engineering Data*, 28(3), 300-305.
- Sample-Lord, K., 2015. *Membrane Behavior and Diffusion in Unsaturated Sodium Bentonite*. PhD Dissertation, Colorado State University, Fort Collins, CO.
- Shackelford, C., 1991. "Laboratory Diffusion Testing for Waste Disposal – A review." *Journal of Contaminant Hydrology*, 7(3), 177-217.
- Shackelford, C., 2011. "Membrane Behavior in Geosynthetic Clay Liners." *Geo-Frontiers 2011: Advances in Geotechnical Engineering*, J. Han and D. Alzamora, Eds., Geotechnical Special Publication 211, ASCE, Reston, VA, 1961-1970.
- Shackelford, C., 2013. "Membrane Behavior in Engineered Bentonite-Based Containment Barriers: State of the Art." *Proceedings of Coupled Phenomena in Environmental Geotechnics (CPEG)*, M. Manassero, A. Dominijanni, S. Foti, and G. Musso, eds., July 1-3, Torino, Italy, CRC Press/Balkema, Taylor & Francis Group, London, 45-60.

- Shackelford, C., 2014. "The ISSMGE Kerry Rowe Lecture: The Role of Diffusion in Environmental Geotechnics." *Canadian Geotechnical Journal*, NRC, 51(11), 1219-1242
- Shackelford, C, Benson, C.H., Katsumi, T., Edil, T.B., and Lin, L. 2000. "Evaluating the Hydraulic Conductivity of GCLs Permeated with Non-standard Liquids." *Geotextiles and Geomembranes*, 18(2-4), 133-161.
- Shackelford, C., and Daniel, D., 1991. "Diffusion in Saturated Soil. 1. Background." *Journal of Geotechnical Engineering*, 117(3), 467–484.
- Shackelford, C., and Lee, J., 2003. "The Destructive Role of Diffusion on Clay Membrane Behavior." *Clays and Clay Minerals*, 51(2), 187-197.
- Shackelford, C.D., Malusis, M.A., Majeski, M.J., and Stern, R.T., 1999. "Electrical Conductivity Breakthrough Curves." *Journal of Geotechnical and Geoenvironmental Engineering*, 125(4), 260-270.
- Shackelford, C., Malusis, M., and Olsen, H., 2003. "Clay Membrane Behavior for Geoenvironmental Containment." *Soil and Rock America Conference 2003*, P. J. Culligan, H. H. Einstein, and A. J. Whittle, Eds., Verlag Glückauf GMBH, Essen, Germany, Vol. 1, 767-774.
- Shackelford, C., Meier, A., Sample-Lord, K., 2016. "Limiting Membrane and Diffusion Behavior of a Geosynthetic Clay Liner," *Geotextiles and Geomembranes*, 44(5), 707-718.
- Shackelford, C., and Moore, S.M., 2013. "Fickian Diffusion of Radionuclides for Engineered Containment Barriers: Diffusion Coefficients, Porosities, and Complicating Issues." *Engineering Geology*, 152(1), 133-147.

- Shackelford, C., and Scalia, J., 2016. "Semipermeable Membrane Behavior in Bentonite-Based Barriers: Past, Present, and Future." In: Proceeding of GeoVancouver 2016, Vancouver, BC, Canada, 2-5.
- Stern, R.T. and Shackelford, C.D., 1998. "Permeation of Sand-Processed Clay Mixtures with Calcium Chloride Solutions." *Journal of Geotechnical and Geoenvironmental Engineering*, 124(3), 231-241.
- Tang, Q., Katsumi, T., Inui, T., Li, Z., 2014a. "Membrane Behavior of Bentonite-Amended Compacted Clay." *Soils and Foundations*, Japanese Geotechnical Society, 54(3), 329-344.
- Tang, Q., Katsumi, T., Inui, T., Takai, A., Li, Z., 2014b. "Influence of Compaction Degree on Membrane Behavior of Compacted Clay Amended with Bentonite." *Geo-Congress 2014*, February 23-26, 2014, Atlanta, Georgia, GSP 234, ASCE.
- Tian, K., and Benson, C., 2015. "Effect of Low-Level Radioactive Waste Leachate on Hydraulic Conductivity of a Geosynthetic Clay Liner." *Geosynthetics 2015*, February 15-18, 2015, Portland, Oregon, Industrial Fabrics Association International, Roseville, MN, 236-244
- Tinoco, I., Sauer, K., and Wang, J. C., 1995. *Physical chemistry*, Prentice-Hall, Upper Saddle River, N.J.
- Tong, S., and Shackelford, C., 2016. "Standardized Hydraulic Conductivity Testing of Compacted Sand-Bentonite Mixtures." *Geotechnical Testing Journal* (in-review).
- Yeo, S., Shackelford, C., and Evans, J., 2005. "Membrane Behavior of Model Soil-Bentonite Backfills." *Journal of Geotechnical and Geoenvironmental Engineering*, 131(4), 418-429.

APPENDIX A: WATER ACTIVITY AND SOLUTION DENSITY VALUES FROM THE
LITERATURE USED FOR DEVELOPMENT OF THE ACTIVITY METHOD

Table A1. Water activities of KCl and NaCl solutions at 25 °C (Robinson and Stokes 1959)

Molality, m	KCl a_w	NaCl a_w
0.1	0.996668	0.996646
0.2	0.993443	0.993360
0.3	0.99025	0.99009
0.4	0.98709	0.98682
0.5	0.98394	0.98355
0.6	0.98078	0.98025
0.7	0.97763	0.97692
0.8	0.97448	0.97359
0.9	0.97133	0.97023
1.0	0.96818	0.96686
1.2	0.9619	0.9601
1.4	0.9556	0.9532
1.6	0.9492	0.9461
1.8	0.9428	0.9389
2.0	0.9364	0.9316
2.2	0.9299	0.9242
2.4	0.9234	0.9166
2.6	0.9169	0.9089
2.8	0.9103	0.9011
3.0	0.9037	0.8932
3.2	0.8971	0.8851
3.4	0.8904	0.8769
3.6	0.8837	0.8686
3.8	0.8770	0.8600
4.0	0.8702	0.8515
4.2	0.8634	0.8428
4.4	0.8566	0.8339
4.6	0.8498	0.8250
4.8	0.8429	0.8160
5.0	-	0.8068
5.2	-	0.7976
5.4	-	0.7883
5.6	-	0.7788
5.8	-	0.7693
6.0	-	0.7598

Table A2. Densities of KCl and NaCl solutions at 25 °C (Romankiw and Chou 1983)

KCl		NaCl	
Molality, m	Density (Mg/m³)	Molality, m	Density (Mg/m³)
0	0.997	0	0.997
0.50	1.01977	1.00	1.036
1.00	1.04134	2.00	1.072
1.50	1.06189	3.00	1.106
2.00	1.08152	4.00	1.137
2.50	1.10031	5.00	1.166
3.00	1.11832	5.80	1.188
3.50	1.13562	6.00	1.194
4.00	1.15218	6.10	1.197
4.50	1.16808	-	-

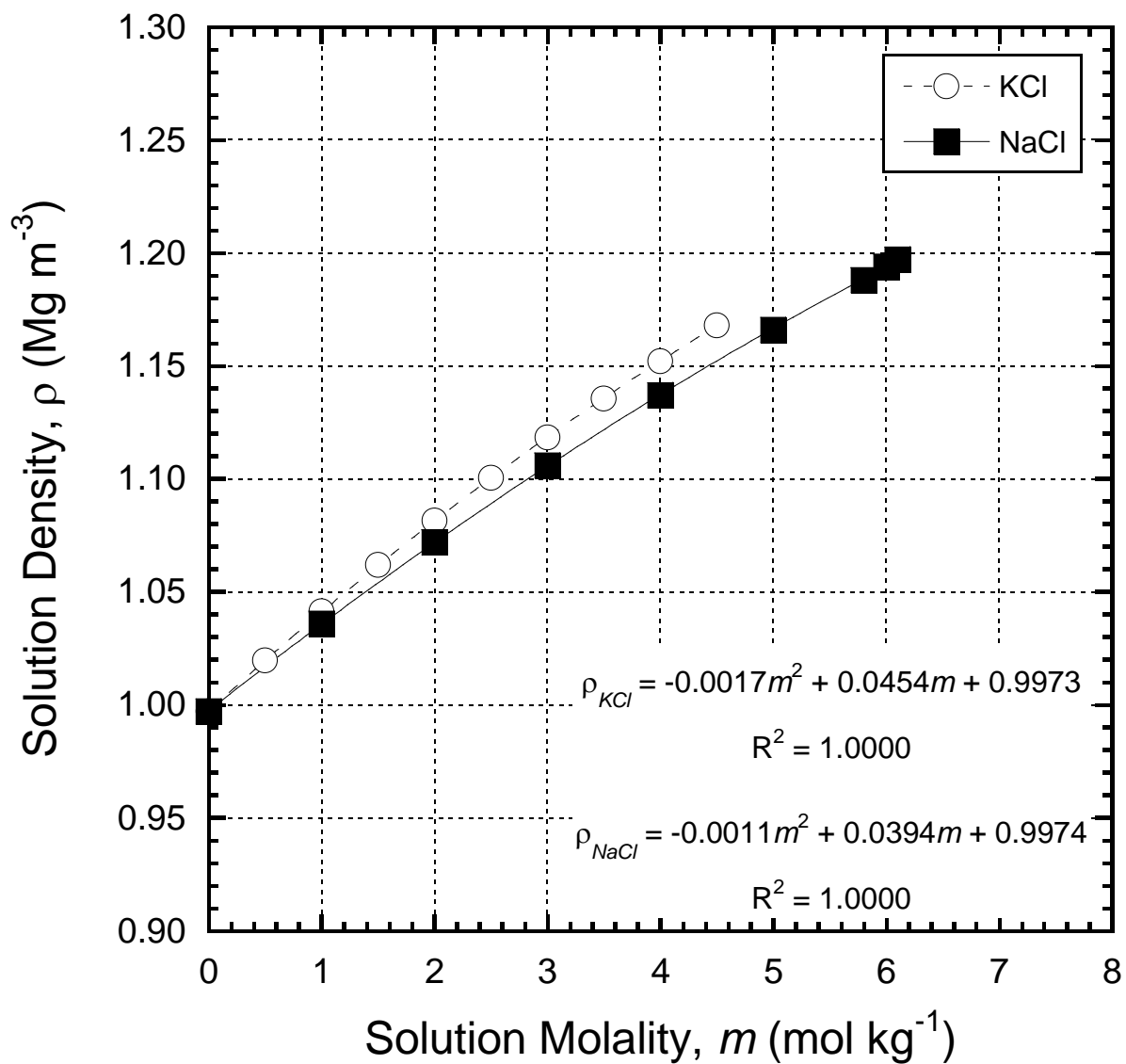


Figure A1. Relationship between solution density and molality for KCl and NaCl solutions.

APPENDIX B: MOLALITY TO MOLARITY CONVERSION

The molality, m (mol/kg), and molarity, C (mol/L), of an aqueous solution can be defined, as follows:

$$m = \frac{n}{W_w} \quad (\text{B1})$$

$$C = \frac{n}{V} \quad (\text{B2})$$

where n is the number of moles of solute (mol), W_w is the mass of water in solution (kg), and V is the total solution volume (L). If the density of the solution, ρ (Mg/m³), is known, and given that the total mass of the solution, W_t (kg), is comprised of W_w and the mass of solute in solution, W_s , then an expression for V can be developed as follows:

$$V = \frac{W_t}{\rho \left(\frac{1000\text{kg}}{\text{Mg}} \right) \left(\frac{1\text{m}^3}{1000\text{L}} \right)} = \frac{W_w + W_s}{\rho} \quad (\text{B3})$$

By rearranging Eq. B1, an expression for W_w can be obtained; furthermore, W_s (kg) can be calculated by multiplying n by the molar mass, M (g/mol), of the solute, as follows:

$$W_w = \frac{n}{m} \quad (\text{B4})$$

$$W_s = M \left(\frac{1\text{ kg}}{1000\text{ g}} \right) \cdot n = \frac{M \cdot n}{1000} \quad (\text{B5})$$

Equation B3 then can be combined with Eqs. B4 and B5 to obtain a new expression for V , as follows:

$$V = \frac{\frac{n}{m} + \frac{n \cdot m}{1000}}{\rho} \quad (\text{B6})$$

Inserting Eq. B6 into Eq. B2 results in the following expression (Eq. B7) for C in terms of m that can be used to convert a concentration from units of molality to units of molarity, assuming the solution density and the molar mass of the solute are known:

$$C = \frac{\frac{n}{\frac{\frac{n}{m} + \frac{n \cdot m}{1000}}{\rho}}}{\frac{1}{m} + \frac{M}{1000}} = \frac{\rho}{\frac{1}{m} + \frac{M}{1000}} \quad (\text{B7})$$

APPENDIX C: COMPARISON OF DIFFERENTIAL PRESSURES OBTAINED USING INLINE VERSUS DIFFERENTIAL PRESSURE TRANSDUCERS

A comparison of ΔP_{inline} and $\Delta P_{differential}$ for the full duration of membrane testing, including the KCl stages conducted by Meier (2016), is presented in Figs. C1 – C4. Although greater error between the two methods was observed for stages where boundary pressure values were lowest (i.e. stages near the beginning and end of testing), no specific evidence is apparent that explains the difference in the relationship between u_{bottom} and u_{top} observed for the two test specimens during the 3.27 M NaCl stage. Thus, the results of this analysis are not conclusive in determining whether the observed relationships between u_{bottom} and u_{top} were a result of unknown behavior within the specimens or a result of pressure transducer measurement error.

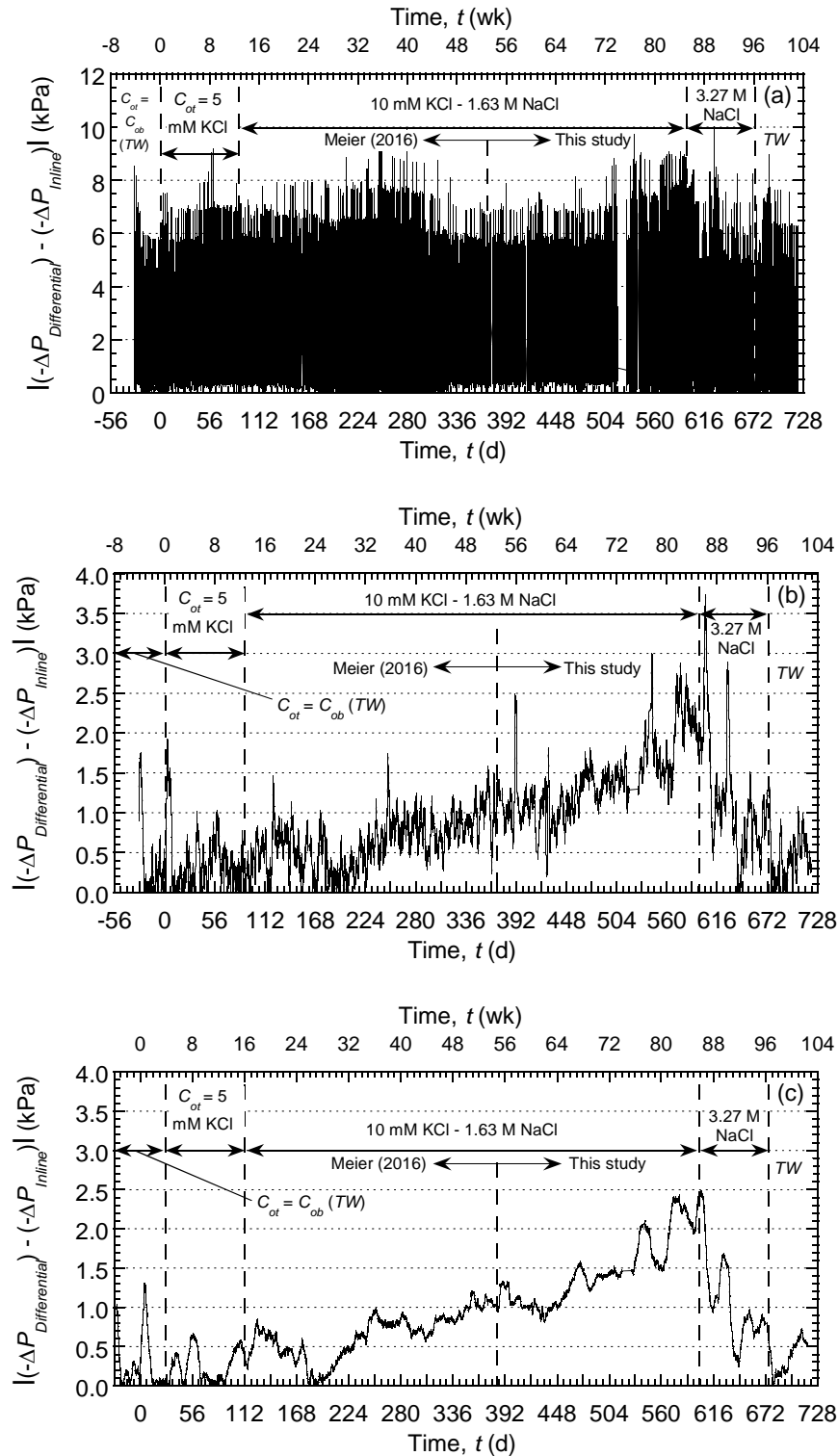


Figure C1. Magnitude of the difference between $-\Delta P$ values obtained from a differential pressure transducer and from inline (gage) pressure transducers for specimen RW-1: (a) using raw $-\Delta P$ data points; (b) using a moving average consisting of ± 100 $-\Delta P$ data points; (c) using a moving average consisting of ± 500 $-\Delta P$ data points.

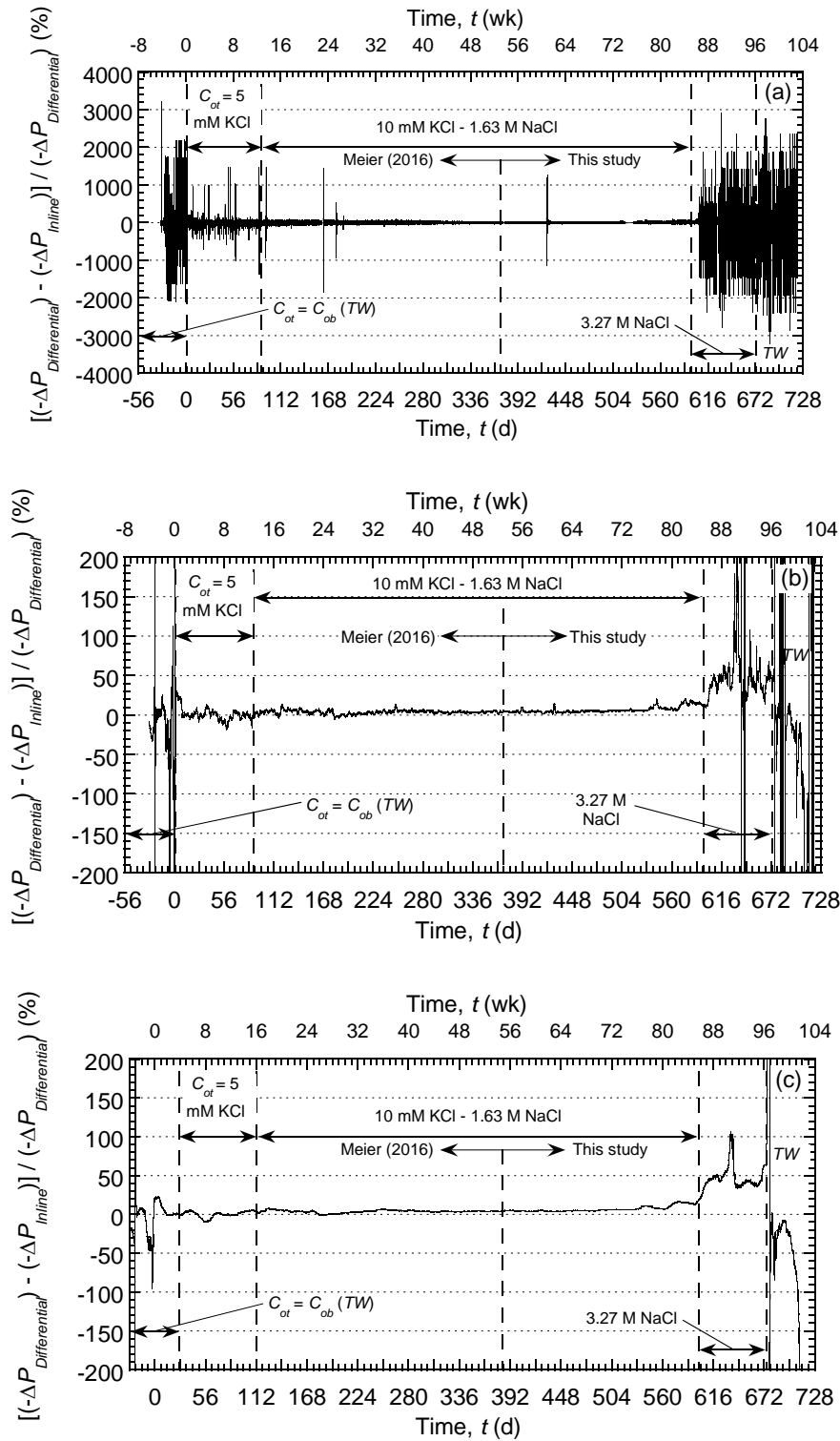


Figure C2. Percent error between $-\Delta P$ values obtained from a differential pressure transducer and from inline (gauge) pressure transducers for specimen RW-1: (a) using raw $-\Delta P$ data points; (b) using a moving average consisting of ± 100 $-\Delta P$ data points; (c) using a moving average consisting of ± 500 $-\Delta P$ data points.

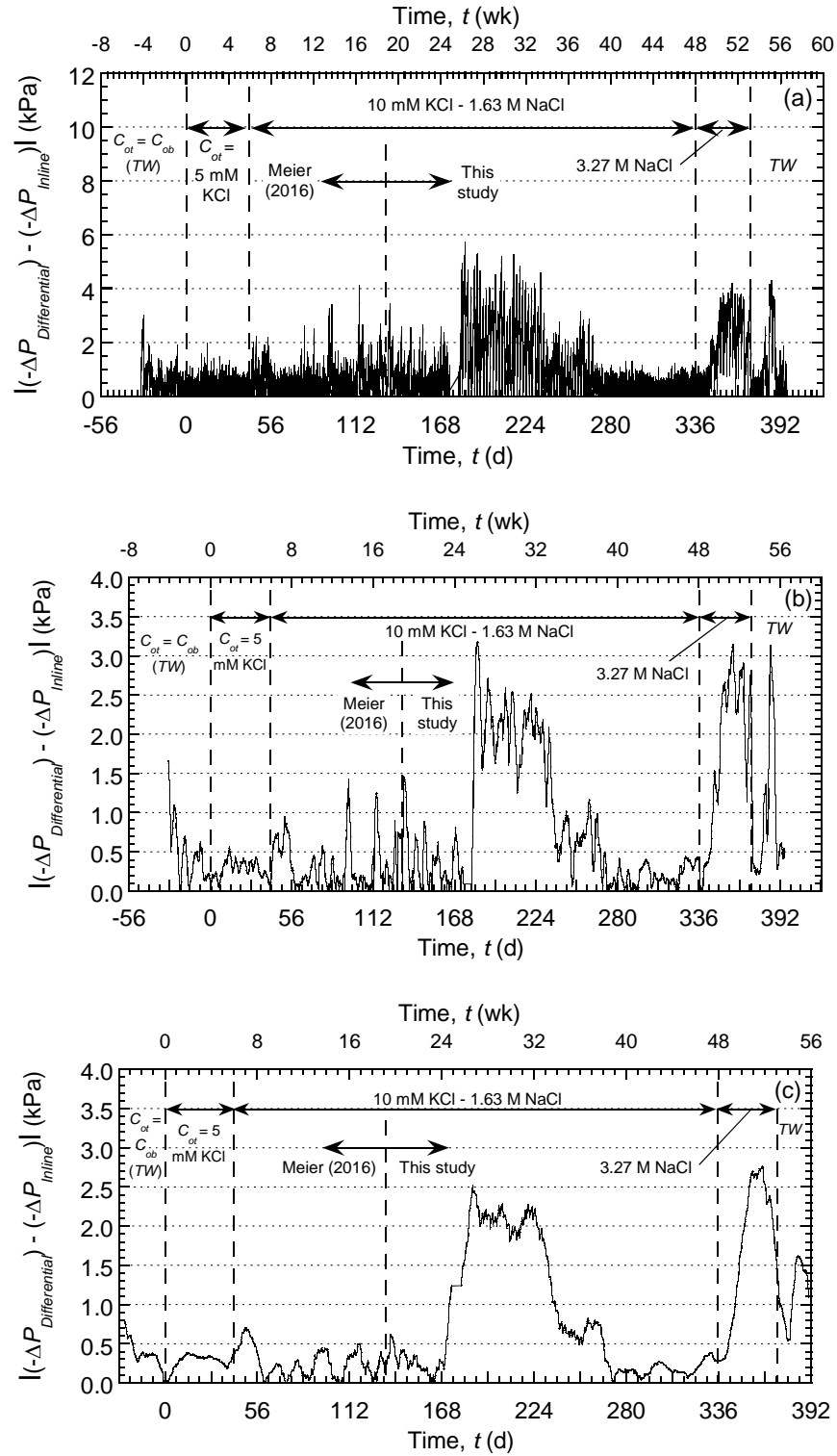


Figure C3. Magnitude of the difference between $-\Delta P$ values obtained from a differential pressure transducer and from inline (gage) pressure transducers for specimen RW-2: (a) using raw $-\Delta P$ data points; (b) using a moving average consisting of ± 100 $-\Delta P$ data points; (c) using a moving average consisting of ± 500 $-\Delta P$ data points.

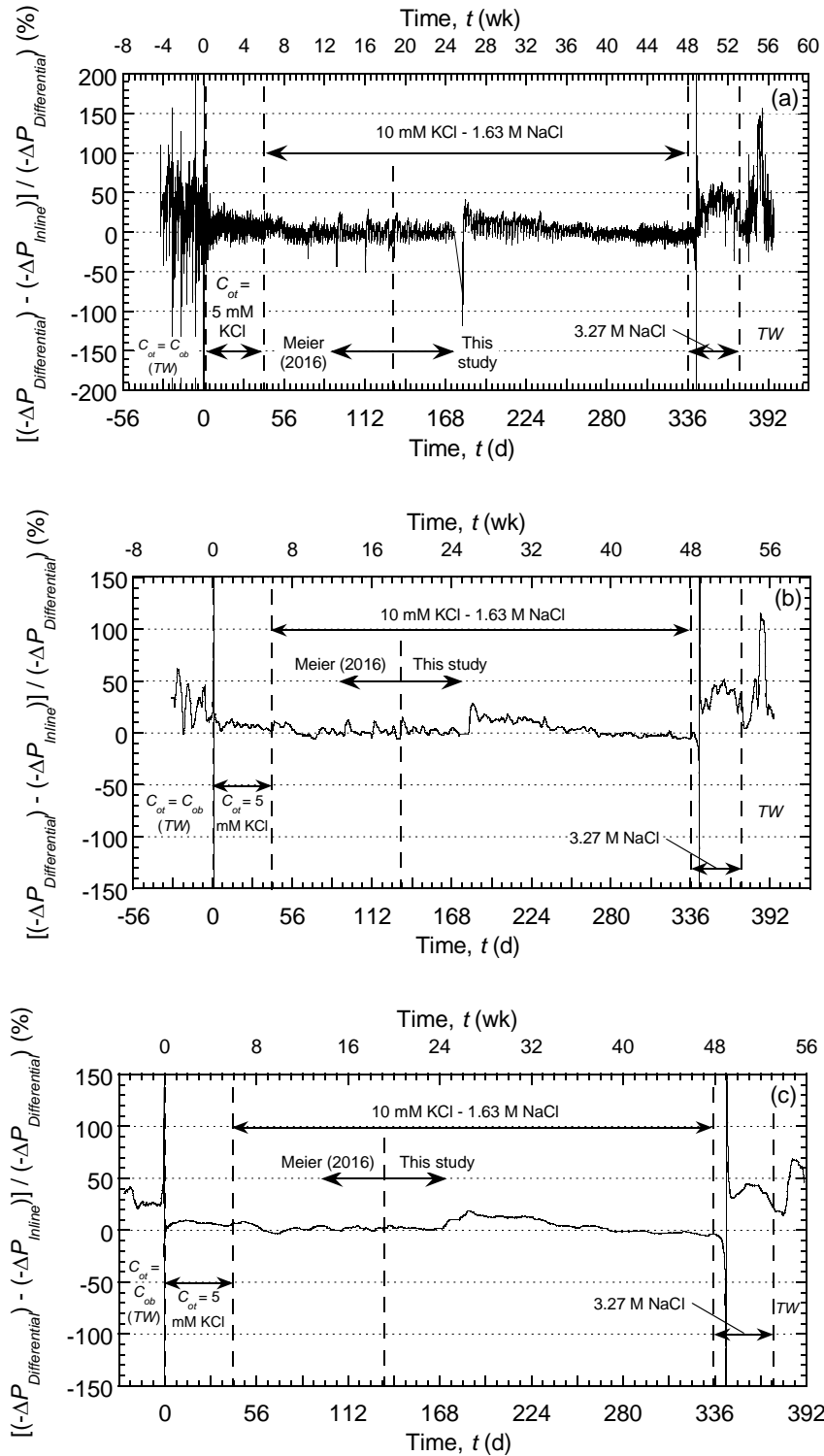


Figure C4. Percent error between $-\Delta P$ values obtained from a differential pressure transducer and from inline (gauge) pressure transducers for specimen RW-2: (a) using raw $-\Delta P$ data points; (b) using a moving average consisting of ± 100 $-\Delta P$ data points; (c) using a moving average consisting of ± 500 $-\Delta P$ data points.

APPENDIX D: METHOD OF REVERSE FITTING FOR DETERMINATION OF STEADY-STATE NET ACCUMULATED SOLUTE MASS FLUX

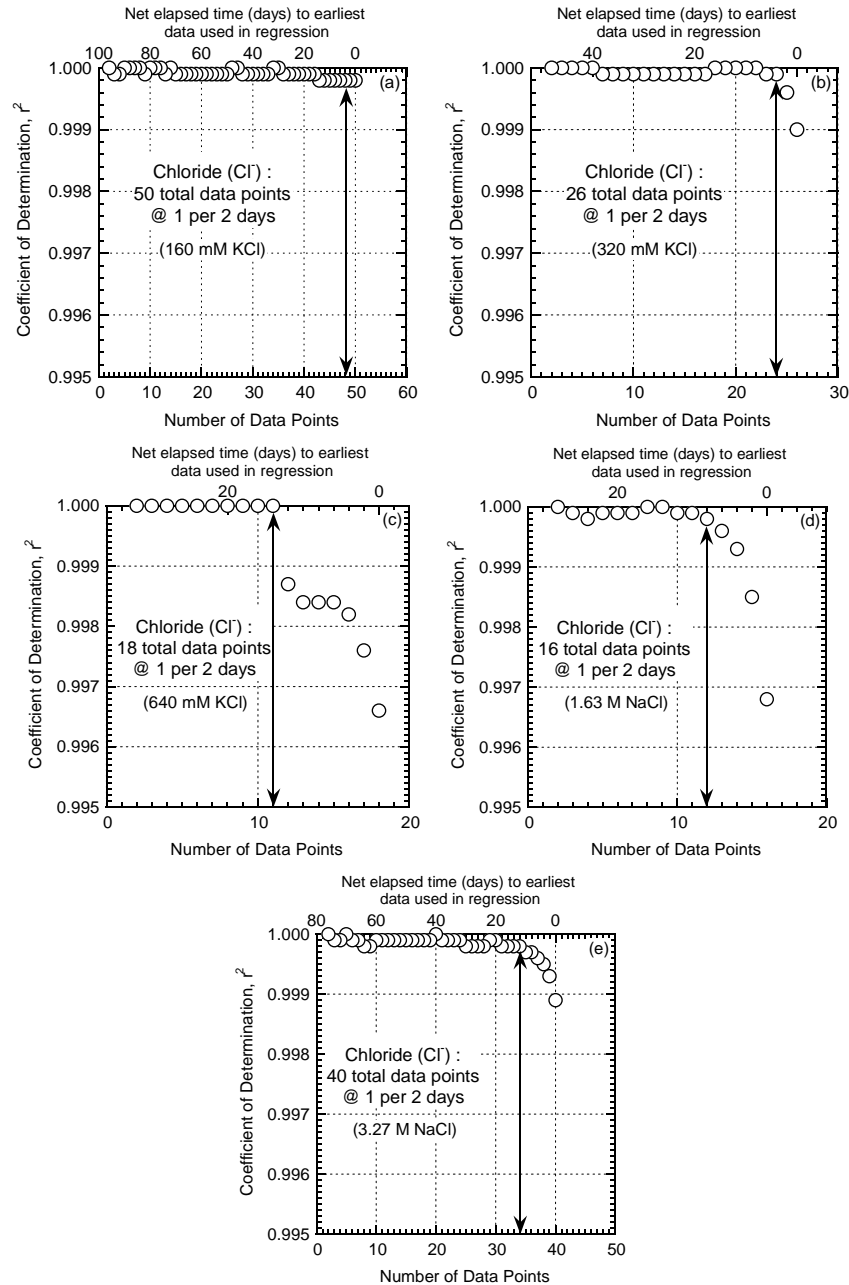


Figure D1. Method of reverse fitting R^2 values to determine the linear regression used to calculate net solute mass flux during steady-state diffusion through specimen RW-1: (a) 160 mM KCl stage; (b) 320 mM KCl stage; (c) 640 mM KCl stage; (d) 1.63 M NaCl stage; (e) 3.27 M NaCl stage.

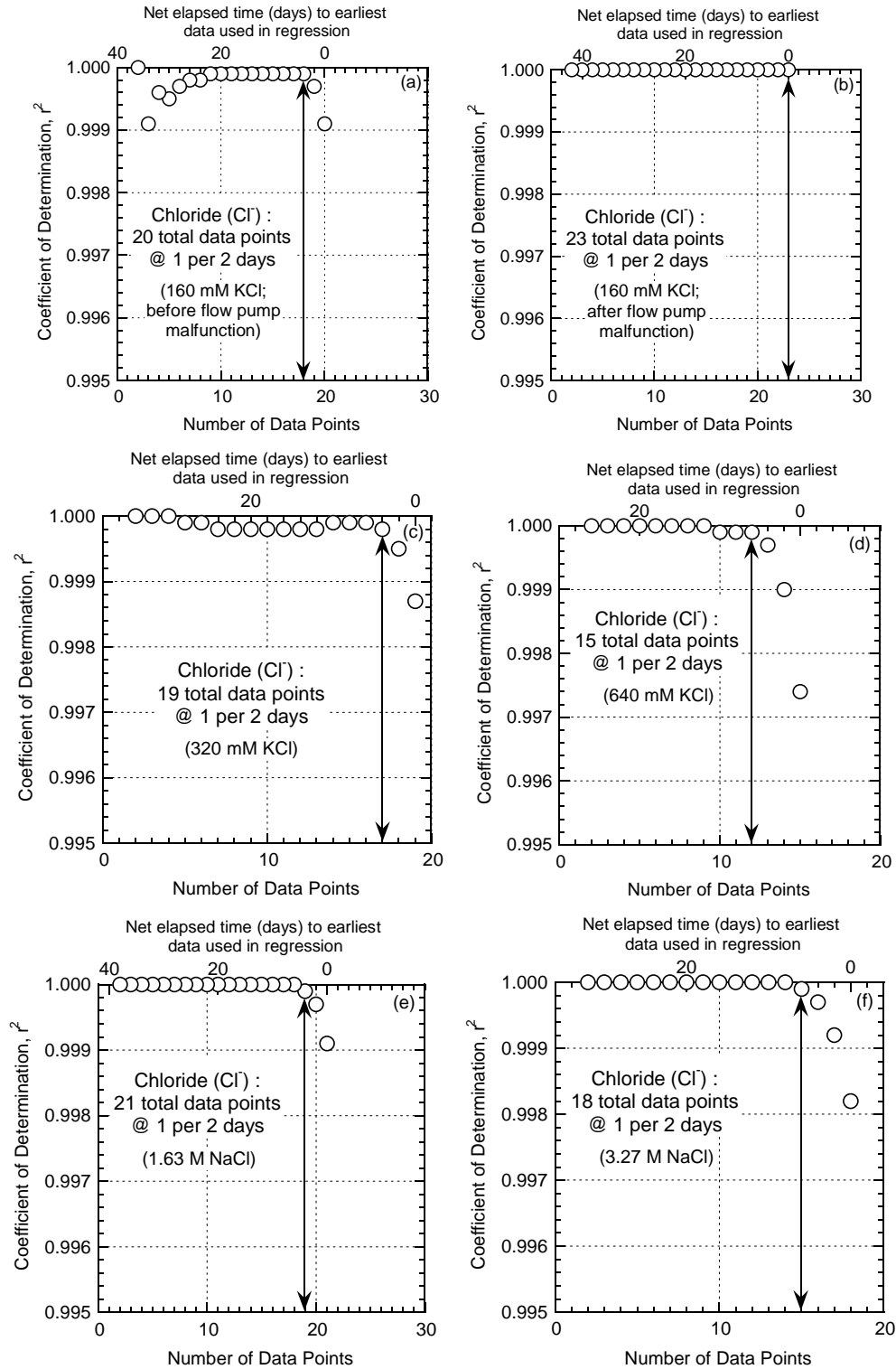


Figure D2. Method of reverse fitting R^2 values to determine the linear regression used to calculate net solute mass flux during steady-state diffusion through specimen RW-2: (a) 160 mM KCl stage, prior to flow pump malfunction; (b) 160 mM KCl stage, after flow pump malfunction; (c) 320 mM KCl stage; (d) 640 mM KCl stage; (e) 1.63 M NaCl stage; (f) 3.27 M NaCl stage.